A NUCLEAR MAGNETIC RESONANCE INVESTIGATION OF THE STRUCTURE OF SOME ALKALI SILICATE GLASSES

Muhammad Golam Mortuza

A thesis submitted to the University of Warwick, England for the admission to the degree of Doctor of Philosophy

Department of Physics

September, 1989

This thesis is dedicated to my

supervisors :

Dr. Raymond Dupree and

Dr. Diane Holland

CONTENTS

A NUCLEAR MAGNETIC RESONANCE INVESTIGATION OF THE STRUCTURE OF SOME ALKALI SILICATE GLASSES

Muhammad Golam Mortuza

A thesis submitted to the University of Warwick, England for the admission to the degree of Doctor of Philosophy

Department of Physics

September, 1989

CONTENTS

LIST OF TABLES

LIST OF FIGURES

ACKNOWLEDGEMENTS

I would like to thank the Commonwealth Scholarship Commission in the United Kingdom for providing me with the financial support and the Department of Physics at the University of Warwick for providing the research facilities. I would also like to thank my fellow countrymen and women, studying at this University, for their friendship.

The technical assistance throughout the course of this research was invaluable and I am deeply grateful to Mr. B. Sheffield, Mr. H.J. Mathers, Mr. R. Lamb and Mr. D. Goodman. I wish to express my sincere thanks to Dr. P.F. James, Sheffield University for encouraging me to investigate the sol-gel prepared lithium silicate glasses and also kindly providing me with the samples. I am grateful to all the members of NMR coffee club for providing me with a pleasant company. I am extremely grateful to Dr. A.T. Boothroyd, Dr. P.R. Dennison, Dr. M. T. -El-Gemal, Dr. A.P. Kemp, Mr. A. Boukara and Mr. K.J. Barnfather for their friendly cooperation during my work. I particularly thank Prof. E.F.W. Seymour, Dr. G. Styles, Dr. D. Mac. Paul, Prof. S.B. Palmer and Dr. H. Mykura for encouraging and inspiring me during the period of this study. I am deeply grateful to Miss L. Lucas for her patience and skilful typing of this thesis.

I am particularly indebted to Dr. M.E. Smith and Dr. I. Farnan who were always happy to discuss topics in NMR and made many invaluable suggestions. By far my greatest debts are to my supervisors Dr. Raymond Dupree and Dr. Diane Holland whose excellent guidance, interest and inspiration made this study possible and made a rewarding experience.

DECLARATION

The work presented here was carried out at the Department of Physics, University of Warwick from October 1985 to September 1988 under the supervision of Dr. R. Dupree and Dr. D. Holland. The results are outcome of my own independent research unless otherwise specified in the text and has not been submitted for any other degrees. A fraction of the work of paper numbers 3 and 4 (see below) was carried out in collaboration with J.A. Collins and M.W.G. Lockyer is not included in this thesis.

Some parts of the thesis have been published, accepted for publication and submitted for publication as follows :

1) "Six Coordinated Silicon in Glasses".
R. Dupree, D. Holland and M.G. Mortuza
Nature, 328, 416 (1987).

2) "The Role of Small Amounts of P_2O_5 in the Structure of Alkali Disilicate Glasses".
R. Dupree, D. Holland and M.G. Mortuza
Phys. Chem. Glasses, 29(1), 18 (1988).

3) "An MAS NMR Study of Network-Cation Coordination in Phosphosilicate Glasses".
R. Dupree, D. Holland, M.G. Mortuza, J.A. Collins and M.W.G. Lockyer
J. Non-Cryst. Solids, 106, 403 (1988).

4) "Magic Angle Spinning NMR of Alkali Phospho-alumino-Silicate Glasses".
R. Dupree, D. Holland, M.G. Mortuza,
J.A. Collins and M.W.G. Lockyer
J. Non-Cryst. Solids, 1989 (in press).

5) "A MAS NMR Investigation of Lithium Silicate Glasses".
R. Dupree, D. Holland and M.G. Mortuza
J. Non-Cryst. Solids, 1989 (submitted).

It is anticipated that some more of the experimental results will be submitted for publication in the future.

ABSTRACT

The potential for the use of MAS and static NMR in the investigation of alkali silicate and alkali phosphosilicate glasses and glass ceramics is the main theme of this thesis. MAS NMR of binary lithium silicate glasses containing 24-29 mol% Li_2O shows that their structure follows the constrained distribution model. However addition of Li_2O in excess of 29 mol% causes deviation from the model and a concentration dependent disproportionation of Q_3 to Q_4+Q_2 occurs. This is observable from MAS NMR in combination with static NMR results. The devitrification of these glasses produces two polymorphs of lithium disilicate. The structural changes during heat treatment occur above the glass transition temperature and are observed from the ^{29}Si chemical shift and full width at half maximum. The static ^{7}Li spectra for the crystallised samples exhibit a Pake doublet indicative of the presence of Li pairs.

The effect of paramagnetic impurity from 0-0.8 mol% on the ^{29}Si T_1 relaxation times in $Na_2O.2SiO_2$ base glasses is discussed.

The heat treatment of the sodium disilicate glasses shows α -, β-, γ - and δ - $Na_2Si_2O_5$ as the devitrification products depending upon heat treatment. A way of estimating the unknown Si-O-Si mean bond angle of the polymorphs is presented.

The effect of the addition of 0-70 mol% P_2O_5 to alkali disilicate glasses is described. Small amounts of P_2O_5 (1-10 mol%) in the glasses results in the scavenging of alkali metal ions by phosphate groups. In sodium and potassium disilicates the phosphate groups resemble orthophosphate and pyrophosphate but only orthophosphate like units are formed in lithium disilicate glasses. As a consequence of the scavenging, the silicate network partially repolymerises. A structural model for the disilicates with (1-10) mol% P_2O_5 is presented. For larger concentrations of P_2O_5 (>10 mol%) in sodium disilicate glasses only metaphosphate species are observed and phosphorus occurs as next nearest neighbour of silicon. However this arrangement gradually changes to Si-O-Si bond with ~25 mol% P_2O_5 and the length of metaphosphate chain increases. On addition of greater than about 30 mol% P_2O_5 some of the network silicon changes radically from its conventional four coordination to six coordination. Both the tetrahedral and octahedral environments of silicon at these concentrations are characteristic of mainly Si-O-P bonds. The six coordinated silicon occupies a SiP_2O_7 like environment. The proportion of "SiP_2O_7" depends upon the alkali content and the cooling rate. The cooling rates cause structural relaxation and are used to measure fictive temperature. This gives an estimate of the change of enthalpy for the conversion of one mole of six coordinated silicon from four coordinated silicon.

The ^{29}Si T_1 relaxation times in alkali silicate glass, glass ceramics and alkali phosphosilicates are presented. The T_1 in sodium disilicate glasses as a function of MnO content is a single exponential but a two component T_1 is observed after heat treatment. The single component relaxation times for the disilicate composition range becomes two component as the Na_2O content is reduced.The T_1 values in all the lithium silicate glasses, glass ceramics and alkali phosphosilicate systems are two component.The conversion of single component exponential to two component because of heat treatment or Na_2O content could be due to either nucleation or glass-in-glass phase separation. Thus the possibilities for obtaining new information about phase separation in glasses are also briefly discussed with the help of TEM micrographs.

CHAPTER 1

INTRODUCTION

1.1 GENERAL

Glasses are characterised by the absence of long range order in their structure and so consequently determination of structure is difficult. Unlike crystalline materials determination of the position of an atom is not of primary interest because the whole structure cannot be expressed as a multiple of a unit cell. The glass structure can be described as a three dimensional configuration of a variety of species termed network formers.

Normally in silicate glasses the network former is the SiO_4 tetrahedron. Unlike the unit cell in a crystalline lattice the local order of the network former, i.e. bond angle and bond length, may vary. Addition of a network modifier, e.g. Na_2O, alters the silicon environment and produces different types of species. Therefore identification of the nearest and next nearest neighbour of the network former, number of species, co-ordination number and a comparison with the respective crystal structure is the major interest for spectroscopists or material scientists. With this in mind the simple binary alkali silicate system has primarily been chosen in this work to interpret the framework structure, mainly by means of the nuclear magnetic resonance (NMR) technique.

1.2 GLASS AND GLASS CERAMICS

Glass can be formed from a melt of one or more glass forming oxides by cooling at a sufficient rate to prevent the formation of crystalline structure [1-4]. The cooling is directly related to the volume temperature characteristics [4] as shown in Figure (1.1). In the region AB the product is

liquid and the viscosity of the melt is comparable to that of water. If the melt cools without crystallisation, the decrease in volume follows the path BE. The product within this region is called a supercooled liquid. The viscosity of the product increases with the decrease of temperature. However, a sudden change of volume may occur along the path BC at a particular temperature T' if the cooling process is accompanied by crystallisation. Further decrease of temperature results either in glass (EF) or crystal (CD) formation depending upon the contraction of volume along the path BE or BC in the diagram (Figure 1.1). The temperature at the point E is called the glass transition temperature, T_g. Thus for a melt to form a glass it has to exhibit this glass transition property during cooling. The contraction of volume along the extrapolation EG or ABE continues if the material is held at the temperature T, a little below T_g. The value of T_g is not well defined and depends upon the rate of cooling.

The glass forming oxides are classified into three categories : (i) network former, (ii) network modifier, and (iii) intermediate. The principal characteristic of the network former is the tetrahedral structural arrangement in the crystalline state, e.g. SiO_2, P_2O_5, B_2O_3 and GeO_2 [5] etc. The tetrahedral configuration of the network former is not strictly valid because there are some oxides, e.g. BeO, which do not form glass [6]. The modifier oxides, e.g. Na_2O, Li_2O, normally break the long chain order and weakens the network of the glass. In the case of an intermediate oxide, e.g. Al_2O_3, Al occupies the network former position in the glass [1] but the oxide itself does not form glass. Geometrical considerations, bonding criteria, nucleation kinetics of the

oxides affect the glass forming region. Consequently the amounts of the chemical compositions of glasses varies from one form of oxide to another.

Glass ceramics are polycrystalline materials which can be produced by controlled crystallisation of glasses [1]. The process of crystallisation is mainly concerned with nucleation and the rate of crystal growth. A typical diagram for the nucleation and the crystal growth is shown in Figure (1.2). The nucleation can be classified as (i) homogeneous nucleation and (ii) heterogeneous nucleation. Homogeneous nucleation is generally caused by fluctuation in ion concentration of the parent liquid phase. This condition is difficult to achieve because glass compositions are not normally free from foreign particles. The general equation to express the rate of homogeneous nucleation is given by Becker [7] as

$$I = A \exp(-\Delta G/kT) \exp(-E/kT) \quad \ldots \quad \ldots \quad (1.1)$$

where A is a constant, ΔG is the maximum free energy of activation for formation of a stable nucleus in the system, E is the activation energy required to diffuse molecules across the phase boundary, k is the Boltzmann constant and T is the temperature.

Heterogeneous nucleation is a result of the presence of foreign particles and doped materials in the glass melt which often behave as nuclei. Epitaxial crystal growth may occur due to presence of these nuclei. The rate of heterogeneous nucleation is given by [8]

$$I = B \exp[-(\Delta Gf(\theta) + E)/kT] \quad \ldots \quad \ldots \quad \ldots \quad (1.2)$$

where B is a constant and the term $f(\theta)$ is given by

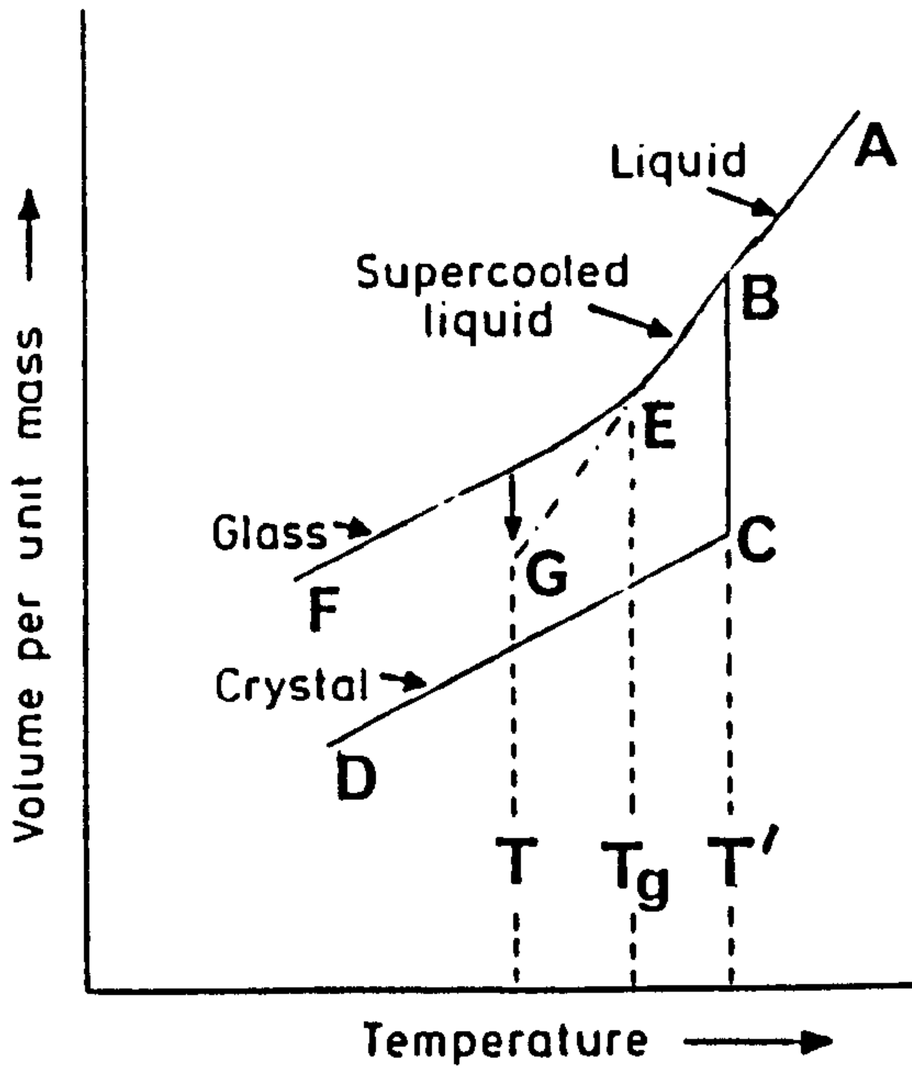

Figure 1.1 Relation between the glassy, liquid and solid states(taken from ref. 2).

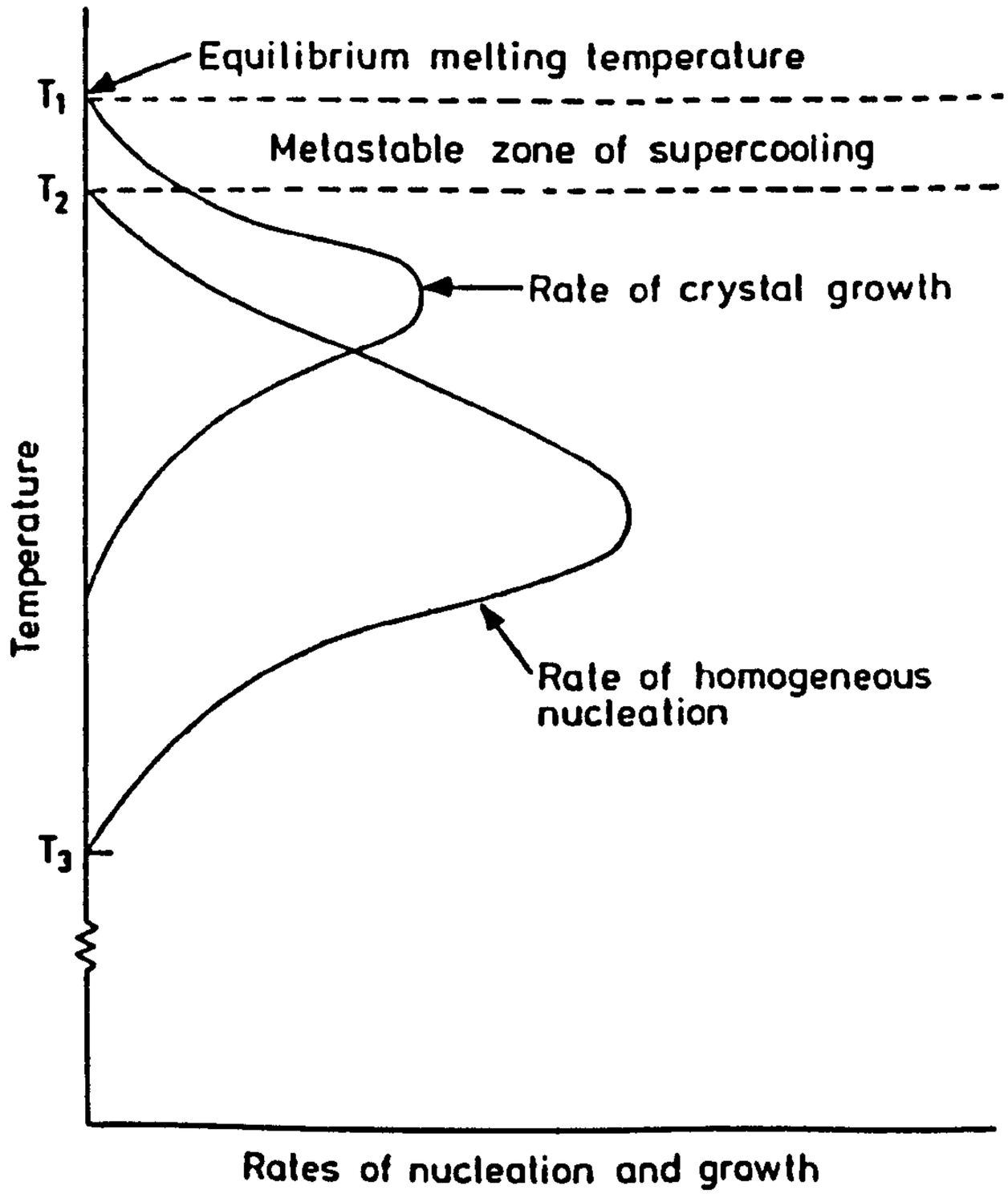

Figure 1.2 Effect of temperature on rates of nucleation and crystal growth(taken from ref. 2).

$$f(\theta) = (2 + \cos\theta)\,(1 - \cos\theta)^2/4 \quad \ldots \quad \ldots \quad (1.3)$$

where θ is the contact angle at the substrate-melt-precipitate junction.

A detailed discussion of the formation of glass, glass-ceramics, nucleation, crystallisation etc. can be found elsewhere [1-4] and these are not discussed here in detail.

1.3 MODELS FOR GLASS STRUCTURE

The random distribution of atoms prevents material scientists from determining an absolute structure of glass. Goldschmidt's prediction [5] followed by the work of Zachariasen [6] led scientists to believe that the framework of silicate glasses consists of SiO_4 tetrahedra. These SiO_4 tetrahedra are randomly linked together by means of Si-O-Si bonds [9] as shown in Figure (1.3). Incorporation of modifier oxides breaks up Si-O-Si bonding and converts some bridging oxygens [bo] to non-bridging oxygens [nbo] [6]. The configuration depending upon the number of [nbo] associated with the network former Si^{4+} is generally described by the nomenclature Q_m [10], where m determines the number of [nbo] connected to Si^{4+} (Q), i.e. for tetrahedral silicon $0 \leq m \leq 4$. Therefore, there are five possible Q species present in amorphous or crystalline states.

In order to determine the number of species or the structure of glasses several models have been proposed :

i) Statistical distribution [11] - the distribution of [nbo] per silicon is determined from probability and composition.

ii) Constrained random [12] - normally only 2Q species

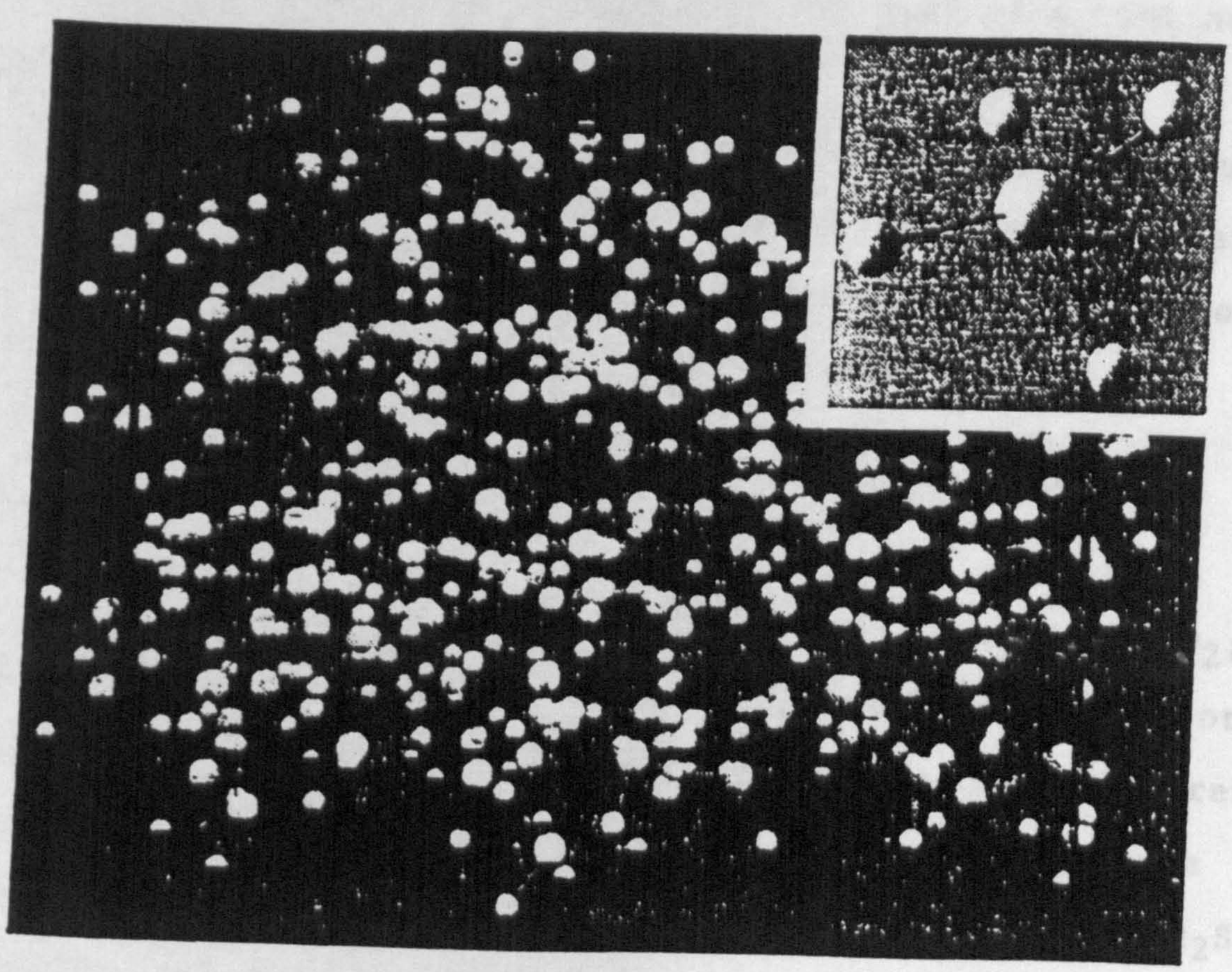

Figure 1.3 A model of vitreous silica, and (inset) a tetrahedral unit (taken from ref. 9).

form where [nbo] are homogeneously distributed. The form of Q_m depends upon the composition.

iii) Mixed Cluster [13] - species appear as clusters.

The models (i) and (ii) give a means of detecting and quantifying the species present in glasses for a particular composition. These two models give extremes of a continuum of possibilities. At high enough temperatures, if the composition forms a glass, a statistical distribution would be best. However at room temperature an intermediate state of the two models may be obtained. Experimental evidence for the cluster model to date has not been provided.

1.4 ALKALI SILICATE GLASSES : THEIR FORMATION AND PHASE DIAGRAMS

The building block of the alkali silicate (R_2O-SiO_2; R = Li, Na, K, Rb, Cs) system is the SiO_4 tetrahedron. According to the phase diagrams [14] and an assumption considered by Grimmer et al. [15] for the R_2O-SiO_2 systems (Figure 1.4) there exist crystalline compounds of SiO_4, $R_2Si_2O_5$, R_2SiO_3, $R_6Si_2O_7$ and R_4SiO_4 corresponding to Q_4, Q_3, Q_2, Q_1 and Q_0 environments. These possible Q species can be shown structurally as [11]

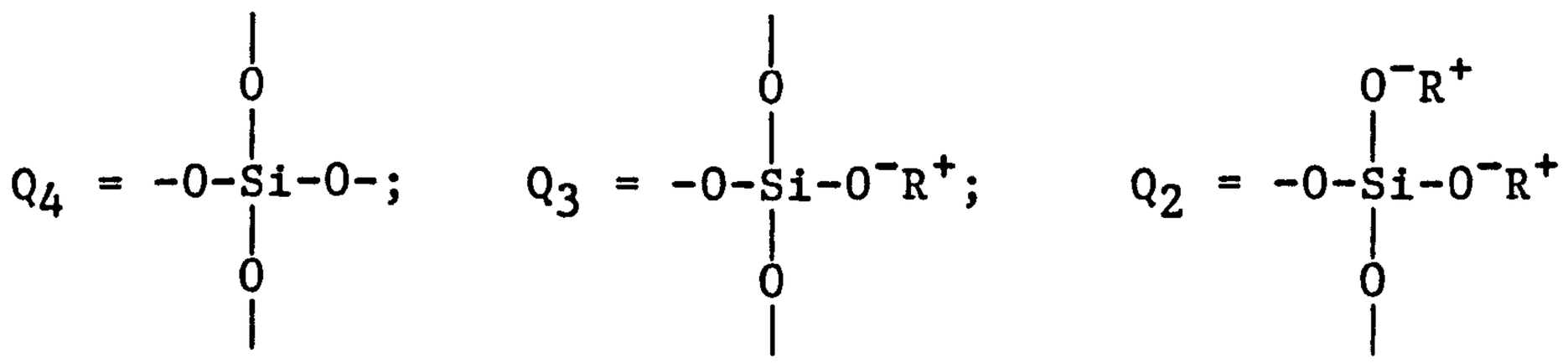

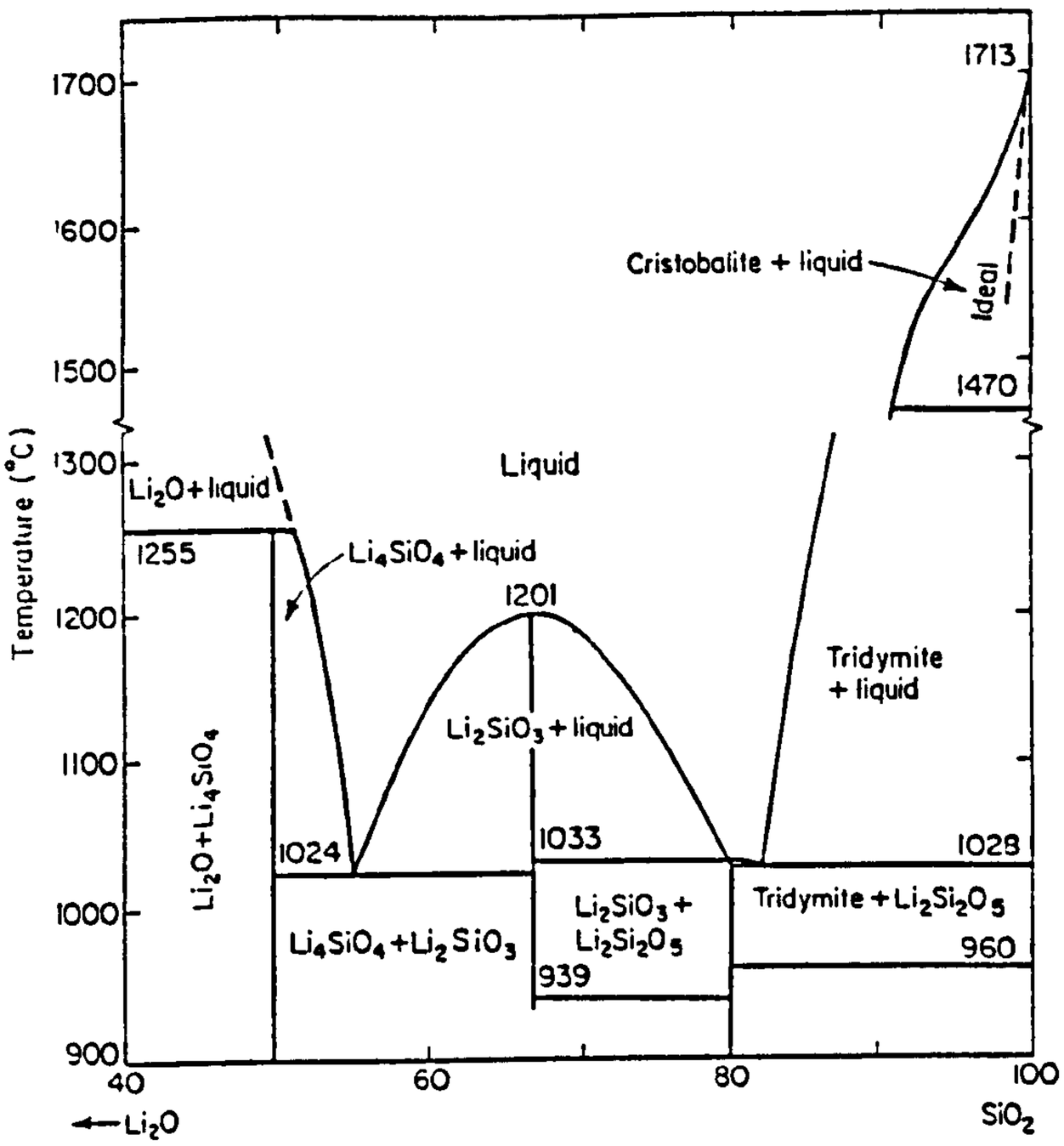

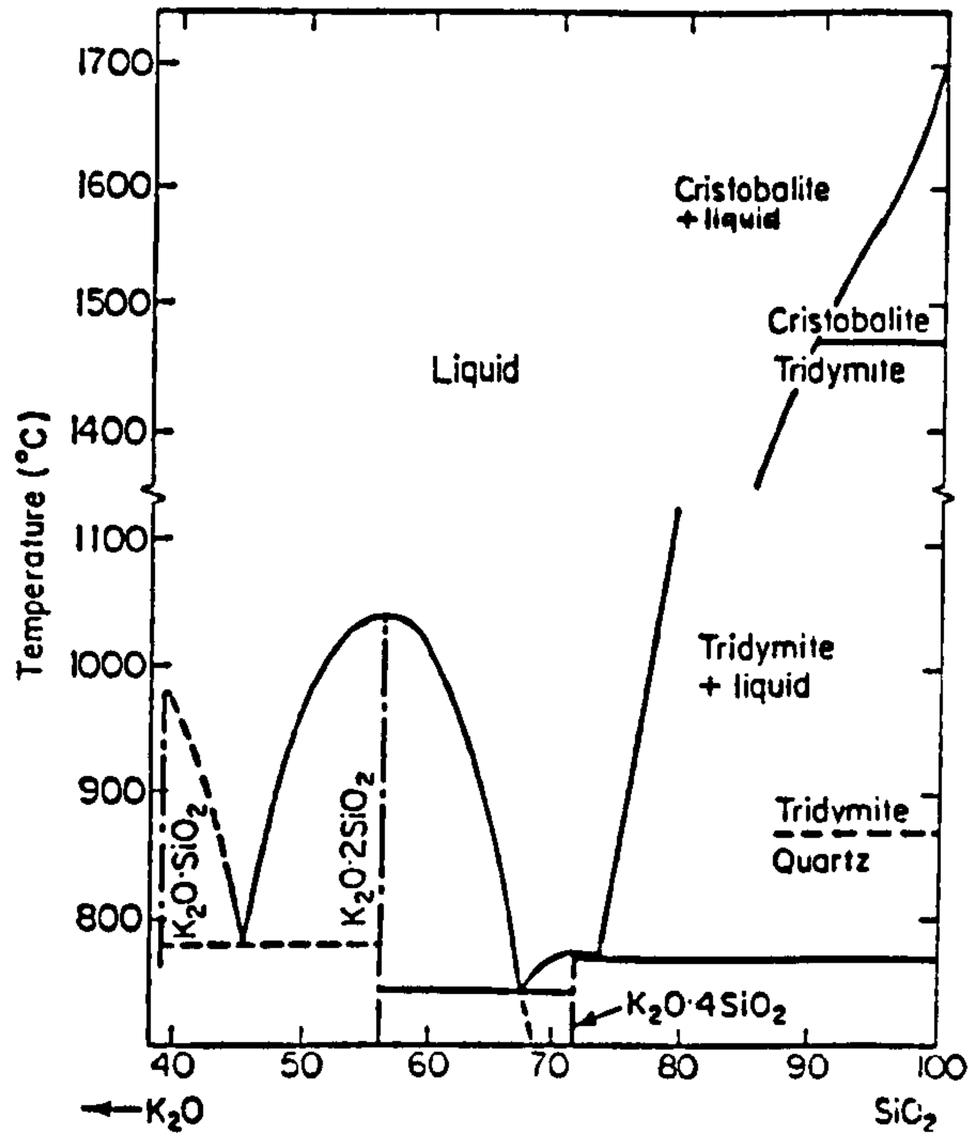

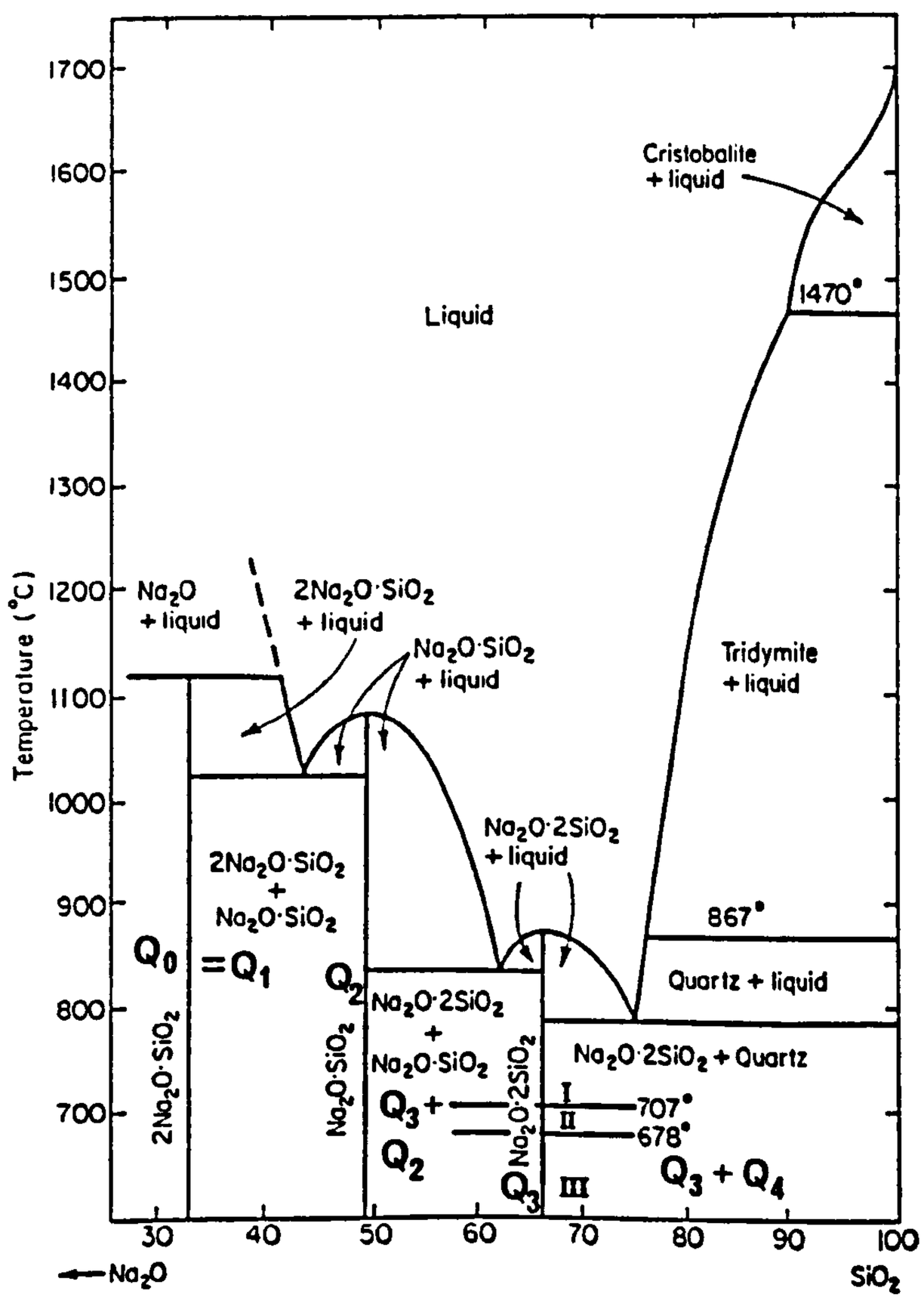

Figure 1.4 Phase diagrams of alkali silicate glasses(taken from ref. 14).

The present work deals with the first three alkali metal ions and in the future R will stand for Li, Na and K only.

In glasses all these environments do not exist. Formation of [nbo] within the continuous three dimensional network of SiO_4 (Q_4) tetrahedra presents a discontinuity in the network. Among the Q_m species Q_0 is an isolated SiO_4 tetrahedron. Thus formation of glass with orthosilicate (Q_0) environment is difficult because that could readily undergo crystallisation. The Q_1 species is a dimer structure and the structural unit may be shown as

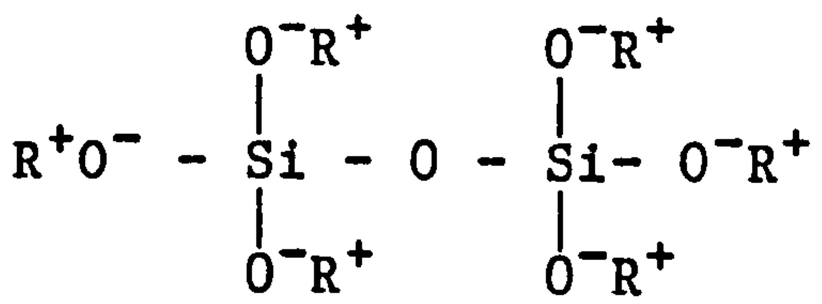

Thus there is a lack of long chains and the formation of glass has also become difficult. Incorporation of large amounts of R_2O(>50 mol%) in the SiO_4 network reduces the viscosity [1], lowers the activation energy for crystallisation [16] and hence lies beyond the glass forming region. However, in general, long chains exist for Q_2, Q_3 species and the formation of alkali silicate glasses with Q_2, Q_3 and Q_4 is possible. The glass formation region also depends upon the type of alkali oxide added to the parent network, amount of a batch and the rate of cooling.

In the phase diagrams (Figure 1.4) of R_2O-SiO_2 systems there is no common feature about the formation of Q_m species. The regions of formation of Q_3 and Q_2 species in alkali silicates become wider with the size of the alkali atom. This could be the effect of steric hindrances (K>Na>Li) which could broaden the glass forming region.

1.5 HIGH RESOLUTION NMR IN SILICATE GLASSES AND GLASS-CERAMICS

Nuclear magnetic resonance (NMR) is the spectroscopy of magnetic materials that possess nuclear magnetic moments. Gorter and Broer [14] first tried to establish the phenomenon but the experiment was unsuccessful. However the effect was demonstrated independently by Purcell et al. [18] and Bloch et al. [19]. The NMR signal depends upon the population difference between two energy levels. In an external magnetic field the nuclear spins follow the Boltzmann distribution and for ^{31}P the population difference is only 23 in 10^6 in a field of 8.45T. In spite of the low sensitivity NMR spectroscopy plays an important role in structural investigation of liquid and solid state materials through high resolution NMR and relaxation time measurements.

The resonance frequencies of slightly different environments are different [20-22]. However the presence of broadening may prevent their observation. In liquids well resolved NMR spectral detail can be obtained because of the random motion of the atoms, ions and molecules which averages the various broadening interactions and provides narrow resonances. In the case of solids such phenomena do not often occur and very broad lines are obtained. Solid samples may be obtained either as single crystals or as powders. The former is not always available and is not appropriate to glasses.

In the early days of NMR, measurement of relaxation times as a function of temperature was of primary interest in polycrystalline samples. However, static (wide line) NMR has also been applied to obtain structural information in borate glasses [23-29], alkali borate glasses [30-34], borophosphate

glasses [36] and boroaluminate glasses [36] etc. Much of the attention has been given to the relative ratio of the different species present in the sample in order to interpret the structure. The profile of the wide line NMR resonance merges peaks together very often and therefore creates a problem to identify the species. But with the advent of magic angle spinning (MAS) NMR in 1958 [37-39] high resolution NMR of powders became possible. Application of MAS narrows the lineshape, i.e. lengthens the time domain NMR signal. An example for the ^{23}Na nucleus in sodium disilicate crystal is shown in Figure (1.5).

Following Lippmaa et al's. [40] first NMR investigation of crystalline silicates, several studies of alkali silicate glasses and crystals have been carried out. However the results are controversial to some extent. Schramm et al. [11] studied the lithium silicate system in which they obtained a statistical distribution of Q_m species. Grimmer et al. [15] investigated similar compositions and found not more than two species present. Similar results were found by them for sodium silicate glasses as well. Almost at the same time Dupree et al. [12] presented an experimental verification of Q_m species in alkali silicate glasses with their calculated values obtained from alkali concentration. The presence of only two species in a particular alkali silicate composition was also confirmed by Murdoch et al. [41] and Schneider et al. [42]. There could be a low concentration of Q_4 species, along with Q_3 and Q_2 units, in high alkali (34-41 mol%) [43] containing sodium silicate glasses which can be merged in the wings of the MAS NMR spectrum. The K_2O-SiO_2 system has been investigated by Grimmer et al. [44] and is consistent with

sodium silicate results of Dupree et al. [12], i.e. only 2 Q species detected. The Rb_2O-SiO_2 and Cs_2O-SiO_2 glasses of a wide range of composition have been investigated by Dupree et al. [45]. The structural arrangement of the network former, Si^{4+} is the same as Na_2O-SiO_2 system for <45 mol% Rb or Cs. However for >45 mol% Rb or Cs as many as three species, namely Q_3, Q_2 and Q_1 may be present in the glasses. This deviation is explained by the authors as a fact of coulombic interaction between the alkali metal ions and bridging oxygens. This has an implication on glass properties [46, 47] and that might affect the structure of other alkali containing glasses as well.

Dupree et al. [48] also investigated the PbO - SiO_2 glasses with 25-70 mol% PbO. The structural arrangement is different from the alkali silicate system. The results suggested that statistical distribution of Q_m species dominates for >30 mol% but that binary distribution [12] is valid for <30 mol% PbO. Recently Dupree and Holland [49] and Dupree and Smith [50] have presented two reviews encompassing most of the glass systems studied using NMR and MAS NMR.

In the case of ternary and quarternary glasses [41,51-54] the resolution of the ^{29}Si spectra is worse than the binary glasses. In glass system of the type CaO-SiO_2-Al_2O_3 alumina may be present either as Si-O-Al or neutral species [51]. This would help to form a particular Q_m^n species with Al neighbours, where n= number of Si-O-Al. The occupancy of one Al shifts the ^{29}Si position by ~5.5 PPM [55] and gives broad ^{29}Si lines. Study of the system $CaMgSi_2O_6$-$CaAl_2SiO_6$ [41,52] showed that glass may contain all the Q_m species within a single broad ^{29}Si spectrum. This sort of

identification must be somewhat speculative and one has to depend upon other techniques as well.

The Q_3 and Q_2 ^{29}Si spectra of glasses show spinning sidebands. No such sideband is observed for Q_4 species because of its near spherically symmetric chemical shift anisotropy [12]. Spinning sidebands provide a means of calculating the chemical shift anisotropy [56-58] which gives some idea of the electronic shielding around the investigated nuclei. High resolution NMR in silicate glasses is not limited to ^{29}Si and a range of nuclei has been investigated to elucidate the glass structure and will be discussed briefly in section (1.7).

1.6 REVIEW OF THE INTERACTION OF SOME PENTAVALENT ATOMS WITH ALKALI AND ALKALI SILICATES

Among the several pentavalent atoms phosphorus, as P_2O_5, forms glass on its own and vanadium, as V_2O_5, forms glass in combination with a second oxide [1,2]. The melt of V_2O_5 crystallises readily at room temperature and therefore glass formation is difficult. P_2O_5 forms glasses in combination with one or more glass forming oxides. Although most of the commercial glasses are silicate and borosilicate composition, this thesis is partly concerned with the interaction of P_2O_5 with alkalisilicate glasses. In this section a general review is presented for the interaction of P_2O_5 with alkali and alkali silicate glasses.

There are three crystalline forms of P_2O_5 known to exist [59]. The PO_4 tetrahedron is the basis of all three P_2O_5 structures and all the melts form glasses between 415-585^oC [59]. The reaction mechanism of P_2O_5 with different types of

alkali metal oxides are different [60-62]. Binary phosphate glasses with different levels of modifier oxides have been prepared by Elyard et al. [63] and Imaoka et al. [64]. The glasses were not phase separated and this was explained by the relatively strong P-O bond compared to Si-O and B-O bond [65]. However Vogel [66] has observed glass-in-glass phase separation in $MgO-P_2O_5$ glasses. The phase separated droplets were so small that scattered light from them was not detectable by the naked eye. Sodium metaphosphate glass may phase separate in presence of a nucleating agent like platinum [67].

The structures of binary phosphate glasses have been investigated by several techniques [68-74]. All these studies unequivocally confirmed that phosphorus occurs as PO_4 tetrahedra. A paper chromatographic study [74] of sodium metaphosphate glass showed that the PO_4 tetrahedra remain as long chains similar to binary alkali silicates. Similar results have been obtained in $Li_2O-P_2O_5$ and $K_2O-P_2O_5$ systems.

Incorporation of SiO_2 in $R_2O-P_2O_5$ (R=Li,Na,K) creates a ternary $R_2O-SiO_2-P_2O_5$ system. Both the silicon and phosphorus are known to be network formers and R_2O is a modifier oxide. Glasses with more than one network former have a tendency to phase separate easily [1]. Among the different oxides only the $Na_2O-SiO_2-P_2O_5$ phase diagram is partially available in the literature [61]. Although phase diagram gives an indication of stable crystalline phases, this cannot be considered as providing evidence for the distribution of the species in a glass melt [1,2].

The kinetics of nucleation and morphology of crystallisation in $Li_2O-SiO_2-P_2O_5$ have been investigated by

several authors [75-77] using high resolution microscopy. P_2O_5 acts as a nucleating agent in the system and hence accelerates nucleation, crystallisation etc. Differential thermal analysis (DTA) has also been used to elucidate the crystallisation kinetics of the glasses. The phase diagrams [61] of the Na_2O-SiO_2-P_2O_5 have shown the existence of phosphate groups, silicophosphates, sodium silicates and SiO_2 in the crystalline state. Raman and infrared spectroscopy [78-80] has been applied to interpret the sodium phosphosilicate glass structure. However the presence of multiple peaks makes it difficult to interpret the spectra. A detailed study of crystallisation kinetics in Na_2O-SiO_2-P_2O_5 glasses has yet to be made.

P_2O_5 is generally used as a nucleating agent in industry to produce fine grained micro-structural glass ceramics [1]. However P_2O_5 cannot be considered as a universal nucleating agent [81]. P_2O_5 mainly works in Li_2O-SiO_2 glasses but not in other alkali silicates as it does in lithium silicates. This striking anomaly creates a need for further investigation.

1.7 MULTINUCLEAR STUDIES

Modern high field, broad band NMR spectrometers can detect signals from a wide range of nuclei. Most of the elements in the periodic table are now accessible to NMR study. Nuclei of NMR active isotopes can be divided into two groups :

i) spin, $I=\frac{1}{2}$ or dipolar isotopes and

ii) $I \geqslant 1$ or quadrupolar isotopes.

Quadrupolar nuclei can again be classified as (i) integral spin and (ii) half integral spin. The charge distribution for

a quadrupolar nucleus is non spherical and gives rise to an electric quadrupole moment. The quadrupolar interaction is considered as a perturbation to the Zeeman levels and lifts the degeneracy of (2I+1) states.

For high resolution NMR studies each group of nuclei has certain advantages and disadvantages over the others. In the case of solids the spin-lattice relaxation time, i.e. time taken by the spins to relax back from the excited state to thermal equilibrium with the lattice, for $I=\frac{1}{2}$ nuclei is typically 10^3 - 10^7 times greater than that of $I\geqslant 1$ nuclei. Therefore the time taken to investigate $I=\frac{1}{2}$ nuclei is much longer than for quadrupolar nuclei. Moreover the NMR signal from $I=\frac{1}{2}$ nuclei is broadened only by the chemical shift (see Section 2.2.1) and by the dipolar interaction both of which can be removed by magic angle spinning [37-39]. Thus intense narrow lines can be obtained from $I=\frac{1}{2}$ isotopes. On the other hand the quadrupolar interaction, for $I\geqslant 1$ nuclei, can only be partially removed (see section 2.4.3) by spinning the sample and relatively broad lines are often obtained.

The principal use of multinuclear study is the identification of phases and the particular environment of the nuclei. A phase may contain different types of nuclei. Therefore an understanding of the local order of all the nuclei is essential to interpret the structure. However there is a difficulty in this respect. For example, $Li_2Si_2O_5$ consists of three kinds of nuclei. Among these nuclei naturally abundant lithium and silicon have magnetic moments but oxygen-16 has not. Thus the local order of oxygen can only be understood if the sample is enriched with expensive oxygen-17.

As the NMR signal is proportional to the number of nuclei present in the sample [82], the NMR signal from different nuclei can be used to quantify various components. Quantification can be made from this signal directly for $I=\frac{1}{2}$ nuclei provided that the standard and the sample of interest run under the same conditions and no saturation occurs due to relaxation delay. But for $I>1$ nuclei several factors must be taken into account. One of the most important factors is the electric field gradient (efg) at the site of the nucleus which varies with symmetry of the electron distribution around the nucleus. Signals from a nucleus with large efg. may be relatively small and quantification will be inaccurate.

Quadrupolar lineshape studies of integral spin nuclei are different from the $I=\frac{1}{2}$ nuclei because the shape is governed by strong first order quadrupolar interaction. For the half integral spin the shapes of $+\frac{1}{2} \longleftrightarrow -\frac{1}{2}$ and $\pm\frac{3}{2} \leftrightarrow \pm\frac{1}{2}$ transitions may provide some useful information about efg., symmetry of the electron distribution etc.

In multi-nuclear studies the relative sensitivity of the investigated nuclei are of common interest. For a nucleus, x, the receptivity is defined as [82]

$$R_x = |\gamma^3_x \, a_x \, I_x \, (I_x + 1)| \quad \ldots \quad \ldots \quad (1.4)$$

where γ = gyromagnetic ratio
a = natural abundance
I = nuclear spin

For $I=\frac{1}{2}$ nuclei R_x can be obtained readily from equ. (1.4) but for quadrupolar nuclei certain precautions are necessary. The line width of quadrupolar nuclei is dependent upon the static field applied to the sample, nuclear spin and quadrupole

moment. Therefore line width is one of the important factors to be taken into account for the calculation of receptivity. The relative sensitivity of the isotopes studied in this thesis along with their line width factor (for quadrupolar nuclei only) and operating frequency at 8.45 T are presented in Appendix A.

Among the nuclei in the periodic table ^{29}Si, ^{31}P, ^{27}Al are of major interest because of their sensitivity to local order and relative ease of obtaining an NMR signal. ^{29}Si is the most studied isotope in minerals, glasses and zeolites [48-54, 83-86]. High resolution spectra obtained from MAS NMR can be used to identify the co-ordination number and the local order of the ^{29}Si. ^{29}Si NMR can also provide an estimate of Si-O-Si/Al bond angle, Si-O bond distance and polymeric state etc. The degree of crystallisation can also be determined from the relatively narrow line of the ^{29}Si NMR. Figure (1.6) shows the ^{29}Si spectra of lithium silicate glass and that heat treated at $525^{o}C/6h$. The peak at -91 PPM for the latter is comparatively narrow and this shows the presence of lithium disilicate crystal in the material.

Phosphorus is one of the major constituents of inorganic solids, e.g. teeth, bone, synthetic and natural silicate glasses etc. [87]. Addition of small amounts of phosphorus to optical fibres improves the overall properties [88]. Phosphorus may also play an important role on crystallisation and thermodynamic behaviour of natural silicate glasses [89]. The wide chemical shift range of ^{31}P, 711 PPM [90], allows identification of the phosphate species in the material. The ^{31}P chemical shift mainly depends upon the oxidation state, structural configuration, electronegative substituents etc.

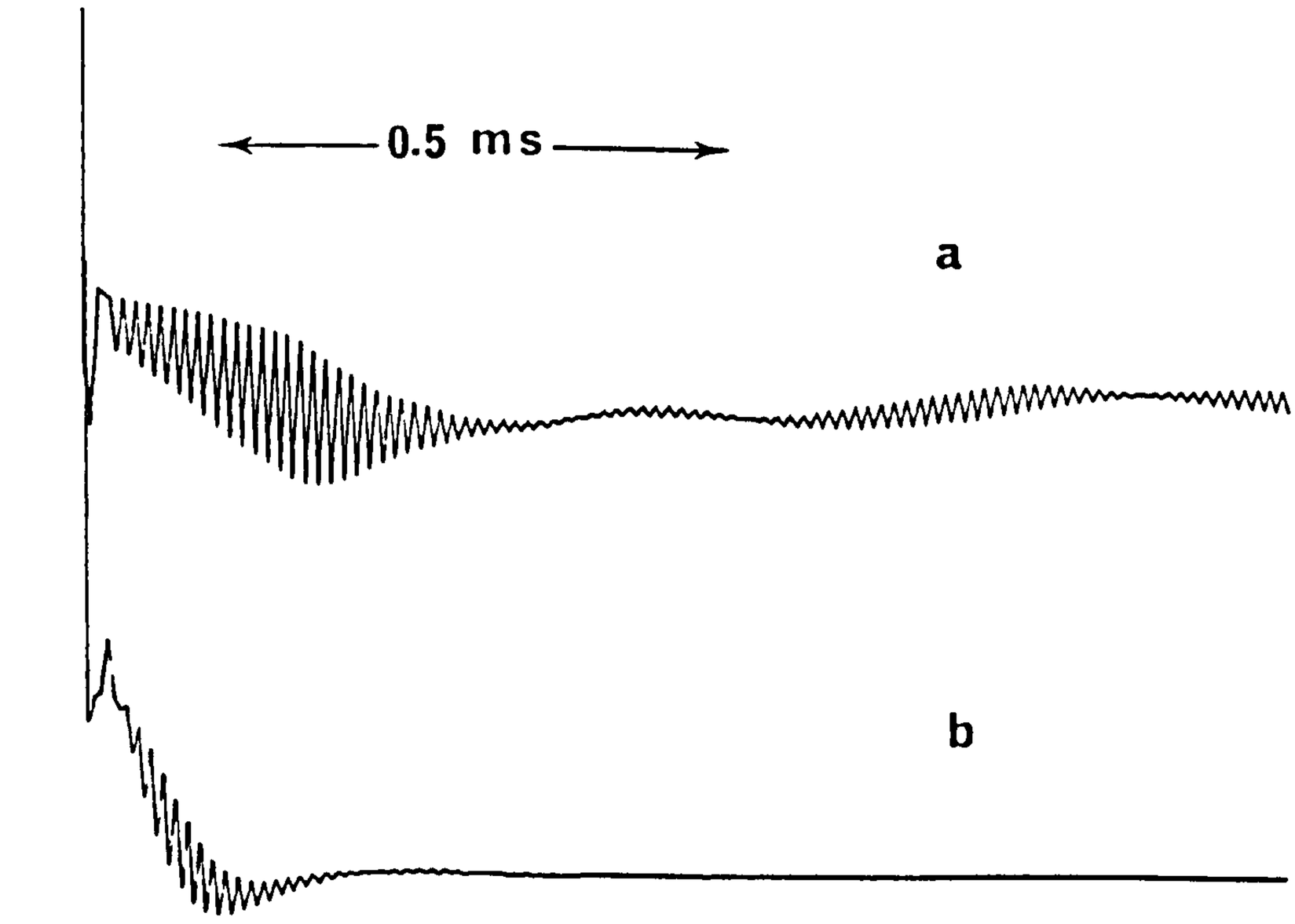

Figure 1.5 Line narrowing of Na nucleus in sodium disilicate crystalline material due to magic angle spinning. (a) Spinning (b) static.

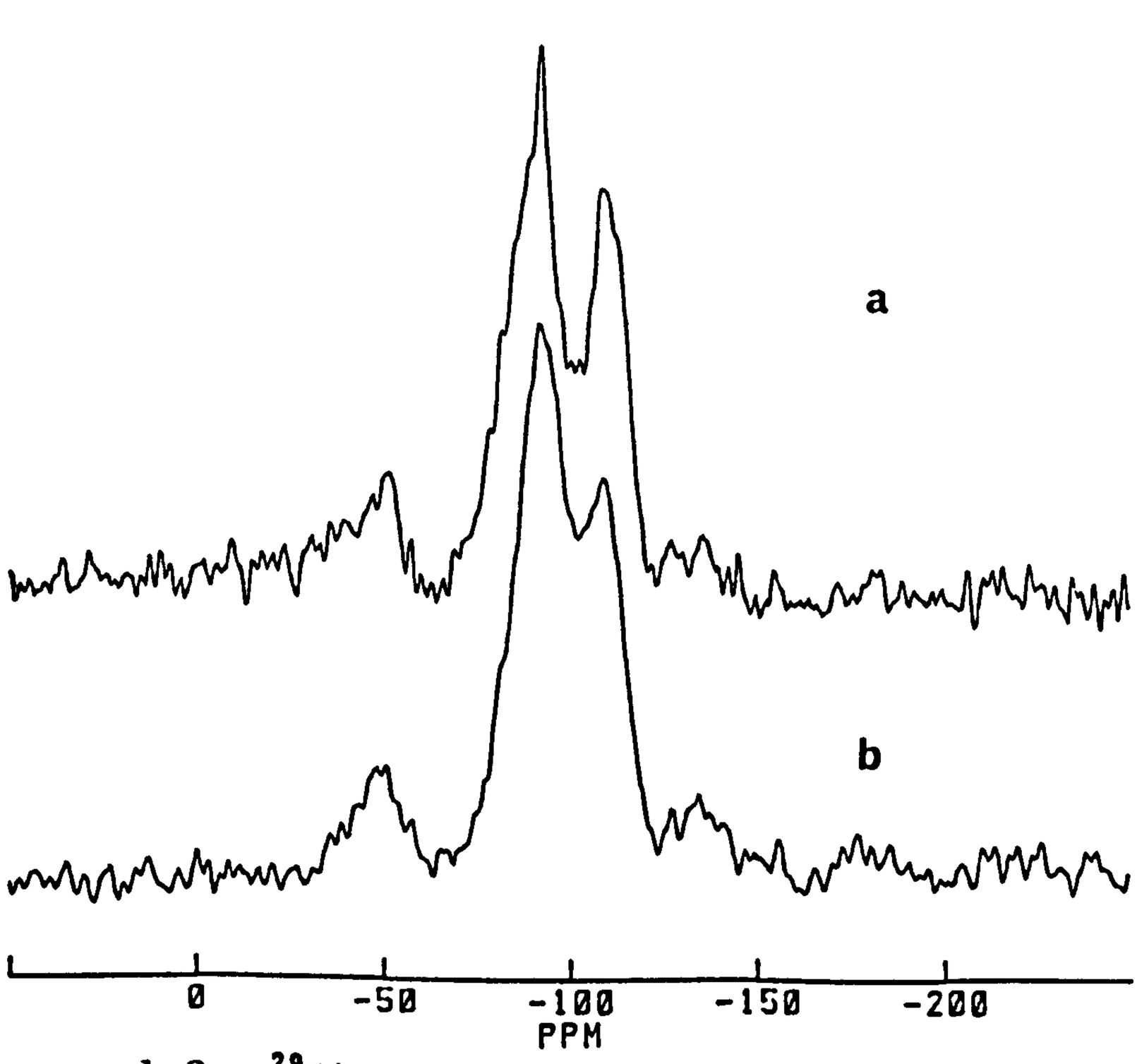

Figure 1.6 ^{29}Si resonance of $24.6Li_2O.75.3SiO_2$.(a) Heat treated at 525 C/6h and (b) glass showing the line narrowing due to the presence of crystalline $Li_2Si_2O_5$.

Therefore from the chemical shift most of the structural parameters, e.g. nearest neighbour, next nearest neighbour, state of polymerisation etc. can be determined. However long chain and ring phosphate species have a large (~ 4.0 kHz) dipolar interaction. Therefore in a MAS NMR experiment the isotropic lineshape is flanked on both sides by spinning sidebands which can only be resolved if the spinning rate is >4 kHz. Thus a high speed spinning probe is essential to identify the chain or ring phosphates. Identification of species in glasses requires comparison with a crystal of known structure. But the ^{31}P chemical shift in glasses does not always correspond exactly to that of the crystalline environment [11,91] and therefore multi-nuclear approach e.g., ^{29}Si resonance in SiP_2O_7 like environments, could help to resolve the problem.

The most common use of ^{27}Al is the identification of Al(4), Al(5) and Al(6) co-ordination in crystalline and glassy materials [92-94] as there is a distinct range of chemical shifts for each of the Al co-ordinations. However care in interpreting aluminium spectra is essential because both the peak position and line width can vary with magnetic field due to quadrupolar effects. Quantitative ^{27}Al is very effective if a suitable standard material is used.

Apart from ^{29}Si, ^{31}P and ^{27}Al other nuclei, e.g. ^{1}H [95,96], ^{23}Na [12], ^{25}Mg [97], ^{11}B [98], ^{85}Rb [12], ^{89}Y [99], ^{133}Cs [12] etc. are also of interest in identifying phases of glasses and minerals etc. Either NMR or MAS NMR of these nuclei provide lines characteristic of the local order of them and so the respective environments can be identified.

1.8 AIM OF THE THESIS

High resolution microscopy is not very effective in identification of species in glasses because of the low contrast. The use of spectroscopic techniques, e.g. infrared, Raman have provided some interesting but not conclusive results [100-102]. Some other techniques, e.g. molecular dynamics method [103], predicts four and five coordinated silicon whereas neutron diffraction [104] predicts four coordinated silicon in alkali silicate glasses. Therefore, results presented to date are contradictory.

Although NMR spectroscopy has been successfully applied to investigate glass structures; the results, even in simple binary alkali silicate system, are interpreted within various models which results in contradictory conclusions. It is well known that, in the crystalline state, silicon exists in octahedral co-ordination [105]. However in glasses the existence of Si(6) has not been observed. In order to resolve these problems an attempt is made

i) to determine the relative amounts of Q_m species present in Li_2O-SiO_2 glasses,

ii) to investigate new co-ordination states of the network formers,

iii) to describe the effect of phosphate addition, and

iv) to determine the early phase separation in binary alkali silicate glasses.

REFERENCES

1. P.W. McMillan, Glass Ceramics, Academic Press, London, 1979.

2. H. Rawson, Inorganic Glass-Forming systems, Academic Press, 1967.

3. H. Rawson, Properties and Application of glass, Elsevier, 1980.

4. G.O. Jones, Glass, Methuen, London, 1956.

5. V.M. Goldschmidt, Geochemische Verteilungspesetze der Elemente, viii, Vid. Akad., 1926.

6. W.H. Zachariasen, J. Am. Ceram. Soc., 54, 3841 (1932).

7. R. Becker, Ann. Phys., 32, 128 (1938).

8. S.D. Stoky, Glasstech. Ber. V International glass congress, 32k, Heft V (1959).

9. R.J. Bell and P. Dean, Nature, London, 212, 1354 (1966).

10. G. Engelhardt, D. Zeigan, H. Jancke, D. Hoebbel and W. Weiker, Z. anorg. allg. Chem., 418, 17 (1975).

11. C.M. Schramm, B.W.H.S. de Jong and V.E. Parzialy, J. Am. Chem. Soc., 106, 4396 (1984).

12. R. Dupree, D. Holland, P.W. McMillan and R.F. Pettifer, J. Non-Cryst. Solids, 68, 399 (1984).

13. C.H.L. Goodman, International Symposium on Structure and Bonding in Non-Crystalline Solids, Reston, Virginia, 23rd-26th May, 1983.

14. E.M. Levin, C.R. Robins, H.F. McMurdie, Phase diagrams for ceramists, Am. Ceram. Soc. (1964), P.601.

15. A.R. Grimmer, M. Magi, M. Hahnert, H. Stade, A. Samoson, W. Weiker and E. Lippmaa, Phys. Chem. Glasses, 25 (4), 105 (1984).

16. J.E. Stanworth, Physical properties of glass, Clarendon Press, 1950.

17. C.J. Gorter and L.J.F. Broer, Physica, 9, 591 (1942).

18. E.M. Purcell, H.C. Torrey and R.V. Pound, Phys. Rev., 69, 37 (1946).

19. F. Bloch, W.W. Hanseu and M. Packard, Phys. Rev., 69, 127 (1946).

20. W.D. Knight, Phys. Rev., 76, 1259 (1949).

21. W.G. Proctor and F.C. Yu, Phys. Rev., 77, 719 (1950).

22. W.C. Dickinson, Phys. Rev., 77, 736 (1950).

23. A.H. Silver and P.J. Bray, J. Chem. Phys., 29, 984 (1958).

24. D. Kline, P.J. Bray and H.M. Kriz, J. Chem. Phys., 48, 5277 (1968).

25. J. Krogh-Moe, J. Non-Cryst. Solids, 1, 269 (1969).

26. H.M. Kriz and P.J. Bray, J. Non-Cryst. Solids, 6, 27 (1971).

27. G.E. Jellison Jr., L.W. Panek, P.J. Bray and G.B. Rouse Jr., J. Chem. Phys., 66, 802 (1977).

28. G.E. Peterson, A. Carnavale and C.R. Kurkjian, Phys. Phys. Chem. Glasses, 18, 41 (1971).

29. G.E. Jellison Jr., and P.J. Bray, Solid State Commun., 19, 517 (1976).

30. P.J. Bray and J.G. O'Keefe, Phys. Chem. Glasses, 4, 37 (1963).

31. S.E. Savanson, E. Forslind and J. Krogh-Moe, J. Phys. Chem., 66, 174 (1962).

32. S. Greeblatt and P.J. Bray, Phys. Chem. Glasses, 8, 213 (1967).

33. Y.H. Yun and P.J. Bray, J. Non-Cryst. Solids, 44, 227 (1981).

34. W. Muller-Warmuth, W. Poch and G. Sielatf, Glasstechn. Ber. 43, 5 (1970).

35. Y.H. Yun, S.A. Feller and P.J. Bray, J. Non-Cryst. Solids, 33, 273 (1979).

36. Y.H. Yun and P.J. Bray, J. Non-Cryst. Solids, 30, 45 (1978).

37. E.R. Andrew, A. Bradbury and R.G. Eades, Arch. Sci. (Geneva), 11, Fasc. Spec., 223 (1958).

38. E.R. Andrew, A. Bradbury and R.G. Eades, Nature, Lond., 182, 1659 (1958).

39. I.J. Lowe, Phys. Rev. lett., 2(7), 285 (1959).

40. E. Lippmaa, M. Magi, A. Samoson, G. Engelhardt and A.R. Grimmer, J. Chem. Soc., 102, 4889 (1980).

41. J.B. Murdoch, J.F. Stebbins and I.S.E. Carmichael, Am. Mner., 70, 332 (1985).

42. E. Schneider, J.F. Stebbins and A. Pines, J. Non-Cryst. Solids, 89, 371 (1987).

43. J.F. Stebbins, Nature, 330, 465 (1987).

44. A.R. Grimmer and W. Muller, Monatsch Chem., 117 (6-7), 799 (1986).

45. R. Dupree, D. Holland and D.S. Williams, J. Non-Cryst. Solids, 81, 185 (1986).

46. R.J. Charles, J. Am. Ceram. Soc., 50 (12), 631 (1967).

47. R.E. Tickle, Phys. Chem. Glasses, 8, 101 (1967).

48. R. Dupree, N. Ford and D. Holland, Phys. Chem. Glasses, 28, 78 (1987).

49. R. Dupree, D. Holland, in New Horizons in Glass and Glass Ceramics, Ed. M.H. Lewis, Chapman and Hall (1988).

50. R. Dupree, M.E. Smith, Reports in Progress in Physics (to be published).

51. G. Engelhardt, M. Nofz, K. Forkel, F.G. Wihsmann, M. Magi,. A. Samoson and E. Lippmaa, Phys. Chem. Glasses, 26(5), 157 (1985).

52. R.J. Kirkpatrick, R. Oestrike, C.A. Weiss, Jr., K.A. Smith, E. Oldfield, Am. Miner., 71, 705 (1986).

53. R.A. Kinsey, R.J. Kirkpatrick, J. Hower, K.A. Smith and E. Oldfield, Am. Miner., 70, 537 (1985).

54. G.L. Turner, R.J. Kirkpatrick, S.J. Risbud and E. Oldfield, Am. Ceram. Soc. Bull., 66 (4), 656 (1987).

55. G. Engelhardt and D. Michel, High Resolution Solid State NMR of Silicates and Zeolites, John Wiley, P.115 (1987).

56. M. M. Maricq and J.S. Waugh, J. Chem. Phys., 70 (7), 3300 (1979).

57. J. Herzfield and A.E. Berger, J. Chem. Phys., 73(12), 6021 (1980).

58. N.J. Clayden, C.M. Dobson, Lu-Yun Lian and D.J. Smith J. Magn. Reson., 69, 476 (1986).

59. W.L. Hill, G.T. Faust and S.B. Hendricks, J. Am. Chem. Soc., 65, 794 (1943).

60. G.W. Morey and E. Ingerson, Am. J. Sci., 242 (1), 4 (1944).

61. E.T. Turkdogan and W.R. Maddocks, J. Iron and Steel Inst., 172, 1 (1952).

62. G.W. Morey, J. Am. Chem. Soc., 76 (18), 4726 (1954).

63. C.A. Elyard, P.L. Baynton and H. Rowson, Glastech. Ber. 32K, V, 35 (1959).

64. M. Imaoka, in "Advances in Glass Technology, Part 1", Plenum press, New York, P.149 (1962).

65. A. Dietzel, Naturwissenschafteu, 29, 537 (1941).

66. W. Vogel, Silikattechnik, 10, 241 (1959).

67. G.E. Rindone and R.J. Ryder, Glass Ind., 38, 29-31, 51 (1957).

68. J. Biscoe, A.G. Pincus, C.S. Smith and B.E. Warren, J. Am. Ceram. Soc., 24, 116 (1941).

69. G.W. Brady, J. Chem. Phys., 28, 48 (1958).

70. M. Goldstein and T.H. Davis, J. Am. Ceram. Soc., 38, 223 (1955).

71. M.E. Milberg and M.C. Dally, J. Chem. Phys., 39, 2966 (1963).

72. B.C. Bunker, D.R. Tallant, C.A. Bafle, R.J. Kirkpatrick, G.L.Turner and M.R. Reidmeyer, J. Am. Ceram. Soc., 70(9), 675 (1987).

73. S. Prabhakar, K.J. Rao, and C.N.R. Rao, Chem. Phys. Lett., 139(1), 96 (1987).

74. A.E.R. Westman and P.A. Gartaganis, J. Am. Ceram. Soc., 40, 293 (1957).

75. P.W. McMillan and G. Partridge, British Ceramic Society Proceedings, 3, 241 (1965).

76. P.F. James and P.W. McMillan, J. Mater. Sci., 6, 1345 (1971).

77. P.F. James and P.W. McMillan, Phys. Chem. Glasses 25 (2), 31 (1984).

78. C. Nelson and D.R. Tallant, Phys. Chem. Glasses, 26 (4), 119 (1985).

79. I.N. Chakraborty and R.A. Condrate, Snr., Phys. Chem. Glasses, 26 (3), 68 (1985).

80. C. Nelson and D.R. Tallant, Phys. Chem. Glasses, 25(2), 31 (1984).

81. P.W. McMillan and G. Partridge, British Ceramic Society Proceedings, 3, 241 (1965).

82. R.K. Harris, Nuclear magnetic resonance spectroscopy, Longman Scientific Technical, 1983.

83. R. Dupree, M.H. Lewis and M.E. Smith, J. Appl. Cryst., 21, 109 (1988).

84. R. Dupree, D. Holland and D.S. Williams, J. De Physique, Colloque, C8, Supplement au No 12, Tome 46, 1985.

85. K.A. Smith, R.J. Kirkpatrick, E. Oldgield and D.M. Henderson, Am. Mineral., 68, 1206 (1983).

86. E. Schneider, J.F. Stebbins and A. Pines, J. Non-cryst. Solids, 89, 371 (1987).

87. H.H. Roseberry, A.B. Hastings and J.K. Morse, J. Biol. Chem., 90, 395 (1931).

88. D.C. Douglass, T.M. Duncan, K.L. Walker and R. Csencsits, J. Appl. Phys., 58 (1), 197 (1985).

89. B.O. Mysen, F.J. Ryerson and D. Virgo, Am. Mineral, 66, 106 (1981).

90. B.E. Mann, The Common Nuclei in NMR and the Periodic Table, Eds. R.K. Harris and B.E. Mann, Academic Press, 101 (1978).

91. J.E. Dickenson Jr., B.W.H.S. de Jong and C.M. Schramm, J. Non-Cryst. Solids, 102, 196 (1988).

92. R. Dupree, I. Farnan, A.J.Forty, S. -El-Mashri and L. Bottyan, J. Phys. (paris), 46, C8-113 (1985).

93. D. Muller, G. Berger, I. Grunze, G. Ladwig, E. Hassas and U. Haubenreisser, Phys. Chem. Glasses, 24 (2), 37 (1983).

94. S.H. Risbud, R.J. Kirkpatrick, A.P. Taglialavore and B. Montez, Commun. Am. Ceram. Soc., C-10 (1987).

95. C.I. Ratcliffe, J.A. Ripmeester and J.S. Tse, Chem. Phys. Lett., 120 (4,5), 427 (1985).

96. J.P. Yesinowski, H. Eckert and G.R. Rossman, J. Am. Chem. Soc., 110, 1367 (1988).

97. S. Forsen and B. Lindman, Ann. Rep. NMR Spectrosc. 11A, 183 (1981).

98. P.J. Bray, D.E. Hintenlaug, R.V. Mulkern, S.G. Greenbaum, D.C. Tran and M. Drexhage, J. Non-cryst. Solids, 56 27 (1983).

99. R. Dupree, M.E. Smith, Chem. Phys. Lett., 148 (1), 41 (1988).

100. D.M. Sanders, W.B. Person and L.L. Hench, Appl. Spectroscopy, 28, 247 (1974).

101. D.W. Matson, S.K. Sharma and J.A. Philpotts, J. Non-Cryst. Solids, 58, 323 (1983).

102. R. Hanna and G.J. Su., J. Am. Ceram. Soc., 47, 597 (1964).

103. T. Soules, J. Chem. Phys., 71, 4570 (1979).

104. S.K. Mitra and R.W. Hockney, Phil. Mag., B48, 151(1983).

105. F. Liebau, Structural Chemistry of Silicates, Springer Verlag, P.31 (1985).

CHAPTER 2

THEORETICAL FRAMEWORK

2.1 NUCLEAR MAGNETIC RESONANCE (NMR)

The term magnetic resonance refers to the fact that at certain critical frequencies the material under study absorbs energy from an imposed radio frequency (rf) field which is in tune with a natural frequency of the magnetic system corresponding to the frequency of gyroscopic precession of the magnetic moment in an external static magnetic field B_0.

A nucleus may possess a total magnetic moment $\vec{\mu}$ and a total angular momentum $\vec{J}$ which are parallel and can be written as

$$\vec{\mu} = \gamma \vec{J} = \gamma \hbar I \quad \ldots \quad \ldots \quad \ldots \quad (2.1)$$

where γ is the gyromagnetic ratio and I is the nuclear spin number. In the presence of the field $\vec{B}_0$ an energy of interaction between the magnetic moment $\vec{\mu}$ and the field $\vec{B}_0$ can be expressed by a simple Hamiltonian

$$H = \vec{\mu} . \vec{B}_0 \quad \ldots \quad \ldots \quad \ldots \quad \ldots \quad (2.2)$$

Considering $\vec{B}_0$ along the Z direction, one can have from equs. (2.1) and (2.2)

$$H = - \gamma \hbar B_0 I_z \quad \ldots \quad \ldots \quad \ldots \quad (2.3)$$

Therefore the allowed energies are

$$E_m = \gamma \hbar B_0 m \quad \ldots \quad \ldots \quad \ldots \quad (2.4)$$

where m=I, I-1, ... , -I i.e., m can have (2I+1) values. The difference between two states is therefore

$$\Delta E = \hbar \omega_0 = - \gamma \hbar B_0 \quad \ldots \quad \ldots \quad \ldots \quad (2.5)$$

From equ. (2.5)

$$\vec{\omega}_0 = - \gamma \vec{B}_0 \qquad \ldots \qquad \ldots \qquad \ldots \quad (2.6)$$

in which $\vec{\omega}_0$ is the Larmor angular frequency. Equ. (2.6) describes the precession of a magnetic dipole moment $\vec{\mu}$ placed in a magnetic field $\vec{B}_0$ as shown in Figure (2.1.a). The negative sign means the motion is in the indicated direction. The precession of $\vec{\mu}$ in $\vec{B}_0$ will result in a torque and the equation of motion can be expressed in the laboratory frame as

$$\frac{d\vec{J}}{dt} = \vec{\mu} \times \vec{B}_0$$

$$\frac{d\vec{\mu}}{dt} = \gamma \vec{\mu} \times \vec{B}_0 \qquad \ldots \qquad \ldots \qquad \ldots \quad (2.7)$$

In the rotating frame the rate of change of $\vec{\mu}$ with angular velocity $\vec{\omega}$ is given by [1,2]

$$\frac{d\vec{\mu}}{dt} = \gamma \vec{\mu} \times (\vec{B}_0 + \vec{\omega}/\gamma) \qquad \ldots \qquad \ldots \quad (2.8)$$

Equ. (2.8) in conjunction with equ. (2.6), if $\vec{\omega} = \vec{\omega}_0$, gives

$$\frac{\delta\vec{\mu}}{\delta t} = 0 \qquad \ldots \qquad \ldots \qquad \ldots \quad (2.9)$$

i.e. in the rotating frame $\vec{\mu}$ is constant but in the laboratory frame it is rotating with angular velocity $\vec{\omega}_0$. If an additional oscillating magnetic field $\vec{B}_1$ applied at right angles to $\vec{B}_0$, in the plane containing $\vec{\mu}$ and $\vec{B}_0$, equ. (2.8) becomes

$$\frac{\delta\vec{\mu}}{\delta t} = \gamma \vec{\mu} \times (\vec{B}_0 + \vec{B}_1 + \vec{\omega}/\gamma) \qquad \ldots \qquad \ldots \quad (2.10)$$

The resonance occurs when the frequency $\vec{\omega}$ of the oscillating field $\vec{B_1}$ becomes equal to the Larmor frequency of precession, i.e. $\vec{\omega} = \vec{\omega_0}$ and equ. (2.10) becomes

$$\frac{\delta \vec{\mu}}{\delta t} = \gamma \vec{\mu} \times \vec{B_1} \quad \ldots \quad \ldots \quad \ldots (2.11)$$

Therefore on resonance the effective field in the rotating frame $B_{eff} = B_1$ and the magnetization rotates around the direction of $\vec{B_1}$ with angular velocity $\gamma \vec{B_1}$ in the laboratory frame. If $\omega \neq \omega_0$, equ. (2.10) takes the form

$$\frac{\delta \vec{\mu}}{\delta t} = \gamma \vec{\mu} \times \frac{\vec{\omega} - \vec{\omega_0}}{\gamma} + \vec{B_1} \quad \ldots \quad \ldots (2.12)$$

So, for off - resonance, $\vec{B_{eff}}$ is the resultant of $\vec{B_1}$ and $(\vec{\omega} - \vec{\omega_0})/\gamma$ as shown in Figure (2.1.b). Therefore the field $\vec{B_1}$ required to flip the polarisation vector $\vec{M}$ for off-resonance is less than the on-resonance case.

Theoretical details of NMR can be found in Farar and Becker [1], Slichter [2], Abragam [3], Harris [4], Derome [5] etc.

2.2 NUCLEAR SPIN INTERACTIONS

Nuclear spins interact with the lattice and with each other. The magnitude of these interactions depends on the magnitude, orientation and relative positions of the nuclei magnetic moments. Mehring [6] and Haeberlin [7] suggested seven different type of spin interactions in solids. Out of these interactions the principle nuclear interactions are

i) Zeeman interaction
ii) Chemical shift interaction
iii) Dipole-dipole interaction and
iv) Nuclear electric quadrupole interaction.

The shape of the NMR spectra of powder samples for half spin ($I=\frac{1}{2}$) nuclei depends upon the chemical shift, and the indirect and direct dipole-dipole interactions. The quadrupolar interaction is often dominant for nuclei of spin, $I>\frac{1}{2}$. A brief account of the Zeeman interaction has already been discussed in Section 2.2 and the rest will now be discussed in brief.

2.2.1 CHEMICAL SHIFT INTERACTION

The origin of the chemical shift is the screening produced by the electrons surrounding the nucleus. The resonance frequency of a nucleus depends on the state of its chemical environment [8-11] and the first separate resonance lines are observed for chemically different environment protons in the same molecule in 1951 [12]. For $I=\frac{1}{2}$ nuclei the different resonance positions corresponding to nuclei of different environments are called chemical shifts. In metal this shift is generally more positive than in insulators and is known as the Knight shift after the name of the discoverer [8]. The chemical shifts can provide structural information.

The Larmor precession of the electronic charges and polarisation of the electronic shells due to applied magnetic field $\vec{B}_0$ cause a change of local field at the site of nuclei. Thus at the nucleus the magnetic field is [3]

$$\vec{B} = \vec{B}_0 (1 - \sigma) \quad \ldots \quad \ldots \quad \ldots \quad (2.13)$$

where σ is a rank 2 tensor and is a measure of the chemical shift. The magnitude of shielding depends upon the response of the electrons charges surrounding the nucleus relative to the applied field $\vec{B}_0$. Therefore the chemical shift is related

to electron density (ED), bond angle (BA), bond length (BL), bond strength (BS), nearest neighbour (NN) and next nearest neighbour (NNN) etc., i.e.

$$\sigma' = f\,(ED, BA, BL, BS, NN, NNN) \quad \ldots \quad \ldots \quad (2.14)$$

The Hamiltonian describing the interaction can be written as

$$H_c = \hbar \sum_i \gamma_i \, I_i \cdot \sigma_i \cdot B \quad \ldots \quad \ldots \quad \ldots \quad (2.15)$$

The term $\sigma_i.B$ is the magnetic field induced by the electrons at the site of the ith nucleus. From equ. (2.13), one can write

$$\omega = \gamma B = \gamma B_0 (1 - \sigma) \quad \ldots \quad \ldots \quad \ldots \quad (2.16)$$

where ω is the resonance frequency.

The shielding factor σ for a nucleus of interest is measured relative to a reference material. From equ. (2.16) one can write

$$\nu_S - \nu_R = (\gamma / 2\pi)(\sigma_R - \sigma_S) B_0 \quad \ldots \quad \ldots \quad (2.17)$$

The subscripts S and R refer to the sample of interest and reference respectively. The term $\sigma_R - \sigma_S$ is called the chemical shift, δ_i. The δ_i is defined in the dimensionless unit of parts per million (PPM) and can be written from equ. (2.17) as

$$\delta_i = \frac{\nu_S - \nu_R}{\nu_R} \times 10^6 \quad \text{PPM} \quad \ldots \quad \ldots \quad (2.18)$$

where ν_S and ν_R are the resonance frequency due to different amounts of field at the site of the sample of interest and reference respectively.

2.2.2 MAGNETIC DIPOLE-DIPOLE INTERACTION

The dipole-dipole interaction is the coupling between two spins of magnetic moment $\vec{\mu}_i$ and $\vec{\mu}_j$ separated by the internuclear vector $\vec{r}_{ij}$ describing their relative positions. This interaction could be direct between the spins, i,j and could be indirect. Detailed description of these interactions can be found in references [1-7].

The dipolar Hamiltonian H_D can be written in truncated form [3] as

$$H_D = \frac{\hbar^2}{2} \sum_{i<j} \frac{\gamma_i \gamma_j}{r_{ij}^3} \quad (3\cos^2 \theta_{ij} - 1)(\vec{I}_i.\vec{I}_j - 3I_{iz}I_{jz}) \quad (2.19)$$

where θ_{ij} is the angle between the Zeeman field $\vec{B}_0$ and $\vec{r}_{ij}$. From equ. 2.19 it is evident that H_D depends on the internuclar vector $\vec{r}_{ij}$, the angle θ_{ij}, and on the spin interactions.

During the Larmor precession around the field $\vec{B}_0$ the projections of the dipole of magnetic moment $\vec{\mu}_i$ generates a static component along the field $\vec{B}_0$ and a rotational component perpendicular to $\vec{B}_0$. The static component of $\vec{\mu}_i$ produces a static field at the site of $\vec{\mu}_j$ which is either parallel or antiparallel to $\vec{B}_0$ and this causes a spread in the Larmor frequences for a polycrystalline sample [6,7] and hence a broadening of the line shape. The rotating component of $\vec{\mu}_i$ produces a local magnetic field at the site of $\vec{\mu}_j$ and also broadens the lineshape. The broadening caused by dipolar interaction obscures the information in the NMR spectra of amorphous and polycrystalline materials.

2.2.3 NUCLEAR QUADRUPOLAR INTERACTION

The nuclear quadrupolar moment is a measure of the deviation of electric charge distribution from its spherical symmetry. Thus the interaction dominates in a nucleus of spin, $I > \frac{1}{2}$. The nuclear electric quadrupole moment interacts with the electric field gradient which is produced by the electric charges close to the nucleus. For high resolution NMR, the static magnetic field $\vec{B}_0$ is very large and the quadrupolar interaction energy is assumed to be small compared to the interaction between the nuclear magnetic moment and the external magnetic field $\vec{B}_0$. In the calculation of energy, the quadrupolar interaction is therefore considered as a perturbation on the Zeeman interaction [13]. The quadrupolar interaction produces a fine structure of resonance lines and can cause broadening or apparent loss of intensity of the resonance line.

The Hamiltonian of a nuclear spin with a quadrupole moment can be written as [3]

$$H = H_Z + H_Q \quad \ldots \quad \ldots \quad \ldots \quad (2.20)$$

where $H_Z = - \gamma \hbar B_0 I_Z$ ... ... (2.21)

is the Zeeman Hamiltonian and

$$H_Q = \frac{e^2qQ}{4I(2I-1)} \Big[\tfrac{1}{2} (3\cos^2\theta - 1) \{ 3I_Z^2 - I(I+1) \} + \frac{3}{2} \sin\theta \cos\theta \{ I_Z (I_+ + I_-) + (I_+ - I_-) I_Z \} + \frac{3}{4} \sin^2\theta (I_+^2 + I_-^2) \Big] \quad \ldots \quad \ldots \quad (2.22)$$

is the quadrupolar Hamiltonian. Here

eq = electric field gradient
eQ = quadrupole moment and
$I_{\pm} = I_x \pm iI_y$

represent the creation and destruction operator respectively. The diagonal ($\Delta m = 0$) and off-diagonal ($\Delta m = \pm 1, +2$) matrix elements in equ. (2.22) can be considered as perturbations. Using the standard perturbation theory the energy levels can be calculated as [3]

$$E_m = \sum_{k \geq 0} E_m^{(k)} \quad \ldots \quad \ldots \quad \ldots \quad (2.23)$$

where $E_m^{(0)} = - h \nu_L m \quad \ldots \quad \ldots \quad \ldots \quad (2.24)$

$$E_m^{(1)} = \tfrac{1}{4} h \quad \nu_Q (3 \mu^2 - 1) (m^2 - 1/3\ a) \quad \ldots \quad \ldots \quad (2.25)$$

$$E_m^{(2)} = -h \frac{\nu_Q}{12} \frac{}{\nu_L} m \left[\frac{3}{2} \quad \mu^2 \quad (1 - \mu^2) (8m^2 - 4a + 1) \right.$$

$$\left. + \quad \frac{3}{8} \quad (1 - \mu^2)^2 (-2m^2 + 2a - 1) \right] \quad \ldots \quad \ldots \quad (2.26)$$

etc. Here

$$\nu_L = \frac{\gamma B_0}{2\pi}$$

$$\nu_Q = \frac{3e^2 qQ}{2I(2I-1)\ h} \quad \ldots \quad \ldots \quad \ldots \quad (2.27)$$

$$\mu = \cos\theta$$

$$a = I(I+1)$$

The higher order energies can be found in ref. [14]. Equ. (2.24) represents the Zeeman interaction and equs. (2.25), (2.26) represent the first and second order energies due to quadrupole interaction respectivly. From the equs. (2.24 - 2.26) the zero, first and the second order perturbation energies for the different m values (m =-3/2, -½, ½, 3/2) due to spin, I = 3/2 can be written as

$$E^{(0)} = h\nu_L \left(\frac{3}{2}, \frac{1}{2}, \frac{1}{2}, \frac{3}{2} \right) \quad \ldots \quad \ldots \quad (2.28)$$

$$E^{(1)} = \tfrac{1}{4}\, h\, \nu_Q\, (3\cos^2\theta - 1)\, (1, -1, -1, 1) \quad \ldots \quad (2.29)$$

$$E^{(2)} = \frac{3}{16} \frac{h\nu_Q^2}{\nu_L} \left[\sin^2 2\theta\, (1,-1,1,-1) + \frac{\sin^4\theta}{2}\, (1,1,-1,-1) \right] \quad (2.30)$$

The numbers separated by commas within the brackets represent the splitting of the magnetic resonance lines corresponding to m = -3/2, $-\frac{1}{2}$, $\frac{1}{2}$, 3/2 values as shown in Figure (2.2). From equations (2.28 - 2.30) it is obvious that the line shape will be a combination of several resonance frequences

$$\nu_m = \sum_{k>0} \nu_m(k) \quad \ldots \quad \ldots \quad (2.31)$$

where $$\nu_m(0) = \frac{E_{m-1}^{(0)} - E_m^{(0)}}{h} = \nu_L \quad \ldots \quad \ldots \quad (2.32)$$

$$\nu_m(1) = \frac{E_{m-1}^{(1)} - E_m^{(1)}}{h}$$

$$= - \nu_Q \left(m - \frac{1}{2}\right) \frac{3\ \mu^2 - 1}{2} \quad \ldots \quad \ldots \quad (2.33)$$

$$\nu_m(2) = \frac{E_{m-1}^{(2)} - E_m^{(2)}}{h}$$

$$= \frac{\nu_Q^2}{12\ \nu_L} \left[\frac{3}{2}\ \mu^2\ (1-\mu^2)\ (8m^2 - 4a + 1) \right.$$

$$\left. + \frac{3}{8}\ (1-\mu^2)^2\ (-2m^2 + 2a - 1) \right] \quad \ldots \quad (2.34)$$

From equ. (2.33) $\nu_{\frac{1}{2}}^{(1)} = 0$ i.e. for $\frac{1}{2}$ integral spin the $-\frac{1}{2} \longleftrightarrow +\frac{1}{2}$ transition is unaffected by quadrupolar interaction. But other transitions, $m \longleftrightarrow (m-1)$ with $m \neq \frac{1}{2}$,

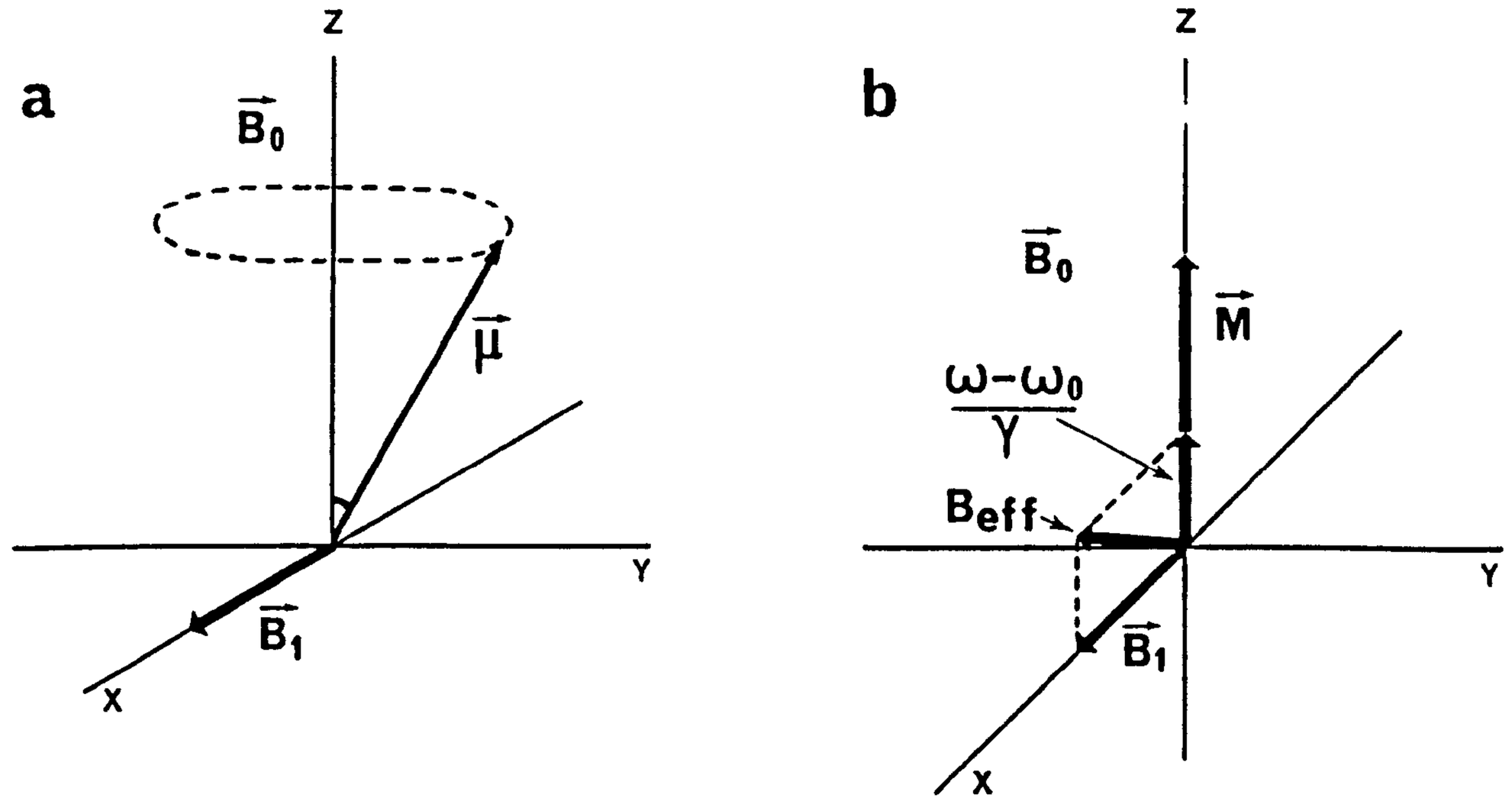

Figure 2.1 (a) Precession of a magnetic moment about a fixed magnetic field $\vec{B_0}$. (b) The effect of off-resonance pulse.

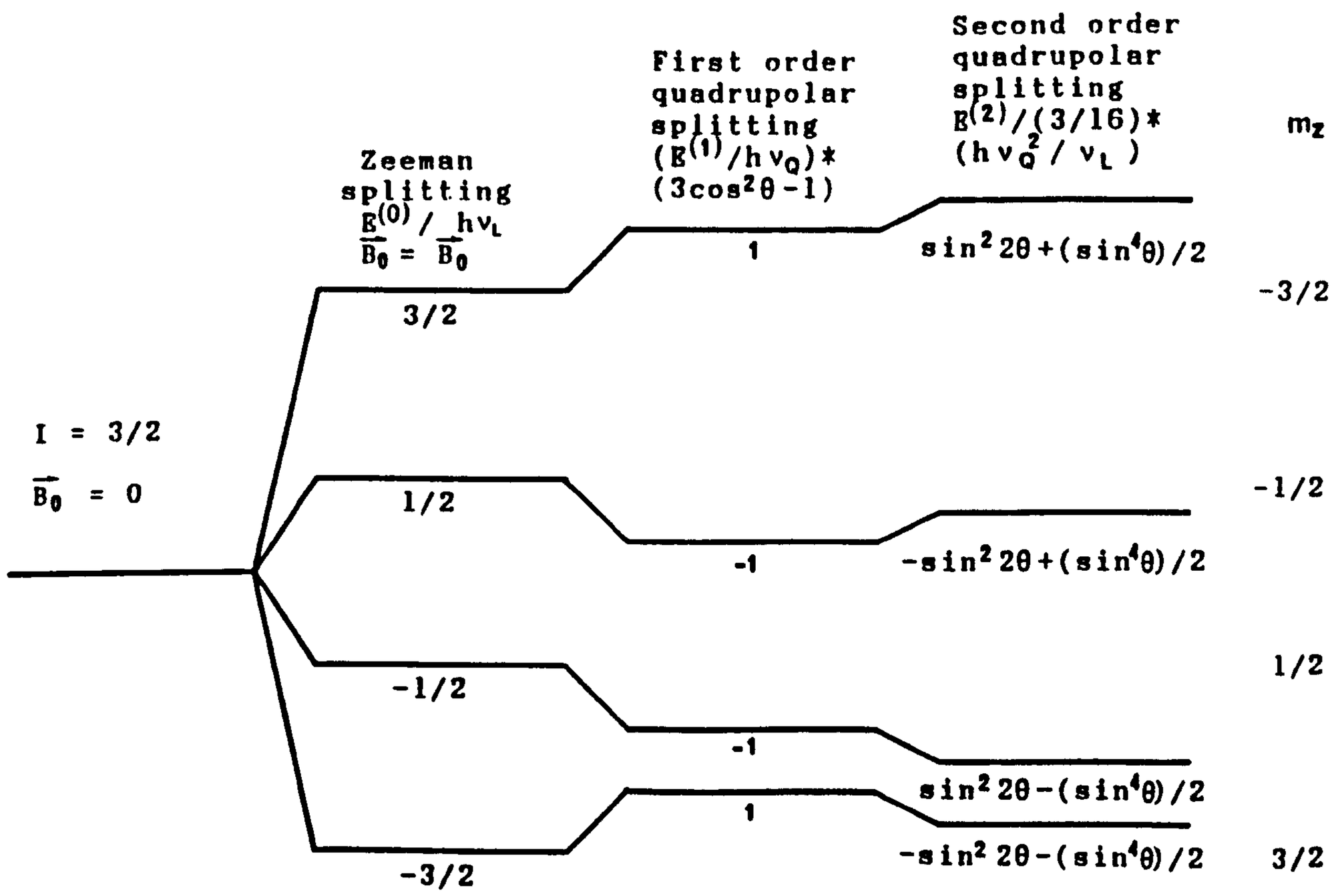

Figure 2.2 Splitting of energy levels of I = 3/2 due to Zeeman and quadrupolar interactions.

are shifted by $|(\nu_Q/2)(3\cos^2\theta - 1)|$ on the both sides of the $-\frac{1}{2} \longleftrightarrow +\frac{1}{2}$ transitions. Equ. (2.34) shows that

$$\Delta\nu^{(2)} = \nu_m^{(2)} - \nu_{-m}^{(2)} = 0 \quad \ldots \quad \ldots \quad (2.35)$$

and the first order frequency shift

$$\Delta\nu^{(1)} = \nu_m^{(1)} - \nu_{-m}^{(1)}$$
$$= \nu_Q (m-\tfrac{1}{2})(3\cos^2\theta - 1) \quad \ldots \quad \ldots \quad (2.36)$$

can be used to calculate the distance between the two satellite lines $(m-1) \longleftrightarrow m$ and $-m \longleftrightarrow -(m-1)$.

2.3 STATIC POWDER SPECTRUM LINE SHAPES IN SOLIDS

A powder consists of randomly oriented single crystals which gives rise to a powder spectrum which is a continuous distribution of frequencies. The calculation of this powder line shape considering anisotropic effects was first done by Bloembergen and Rowland [15,16]. They showed that for spin ½ nuclei the intensity of the NMR signal at a frequency ω with the convention $\omega_{33} > \omega_{22} > \omega_{11}$ is

$$I(\omega) = \frac{1}{\pi}[(\omega - \omega_{11})(\omega_{33} - \omega_{22})]^{-\frac{1}{2}} K(M) \quad \ldots (2.37)$$

where

$$K(M) = \int_0^{\pi/2} d\gamma \; (1 - M\sin^2\gamma)^{-\frac{1}{2}}$$

is the elliptic integral of the first kind in which

$$M = \frac{(\omega_{22} - \omega_{11})(\omega_{33} - \omega)}{(\omega_{33} - \omega_{22})(\omega - \omega_{11})} \quad \ldots \quad \ldots \quad (2.38)$$

For axially symmetric case $\omega_{11} = \omega_{22}$ and the equ. (2.37) can be expressed as

$$I(\omega) = \tfrac{1}{2}\,[(\omega - \omega_{11})(\omega_{33} - \omega_{22})]^{-\frac{1}{2}} \quad \ldots \quad (2.39)$$

The plots of equs. (2.37) and (2.39) with and without additional broadening are shown in Figure (2.3). The principal components of the chemical shift tensors (σ_{xx}, σ_{yy} and σ_{zz}) can be obtained directly from the discontinuities at ω_{11}, ω_{22} and ω_{33} in the diagram.

In a sample the internuclear distance between identical spins may be short and as a result the dipolar interaction becomes strong. Under these circumstances nuclear spins form groups of either two, three or four etc. spins. The NMR shape for such a case exhibits fine structure [17].

In the presence of an external magnetic field $\vec{B}_o$ the energy levels for the interaction between pairs of $I=\frac{1}{2}$ spins can be calculated [3]. The separation between the resonances with respect to the centre of gravity is given by

$$h = \pm \frac{3}{4} \frac{\gamma^2 \hbar}{r^3} (3\cos^2\theta - 1) \quad \ldots \quad \ldots \quad (2.40)$$

The total spectrum for the range $-2d<h<+2d$, where

$d = (3/4)\,\gamma^2 \hbar\, r^{-3}$ can be defined by [3]

$$f(h) = \left(-\frac{h}{d} + 1\right)^{-\frac{1}{2}} \quad ; (-2d<h<-d)$$

$$= \left(-\frac{h}{d} + 1\right)^{-\frac{1}{2}} + \left(\frac{h}{d} + 1\right)^{-\frac{1}{2}} \quad ; (-d<h<d) \quad (2.41)$$

$$= \left(\frac{h}{d} + 1\right)^{-\frac{1}{2}} \quad ; (d<h<2d)$$

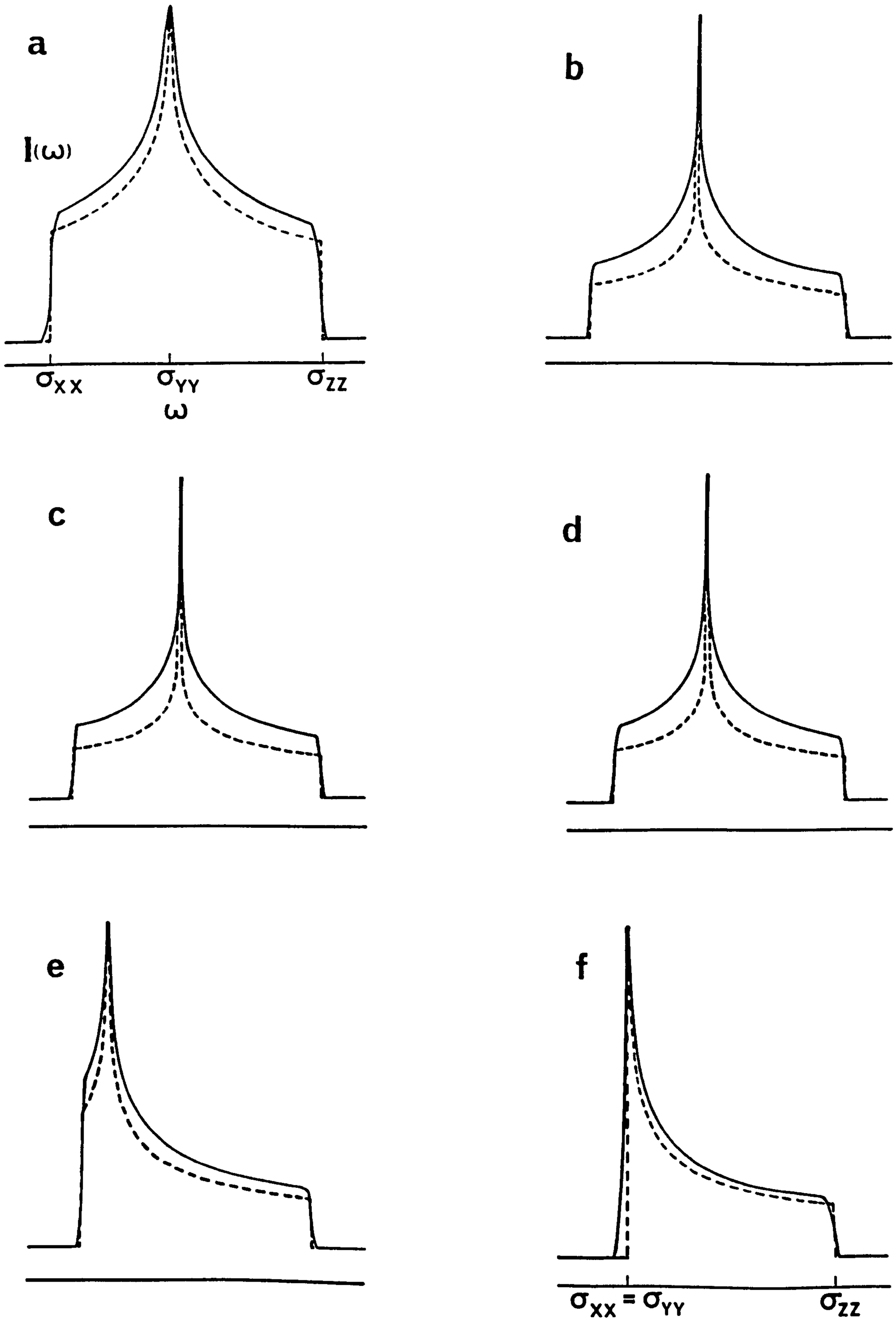

Figure 2.3 Nuclear magnetic resonance powder line shapes in solids for different asymmetry. (a) to (e) are shown for $\omega_{11} \neq \omega_{22}$ and (f) is for axially symmetric ($\omega_{11} = \omega_{22}$). Solid lines are drawn with additional line broadening.

is shown in Figure (2.4) for proton resonance in gypsum (broken line). In practice this line shape will be broadened by the interaction of the other pairs of spins of crystallites which are oriented randomly within the powder sample. The resulted spectrum is shown by the solid line (Figure 2.4).

For quadrupolar nuclei (spin, $I>\frac{1}{2}$) the situation is quite different because of their quadrupole moment. The quadrupole interaction must be small compared to the Zeeman interaction for the line to be observable directly from NMR. Bloembergen [18] also calculated the first and second order line shapes as shown in Figure (2.5) for I = 3/2 and η =0.

2.4 NMR IN ROTATING SOLIDS

2.4.1 INTRODUCTION

In 1958 Andrew et al. [19,20] discovered a novel way of eliminating the broadening caused by different interactions from the NMR spectra of solids by rotating the sample at $54^{o}44'7"$ to the field direction. The major interactions are $(3\cos^2\beta -1)$ dependent, where β is the angle between the axis of rotation and the applied field $\vec{B}_0$, and for $\beta = \cos^{-1}(1/\sqrt{3}) = 54^{o}44'7"$ most of the interactions become insignificant. Andrew et al. also proved that the square root of the second moment [21] remains invariant considering the spinning effect along with the isotropic lineshape. Later in 1959 Lowe [22] also showed the motional narrowing and invariance of the second moment for ^{19}F in powdered CaF_2 and teflon due to rapid rotation of the sample at the angle β . NMR in rotating samples has played an important role for elucidation of structural problems in solids since that time.

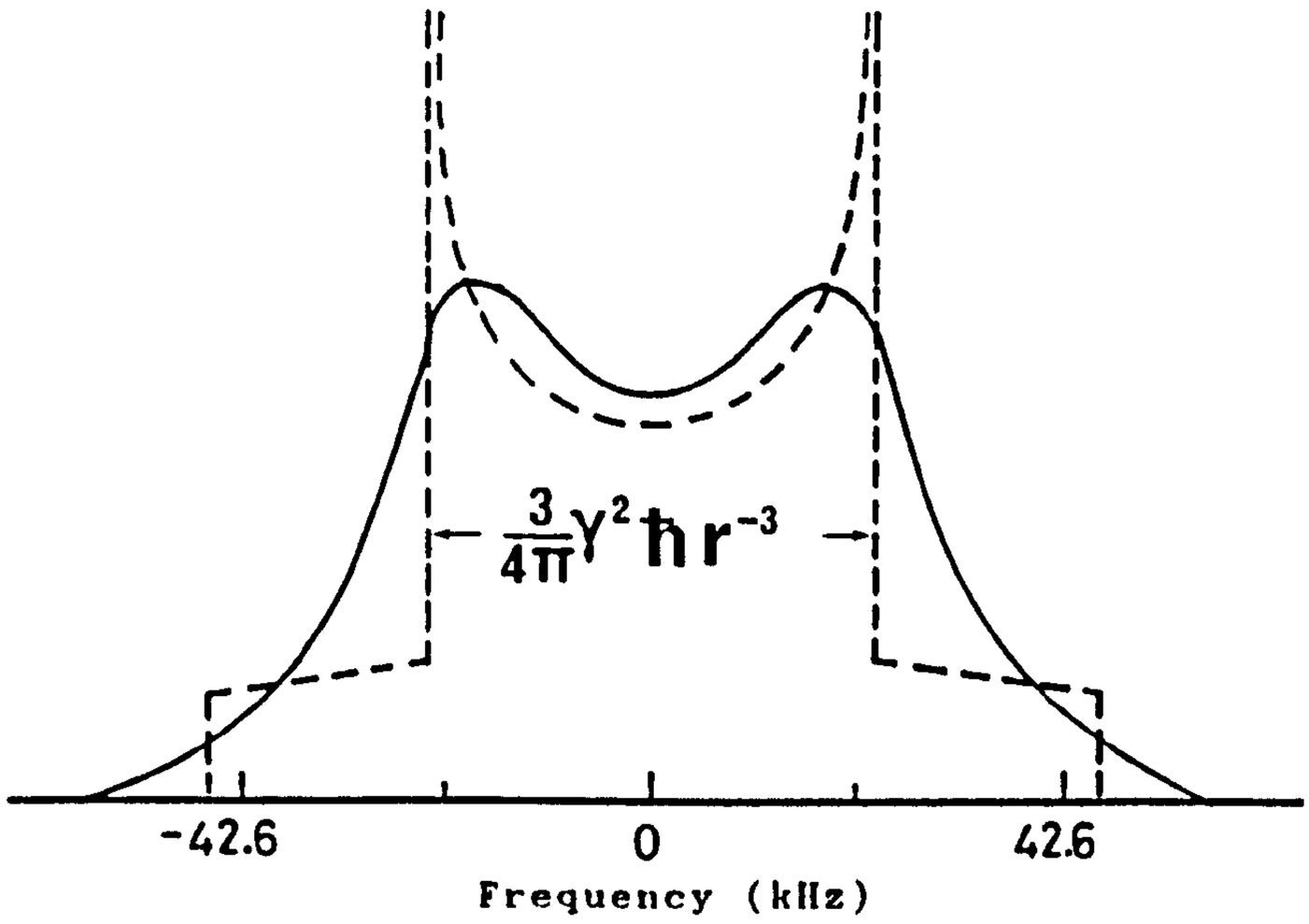

Figure 2.4 Powder pattern for proton resonance in gypsum. The broken line is theoretical shape (equ. 2.41) and the solid line is gaussian broadening superimposed (ref.17).

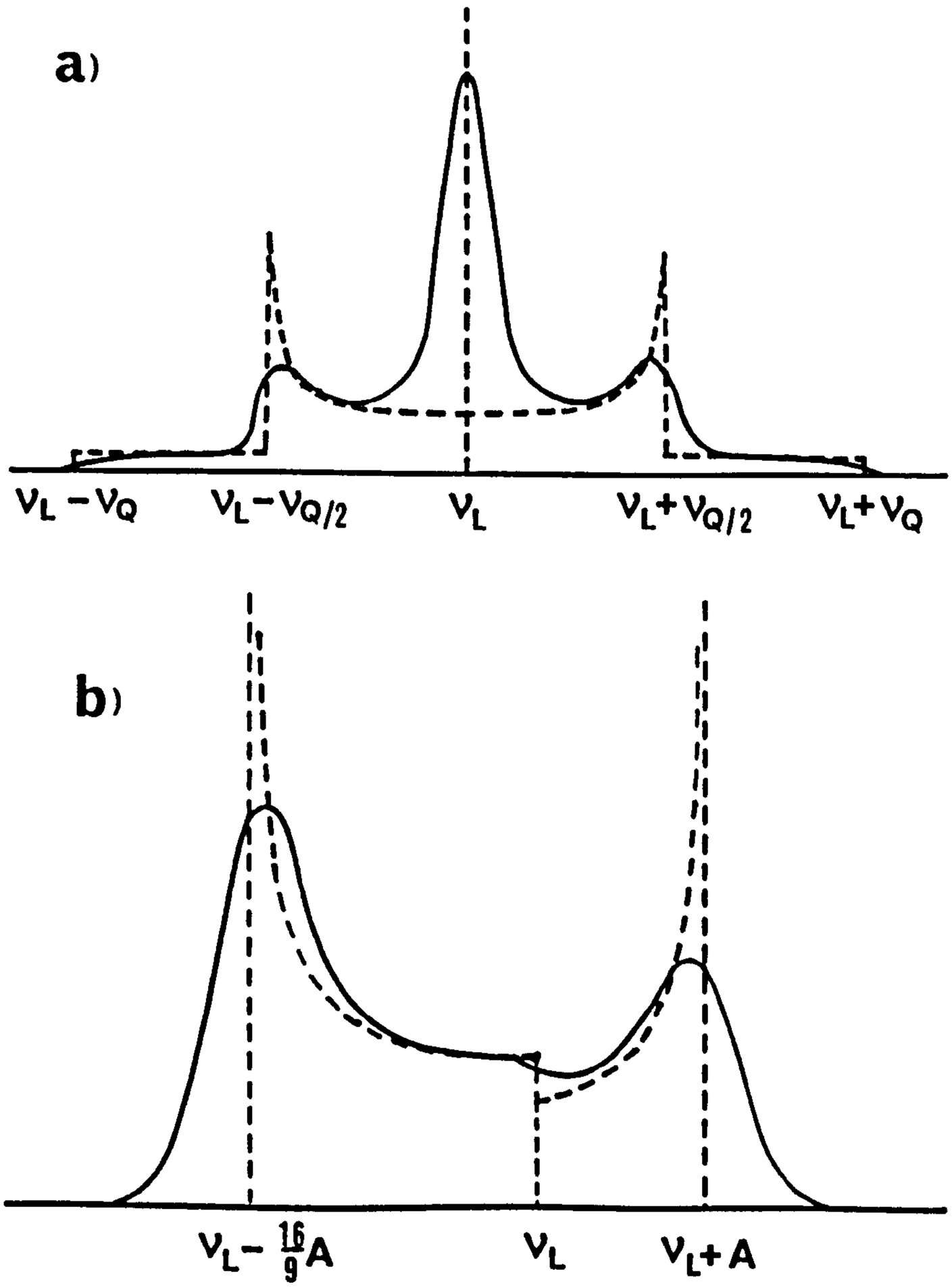

Figure 2.5 (a) First order quadrupolar powder pattern for $I = 3/2$ and $\eta = 0$. (b) Second order pattern for the centre band. $\nu_Q = e^2qQ/2h$ and $A = (a-3/4)\nu_Q^2/16\nu_L$ (ref. 15).

2.4.2 GENERALISATION OF HAMILTONIAN FOR A ROTATING SAMPLE

The Hamiltonian for the spin interactions K (chemical shift, dipolar etc.) of the spins i,j, ... etc. can be written as [7,23]

$$H^K = C^K \sum_{l=0}^{2} \sum_{m=-l}^{l} (-1)^m R_{l,-m} T_{lm} \quad \ldots \quad \ldots (2.42)$$

l=0,1,2 represent the interactions requiring tensors upto second rank, C^K depends on physical constants appropriate to K. $R_{l,-m}$ and T_{lm} are irreducible spherical tensor components expressing the spatial and spin dependence of H^K. Both the tensors can be written in a co-ordinate system fixed in the laboratory with its polar axes parallel to $\vec{B_0}$ [20]. In order to transform from the laboratory to the rotating frame T_{lm} can be written using the Wigner rotation matrix [24] as

$$T_{lm'} = \sum_m D_m^{\,l} (0,0,i\,\omega_0 t) \; \tau_{lm}$$

$$= \sum_m \exp(-im'\,\omega_0 t) \; \tau_{lm} \quad \ldots \quad \ldots \quad (2.43)$$

where τ_{lm} represent the components of T_{lm}. Due to rotation of the sample, the Hamiltonian becomes time dependent and can be expressed for the order (m=0) as

$$H_0 = \frac{\omega_0}{2\pi} \int_0^{2\pi/\omega} H(t')\, dt'$$

$$= CR_{00} \; \tau_{00} + CR_{10} \; \tau_{10} + CR_{20} \; \tau_{20} \quad \ldots \quad (2.44)$$

The first and the second term contribute to the chemical shift interaction and only the last term contributes to the dipolar

and quadrupole interactions because of the matrix elements of R. The term R_{00} represents the isotropic contribution and the terms R_{1m} (m=-1,0,1) are traceless and antisymmetric, and R_{2m} (m = -2,-1,0,1,2) are also traceless but symmetric. The antisymmetric components cannot be observed by spectroscopic technique and the tensor R_{2m} can be re-written in a coordinate system fixed in the rotor using the Wigner rotation matrix as

[7]

$$R_{2m}' = \tfrac{1}{2}(3\cos^2\beta - 1)r_{20} + \sqrt{3/8}\,\sin 2\beta\,(r_{21}\exp(i\,\omega_r t) - r_{2,-1}\exp(-i\omega_r t))$$

$$+\sqrt{3/8}\,\sin^2\beta\,(r_{22}\exp(2i\,\omega_r t) + r_{2,-2}\exp(-2i\,\omega_r t)) \quad ..(2.45)$$

where β = angle between the axis of rotation and the field B_0

ω_r = rotational frequency

$2m'$ = components of R_{2m}

Therefore equ. 2.39 can be written as

$$H_0 = C r_{00}\tau_{00} + C\tau_{20}\,[\tfrac{1}{2}(3\cos^2\beta - 1)\quad r_{20} +$$

$$\sqrt{3/8}\quad \sin 2\beta\quad (r_{21}\exp(i\,\omega_r t) - r_{2,-1}\exp(i\,\omega_r t))\quad +$$

$$\sqrt{3/8}\quad \sin^2\beta\,(r_{22}\exp(2i\,\omega_r t) - r_{2,-2}\exp(-2i\,\omega_r t))] \quad (2.46)$$

The symmetric tensor r_{1m} can be diagonalised by a rotation Ω (α', β', γ') into its principal axis system (PAS), where α', β' and γ' are Euler angle. The tensor r_{1m} can be transformed as before and can be written as

$$r_{2m'} = \frac{3\cos^2\beta - 1}{2}\quad \rho_{20} + \sqrt{3/8}\,\sin^2\beta'\,\exp(2i\,\gamma')\,\rho_{22}$$

$$+\sqrt{3/8}\quad \sin^2\beta'\,\exp(-2i\,\gamma')\,\rho_{2,-2} \quad \ldots \quad \ldots \quad (2.47)$$

Conventionally ρ_{00}, ρ_{20} and $\rho_{2,\ \pm2}$ are defined as

$$\rho_{00} = \frac{1}{3} \mathrm{TrR}$$

$$\rho_{20} = \sqrt{\frac{3}{2}}\,\delta \qquad \ldots \qquad \ldots \qquad \ldots \qquad (2.48)$$

$$\rho_{2,\ \pm2} = \tfrac{1}{2}\,\eta\,\delta$$

where δ and η represent the anisotropy and asymmetry in the sample respectively. According to Haeberlin [7] the anisotropic range, and the asymmetry parameter η are defined as

$$\Delta\sigma = \frac{3}{2}\,\delta = \sigma_{zz} - \tfrac{1}{2}(\sigma_{xx} + \sigma_{yy}) \qquad \ldots \qquad \ldots \qquad (2.49)$$

and
$$\eta = \frac{\sigma_{yy} - \sigma_{xx}}{\sigma_{zz} - (1/3)\mathrm{Tr}\,\sigma} \qquad \ldots \qquad \ldots \qquad \ldots \qquad (2.50)$$

where σ_{xx} , σ_{yy} and σ_{zz} are the principal components of the chemical shift tensor σ . Using the Equs. (2.46, 2.47) and the definition (2.48), and collecting terms the truncated Hamiltonian of Equ. (2.44) can be written as [23]

$$H_0 = C\,\rho_{00}\,T_{00} + \sqrt{3/2}C\,\delta\,T_{20}\,[\tfrac{1}{2}(3\cos^2\beta - 1)]$$

$$[\tfrac{1}{2}(3\cos^2\beta' - 1) + (\eta/2)\sin^2\beta'\cos 2\gamma'] + \sqrt{3/2}C\delta\,T_{20}\quad\xi(t) \qquad (2.51)$$

where

$$\xi(t) = \tfrac{1}{2}\sin 2\beta \sin\beta'(X_1\cos\alpha' - \eta\sin 2\gamma' \sin\alpha')\cos\omega_r t$$

$$-\tfrac{1}{2}\sin 2\beta \sin\beta'(X_1\sin\alpha' + \eta\sin 2\gamma' \cos\alpha')\sin\omega_r t$$

$$+\tfrac{1}{2}\sin^2\beta\,(X_2\cos 2\alpha' - \eta\cos\beta' \sin 2\gamma' \sin 2\alpha')\cos 2\omega_r t$$

$$-\tfrac{1}{2}\sin^2\beta\,(X_2\sin 2\alpha' + \eta\cos\beta'\sin 2\gamma'\cos 2\alpha')\sin 2\omega_r t \qquad (2.52)$$

Here $X_1 = \cos\beta' \ (\eta \cos 2\gamma' - 3)$ and

$$X_2 = (3/2) \sin^2\beta' + (\eta/2)\cos 2\gamma' \ (1 + \cos^2\beta') \quad \ldots \quad (2.53)$$

H_0 in equ. (2.51) is the generalised Hamiltonian. The first term gives the isotropic line shape. The second and the third term give the reduced chemical shift, dipolar etc. interactions. The fourth term is periodic with ω_r, i.e. the effect of rotation will be obtained periodically.

2.4.3 MAGIC ANGLE SPINNING AND LINE NARROWING

When a powder sample is rotated uniformly with an angular velocity ω_r inclined at an angle β to the Zeeman field direction, all the interactions become time dependent with a period $2\pi/\omega_r$ as shown in equ. (2.51) which can be written as

$$H = H + H(t) \quad \ldots \quad \ldots \quad \ldots \quad (2.54)$$

where H represents the isotropic Hamiltonian and H(t) is the sum of the anisotropic interaction Hamiltonians. For $\beta = 54.7^{o}$, most of the anisotropic interactions reduce to zero; so that polycrystalline powders exhibit sharp resonances corresponding to different environments of the nuclei, and spinning at this particular angle is called magic angle spinning.

At the magic angle $\frac{1}{2}(3 \cos^2\beta - 1) = 0$ and equ. (2.51) for the chemical shift interaction (K=CS) can be written as

$$H_0^{CS} = C^{CS} \ \rho_{00} \ T_{00} + C^{CS} \ \int (3/2) \ T_{20} \ \delta \ \xi(t)$$

$$= \gamma_i \ B_0 \ I_{zi} \ [\ \sigma_i + \ \delta_i \ \xi^{CS} \ (t)] \quad \ldots \quad (2.55)$$

σ_i can be expressed in terms of principal components of chemical shift tensors as

$$\sigma_i = 1/3 \; (\; \sigma_{xx} \; + \; \sigma_{yy} \; + \; \sigma_{zz}) \qquad \ldots \qquad \ldots \quad (2.56)$$

Equ. (2.55) provides a narrow isotropic line shape along with spinning sidebands periodic with ω_r. An example of reducing chemical shift anisotropy is shown in Figure (2.6).

For the case of dipolar interaction (K=D) at the magic angle, equ. (2.57) takes the form

$$H^D = \sqrt{3/2}\; C^D \delta \;\; T_{20} \;\; \xi^D \; (t)$$

$$= \gamma_i \; \gamma_j \hbar \;\; r_{ij}^{-3} \; (\vec{I}_i . \vec{I}_j - 3 I_{zi} \; I_{zj}) \;\; \xi^D(t) \; \ldots \quad (2.57)$$

The Hermitian dynamical variables I_x, I_y and I_z of the spins I_i and I_j for different pair (ij) and (i k) do not commute and therefore the resultant interaction can be described as (i) homogeneous and (ii) inhomogeneous interactions [25]. Dipolar interaction between like spins causes homogeneous broadening in the spectra, but that interaction between unlike spins, i.e. spins with different Larmor frequences causes inhomogeneous broadening. The periodicity of equ. (2.57) will provide dipolar spinning sidebands on both sides of the isotropic line shape as shown in Figure (2.7). For some special cases, the coupling between spin half nuclei and quadrupolar nuclei, the angular dependence become different from equ. (2.51). If quadrupolar nuclei have a large efg (MHz) and this has an impact on the isotopically abundant nuclei like ^{31}P, ^{1}H etc.; the spinning at the magic angle cannot totally reduce the broadening from the NMR spectra of these nuclei [26].

The spread of spinning sidebands is comparable with the static line width Δ . Therefore one would expect spinning sidebands if $\omega_r < \Delta$. Once $\omega_r >> \Delta$, the resolution does not

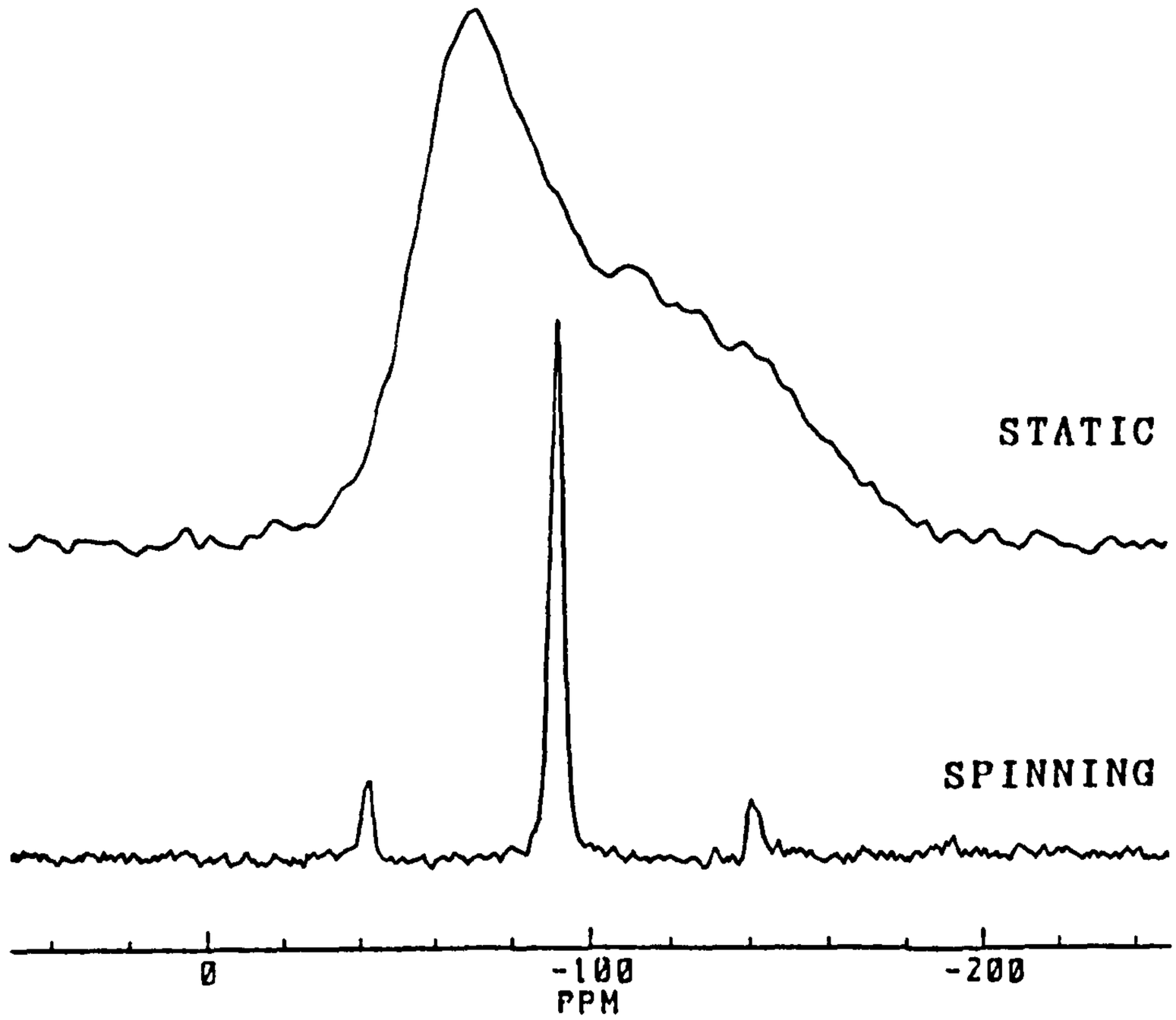

Figure 2.6 Reduction of chemical shift anisotropy from the ^{29}Si spectra of crystalline $Li_2O.2SiO_2$.

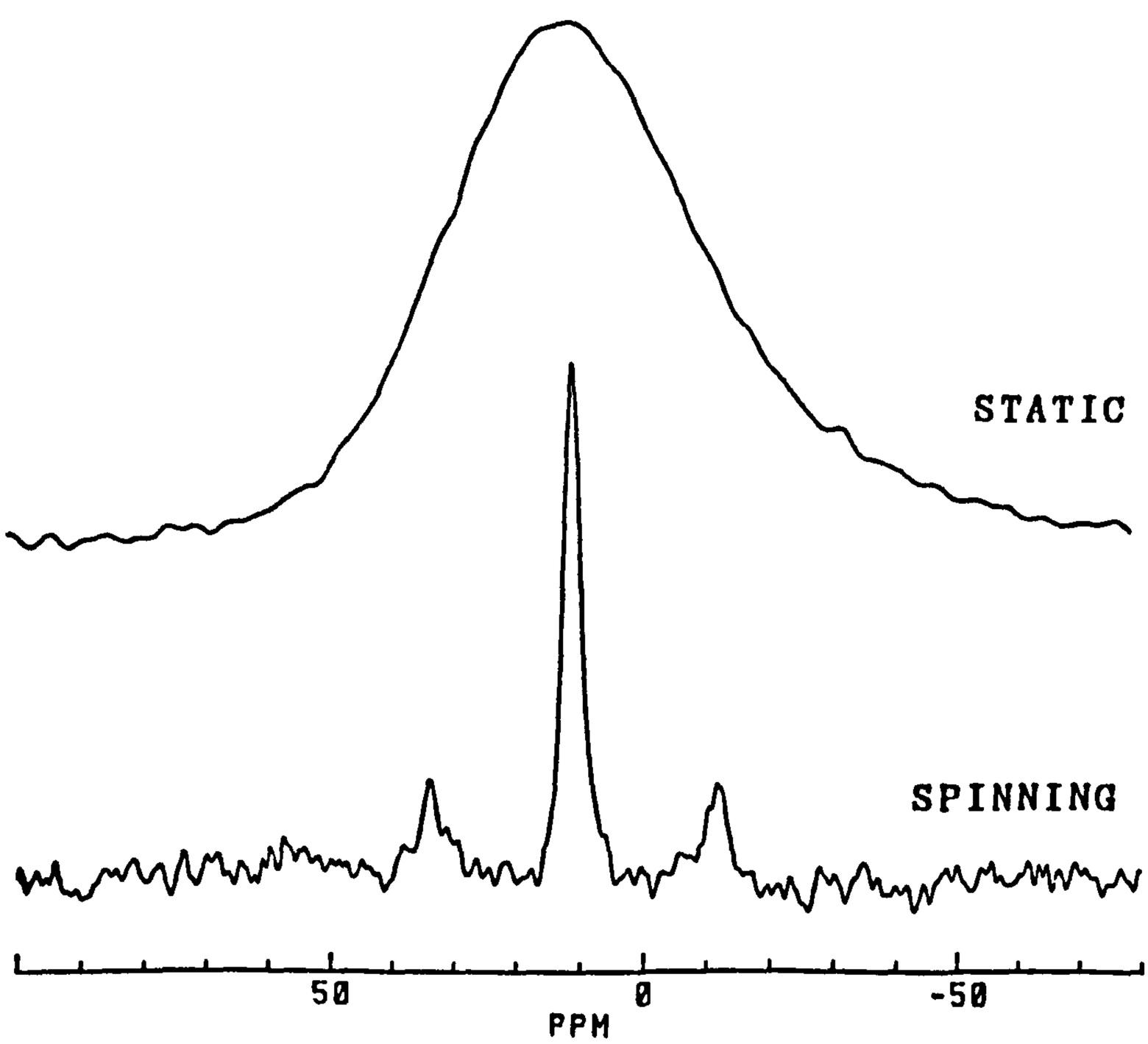

Figure 2.7 Reduction of dipolar interaction from the ^{31}P spectra of Li_3PO_4. There may be little chemical shift anisotropy as well.

further increase but the sensitivity increases until $\omega_r > \Delta$ because all the signal appears as isotropic line shape.

The $\xi^{CS}(t)$ in equ. (2.55) is an oscillating function and the spin system returns back to its initial position after one complete rotation. The resultant of this effect is that the FID assumes the form of rotational echoes whose shape function g(t) is given by [23]

$$g(t) = \sum p_n \exp(i\,\omega_0\,\sigma_n t) \sum_s \exp[i\,\omega_0\,\delta_n \int_0^t \xi_{sn}(t')dt']\ldots \quad (2.58)$$

where p_n represents the population of the species n, s represents the spin packets and ω_0 is the Larmor frequency. For t= q $(2\,\pi/\,\omega_r)$, where q is an integer,

$$\int_0^t \xi_{sn}(t')dt' = 0 \qquad \ldots \qquad \ldots \qquad (2.59)$$

and the sum over s represents a train of echoes, all having the same shape $g_{en}\,[t - q\,(2\,\pi\,/\,\omega_r)]$ which can be represented as [27]

$$W\,[\,t - (2\pi\,/\,\omega_r)\,] * g_{en} \qquad \ldots \qquad \ldots \qquad (2.60)$$

where W $[t - (2\,\pi\,/\,\omega_r)\,]$ is the sampling function and * represents convolution. The term preceding s in equ. (2.58) represents the FID corresponding to isotropic contribution, $g_{In}(t)$. Therefore equ. (2.58) can be written as

$$g(t) = \sum_n g_{In}\,(t)\,[W(t - 2\,\pi\,/\,\omega_r) * g_{en}\,(t)] \quad \ldots \quad (2.61)$$

Fourier transform of this equ. will give a series of spinning sidebands separated by frequency $\omega_r/2\pi$ representative of the spinning echoes, on the both sides of the isotropic line. The effect of spinning at different ω_r will be the displacement

of the spinning sidebands by different amounts but the isotropic line will be at the same position; from which the isotropic line can be identified. The formation of echoes and the spinning sidebands are shown in Figure (3.6.b)

The effect of MAS on quadrupolar nuclei is different from the chemical shift or the dipolar interaction because of different angular dependence of the quadrupolar Hamiltonian [28,29]. Calculation showed that the first order quadrupolar interaction is proportional to $(3\cos^2\beta - 1)$ but that of second order is not. Therefore MAS could reduce the first order quadrupolar broadening more effectively than that of the second order as shown in Figure (2.8 and 2.9). For the second order quadrupolar interaction Freude et al. [30] showed that the square root of the ratio of the second moment, M_2, for static and MAS in $(M_2/M_{2,MAS})^{\frac{1}{2}} = 3.625$. Thus the second order quadrupolar interaction can be reduced by a factor of 3.6 to 4.0 due to spinning at the magic angle (Figure 2.9). Variable angle spinning could more efficiently reduce the second order effect and it would provide a somewhat narrow line shape [31] at the expense of extra broadening from dipolar and chemical shift anisotropy effects.

2.4.4 EXTRACTION OF σ_{xx}, σ_{yy} AND σ_{zz} FROM SPINNING SIDEBANDS

So far three methods have been designed to extract chemical shift parameters from the spinning sidebands (SS). (i) Moment analysis [23] which needs an accurate measurement of sideband intensity, (ii) graphical analysis [32] which is based on the ratios of the intensity of spinning sidebands to the isotropic lineshape and (iii) computer simulation [33].

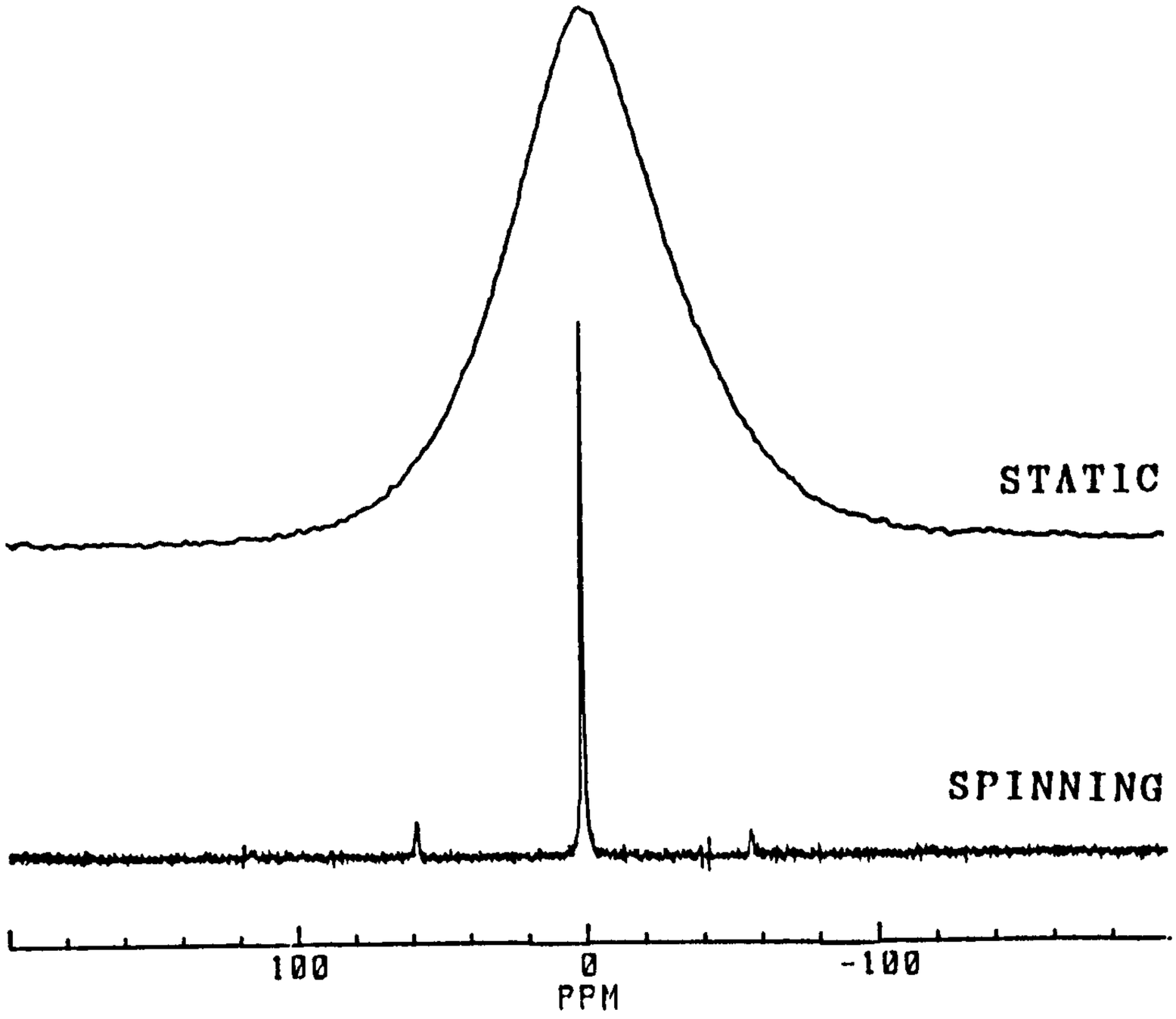

Figure 2.8 Reduction of first order quadrupolar and non-homogeneous dipolar interactions from the ^{6}Li spectra of lithium disilicate glass.

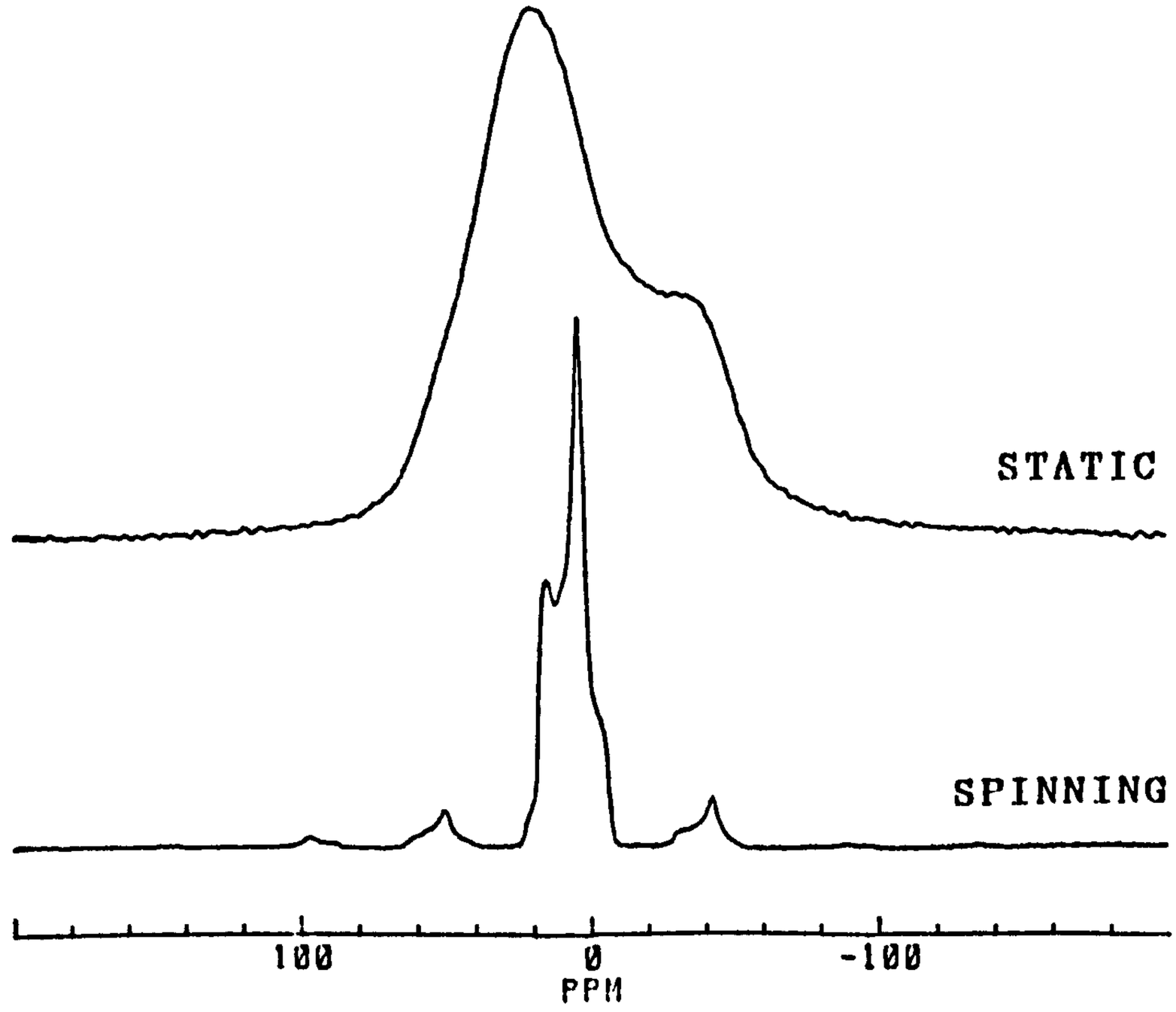

Figure 2.9 Reduction of second order quadrupolar interaction from the ^{23}Na spectra of crystalline $Na_2O.2SiO_2$.

Normally the higher order SS have lower intensities and may also be obscured by noise. This occurs frequently for glasses, glass-ceramics and ceramics because of long T_1 relaxation times. Therefore the accuracy of the chemical shift tensors and hence the anisotropic ranges are severely affected due to neglect of higher order SS [33]. However, in the graphical method the tensor components are unaffected by missing the higher order SS [33]. The computer simulation method has no great advantage over graphical analysis but it has been employed to extract the chemical shift parameters in glasses and glass-ceramics of interest [33-36]. In this thesis both the graphical analysis and the simulation method are employed to extract the chemical shift parameters.

For slow spinning speeds, i.e. $\omega_r < \Delta$ but greater than the broadening caused by homogeneous interactions, the shape of the sideband pattern is governed by the powder lineshape. The line intensities are dependent only upon [32]

$$\Delta_- = (\omega_0 / \omega_r) (\sigma_{yy} - \sigma_{xx}) \quad \ldots \quad \ldots \quad (2.62)$$

and $\Delta_+ = (3 \omega_0 / \omega_r) (\sigma_{zz} - \sigma_i)$

The relative intensities of the Nth sidebands, I_N, can be calculated from the equations described by Herzfield and Berger [32] for different values of Δ_- and Δ_+. In order to cover all possible values of the chemical shift parameters the quantities

$$\mu = (\omega_0 / \omega_r) (\sigma_{zz} - \sigma_{xx}) \quad \ldots \quad \ldots \quad (2.63)$$

and $\rho = (\sigma_{xx} + \sigma_{zz} - 2 \sigma_{yy}) / (\sigma_{zz} - \sigma_{xx}) \ldots \quad (2.64)$

are defined. μ is always positive for positive ω_r and $\rho = \pm 1$ corresponding to axially symmetric tensors. Therefore $\mu \geqslant 0$

and $-1 \leqslant \rho \leqslant +1$ can cover all the chemical shift parameters and the dependence of $(I_{\pm N} / I_0)$, where I_0 is the intensity of isotropic line, on μ and ρ are shown by Herzfield and Berger using a set of contour maps [32]. An example for $(I_{\pm 1}/I_0)$ is shown in Figure (2.10) and a typical plot showing the analysis of the sideband intensities to extract the chemical shift parameters in glass using the graphs of Herzfield and Berger is shown in Figure (2.11). Therefore extracting the values of μ and ρ the values of the chemical shift tensors, asymmetry parameter and anisotropic range can be calculated by using equs. (2.49) and (2.50) of the preceding section.

2.5 SPIN-LATTICE RELAXATION IN ROTATING SOLIDS

When a system of spin ½ nuclei placed in an external strong magnetic field $\vec{B}_0$, which is strong enough to consider broadening interactions as a small perturbation on $\vec{B}_0$, the spin system relaxes to equilibrium via different paths following an excitation pulse [37]. If a second pulse is applied after a time t to sample the magnetisation, the amount of the recovered magnetisation is a characteristic of the time T_1, generally called the spin-lattice relaxation time. Thus T_1 serves as a measure of the rate with which the spin system comes into equilibrium with its environment. When the coupling between the spins is stronger than the coupling with the lattice, the value of T_1 can be computed from the population changes of nuclei due to coupling to the lattice [38]. In the case of motional narrowing, a density matrix is used to compute both the spin-spin relaxation time T_2 and T_1. The general treatment of these times for liquids and gases can be found in Abragam [3]. This thesis will be concerned with

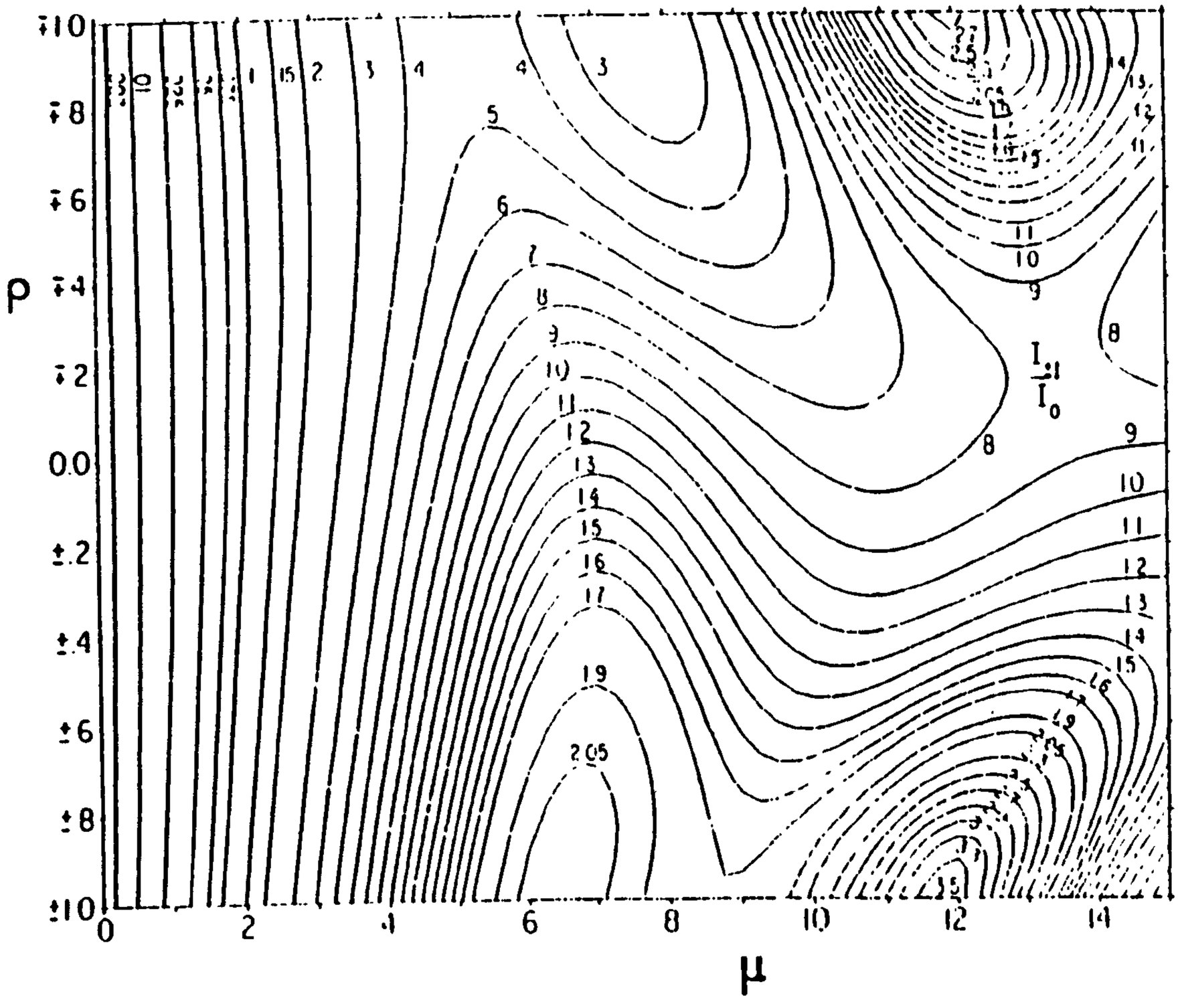

Figure 2.10 Contour plots of ρ versus μ for the ratio of first pair of sidebands to the isotropic line (ref. 32).

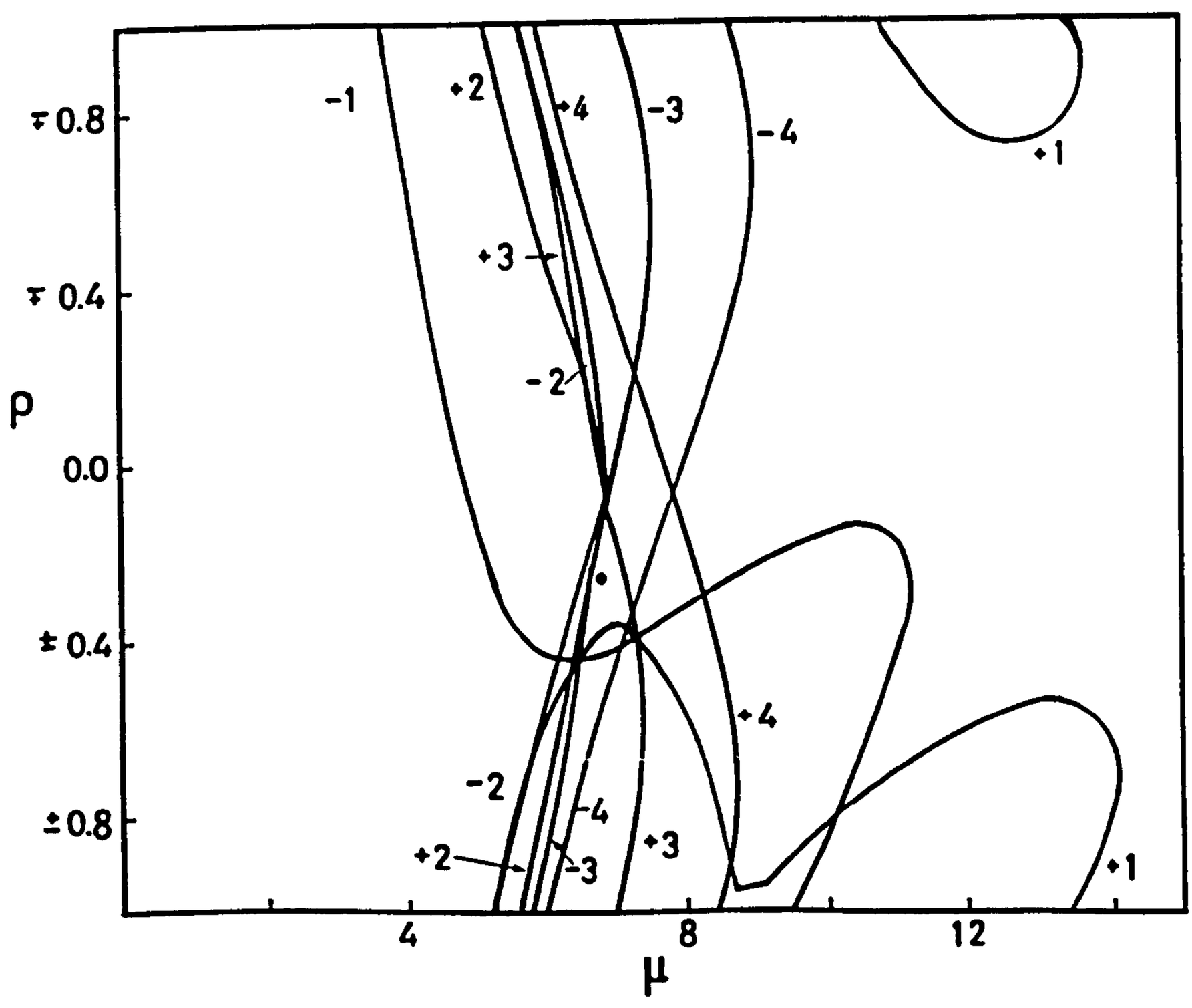

Figure 2.11 Graphical analysis of the sidebands of $Na_2O.2SiO_2.2P_2O_5$ glass.

the T_1 of some rotating solids with ($I=\frac{1}{2}$) and a brief theoretical background [39] is presented here.

The Hamiltonian for spin interaction of a sample in an irreducible spherical tensor notation is given by equ. (2.42)

$$H^K = C\ (-1)^m\ R_{2,-m}\ \tau_{2m}\ \exp(im\ \omega_0 t) \quad \ldots \quad \ldots \quad (2.65)$$

where τ_{2m} are the components of T_{1m} (1=2 is considered only) and $\omega_0 = \gamma B_0$.

The Hamiltonian for the rotating sample experiment, in PAS rotates in spin space but is stationary with respect to the time dependent latticevariables, can be written as

$$H = C\ (-1)^m\ R_{2,-m}(t)\ \tau_{2m}\ \exp(im\omega_0 t) \quad \ldots \quad (2.66)$$

A rotation of the sample at an angular velocity ω_r leads to

$$H = C(-1)^m\ D^2_{-m,-m'}\ r_{2,-m'}\ \tau_{2m}\ \exp(im\ \omega_0 t)\ \exp(im'\ \omega_r t) \quad \ldots \quad (2.67)$$

The equation of motion for the average density matrix can be written as

$$\frac{d\psi}{dt} = \int_0^{\infty} d\tau\ \langle\ [H(t),\ [H(t-\tau),\sigma]]\ \rangle \quad \ldots \quad \ldots \quad (2.68)$$

Using equ. (2.65) and (2.66) Haeberlin and Waugh [39] showed that the spin-lattice relaxation due to dipolar interaction is

$$\frac{1}{T_1} = \frac{2}{5}\sum_r \frac{\gamma^4\ \hbar^2}{r^6}\ I(1+1)\left(\frac{\tau}{1+\omega_0^2\ \tau^2} + \frac{4\tau}{1+4\ \omega_0{}^2\tau^2}\right) \quad (2.69)$$

This equation is exactly the same as the spin-lattice relaxation time T_1 in a liquid where the motional narrowing is caused by the natural phenomena. They also showed by considering the mechanical rotation of solids, e.g. by

considering equs. (2.67) and (2.68) for $\omega_0 >> \omega_r$ and m = 0, that there is no dramatic change in the value of T_1 compared to equ. (2.69). However the spin-spin relaxation time T_2 changes considerably [37].

2.6 RELAXATION CAUSED BY PARAMAGNETIC SUBSTANCES

In this study paramagnetic impurities have been introduced into the samples and a brief account of the effect of paramagnetic substances is given here.

Bloembergen [37] in 1949, using a rigid lattice approximation, showed that for spin ½ nuclei relaxation is caused by the diffusion of the spin magnetic energy to the paramagnetic centres. The diffusion may take place via the flip-flop term $(I_+^i I_-^j + I_-^i I_+^j)$ in equ. (2.20). Out of several ways there are two important ways to be considered. First the rate at which spin magnetic energy can diffuse to the paramagnetic centres and second, the rate at which the impurity can equilibrate spins in its immediate neighbourhood. Theoretically, paramagnetic impurities, even 1 PPM increase the linewidth [21]. But according to Bloembergen [37] the paramagnetic interaction is not effective until the number of paramagnetic centres become 1000 PPM. For ionic solids paramagnetic impurity levels as low as 10 PPM could change the temperature dependence of T_1 relaxation time [40].

In the vicinity of the paramagnetic impurity the local field produced by the electron moment is very large. Therefore the Larmor frequencies of the nuclei within this region will be significantly different from the nuclei beyond this vicinity. Therefore spin diffusion will be prevented in

this region. There is no sharp boundary to this region but Blumberg [41] defined the radius of this region as

$$b = \left[\frac{3 < \mu_p >}{\mu_n}\right]^{\frac{1}{4}} a \qquad \ldots \qquad \ldots \qquad \ldots \quad (2.70)$$

by equating the field change in moving one lattice spacing with the nuclear linewidth determined by the local field, where

$$< \mu_p > = \gamma_p \hbar J \left[B^2(X) + \frac{\delta B(X)}{\delta X} \frac{2}{\pi} \tan^{-1}\left(\frac{T_{1P}}{T_2}\right)\right]^{\frac{1}{2}} \qquad (2.71)$$

Here $\gamma_p \hbar = p_{Mn} \mu_B$; p_{Mn} is the effective Bohr magneton number, μ_B is the Bohr magneton, μ_n is the nuclear moment and

$$B(X) \approx \frac{X}{3} \left(\frac{J+1}{J}\right) \qquad \ldots \qquad \ldots \qquad \ldots \quad (2.72)$$

where $X = \gamma_p \hbar J B_0 / kT$,

T_{1p} = spin-lattice relaxation time of the paramagnetic impurity,

a = lattice constant

J = impurity spin and

T_2 = spin-spin relaxation time of the investigated nuclei.

At a nuclear site, $|\vec{r} - \vec{r}_n| <$ b, the contribution to the dipolar field can be ignored compared to the field produced by the randomly fluctuating impurity spin, where r_n is the position of the nth impurity atoms. Considering spin diffusion Rorschach [42] showed that the spin-lattice relaxation time in a static sample is inversely proportional to the concentration of the paramagnetic impurity.

As the dipolar Hamiltonian (equ. 2.19) is proportional

to $(3\cos^2\theta - 1)$ and for magic angle spinning the Hamiltonian can be shown to be periodic with rotational frequency, the spin diffusion might be affected by the mechanical rotation of the sample. Kessemeier and Norberg [43] showed the dependence of the time rate of change of magnetisation on ω_r in rotating solids at the magic axis as

$$\frac{\delta M_z(t)}{\delta t} = -\frac{1}{T_1(B_0, \omega_r)} [M_z(t) - M_0] \quad \ldots \quad \ldots (2.73)$$

where

$$\frac{1}{T_1(B_0\ \omega_r)} = \frac{8}{3}\ \pi\ NC^{\frac{1}{4}}(B_0)\ D^{\frac{3}{4}}(\omega_r)\ K_{3/4}(\zeta)/K_{-3/4}(\zeta) \quad (2.74)$$

Here

N = impurity concentration and

$K_m(\zeta) = i^{-m}\ J_m(i\zeta)$ is the hyperbolic Bessel function

with $\zeta = (\frac{1}{2})b^{-2}\ (B_0)\ [C(B_0) / D(\omega_r)]^{\frac{1}{2}}$

where

$$C(B_0) = 3\gamma_p^2\ \gamma_n^2\ \hbar^2 J(J+1)\sin^2\beta\ \cos^2\beta\ \tau_e[1+(\omega\tau_e)]^{-1} \text{ and}$$

$$D(\omega_r) = a^2\ W(\omega_r)$$

with a is the lattice constant and W (ω_r) is the probability of a flip-flop transition in the presence of ω_r. The value of W (ω_r) is inversely proportional to the spin-spin relaxation time, T_2 [37]. Thus W (ω_r) decreases with the increase of ω_r. Physically $C(B_0)$ defines the coupling strength between an impurity ion and a nuclear spin in its vicinity and $D(\omega_r)$ is the diffusion coefficient. In the case of diffusion limited relaxation $\zeta >> 1$;

$K_m(\zeta) = K_{-m}(\zeta)$ and equ. (2.74) simplifies to

$$\frac{1}{T_1} = \frac{8}{3} \pi N C^{\frac{1}{4}} (B_o) D^{3/4} (\omega_r) \quad \ldots \quad \ldots \quad (2.75)$$

An increase of ω_r should increase the value of T_1 until it fully reduces the interactions. For the fast diffusion limit $\xi \ll 1$,

$$\frac{1}{T_1} = \frac{4\pi}{3} \frac{NC(B_0)}{b^3}$$

independent of ω_r. In both cases the plot of relaxation rate as a function of impurity concentration should give a straight line.

REFERENCES

1. T.C. Farrar and E.D. Becker, Pulse and Fourier Transform NMR, Academic Press, London, 1971.

2. C.P. Slichter, Principles of Magnetic Resonance, 2nd Edn. Springer Verlag, 1980.

3. A, Abragam, Principles of Nuclear Magnetism, Oxford, 1985.

4. R.K. Harris, Nuclear Magnetic Resonance Spectroscopy, Longman Scientific and Technical, 1986.

5. A.E. Derome, Modern NMR techniques for Chemistry Research, Oxford, 1987.

6. M. Mehring, High Resolution NMR in Solids, Springer Verlag, 1983.

7. U. Haeberlin, High Resolution NMR in Solids, Academic Press, 1976.

8. W.D. Knight, Phys. Rev., 76, 1259 (1949).

9. W.C. Dickinson, Phys. Rev., 77, 736 (1950).

10. G. Lindstrom, Phys. Rev., 78, 817 (1950).

11. W.G. Proctor and F.C. yu, Phys. Rev., 77, 717 (1950).

12. J.T. Arnold, S.S. Dharmati and M.E. Packard, J. Chem. Phys., 19, 507 (1951).

13. M.H. Cohen and R. Reif, Solid State Physics, Academic Press, 5, 325 (1957).

14. G.M. Volkoff, Canad. J. Phys., 31, 820 (1953).

15. N. Bloembergen and T.J. Rowland, Acta Metallurgica, 1, 731 (1958).

16. N. Bloembergen and T.J. Rowland, Phys. Rev., 55, 1679 (1955).

17. G.E. Pake, J. Chem. Phys., 16, 327 (1948).

18. N. Bloembergen, Rept. Conf., on defects in crystalline solids, Bristol, 1954, P.1., The Physical Society, London, 1955.

19 E.R. Andrew, A. Bradbury and R.G. Eades, Arch. Sci. (Geneva), 11, Fasc. Spec., 223 (1958).

20. E.R. Andrew, A. Bradbury and R.G. Eades, Nature (London) 182, 1659 (1958).

21. J.H. Van Vleck, Phys. Rev., 74, 1168 (1948).

22. I.J. Lowe, Phys. Rev., 2(7), 285 (1959).

23. M.M. Maricq and J.S. Waugh, J. Chem. Phys., 70(7), 3300 (1979).

24. A.R. Edmond, Angular momentum in Quantum Mechanics, Princeton University Press, New Jersey, 1957.

25. A.M. Portis, Phys. Rev., 91, 1971 (1953).

26. J. Bohm, D. Fenzke and H. Pfeifer, J. Magn. Reson., 55, 197 (1983).

27. R. Bracewell, The Fourier transform and its applications, McGraw Hill, New York, 1965.

28. F. Lefebvre, J.-P. Amoureux, C. Fernandez and E.G. Derouane, J. Chem. Phys., 86(11), 6070 (1987).

29. D.J. Behrens and B. Schnabel, Physica, 114B, 185 (1982).

30. D. Freude, J. Hasse, J. Klinowski, T.A. Carpenter and G. Ronikier, Chem. Phys. Lett., 119(4), 365 (1985).

31. S. Ganapathy, S. Schramm and E. Oldfield, J. Chem. Phys., 77(9), 4360 (1982).

32. J. Herzfield and A.E. Berger, J. Chem. Phys., 73(12), 6021 (1980).

33. N.J. Clayden, C.M. Dobson, Lu-Yun Lian and D.J. Smith, J. Magn. Reson., 476 (1986).

34. R. Dupree, D. Holland and D.S. Williams, J. Non-cryst. solids, 81, 185 (1986).

35. R. Dupree, D. Holland and M.G. Mortuza, Phys. Chem. Glasses, 29(1), 18(1988) (This Thesis, P.).

36. E. Schneider, J.F. Stebbins and A. Pines, J. Non-cryst. Solids, 89, 371 (1987).

37. N. Bloembergen, Physica, 15 (3-4), 386 (1949).

38. C.J. Gorter, Paramagnetic relaxation, Elsevier Publishing Co., New York, 1947.

39. U. Haeberlin and J.S. Waugh, Phys. Rev.,182(2),420, 1969.

40. T.T. Phua, B.J. Beudry, D.T. Paterson, D.R. Torgeson, R.G. Barnes, M. Belhoul, G.A. Styles and E.F.W. Seymour, Phys. Rev.B, 28(11) 6227 (1983).

41. W.E. Blumberg, Phys. Rev., 119(1), 79 (1960).

42. H.E. Rorschach, Jr., Physica 30, 38 (1964).

43. H. Kessemeier and R.E. Norberg, Phys. Rev., 155(2), 321 (1967).

CHAPTER 3

INSTRUMENTATION AND TECHNIQUES

3.1 INTRODUCTION TO PULSED FOURIER TRANSFORM (PFT) SPECTROMETRY

The basic principle involved in pulsed spectrometry is the excitation of a spin system by a short discontinuous, e.g. rectangular radio frequency (rf) wave form, $\vec{B}_1$, in the presence of a large magnetic field $\vec{B}_0$. In the pulse experiment the B_1 field is switched on at t=0 for a short time (usually 0.5 - 40 μs) compared to T_1 and T_2 and then switched off at t=t'. The field $\vec{B}_1$ is orthogonal to $\vec{B}_0$ and induces an alternating magnetic field

$$\vec{B}_1 = B_1 \ (I_x \cos\omega t + I_y \sin \omega t) \quad \ldots \quad (3.1)$$

of frequency ω in the sample via the NMR coil. The oscillating frequency is almost equal to the Larmor frequency of the investigated nuclei. The $\vec{B}_1$ field nutates the spin magnetisation M_z from the OZ axes by a given angle θ described by

$$\theta = \gamma B_1 \ t_p \quad \ldots \quad \ldots \quad \ldots \quad (3.2)$$

where γ is the gyromagnetic ratio and t_p is the pulse width. At resonance the effective field $\vec{B}_{eff} = \vec{B}_1$ in the rotating frame [1-4]. The magnetisation will precess about $\vec{B}_1$ in a plane (0,y',z') perpendicular to $\vec{B}_0$ following a π/2 pulse in the laboratory frame if $\vec{B}_1$ is applied along the (x',0,0) direction. During the experiment, the NMR coil lies in the (x,y,0) plane and, following the pulse, the magnetisation of the individual spins will fan out on the (x',y',0) plane which will induce a decaying voltage at the rate $\exp(-t/T_2)$ in the coil, where T_2 is the spin - spin relaxation time. This signal following a pulse is called the Free Induction Decay

(FID) and the whole process is shown in Figure (3.1). This was first predicted theoretically by Torrey [5] and demonstrated practically by Hahn [6].

The FID is a time domain signal and the information about multicomponent phases is almost obscured. In 1957 Lowe and Norberg [7] theoretically demonstrated that this time domain signal is the Fourier transform (FT) of the corresponding steady state resonance line shape. This idea was implemented by Clark [8] using a box car integrator to find the absorption and dispersion mode signal from the FID. He used the integrator to integrate the area under the FID obtained as a function of magnetic field. In 1966 a detailed study was made by Ernst and Anderson [9] using the Bloch equations [10] of the conditions, i.e. the decaying mechanism of the spin system. According to their investigation Fourier transform of the FID using a Fast Fourier transform (FFT) algorithm [11] could provide spectral information in a more efficient manner than direct observation of the ordinary spectrum. They pointed out that Fourier transforming the FID obtained by a pulsed NMR spectrometer could provide the multi-line spectra corresponding to different environments of nuclei. The two techniques merged and the principle of pulsed Fourier transform (PFT) NMR spectrometry was established.

The PFT NMR spectrometer has to have at least

a) a magnet capable of providing a homogeneous high magnetic field since the signal intensity, $I \propto B_0^2$. Particularly for high resolution experiments, a super-conducting magnet is preferable.

b) a transmitter capable of providing short (0.5 - 40 μs), strong (100 - 1000V) and homogeneous rf pulses to ensure

the same rotation of all the investigated nuclei and provide an undistorted FID.

c) a pulse programmer capable of providing very stable time base pulses for all time intervals. The switch on-off can be expressed as

$$V = 0 \text{ for } t=0 \text{ and } t > t'$$
$$V = V \text{ for } t < t' ,$$

i.e. the power must be turned on and off very quickly (~ ns).

d) a receiver to receive the signal following excitation which induces a voltage in the coil. The receiver must amplify the signal linearly from its initial microvolts to the voltage required to drive the analog to digital converter.

e) probes of different frequency range to match the resonance frequency of different nuclei. The solid state NMR experiments require a special type of probe and spinner and these will be discussed briefly in section (3.3).

f) the facilities to store the data for later manipulation.

The exact resonance positions of nuclei in a sample depend upon the environments of the nuclei and are not known in advance and therefore a range of frequencies Δ is selected to cover the resonance frequencies of the spectrum. The applied rf of the carrier wave ν_0 can be chosen at the centre of those frequencies and positive and negative frequencies are observed after Fourier transforming the FID. The frequency range Δ is called the spectral width. The value of Δ must also be large enough to provide a resonable base line. In practice $\Delta = 6\ \nu_{1/2}$ gives an unambiguous base line, where $\nu_{1/2}$ is the line width. The FID is a combination of absorption and

dispersion mode signals and a detector cannot detect the different phases of the complex waveform. Therefore two phase sensitive detectors (PSD) in quadrature, i.e. 90^{o} out of phase with each other are used to detect the signal as shown in Figure (3.2). This technique increases the signal - to - noise ratio by $\sqrt{2}$ giving a time saving factor of 2. The detected signals are amplified, passed through low pass filters and are further amplified to switch on the analog to digital convertor (ADC). The signals are then digitised and saved in the memory blocks of a computer. A schematic diagram of a PFT NMR spectrometer is shown in Figure (3.2).

3.2 THE BRUKER MSL 360 SPECTROMETER SYSTEM

The Multipurpose Solid and Liquid (MSL-360) spectrometer is commercially available from Bruker Spectrospin. It is a compact assembly of the necessary components required for a PFT NMR spectrometer. A brief description extracted from the Bruker catalogues [13,14] is given here.

The spectrometer is equipped with an Oxford super-conducting wide bore (89 mm) high field (8.45 T) magnet and an Aspect 3000 computer with Winchester disc system. The optimum homogeneity of the magnetic field is achieved by using the shim coils which generate very small local field gradients in comparison to the $\vec{B}_0$ field. For the proton signal in water a linewidth of 28 to 36Hz was obtained by shimming the magnet. The rf electronics of the system consists of frequency generator, modulator, converter, receiver, transmitter, filter and rf - interface. The basic frequency is generated by a PTS-200 frequency synthesizer of standard resolution 1 Hz. Frequencies above 200 MHz are generated by mixing the

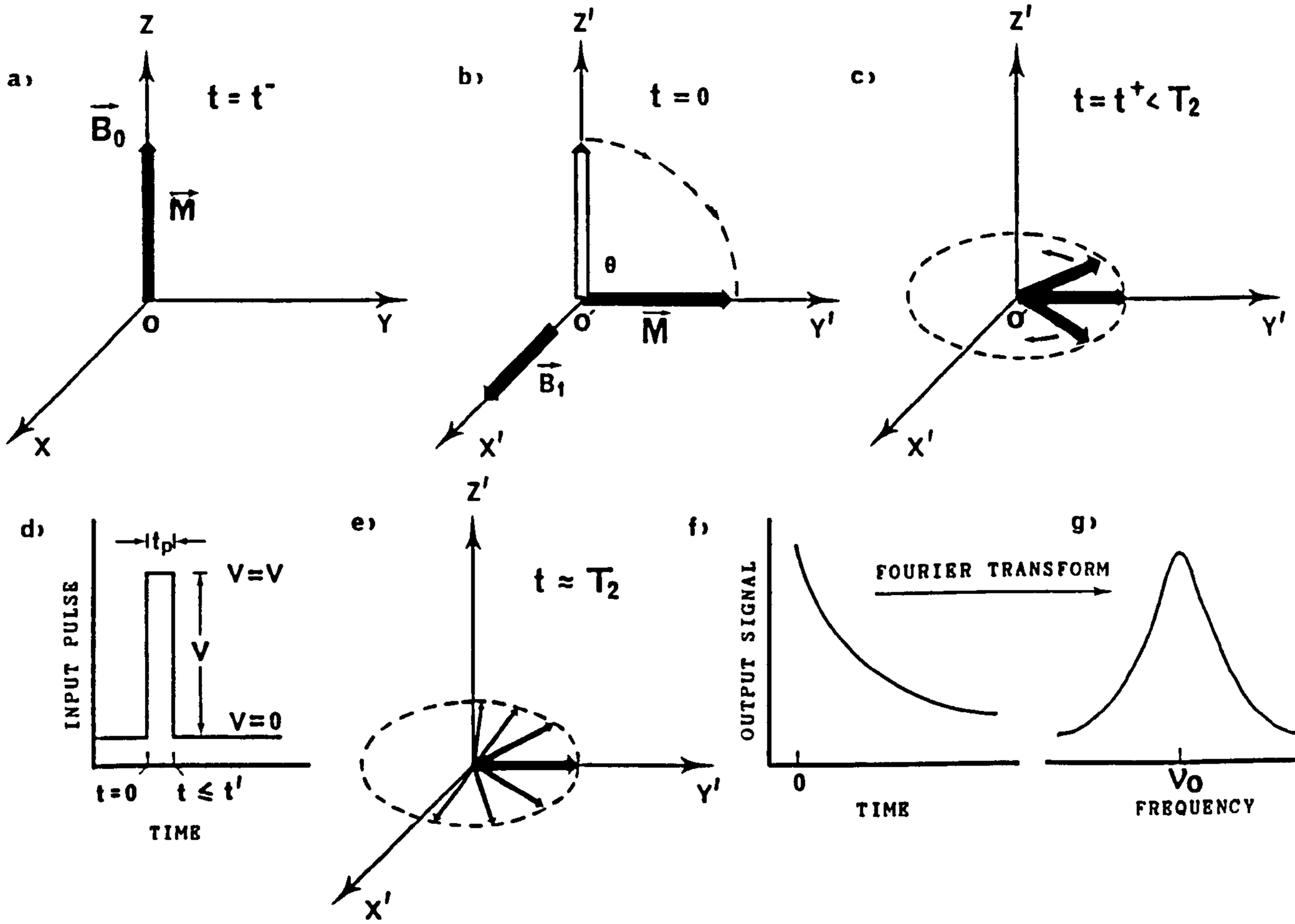

Figure 3.1 (a) Magnetisation $\vec{M}$ in laboratory frame before application of the pulse. (b) A $\pi/2$ pulse rotates the magnetisation M from O'Z' axis to O'Y' axis when pulse is applied along (X',0,0) direction. (c) Dephasing of magnetic moments with time following a $\pi/2$ pulse showing decaying of the output signal. (d) Input pulse applied to (b). (e) Dephasing of magnetic moments continues until $t >> T_2$. (f) Exponential FID corresponding to (c) and (e). (g) Fourier transform of the FID shown in (f).

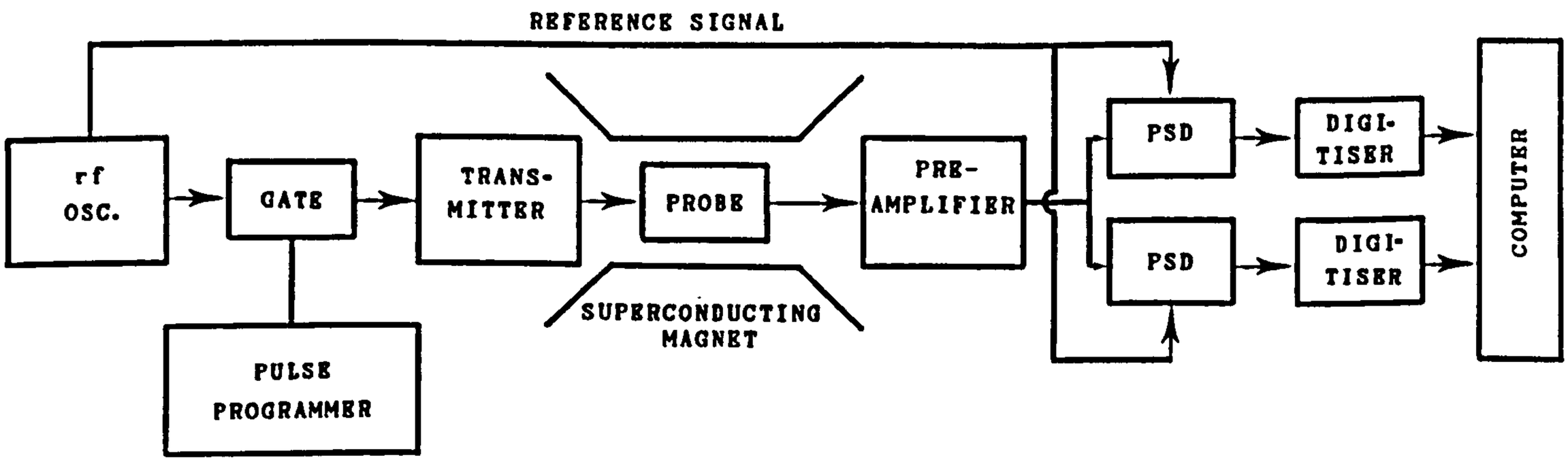

Figure 3.2 Schematic diagram of a PFT NMR spectrometer.

appropriate frequency with the synthesizer frequency. The required frequency is then fed to a modulator unit via a rf gate. A pre-amplifier with appropriate matching receives the signal. The receiver is a broad-banded amplifier with linear gain from 1-404 MHz. A Bessel filter is used to obtain the optimum band width without phase distortion. Similar approach via different devices, wherever necessary, is used for the proton frequency (360.13 MHz).

The experiments are controlled by means of computer programmes using the key board. A high level machine language is used to write the programmes. The system also provides plotter for the spectra, floppy disc drive, visual display unit and a printer for the general purposes. A block diagram for the essential components of the Bruker MSL-360 spectrometer is shown in Figure (3.3).

3.3 THE NMR PROBES AND SPINNERS

The Bruker MSL-360 spectrometer is equipped with static, single and double bearing single coil probes to perform high resolution NMR experiments in solids and liquids. The single and double bearing (DB) probes have the facility for both static and magic angle spinning, with or without decoupling and cross-polarisation [15]. The associated rf electronics in Bruker probes are rather complicated and are described elsewhere [15]. The basic principle involved in the probe circuit is to transfer rf power from the transmitter to the coil and from the coil to the receiver as shown in Figure (3.4) which is based on the non-linear voltage characteristics of semiconductor diodes [16]. All samples were held at ~296°K.

In the static probe the sample was put into the coil

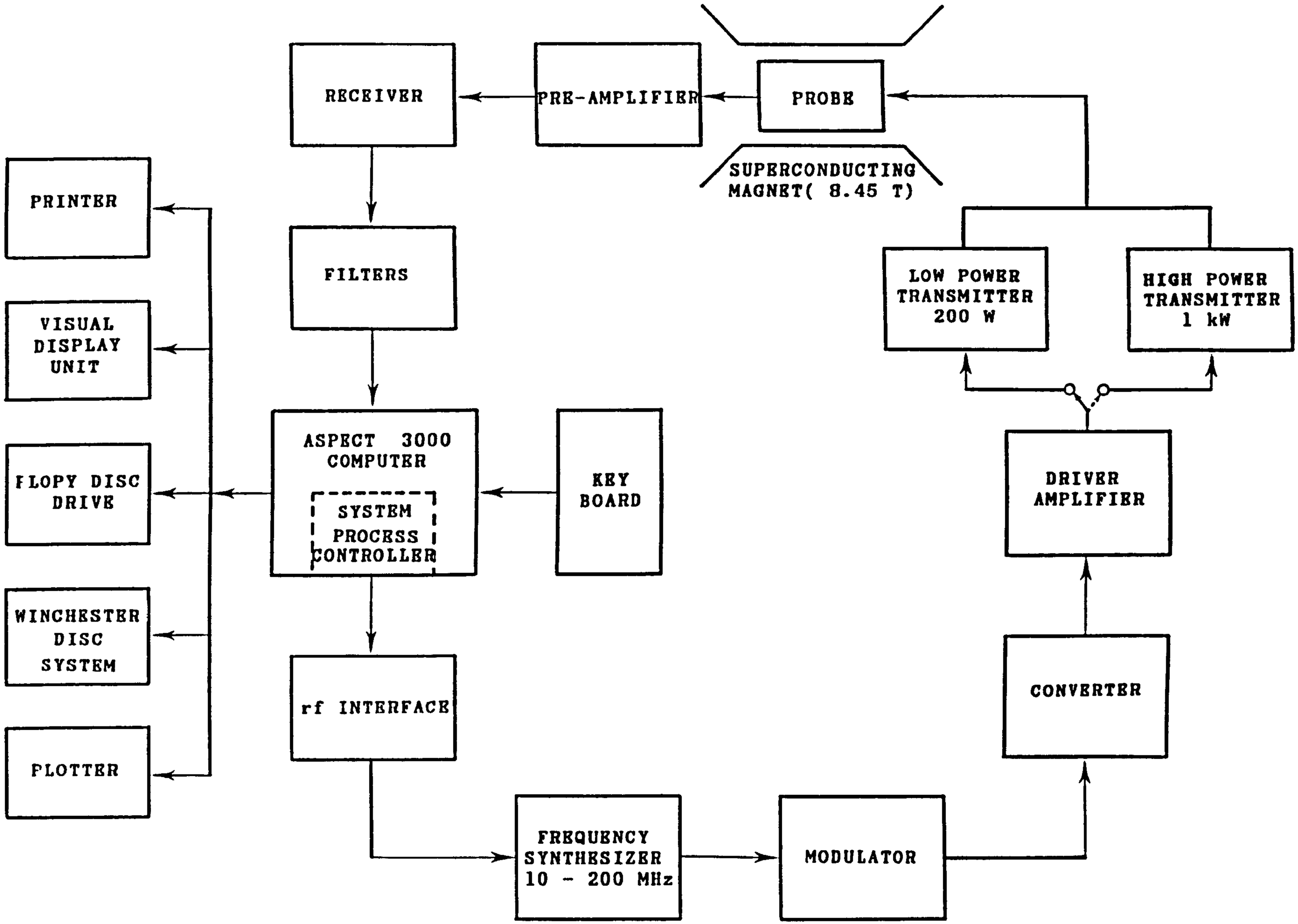

Figure 3.3 The basic components of the Bruker MSL-360 spectrometer.

before inserting into the magnet. But in the spinning probes the sample was held in the coil by air driving generator. After each experiment one had to take the static and single bearing probes out of the magnet to change the sample. This task could be performed remotely in the DB probe by using an insert and eject tube connected with a pneumatic unit operated at 6 bars pressure. The other tubes connected with the pneumatic unit provided the bearing and drive pressure to spin the sample. Bruker-made cylindrical alumina and zirconia rotors of internal diameter 5.5 mm, external diameter 7 mm and length 17.7 mm were used in the DB probe. DB magic angle spinning systems were quite sensitive to sample imbalance, hygroscopicity of the samples, particle size, conductivity, packing fraction etc. and special precautions [13,15] were essential for DB probes sample preparation. The rotors spin at 5 kHz with 1.5 bars bearing and drive pressures. The single bearing probe is commonly known as a mushroom probe because of its mushroom shaped [17] spinners with and without flutes. The rotors with flutes spin easily at 5 kHz with 2 bars air pressure whereas without flutes they spin at only 3 kHz with that pressure. Apart from the Bruker probes home made probes with a simple tuning circuit as shown in Figure (3.4) and a Doty probe [18] were also used to run the experiments. Conical shaped spinners made of Delrin and fitted with glass tubes are used in the home made probe. The Doty probe was equipped with hollow cylindrical silicon nitride, zirconia and sapphire made rotors of inner diameter 3.5 mm and outer diameter 5.0 mm and was designed for high speed rotation of the samples. A system for centering the rotors and two turbine caps helped the rotors to spin very

fast (~ 10 kHz). Additional air filter was also provided with the probe. The sensitivity of the Bruker DB probe was about 18 and 34 percent more than the mushroom and the home made probe respectively. A diagrammatical representation of the spinners used in DB, mushroom, home made and Doty probe is shown in Figure (3.5).

3.4 OPERATION OF THE SPECTROMETER

3.4.1 INTRODUCTION

The Bruker MSL-360 spectrometer was controlled by a computer programme, DISMSL, which operated in conjunction with the ADAKOS disk monitor and a high density disk drive unit. The spectrometer could be run using the commands from the keyboard described in the Bruker manual [14]. The characteristics of the spectrometer do not remain constant with time. Therefore certain parameters, e.g. receiver amplitude, receiver phase, transmitter amplitude etc. needed to be adjusted with time. The experimental gain was rather sample dependent and the receiver needed to be fixed before final data acquisition on the laboratory sample. For high resolution NMR the homogeneity of the field was achieved by shimming the magnet [19]. The shimming depends on the orientation of the probes in the magnet and probe heads. The magnet was shimmed for a particular orientation and the parameters were saved in a file. The file had to be recalled for every experiment to optimise the field homogeneity.

In order to check the sensitivity, resolution, lineshape etc. test spectra were run following a change of the spectrometer conditions. The general procedure for

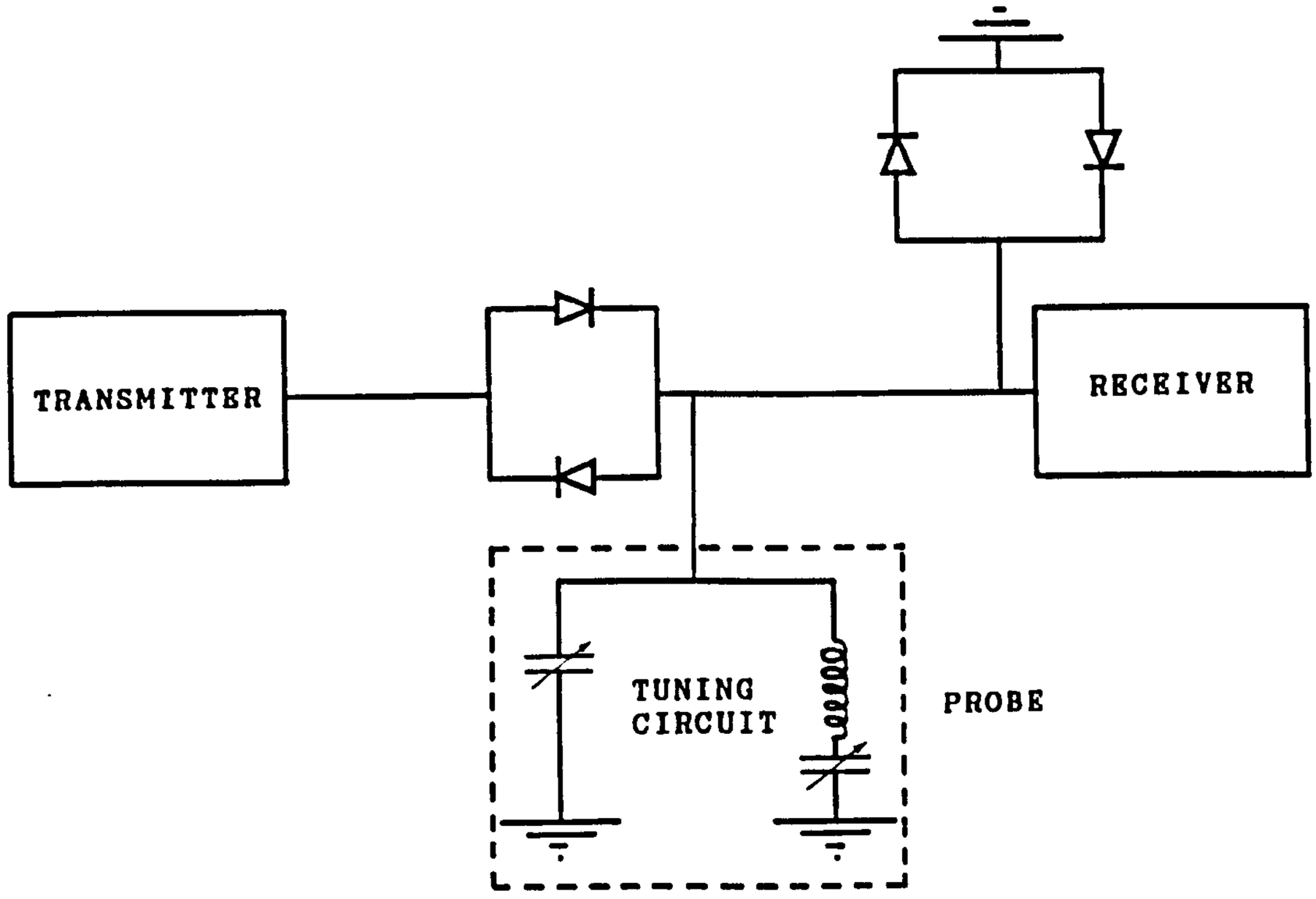

Figure 3.4 Block diagram showing the operation of a single coil probe.

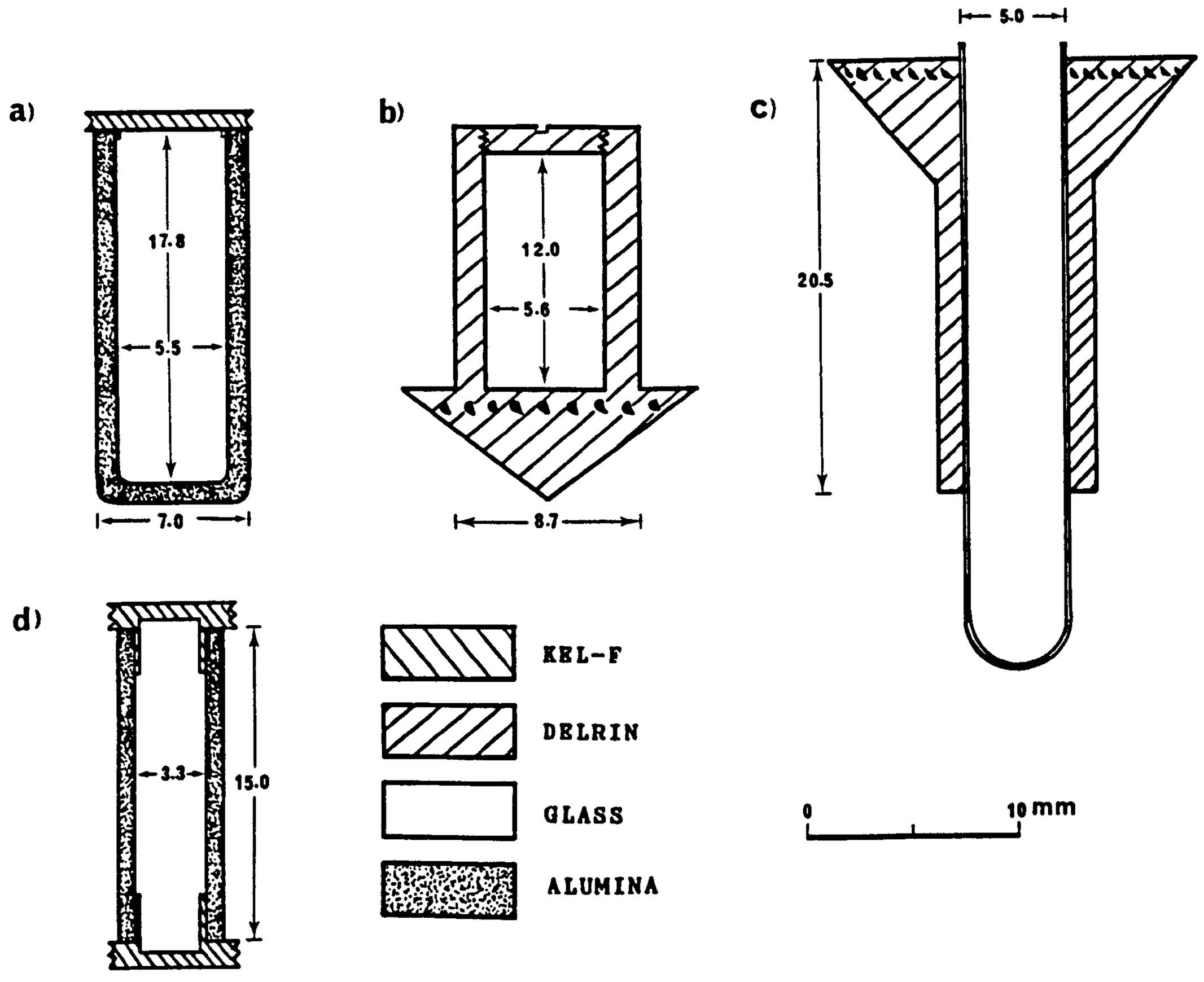

Figure 3.5 Different types of spinners used in (a) DB, (b) mushroom, (c) home made and (d) Doty probe. All the scale is in mm.

observation of any nucleus were not straight forward and certain adjustments had to be made as explained in the following sections (3.4.2 - 3.4.6).

3.4.2 MAGIC ANGLE SETTING

In order to reduce the broadening from the isotropic lineshape caused by different interactions, e.g. chemical shift interaction, dipolar interaction, quadrupolar interaction etc., rotation of the sample at the magic angle was essential. This was achieved by setting the axis of rotation at the angle of $54^{o}44'\ 7''$ to the Zeeman field direction. This was first done by Andrew et al. [20-22] and following their work Lowe [23] also observed the narrowing of resonance lineshape due to mechanical rotation of the sample at the magic angle. For high resolution solid state NMR spectroscopy the closer to the correct 'magic angle' setting the better the resolution as shown in Figure (3.6).

The ^{79}Br nucleus [24] in a powdered KBr sample was used to set the magic angle for the high frequency range (60-146 MHz). ^{79}Br is a quadrupolar nucleus of spin 3/2, natural abundance 50.54%, $\gamma = 7.2468 \times 10^{7}$ rad $T^{-1}s^{-1}$ and in a relatively symmetric cubic environment provides a huge NMR signal with symmetric spinning sidebands if the spinning axis is at the magic angle [24]. For the lower frequency range, 10-60 MHz, the ^{85}Rb nucleus in RbCl can be used to set the magic angle [25].

The FID can be represented by the equation

$$M = M_0 \exp(-t/T_2) \cos(\omega - \omega_0)t \quad \ldots \quad \ldots \quad (3.3)$$

where M = macroscopic magnetisation,
M_0 = value of M at equilibrium,
ω = observed resonance frequency,
ω_0 = frequency of the rf carrier wave.

At resonance $\omega = \omega_0$ and Equ. 3.3. becomes

$$M = M_0 \exp(-t/T_2) \quad \ldots \quad \ldots \quad \ldots \quad (3.4)$$

Equ.(3.4) represents a decaying exponential with maximum at M_0 and the plot of M versus t, which is a general shape of the FID on resonance, is shown in Figure (3.6.c). This condition was achieved by changing the offset frequency (spectrometer frequency + offset frequency = frequency of the carrier wave) and the shape of the FID was brought to a shape as shown in Figure (3.6.c) with the help of the facility provided as a part of the spectrometer. The mechanical adjustment of the magic angle setting was then turned slowly to $54^{o}44'7"$. When the sample rotation axis was very close to the magic angle, the rotational echos, periodic with the rotor period were observed as spikes as shown in Figure (3.6.b). Minor adjustments were then made to the angular setting to get the maximum number of rotational echos which represent the appropriate setting of the magic angle. Three spectra, one at the magic angle, one close to the magic angle and the other one beyond the magic angle along with their FIDs are shown in Figure (3.6).

3.4.3 SETTING UP ON A NUCLEUS

Setting up on a nucleus basically consists of

i) Hardware changeover for the required nucleus.

ii) Placing the sample in the probe-head.

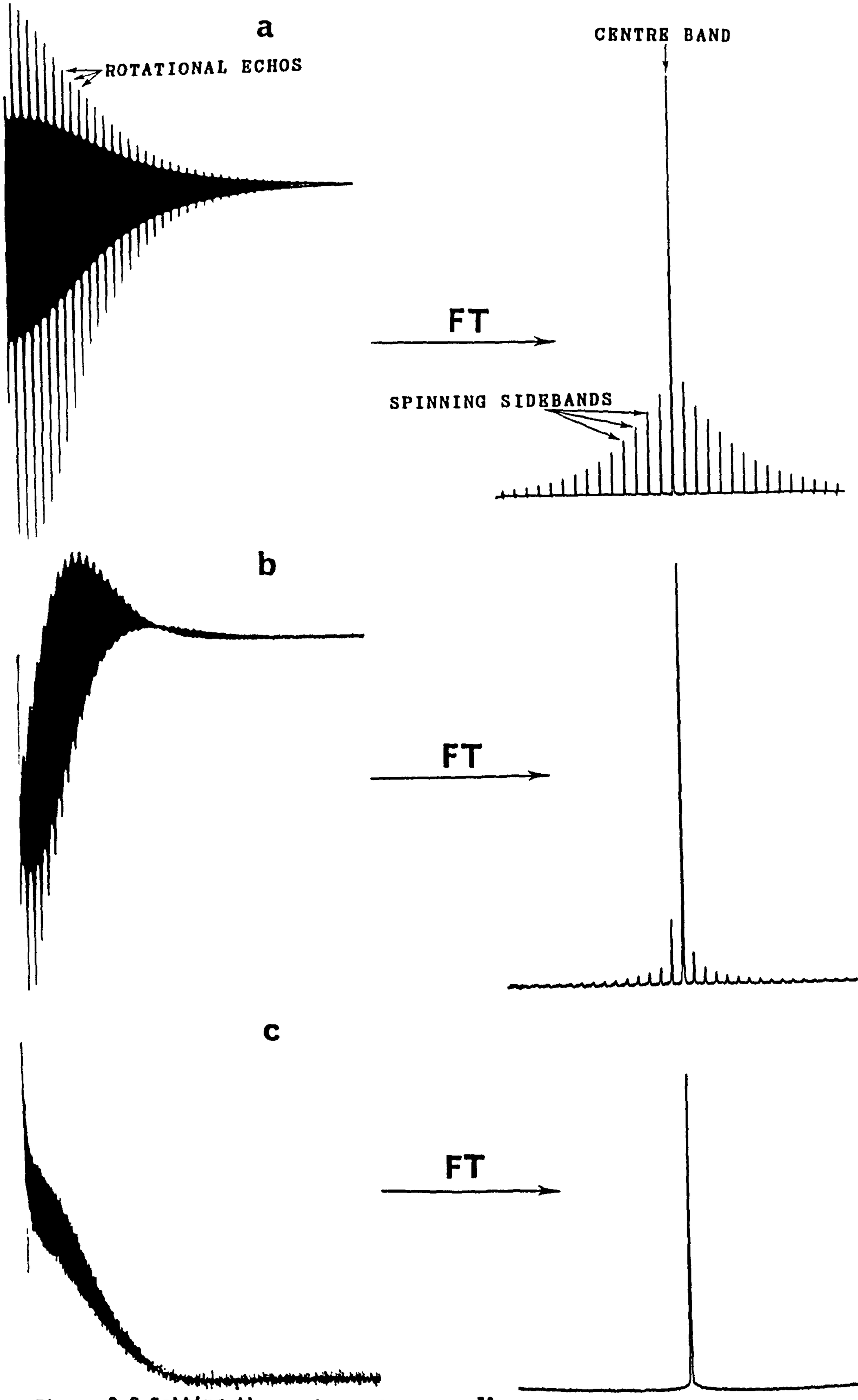

Figure 3.6 Setting the magic angle using ^{79}Br resonance in KBr. (a) At the magic angle, (b) close to the magic angle and (c) on resonance FID beyond the magic angle.

iii) Spinning rate adjustment.

iv) Shimming the magnet.

v) Entering the desired pulse programme into the computer

vi) Entering acquisition parameters.

vii) Tuning the probe.

viii) Adjustment of the receiver gain.

Hardware changeover is essentially the selection of preamplifier box to set the carrier frequency. As the Bruker MSL-360 spectrometer is equipped with a superconducting magnet, the magnetic field $\vec{B}_0$ is fixed, the carrier frequency was selected by choosing the pre-amplifier and transmitter power amplifiers frequency matching boxes provided with the spectrometer. The boxes are plugged in and retuned to appropriate frequency. The offset frequency was typed in on the keyboard to place spectra within the range of spectral width. The offset frequency shifts the zero of the spectrum by exactly the same amount, i.e. it moves the position of the reference signal (discussed in section 3.4.4) keeping the distance between the carrier frequency and the reference signal constant. The static field $\vec{B}_0$ drifts ~30 Hz per week for the ^{29}Si and changes of offset were necessary with time.

Entering the acquisition parameters consisted of fixing the pulse length, delay between pulses, spectral width (SW) etc. which vary from nucleus to nucleus. The B_1 field used was 4.5mT and the $\pi/2$ pulse length different for different muclei, e.g. $\pi/2$ pulse length for ^{29}Si was 6.5 μs and that for ^{31}P was 4 μs. Therefore selection of pulse length is a key factor for the NMR experiments. The delay between pulses depends on the T_1 relaxation time of the nuclei. The signal

will be saturated unless the delay is properly set. Approximately $4T_1$ between pulses gives unsaturated data (98.2%) which is a means of quantitative NMR studies. The delay between pulses can be made shorter by choosing an appropriate flip angle, θ , for the nuclei having long T_1. Ernst et al. [26] and Dupree et al. [27] give a convenient basis for estimating θ and delay between pulses to optimise signal-to-noise. The sampling time (DW) is automatically calculated as (DW)=1/2(SW).

The receiver gain has to be set properly to prevent overloading which is dependent on the isotopic abundance of the nuclei and the number of nuclei present in the sample within the spinner. The instructions for other adjustments can be found elsewhere [28-30]. Having written a standard file, after setting all these parameters for a specific experiment, one could use that file to run real experiments by recalling that file provided that the probe, pre-amplifier and power amplifier are tuned properly.

3.4.4 MEASUREMENT OF SPECTRUM REFERENCE

The chemical shifts or the peak position of the spectra have been measured relative to standard materials for all the NMR accessible nuclei. Normally a solution state of a material was used for the measurement of spectrum reference (SR). The nucleus of interest of the material has to have a single environment to provide a single resonance line. In fact the SR is the distance in Hz between the centre of the spectral width and this resonance position. The $\vec{B}_0$ field decays with time and as the resonance frequency depends upon the $\vec{B}_0$ field, the measurement of an SR is necessary for both

the high resolution and broad line NMR experiments.

In order to measure an SR, the resonance position obtained from the respective reference material was set to zero and the distance to the centre of the spectral width was found by using the algorithm provided with the spectrometer. A list of the materials chosen for the measurement of SR is given in Table No. 3.1. A detailed list can be made by searching Harris et al. [31] and Laszlo [32,33].

3.4.5 DATA COLLECTION

Having set all the parameters and number of scans (NS) in the standard file one can run the experiment just by recalling the standard file. Data collection was fully automatic and started when the command ZG was typed in by the operator. The accumulation would stop when the NS was completed. If the value of NS was not set before starting the experiment, the experiment could continue until the buffer memory overflows.

Normally a quadrature phase cycling pulse sequence

$$(\pi/m)_{+x} - t(acq) - (\pi/m)_{-y} - t(acq) - (\pi/m)_{-x} - t(acq) - (\pi/m)_{+y} -$$

was used for both the high resolution and static experiments, where m=6 for ^{29}Si and m=2 for other nuclei. For the ^{29}Si the value of t was optimised to get the maximum signal-to-noise ratio [27]. But for quantitative measurements the t was increased until the signal area did not alter. The shape of the signal for $(\pi/2)_{+x}$ and $(\pi/2)_{+y}$ [4] is shown in Figure (3.7).

An analogue to digital convertor performed the digitisation of the signal which was saved in the computer

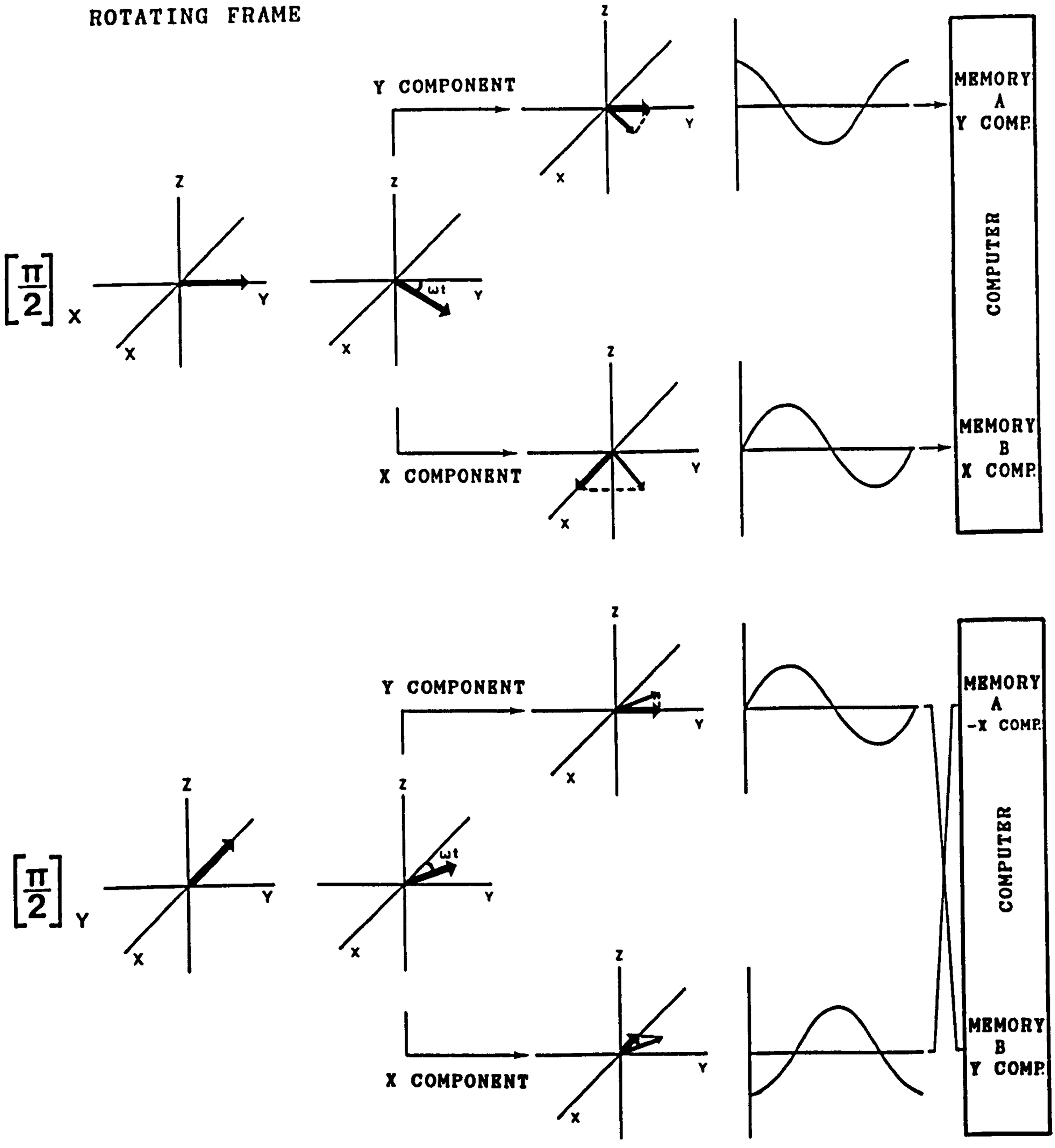

Figure 3.7 Signal corresponding to $(\pi/2)_X$ and $(\pi/2)_Y$ pulse (ref. 4).

TABLE No.3.1 List of the reference materials used for the study of different nuclei.

Name of the nuclei	Name of the reference material	Concentration of the reference material in aqueous solution -(molarity)	Larmor frequency of the nuclei MHz
^{1}H	$Si(CH_3)_4$	-	360.1
^{7}Li	LiCl	0.1	139.91
^{23}Na	NaCl	0.1	95.30
^{27}Al	$Al(NO_3)_3$	0.1	93.83
^{29}Si	$Si(CH_3)_4$	-	71.535
^{31}P	H_3PO_4	85*	145.78

* (%)

memory. The signal was also displayed on the CRT screen at the same time. Finally the accumulated FID was saved on the disc with proper file name and could be retrieved from the memory at any time for processing.

3.4.6 DATA PROCESSING

The achievement of high signal-to-noise (S/N) ratio is essential for accurate interpretation of NMR data. Particularly for minor phases and for absolute signal height measurements the S/N ratio plays an important role. Having the FID on the screen or in the memory of the computer, which is a digitised voltage,a means of increasing the S/N ratio is by multiplying the FID by a Lorentzian function $\exp(-\alpha t)$ or by a Gaussian function $\exp(-\alpha^2 t^2)$ or by the product of these two functions, where α is the line broadening in Hz. The latter can only be applicable to data with very high (S/N) ratio. For the case of Lorentzian function application of α Hz line broadening increases the linewidth $\nu_{1/2}$ to $\nu_{1/2} + \alpha/\pi$ and decreases the signal height as

$$I_2 = \frac{I_1}{1 + \frac{\alpha}{\pi \nu_{1/2}}} \quad \ldots \quad \ldots \quad \ldots \quad (3.5)$$

where $\nu_{1/2}$ = full width at half maximum,
I_2 = signal height with α Hz line broadening and
I_1 = signal height without line broadening.

The area under the spectrum remain constant but an injudicious use of line broadening distorts the line shape.

In this high resolution solid state NMR work the enhancement of S/N was achieved by multiplying the FID by

exp(- α t) and the frequency dependent spectrum was then obtained by Fourier transforming the FID which generally contained a mixture of absorption and dispersion mode signal. The two modes of signal arose because of improper setting of the detector phase which was not a trivial problem. The dead time, i.e. time before data collection, the time required for receiver recovery etc. causes distortion of phase in the spectrum. The effective phase shift becomes larger as the frequency offset becomes larger. Truncation of the FID at the beginning causes distortion of the lineshape because Fourier transformation of the time shifted FID is multiplied by a phase factor which varies linearly with frequency and is proportional to the time shift[29]. Therefore the limit of truncation and the value of α were chosen very carefully, even to be zero, wherever necessary. The Fourier transformed spectrum was then phased by using the algorithm provided with the spectrometer which add the signals from the two phase sensitive detectors to produce an absorption mode signal.

3.5 MEASUREMENT OF T_1 RELAXATION TIME

The spin-lattice relaxation time T_1 is characteristic of the rate of transfer of energy from the nuclear spin system to its surroundings following a perturbation. Therefore, it can be measured by recovering the magnetization along the static field direction by applying a sampling pulse at a time t after a pulse or a group of pulses which perturbs the magnetisation from its equilibrium state. From the several methods [29] for the measurement of relaxation time, a saturating comb was selected for T_1 measurement because in the glasses $T_1 >> T_2$ (T_2 is the spin-spin relaxation time). In

this method a series of $\pi/2$ pulses [34] is applied to saturate the spin system, i.e. the total magnetization M_z=0 at t=0 and then the $\pi/2$ sampling pulse is applied at t=t to sample the recovered magnetization.

The recovery of the magnetization M_z is given by [35]

$$\frac{dM_z}{dt} = \frac{M_0 - M_z}{T_1} \quad \ldots \quad \ldots \quad \ldots \quad (3.6)$$

where M_0 is the thermal equilibrium magnetization. Integration of equ.(3.6) with M_z= 0 at t=0 yields

$$M_z = M_0 [1 - \exp(- t/T_1)] \quad \ldots \quad \ldots \quad (3.7)$$

$$\ln (M_0-M_z) = \ln M_0 - \frac{t}{T_1} \quad \ldots \quad \ldots \quad (3.8)$$

Therefore, for sufficiently long times after saturation, the nuclear spin system has approached a single spin temperature and the relaxation can be described by a simple exponential recovery [36] of the form shown in equ. (3.7). The plot of ln (M_0-M_z) versus t will provide a relaxation pattern of the investigated nuclei.

A series of eight pulses, each of 6.5 μs ($\pi/2$), with 2 ms delay between pulses was employed at t=0 to saturate the ^{29}Si spin system. The separation 2.5ms was chosen to decay the signal completely after each pulse, i.e. the length of the FID is roughly equal to 2 ms. The sampling pulse of 6.5 μs ($\pi/2$) was then applied at t=t to observe the FID. The magnitude of the signal was proportional to the Z component of the partially recovered spin magnetization $M_z(t)$ existing at time t. A pulse sequence used to measure T_1, successive saturation of signal after every pulse, observation of the FID after the

sampling pulse and the spectra showing recovered magnetization for different values of t are shown in Figure No. (3.8).

Typically fifteen experiments with different number of scans (NS) were carried out for diffent values of t. The NS was selected to give a reasonable S/N ratio, approximately 10:1. The values of M_z were then obtained as signal height by Fourier transforming the FID. A set of spectrum collected to measure T_1 in $Li_20.2SiO_2.0.1MnO$ is shown in Figure (3.8). In order to measure M_0, the value of t was varied until the signal height did not alter. According to equ. (3.7), $t=5T_1$ allows almost complete recovery (99.3%) of the magnetization. But when $T_1 > 1500$ s, this is rather time consuming and the corrected values of (M_0-M_z) were obtained as

$$(M_0-M_z)_{corrected} = (M_0-M_z)_{t=t} - (M_0-M_z)_{t=\infty} \quad \ldots (3.9)$$

The corrected values were obtained for $t \sim 3T_1$. However two experiments on the samples having $T_1 \gtrsim 1500$ s were also carried out with $t=5T_1$ and within the experimental error ($\pm$11%), there was no difference in T_1 values. In the case of $24.6Li_20.75.3SiO_2.0.1MnO$ (LS1) two distinct resonance positions were observed. Partial overlap of the resonances may affect the signal height and to examine this effect the area under each was measured by fitting to a Gaussian. The value of T_1 obtained from the plot of these ln (M_0-M_z) versus t was the same as that obtained from the normal signal height measurement.

The longest T_1 recorded in this work was 2300s and an experimental time required to perform this experiment was 72 hours. Despite many lengthy runs and a poor S/N ratio, it was

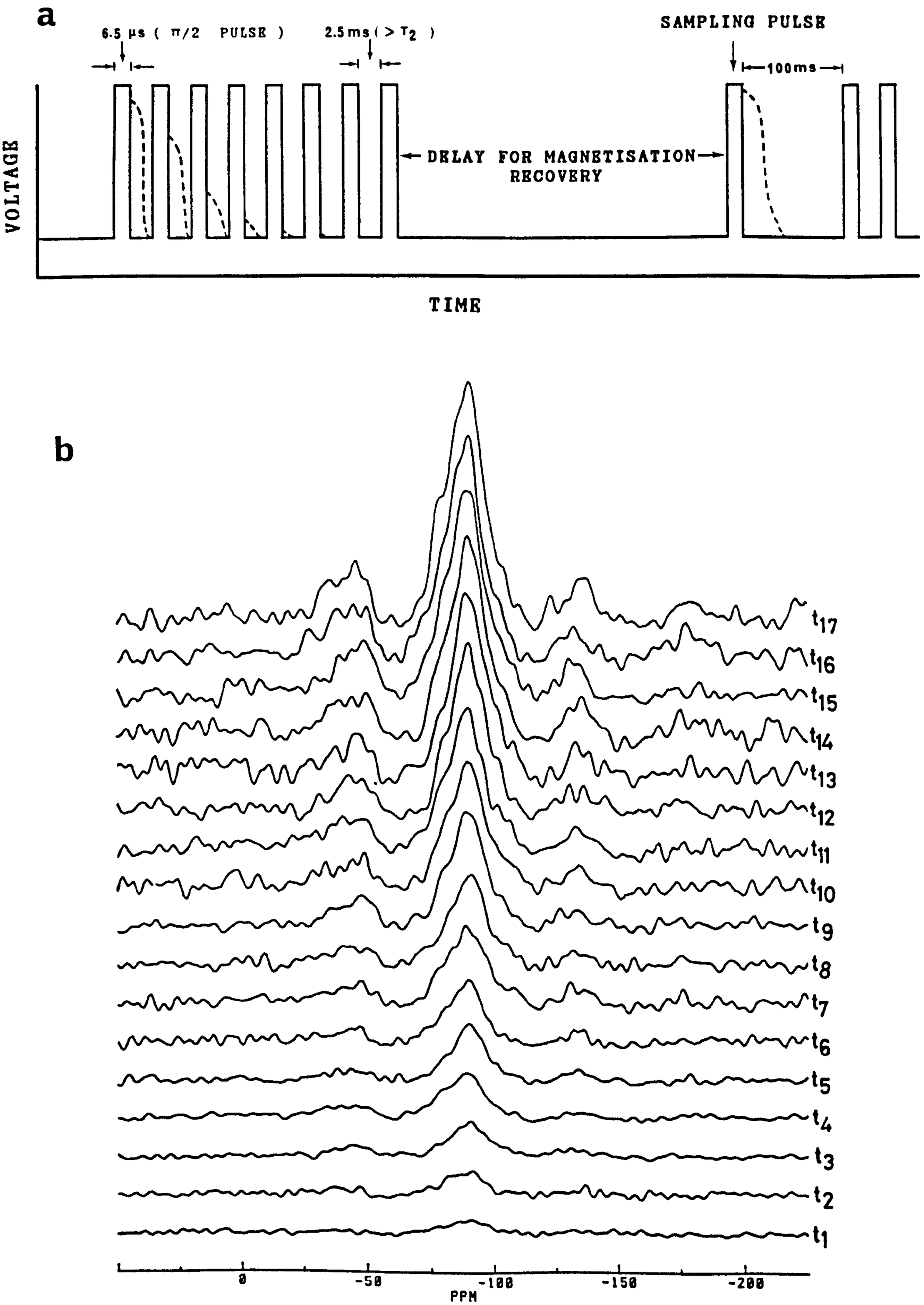

Figure 3.8 (a) Pulse sequence for saturation recovery method. (b) Increase of signal height due to increase of relaxation delays (t) in $Li_2O.2SiO_2.0.1MnO$ (LS3) base glass($t_1 < t_2 < t_3 < ----- < t_{17}$).

estimated from the reproducibility of the results that the T_1 values presented here are correct within an accuracy of measurements of $\pm$ 11%.

3.6 MATERIALS PREPARATION AND CHARACTERISATION

3.6.1 INTRODUCTION

Since we are interested in investigating the structural properties of alkali silicate glasses, simple binary alkali silicates and alkali phosphosilicates were prepared and characterised. According to the National Research Council [37] "characterisation describes those features of the composition and structure (including defects) of a material that are significant for a particular preparation, study of properties, or use and suffice for the reproduction of the material". Therefore quantitative characterisation is the foundation of structural analysis and several methods were employed to characterise the materials. A brief description of the methods used for the characterisation of materials can be obtained from Hench and Gould [38].

3.6.2 CHOICE OF INITIAL MATERIALS

In order to make alkali silicates and alkali phosphosilicates commercially available SiO_2, R_2CO_3, R_3PO_4 and $(NH_4)_2HPO_4$ were chosen as starting materials for the glasses, where R stands for Li, Na and K respectively. The metal carbonate and phosphates decompose at different temperatures [39] as

$$
\begin{aligned}
R_2CO_3 &\xrightarrow{\Delta} R_2O + CO_2 \\
2\,R_3PO_4 &\xrightarrow{\Delta} 3R_2O + P_2O_5 \qquad \ldots (3.10) \\
2\,(NH_4)_2HPO_4 &\xrightarrow{\Delta} 4NH_3 + 3H_2O + P_2O_5
\end{aligned}
$$

and provide required amounts of alkali oxide, phosphorus etc. in the composition. High phosphorus glasses (> 10 mol % P_2O_5) were made using $(NH_4)_2HPO_4$ instead of R_3PO_4 because of additional R provided by R_3PO_4.

3.6.3 PREPARATION OF GLASSES

The nominal composition, melting temperature, time and the optical quality of the glasses included in this study are given in Table 3.2. Powdered raw materials (usually 100g batch) of appropriate amounts were homogenised by rolling for 12 hours prior to melting in electric furnace. The melting temperatures for the glasses LS1-LS5, NS1-NS6 and KS1 were estimated from the temperature composition phase diagram [40-43]. The phase diagrams for Na_2O : SiO_2 = 1:2 with different amounts of P_2O_5 are not available in the literature and the melting temperature was found by trial and error. For sodium disilicate with $10.0 \lesssim P_2O_5 \lesssim 30.0$ mol%, glass making is difficult because of high liquidus temperatures but becomes easier beyond 30.0 mol% P_2O_5. The samples of this compositional region crystallise more readily than the low (<10.0 mol%) and high (>40.0 mol%) phosphorus containing samples.

In order to facilitate the MAS NMR experiments, paramagnetic impurity ($MnCO_3$) was added to most of the batches, as given in Table (3.2), to reduce the ^{29}Si relaxation time, since this is typically 10-60 minutes in an undoped sample. The samples LSP4(b) and NSP11(d) were made without $MnCO_3$ and the control experiments on these samples showed that there was no difference in relative peak intensities due to small additions of $MnCO_3$ (up to 0.1 mol %).

TABLE NO. 3.2 SAMPLE COMPOSITION, PREPARATION AND STATE OF THE GLASSES AND CRYSTALLINE MATERIAL STUDIED

Name of the glasses	Nominal compsition (mol %)				Melting temp. (°C)/ t (h)	Optical quality	XRD of the glasses (NHT)
	R_2O	SiO_2	P_2O_5	MnO			
LS1	25.0	75.0	-	0.1	1400/3	clear	amorphous
LS2	30.00	70.0	-	0.1	1400/3	clear	amorphous
LS3	33.33	66.67	-	0.1	1350/3	clear	amorphous
LS4	37.5	62.5	-	0.1	1250/3	clear	amorphous
LS5	40.0	60.0	-	0.1	1250/3	clear	amorphous
LSP1	33.0	66.0	1.0	0.1	1350/3	clear	amorphous
LSP2	32.5	65.5	2.0	0.1	1350/3	clear	amorphous
LSP3	32.5	65.5	2.0	0.1	1350/3	milky	amorphous
LSP4(a)	32.0	63.0	5.0	0.1	1350/3	milky	crystalline (Li_3PO_4)
LSP4(b)	32.0	63.0	5.0	-	1350/3	milky	crystalline (Li_3PO_4)
LSP5	16.67	33.33	50.0	0.05	200/1.5;1100/2.5	clear	amorphous
NS1	33.33	66.67	-	-	1250/3	clear	amorphous
NS2	33.33	66.67	-	0.05	1250/3	clear	amorphous
NS3	33.33	66.67	-	0.1	1250/3	clear	amorphous
NS4	33.25	66.55	-	0.2	1250/3	clear	amorphous
NS5	33.2	66.4	-	0.4	1250/3	clear	amorphous
NS6	33.05	66.15	-	0.8	1250/3	clear	amorphous
NS7	28.6	71.4	-	0.1	1300/3	clear	amorphous
NS8	25.0	75.0	-	0.1	1350/3	clear	amorphous
NS9	20.0	80.0	-	0.1	1400/3	clear	amorphous
NSP1	33.0	66.0	1.0	0.1	1250/3	clear	amorphous
NSP2	32.5	63.5	2.0	0.1	1250/3	clear	amorphous
NSP3	32.0	63.0	5.0	0.1	1250/3	clear	amorphous
NSP4	30.83	61.67	7.5	0.1	1300/3	clear	amorphous
NSP5	30.0	60.0	10.0	0.1	1500/3	slightly milky	amorphous
NSP6	28.3	56.67	15.0	0.1	200/1.5;1580/4	slightly nucleated + clear	clear portion amorphous
NSP7	26.67	53.33	20.0	0.1	200/1.5;1575/4	slightly nucleated + clear	clear portion amorphous
NSP8	25.0	50.0	25.0	0.05	200/1.5;1575/4	slightly nucleated + clear	clear portion amorphous
NSP9	23.33	46.67	30.0	0.05	200/1.5;1574/4	slightly nucleated + clear	clear portion amorphous
NSP10	20.0	40.0	40.0	0.05	200/1.5;1100/2.5	clear, bubbles	amorphous
NSP11(a)	16.67	33.33	50.0	0.05	200/1.5;1100/2.5	clear	amorphous
NSP11(b)	16.67	33.33	50.0	0.05	200/1.5;1050/2.5	clear	amorphous
NSP11(c)	16.67	33.33	50.0	0.05	200/1.5;1200/2.5	clear	amorphous
NSP11(d)	16.67	33.33	50.0	-	200/1.5;1100/2.5	clear	amorphous
NSP12(a)	13.33	26.67	60.0	0.05	200/1.5;1100/2.5	clear	amorphous
NSP12(b)	13.33	26.67	60.0	0.05	200/1.5;1100/2.5	clear	amorphous
KS1	33.33	66.67	-	0.1	1200/3	clear	amorphous
KSP1	33.0	66.0	1.0	0.1	1200/3	clear	amorphous
KSP2	32.5	65.5	2.0	0.1	1200/3	clear	amorphous
KSP3	32.0	63.0	5.0	0.1	1200/3	clear	amorphous

* R = Li, Na and K for L, N and K respectively.

TABLE NO. 3.2 SAMPLE COMPOSITION, PREPARATION AND STATE OF THE GLASSES AND CRYSTALLINE MATERIAL STUDIED

Name of the glasses	Nominal compsition (mol %)				Melting temp. (°C)/ t (h)	Optical quality	XRD of the glasses (NHT)
	R_2O	SiO_2	P_2O_5	MnO			
LS1	25.0	75.0	-	0.1	1400/3	clear	amorphous
LS2	30.00	70.0	-	0.1	1400/3	clear	amorphous
LS3	33.33	66.67	-	0.1	1350/3	clear	amorphous
LS4	37.5	62.5	-	0.1	1250/3	clear	amorphous
LS5	40.0	60.0	-	0.1	1250/3	clear	amorphous
LSP1	33.0	66.0	1.0	0.1	1350/3	clear	amorphous
LSP2	32.5	65.5	2.0	0.1	1350/3	clear	amorphous
LSP3	32.5	65.5	2.0	0.1	1350/3	milky	amorphous
LSP4(a)	32.0	63.0	5.0	0.1	1350/3	milky	crystalline (Li_3PO_4)
LSP4(b)	32.0	63.0	5.0	-	1350/3	milky	crystalline (Li_3PO_4)
LSP5	16.67	33.33	50.0	0.05	200/1.5;1100/2.5	clear	amorphous
NS1	33.33	66.67	-	-	1250/3	clear	amorphous
NS2	33.33	66.67	-	0.05	1250/3	clear	amorphous
NS3	33.33	66.67	-	0.1	1250/3	clear	amorphous
NS4	33.25	66.55	-	0.2	1250/3	clear	amorphous
NS5	33.2	66.4	-	0.4	1250/3	clear	amorphous
NS6	33.05	66.15	-	0.8	1250/3	clear	amorphous
NS7	28.6	71.4	-	0.1	1300/3	clear	amorphous
NS8	25.0	75.0	-	0.1	1350/3	clear	amorphous
NS9	20.0	80.0	-	0.1	1400/3	clear	amorphous
NSP1	33.0	66.0	1.0	0.1	1250/3	clear	amorphous
NSP2	32.5	63.5	2.0	0.1	1250/3	clear	amorphous
NSP3	32.0	63.0	5.0	0.1	1250/3	clear	amorphous
NSP4	30.83	61.67	7.5	0.1	1300/3	clear	amorphous
NSP5	30.0	60.0	10.0	0.1	1500/3	slightly milky	amorphous
NSP6	28.3	56.67	15.0	0.1	200/1.5;1580/4	slightly nucleated + clear	clear portion amorphous
NSP7	26.67	53.33	20.0	0.1	200/1.5;1575/4	slightly nucleated + clear	clear portion amorphous
NSP8	25.0	50.0	25.0	0.05	200/1.5;1575/4	slightly nucleated + clear	clear portion amorphous
NSP9	23.33	46.67	30.0	0.05	200/1.5;1574/4	slightly nucleated + clear	clear portion amorphous
NSP10	20.0	40.0	40.0	0.05	200/1.5;1100/2.5	clear, bubbles	amorphous
NSP11(a)	16.67	33.33	50.0	0.05	200/1.5;1100/2.5	clear	amorphous
NSP11(b)	16.67	33.33	50.0	0.05	200/1.5;1050/2.5	clear	amorphous
NSP11(c)	16.67	33.33	50.0	0.05	200/1.5;1200/2.5	clear	amorphous
NSP11(d)	16.67	33.33	50.0	-	200/1.5;1100/2.5	clear	amorphous
NSP12(a)	13.33	26.67	60.0	0.05	200/1.5;1100/2.5	clear	amorphous
NSP12(b)	13.33	26.67	60.0	0.05	200/1.5;1100/2.5	clear	amorphous
KS1	33.33	66.67	-	0.1	1200/3	clear	amorphous
KSP1	33.0	66.0	1.0	0.1	1200/3	clear	amorphous
KSP2	32.5	65.5	2.0	0.1	1200/3	clear	amorphous
KSP3	32.0	63.0	5.0	0.1	1200/3	clear	amorphous

* R = Li, Na and K for L, N and K respectively.

All the binary silicates and low phosphorus ($\lesssim$ 10.0 mol %) containing samples were melted in Pt crucibles but the high phosphorus ($\gtrsim$15.0 mol%) containing samples were melted in alumina crucibles, since higher concentrations of P_2O_5 attack Pt. A significant level of contamination, contrary to Nelson and Tallant [44], was obtained from the alumina crucibles. Glasses were kept in vacuum desiccators to prevent reaction with atmospheric moisture.

3.6.4 THERMAL ANALYSIS

A measure of the change of any property of a material when heated or cooled at a constant rate can be obtained from thermal analysis. This in turn can provide information about the reaction occuring and may be used to characterise or identify a material of interest under dynamic temperature conditions. Using the thermal analysis method not all the properties can be measured and factors such as pressure, sample preparation etc. which may affect the reaction characteristics must be controlled.

When a material is heated or cooled at a constant rate it may transform from one phase to another by releasing or absorbing energy. This exothermic or endothermic behaviour in the material can be identified by measuring the change of its temperature or differences in heat flux relative to a reference material. Differential Thermal Analysis (DTA) and Differential Scanning Calorimetry (DSC) are based upon these effects and were used to estimate the 'glass transition temperature', T_g, 'crystallisation temperature', T_x, 'liquidus temperature', T_{ls}, 'fictive temperature', T_f and 'relative

specific heat at constant pressure', Cp, from the endothermic and exothermic dips on the trace.

3.6.4.1 DIFFERENTIAL THERMAL ANALYSIS (DTA)

The principle of DTA is the measurement of the differential temperature between two samples, one of which is an inert reference and the other is the material of interest, when heated at some given rate. A typical DTA trace showing endo- and exothermic phenomena is shown in Figure (3.9). The differential temperature is measured using two thermocouple junctions, each in contact with sample or reference crucible and connected in opposition. Detailed theoretical and practical aspects of DTA can be found elsewhere [45-47].

The most important factors to be considered when carrying out a DTA experiment are

1. sample weight,
2. particle size,
3. heating rate,
4. atmospheric condition surrounding the sample,
5. conditions of packing.

As DTA is a comparative method, the above factors were maintained as identical as possible to attain symmetrical conditions. All the DTA experiments, to estimate the T_g, T_x, T_{ls} or softening point (where sharp peak for T_{ls} was not observed), were carried out using a Stanton Redcroft 1500 DTA instrument. The heating rate for the experiments was 6^oC/min and the reference material used was SiO_2 under normal atmosphere and pressure.

3.6.4.2 DIFFERENTIAL SCANNING CALORIMETRY (DSC)

DSC is also a comparative technique like DTA. The major application of DSC are to measure thermodyamic parameters [48-52], e.g. fictive temperature, specific heat, structural

transitions, phase diagram etc. and kinetic parameters [53], e.g. kinetics of phase transition, recrystallisation etc. DSC measures the thermal power flowing between the sample and the thermostated enclosure. The measurement of the heat transfer is made by means of a thermoelectric pile. Therefore the heat absorbed or evolved during the course of heating or cooling can be measured directly either as a function of time or temperature with respect to a reference material.

In the present work the dependence of the limiting fictive temperature on cooling rate of NSP12(b) was estimated according to the method proposed by Moynihan et al. [48] with the help of a Setaram HT1000 calorimeter. The heating and cooling rates, sensitivity and all other experimental conditions, e.g. sample weight (1.805 $\pm$ 0.003 g), crucibles etc. were the same throughout the experiments.

According to Moynihan [48], the fictive temperature, T_f, i.e. the temperature at which the structure of glass would be the equilibrium and which is a function of the cooling rate [55-57] at temperature T' may be calculated from

$$H(T') = H_e(T_f) - \int_{T'}^{T_f} \left(\delta H/\delta T\right)_g \, dT \quad \ldots \quad (3.11)$$

where H is the enthalpy and the subscript e, g refer to the equilibrium and glass respectively. Differentiation followed by integration of equ.(3.11) would give us

$$\left[\left(\frac{dH}{dT}\right) - \left(\frac{\delta H}{\delta T}\right)_g\right]_{T'} = \left[\left(\frac{\delta H}{\delta T}\right)_e - \left(\frac{\delta H}{\delta T}\right)_g\right]_{T_f}$$

$$\int_{T^*}^{T'} (C_p - C_{pg})\, dT = \int_{T^*}^{T_f} (C_{pe} - C_{pg})\, dT_f \quad \ldots \quad (3.12)$$

Here T* is any temperature above the transition region at which the specific heat C_p is equal to the equilibrium liquid value, C_{pe}, and T' is a temperature well below the transition region. Therefore according to equ.(3.12) the value of T_f can be calculated from the boundary of the difference of two integrals as shown in Figure (3.10).

3.6.5 X-RAY DIFFRACTION STUDIES

The amorphicity of the glasses studied in this thesis were checked using a Philips Powder Diffractometer and are presented in Table (3.2). The phases in the devitrified materials were also identified using this technique by comparing the experimental interplanar spacing and the intensity of the diffraction pattern with the standard JCPDS powder diffraction files. Powder samples mounted on thin pyrex glass slides using silicone grease were examined in the experiments using Cu K_α (λ =1.54178 A) radiation. This is an established technique and described already by Klug and Alexander [58].

3.6.6 MICROSTRUCTURE STUDY OF GLASS CERAMICS

3.6.6.1 ELECTRON MICROSCOPY

Electron microscopy could be a useful tool for microstructural analysis in glass-ceramics [59-65]. The technique provides a direct image from which glass-in-glass phase separation, morphology of crystallisation, composition etc. can be predicted. Unfortunately in glasses, except for homogeneity and composition, little structural information can be obtained. Microscopy is suitable for long range order

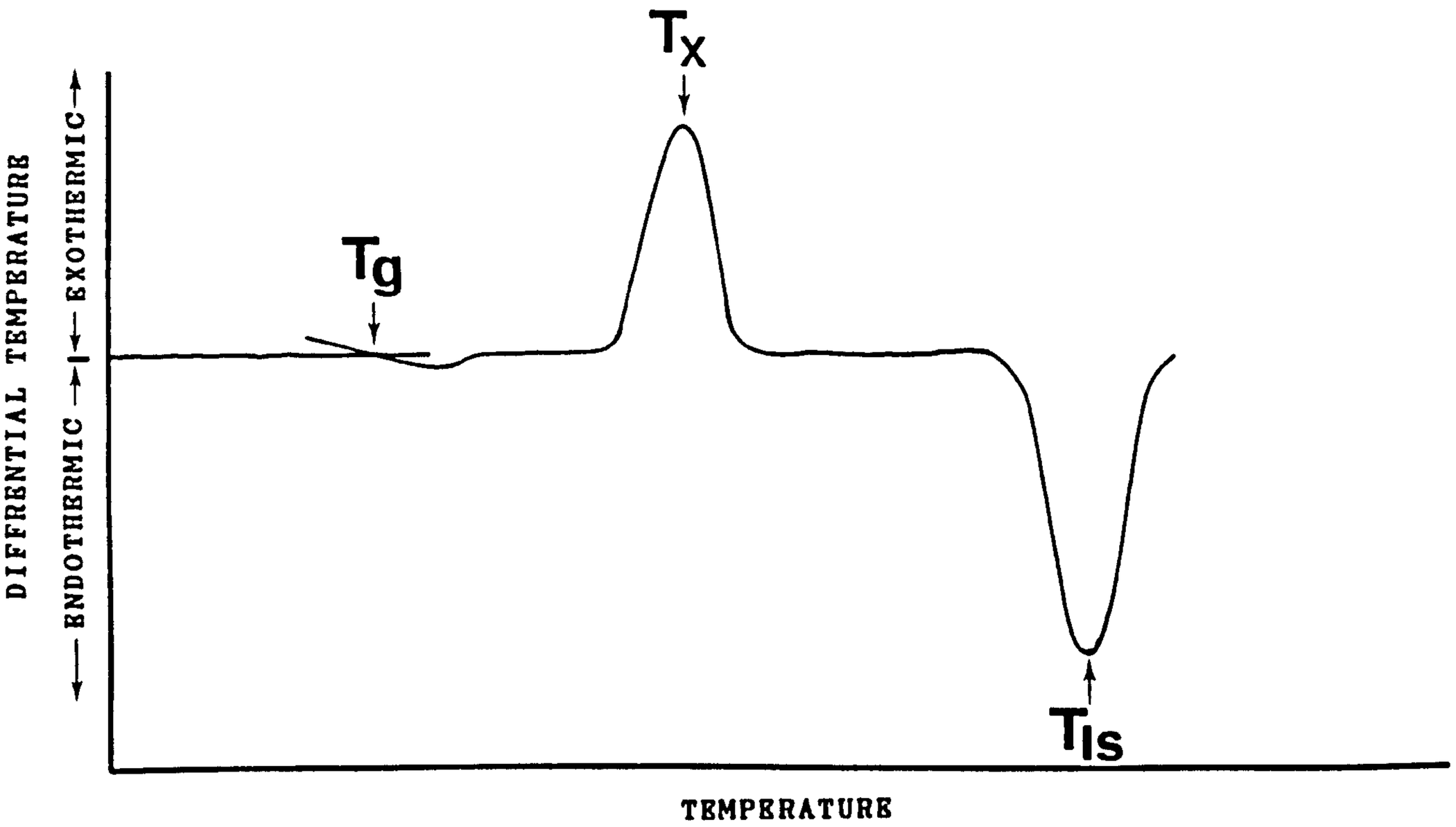

Figure 3.9 A typical DTA curve showing the transformation temperatures.

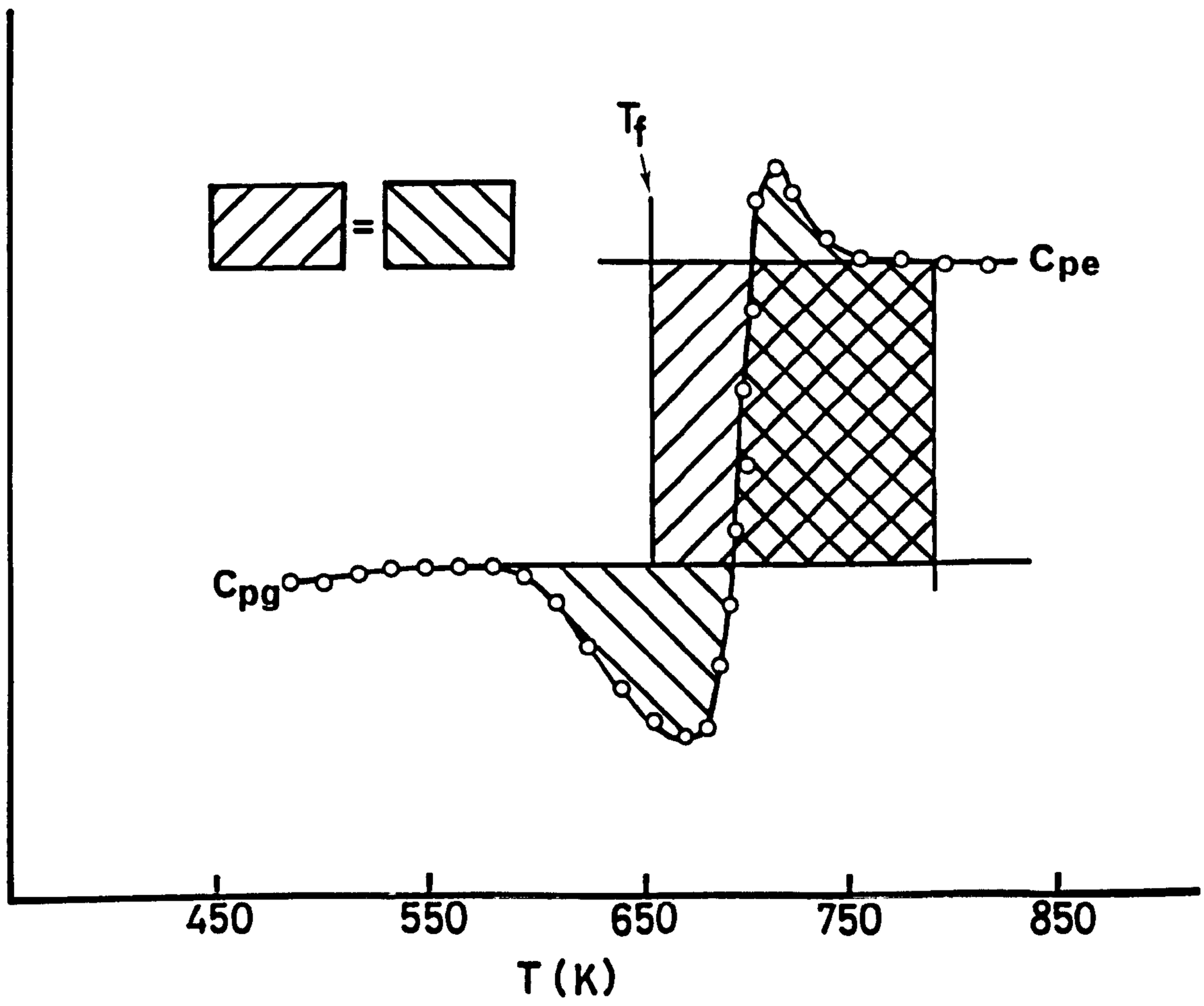

Figure 3.10 Heat capacity vs. temperature for $16.67Na_2O.33.33SiO_2.50.0P_2O_5$ glass determined at a heating rate 300 °K/h. The line indicating the difference between two areas of equ. 3.12 represents the fictive temperature, T_f.

analysis and the principles and applications of the technique are explained in the texts by Bowen and Hall [66] and McMillan [67]. The detailed experimental technique can also be found in microscopy hand books [68].

In the present work Transmission Electron Microscope (TEM) was used to examine the phase separation in LS1, LS2, LSP4(a), NSP5 and in NSP11(a). Scanning Electron Microscope (SEM) was used to analyse the compositions via EDX.

3.6.6.1.1. SAMPLE PREPARATION FOR SEM

In order to analyse composition bulk specimen (10x10x1 mm^3) of sodium phosphosilicate glasses (NSP1- NSP3, NSP11(a)) were mounted in conducting bakelite and were polished using polishing disks, silicon carbide papers (220 - 1200 grit) and polishing pads (1-6 μm) to 1 μm. The specimens were washed with cotton soaked with 1-1-1 trichloroethane (genklene). As the alkali phosphosilicate glasses are water sensitive [39], an oil based lubricant was employed during polishing.

All the specimens were coated with carbon of estimated thickness 10-50 Å to prevent charging in the electron beam. A Cambridge electron microscope was used for imaging and analysis. The typical operating conditions were at 20 KV with beam current around 100 Å.

3.6.6.1.2 SAMPLE PREPARATION FOR TEM

The samples were prepared using two techniques :

i) Chemical Thinning
ii) Ion beam Thinning

as described below:

i) CHEMICAL THINNING : Specimens of LS1 (as cast and heat treated), LS2 and NSP11(a) were prepared from bulk material.

Thin slices (~ 1500 μm) of the samples were cut by using a diamond impregnated wheel. The slices were mounted on a thick glass slides (0.6 cm) using resin and thinned to ~120 μm by polishing as described in section 3.6.6.1.1. The thin specimens were removed from the glass and washed in an ultrasonic bath with genklene. Finally the specimens were prepared by chemical thinning described by James et al. [60].

ii) ION BEAM THINNING : The specimens of LS1, LS2, LSP4(a), NSP5 and NSP11(a) were prepared using ion beam thinning. A portion of the thin (~ 120 μm) slice of the samples were abraded with a stream of 0.5 μm alumina particles (carried by compressed N_2 gas) to thin to~80 μm and 3 mm. diameter discs were then drilled out from the centre using an ultrasonic drill. Silicon carbide powder was used during drilling the specimen. The discs were washed as before and mounted on brass rings of outer diameter 3mm and inner diameter 2.4 mm using glue (araldite). The discs were then thinned in an Edwards Argon ion beam thinning machine. The discs were mounted at an angle about 30^{o} away from the direction of the incident beam and the accelerating potential was 5 kV.

All the specimens were coated with carbon as before. A JEM transmission electron microscope operating at 100 kV was used.

3.7 CHEMICAL ANALYSIS

The nominal compositions of the materials do not remain constant during melting of the glasses. Therefore knowledge of the final composition of the glasses is an essential part of the structural analysis.

Most of the glasses studied in this thesis were analysed chemically using wet chemical analysis and atomic absorption spectrophotometry. The analysis of some of the components, as indicated in Table (3.3), were carried out using these chemical techniques and EDX as well as MAS NMR to compare the results. A good agreement was obtained between the different techniques.

3.7.1 WET CHEMICAL ANALYSIS

The samples LS1-LS4, NS1-NS4, KS1 and KSP1-KSP3 were analysed using the British standard method [69] recommended for the chemical analysis of glasses. In LS1-LS4, NS1-NS4 glasses only the amounts of silica were determined and the amounts of alkalis were obtained by difference by assuming that the amounts of MnO remained unchanged during melting. In addition the concentration of MnO in NS1-NS4 were also analysed using ultraviolet-visible spectrophotometry (discussed in section 3.7.3) and the level of MnO did remain constant within the experimental error. In the KS1, KSP1-KSP3 glasses, the concentrations of silicon were determined using this method and the amounts of P_2O_5 were determined using NMR. The amounts of K_2O were obtained by subtraction.

Commercially available reagents suggested by the British standard [69], British standard glass wares, e.g. sintered glass crucibles of porosity Grade No.4 [70] and platinum crucibles were used to analyse the glasses. A list of the nominal compositions and the final compositions of the aforesaid glasses are given in Table (3.2) and (3.3) respectively.

3.7.2 ATOMIC ABSORPTION SPECTROPHOTOMETRY (AAS)

The chemical analyses of the samples NS1-NS4, and NSP1-NSP12 were carried out using a Varian Techtrons Model AA-6 atomic absorption spectrophotometer and Hilger analytical hollow cathode lamps. The concentrations of Na_2O, SiO_2 and Al_2O_3, in NSP6-NSP12 were determined and the amounts of P_2O_5 were obtained by difference. The standard solutions for Na and Al were prepared using NaCl and aluminium foil respectively and that for Si was obtained from BDH chemicals Ltd. In order to prevent the effects of interference, appropriate reagents were added to the standard solutions as described in the Varian techtrons manual [71]. The working conditions were also set according to the given instructions [71].

The calibration curves were made by plotting the absorption intensity versus the concentrations of the elements. The solutions of the samples were prepared [71] and the levels of each element were then determined from the respective calibration graph. The final compositions of the samples are given in Table (3.3).

Wet chemical analysis and EDX as well as MAS NMR experiments were carried out on some samples, as mentioned in Table (3.3), to confirm the AAS results. Good consistency was obtained within the experimental error ($\pm$ 2%).

3.7.3 UV SPECTROSCOPY

A Varian DMS-90 UV visible spectrophotometer was used to analyse the concentration of MnO in LS1-LS4 and NS3-NS6 glasses. The spectrophotometer was calibrated using Mn metal

TABLE NO.3.3 CHEMICALLY ANALYSED COMPOSITIONS OF THE GLASSES.

Name of the samples	FINAL COMPOSITIONS (mol %) ±2%				
	R_2O	SiO_2	P_2O_5	Al_2O_3	Mno
LS1	24.6	75.3	-	-	0.1
LS2	29.2	70.7	-	-	0.1
LS3	32.9	67.0	-	-	0.1
LS4	36.6	63.3	-	-	0.1
LS5	39.3	60.7	-	-	0.1
LSP1+	32.1	66.87	0.93	-	0.1
LSP2+	31.9	66.12	1.88	-	0.1
LSP4(a)+	31.5	64.1	4.30	-	0.1
NS1*	32.69	67.3	-	-	-
NS2*	32.6	67.3	-	-	0.05
NS3*	32.6	67.3	-	-	0.1
NS4*	32.1	67.7	-	-	0.19
NS5	31.9	67.7	-	-	0.4
NS6	32.2	67.1	-	-	0.81
NSP1++	32.05	67.04	0.91	-	0.1
NSP2++	32.03	66.12	1.84	-	0.1
NSP3++	31.57	64.45	3.98	-	0.1
NSP4	30.12	61.96	6.12	-	0.1
NSP5	29.12	62.95	7.92	-	0.1
NSP6	27.03	59.33	11.04	2.60	0.1
NSP7	25.69	55.02	16.07	3.12	0.1
NSP8	24.4	52.81	19.69	3.10	0.1
NSP9	22.83	48.90	25.02	3.20	0.05
NSP10	19.61	41.30	38.12	0.95	0.05
NSP11(a)++	15.96	36.01	46.79	1.24	0.05
NSP12	13.01	28.32	57.26	1.46	0.05
KS1	32.7	67.2	-	-	0.1
KSP1	32.0	67.0	0.90	-	0.1
KSP2	32.1	66.0	1.79	-	0.1
KSP3	31.6	64.29	4.01	-	0.1

+ amounts of P were estimated by MAS NMR and Si by wet chemical.

* verified by using wet chemical analysis and AAS.

++ checked by using EDX, MAS NMR and AAS.

solution of different concentrations covering the range of interest. Two sets of solutions, with and without manganese were made using the procedure described in Methods of analysis [72]. The difference in optical densities between the Mn-free solution and the Mn-containing solution plotted against the concentration of Mn in the Mn-containing solutions were used to make the calibration curve. The emission intensities were recorded at 545 nm using a 10 mm cell and the scanning speed was 10 nm/min.

The solution of the samples of interest were made using the procedure described in the Methods of analysis [72] and the corresponding optical densities were measured using water as the reference solution. The concentrations of MnO in the samples were then determined from the calibration graph and are presented in Table (3.2). The British standard glass wares and platinum crucibles were used to carry out this analysis.

3.8 INFRARED SPECTROPHOTOMETRY

Infrared spectroscopy is the study of the vibration of inter-atomic bonds in molecules of a material when electromagnetic radiation in the infrared region falls on a sample. The natural vibrational frequencies of bonds in the molecules are different due to different environment and a range of vibrational modes are observed when infrared light of wavelength 2-1000 μm impinges on the material. The vibrational energies contain structural information. The vibrational modes in glasses are generally broad relative to their crystalline form and quantitive information is rather difficult. The transition energies are generally expressed in

terms of wave number (cm^{-1}). Therefore the vibrational frequencies range from 5000 to 10 cm^{-1}. Theoretical and practical aspects of this technique can be obtained elsewhere [73-75].

Transparent pellets of thickness 0.001 cm were made using powder samples intimately mixed with alkali halides (KBr, CsI). A Perkin Elmer PE 983 infrared spectrophotometer was used to carry out the experiments.

REFERENCES

1. A. Abragam, Principles of Nuclear Magnetism, Oxford, 1985.

2. T. C. Farar and E. D. Becker, Pulse and Fourier Transform NMR, Academic Press, London, 1971.

3. C. P. Slichter, Principles of Magnetic Resonance, 2nd Edn., Springer Verlag, 1980.

4. A. E. Derome, Modern NMR techniques for chemistry research Oxford, 1987.

5. H. C. Torrey, Phys. Rev., 76, 1059 (1949).

6. E. L. Hahn, Phys. Rev., 80, 580 (1951).

7. I. J. Lowe and R. E. Norberg, Phys. Rev., 107, 46 (1957).

8. W. G. Clark, Rev. Sci. Inst., 35, 316 (1964).

9. R. R. Ernst and W. A. Anderson, Rev. Sci. Inst., 37, 93 (1966).

10. F. Bloch, Phys. Rev., 70 (7-8), 460 (1946).

11. J. W. Cooley and J.W. Tukey, Math. Comput., 19, 297 (1965).

12. A. G. Redfield and S. D. Kunz, J. Magn. Reson., 19, 250 (1975).

13. 'MSL System description' Bruker Manual, Ref. No. 431001, 1986.

14. 'Aspect 3000 MSL software manual', Bruker Manual, 1986.

15. NMR probehead, series MAS-DB, Bruker manual, 1985.

16. I. J. Lowe and C. E. Tarr, J. Sci. Inst., 2, 320 (1968).

17. E. R. Andrew, Prog. Nucl. Magn. Reson., 8, 1 (1971).

18. User's manual for solid state probes, Doty Scientific Instruments, Columbia, U.S.A.

19. W. A. Anderson, Rev. Sci. Inst., 32, 241 (1961).

20. E. R. Andrew, A. Bradbury and R. G. Eades, Arch. Sci., Geneva 11, Fasc. Spec., 223 (1958).

21. E. R. Andrew, A. Bradbury and R. G. Eades, Nature, London, 182 1659 (1958).

22. E. R. Andrew, A. Bradbury and R. G. Edes, Nature, 183, 1802 (1959).

23. I. J. Lowe, Phys. Rev. Lett., 2 (7), 285 (1959).

24. J. S. Frye and G. E. Maciel, J. magn. Reson., 48, 125 (1982).

25. M. E. Smith, Ph.D. Thesis, Physics Department, Warwick University, U.K, 1988.

26. R. R. Ernst and W. A. Anderson, Rev. Sci. Inst., 37, 93 (1966).

27. R. Dupree and M. E. Smith, J. Magn. reson., 75, 153 (1987).

28. Users Manual, MSL series, Bruker manual, 1985.

29. Eiichi Fukushima and S. B. W. Roeder, Experimental pulse NMR, Addison-Wesley, 1981.

30. M. L. Martin, J. J. Delpuech and G. J. Martin, Practical NMR spectroscopy, Heydew & Son Ltd., 1980.

31. R. K. Harris and B. E. Mann, NMR and the periodic table, Academic Press, 1978.

32. P. Laszlo, NMR of the newly accessible nuclei, Academic Press, Vol.1 (1983).

33. P. Laszlo, NMR of the newly accessible nuclei, Academic Press, Vol.2 (1983).

34. J. L. Markley, W. J. Horsely and M. P. Kleim, J. Chem. Phys., 55, 3604 (1971).

35. F. Bloch, Phys. Rev., 70, 460 (1946).

36. D. Barnard and I. J. Lowe, Phys. Rev. Lett., 11, 258 (1963).

37. Characterisation of materials, "The Materials Advisory Board Publication MAB-229-M, National Academy of Sciences - National Academy of Engineering, Washington, D.C., March 1967.

38. L. L. Hench and R. W. Gould, Characterisation of Ceramics, Marcel Dekker, Inc., New York, 1971.

39. Hand Book of Chemistry and Physics, 55th Edn., CRC Press 1974-75.

40. F. C. Kracek, J. Phys. Chem., 34, 2641 (1930).

41. F. C. Kracek, J. Phys. Chem., 34, 1588 (1930).

42. F. C. Kracek, J. Am. Chem. Soc., 61, 2869 (1939).

43. F. C. Kracek, N.L. Bowen and G. W. Morey, J. Phys. Chem., 41, 1188 (1937).

44. C. Nelson and D. R. Tallant, Phys. Chem. Glasses, 25(2), 31 (1984).

45. W. J. Smothers and Y. Chiang, Differential thermal analysis: Theory and Practice, Chem. Pub. Co., New York.

46. R. C. MacKenzie and B. D. Mitchell, Analyst, 87, 420 (1962).

47. R. Melling, F. W. Wilburn and R. M. McIntosh, Anal. Chem 41(10), 1275 (1969).

48. C. T. Moynihan, A. J. Easteal, M. A. DeBolt and J. Tucker J. Am. Ceram. Soc., 59 (1-2), 12 (1976).

49. M. A. DeBolt, A. J. Easteal, P. B. Macedo and C. T. Moynihan, J. Am. Ceram. Soc., 59 (1-2), 16 (1976).

50. J. P. Bros, E. Calvet, C. Prunier, Acad. Sci., 258, 170 (1964).

51. R. Castanet, J. P. Bros., M. Laffite, J. Chem. Phys., 64, 1536 (1968).

52. I. Avramov, E. Grantscharova and I. Gutzow, J. Non-Cryst. Solids, 91, 386 (1987).

53. A. Souchan, M. Soustelle, R. Lalauze, Bull. Soc. Chim. Fr., 327 (1976).

54. R. O. Davies and G. O. Jones, "Thermodynamic and Kinetic Properties of Glasses", Adv. Phys., 2(7), 370 (1953).

55. A. Q. Tool, J. Am. Ceram. Soc., 29(9), 240 (1946).

56. H. N. Ritland, J. Am. Ceram. Soc., 39(12), 403 (1956).

57. O. S. Narayanaswamy, J. Am. Ceram. Soc., 54(10), 491 (1971).

58. H. P. Klug and L. E. Alexander, X-ray Diffraction Procedures, John Wiley and Sons., 2nd Edn., 1973.

59. J. W. Cahn and R. J. Charles, Phys. Chem. Glasses 6(5), 181 (1965).

60. P. F. James and P. W. McMillan, Phil. Mag., 18, 863 (1968).

61. T. P. III. Seward, D. R. Uhlmann, D. Turnbull, J. Am. Ceramic. Soc. 51, 278 (1968).

62. P. F. James and P. W. McMillan, Phys. Chem. Glasses, 1(3), 59 (1970).

63. P. F. James and P. W. McMillan, Phys. Chem. Glasses, 1193), 64 (1970).

64. P. F. James and P. W. McMilan, J. Mater. Sci., 6, 1345 (1971).

65. M. Ito, T. Sakaino, T. Moriya, Bull. Tokyo Inst. Tech., 88, 127 (1968).

66. D. K. Bowen and C. R. Hall, Microscopy of materials, The MacMillan Press Ltd., London (1975).

67. P. W. McMillan, Glass ceramics, Academic Press, London, 1979.

68. Miscroscopy hand books, Royal Microscopical Society, Oxford University Press, 1984.

69. British standard methods for the analysis of glass, B.5. 2649, Part 2, 1957.

70. British standard methods for the analysis of glass, B.5. 1752, Part 2, 1957.

71. Instruction manual, Varian Techtrons, Atomic Absorption spectrophometer, Model AA-6.

72. Methods of analysis - Materials Science Division, British Glass Industry Research Association, Part 2, Page, No.56.

73. L. J. Bellamy, Infrared spectra of complex molecules, 3rd Edn., 1975.

74. G. Herzberg, Molecular spectra and Molecular structure II, Infrared and Raman spectra of polyatomic molecules, D. Van Nostrand, New York, 1945.

75. E. B. Wilson, J. C. Decius and P. C. Cross, Molecular vibrations, McGraw Hill, New York, 1955.

CHAPTER 4

LITHIUM SILICATE SYSTEM

4.1 INTRODUCTION

Lithium silicate is the basis of many glass ceramics used in industry [1]. Numerous studies [2-13] have already beem made on this system using XRD, high resolution electron microscopy, infrared and Raman spectroscopy etc. MAS NMR is a relatively new technique for the investigation of local order of nuclei in glasses and a few studies [14-18] have also been carried out on the system. However the studies carried out by Schramm et al. [14], Selvaray et al. [15] and Grimmer et al. [16] are not in agreement with each other. The results of Schramm et al. and Selvaray et al. have been criticised by Gladden et al. [19].

X-ray crystallographic studies of [3-6] crystalline lithium silicates confirm the presence of different Q_m ($0 \leqslant m \leqslant 4$) species. However, due to lack of symmetry and overlapped resonances in glasses, determination of structure is rather complicated. The species Q_m in lithium silicate glasses resonate at different frequencies. The observed chemical shifts for the local environment of the Q_m species in lithium silicate crystals are -64 PPM(Q_0), -67 PPM(Q_1), -75 PPM(Q_2), and -93 PPM(Q_3) [14]. The shifts in glasses are not very different from the crystalline species and a comparison would allow identification of the species.

The Li_2O-SiO_2 system has a wide glass forming region [1] and the glasses LS1-LS5 and LSG1-LSG3, prepared by conventional method and by sol-gel respectively, are chosen for this study. The nuclei ^{29}Si and ^{7}Li in both the glass and crystalline compounds are investigated using NMR as well as proton NMR in the glasses LSG1-LSG3. ^{16}O has zero spin and

consequently it has no magnetic moment. Isotopic enrichment of ^{17}O is possible but has not been used in this work. In addition to NMR, DTA, XRD and electron microscopy are also employed to understand the system. A relatively clear picture about the local order of the network former and its next nearest neighbour is presented in this chapter.

4.2 CONVENTIONALLY PREPARED LITHIUM SILICATE GLASSES

4.2.1 ^{29}Si NMR

The ^{29}Si MAS NMR spectra of lithium silicate glasses (LS1-LS5) and their analysed compositions (mol%) are shown in Figure (4.1.a). The static spectra of the respective glasses are shown in Figure (4.1.b). The gradual formation of Q_3 from Q_4 upto 33.3 mol% Li_2O and then Q_2 from Q_3 for higher concentration of Li_2O is evident from the spinning spectra. Such a change is also observed by Dupree et al. [20-22] in other alkali silicate glasses. The spinning side bands (SS) corresponding to Q_2 and Q_3 species have been observed. This is due to the fact that the spinning of the sample at the magic angle removes the anisotropic part of the central lineshape and produces those SS as additional peaks (see section 2.4.3). There is no SS observed corresponding to Q_4 resonance because anisotropy associated with Q_4 is small, as described by Dupree et al. [21]. The variation of electron density around the silicon nuclei due to incorporation of Li^+ ions into the structure causes a change of the resonance position and can be identified from the chemical shift scale.

The ^{29}Si NMR spectral parameters are summarised in table (4.1). From the table it is clear that the chemical shift

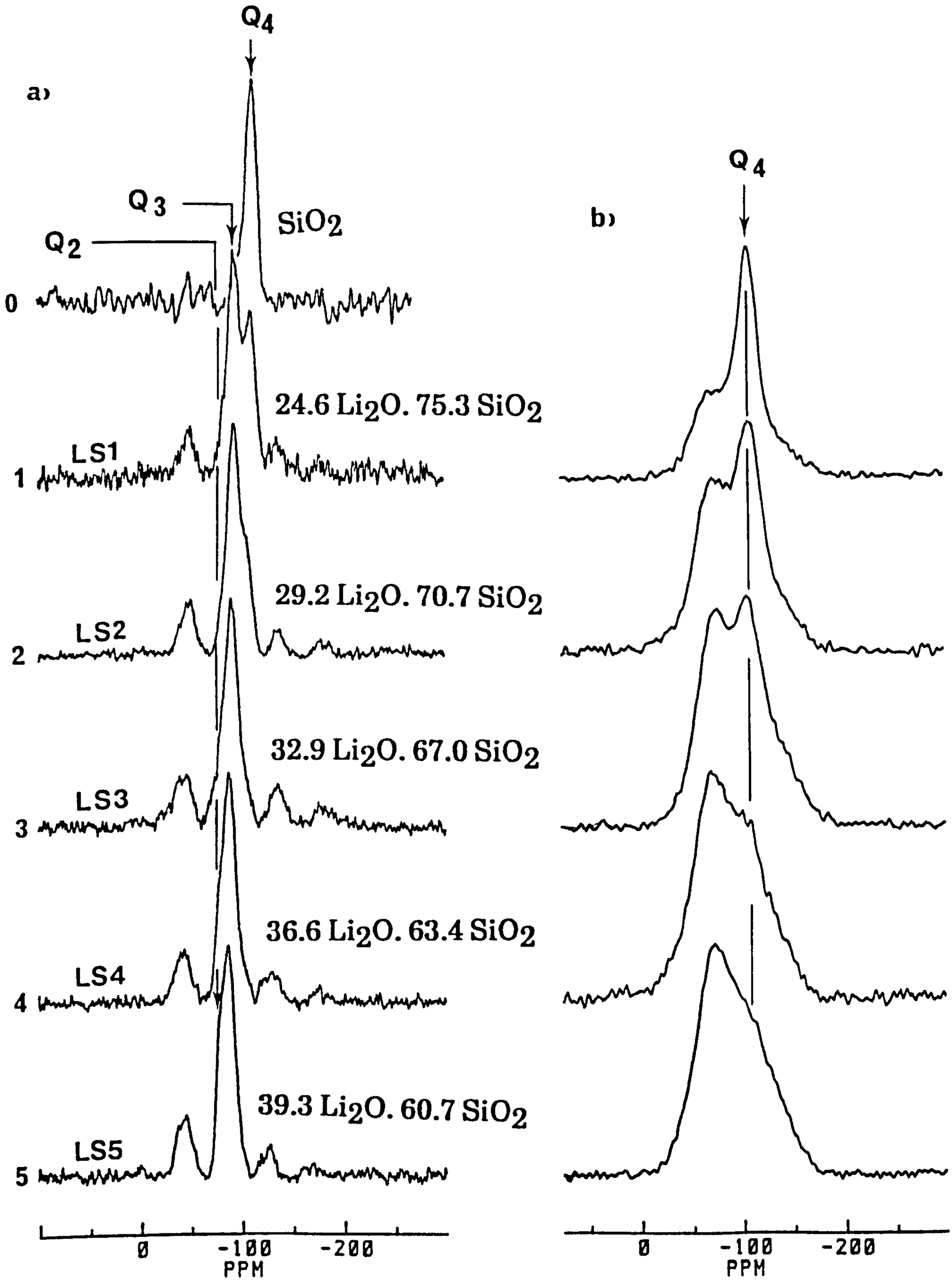

Figure 4.1 ^{29}Si spectra of lithium silicate glasses as prepared: (a) spinning and (b) static. The actual compositions are given in the figure.

TABLE NO.4.1 ^{29}Si NMR DATA FOR Li_2O - SiO_2 SYSTEM

Sample	Concentration of Li_2O (mol%) ±2%	^{29}Si spectral parameters (PPM) ±0.5						Amounts of (%) ±4%		
		Q_4		Q_3		Q_2				
		CS[a]	FWHM[b]	CS	FWHM	CS	FWHM	Q_4	Q_3	Q_2
LS1	24.6	-109.8	13.5	-92.7	15.0	-	-	33.8	66.2	-
LS2	29.2	-107.1	12.2	-91.5	15.9	-	-	16.5	83.5	-
LS3	32.9	-105.3	12.0[c]	-90.0	16.8	-77.4	7.8	10.2[c]	81.5	8.3[c]
LS4	36.6	-103.1[c]	10.3[c]	-88.7	15.0	-76.8	8.1	5.3[c]	75.8	18.9
LS5	39.3	-102.2[c]	9.0[c]	-87.0	14.0	-75.5	10.7	3.4[c]	67.1	29.5

a) CS = Chemical shift

b) FWHM = Full width at half maximum

c) error is ±1.0

changes for both the Q_3 and Q_4 species with the concentration of Li_2O. Thus the resonances of the species cover a wide range as shown in Figure (4.2). A plot of chemical shift versus concentration of Li_2O is shown in Figure (4.3.). However, the resonance positions are not well-resolved for relatively small amounts of Q_4 species in the spinning spectra. Chemical shift dispersion due to structural disorder in glasses often causes a peak of low intensity to merge with one of high intensity. This creates a problem for the identification or quantification of the species.

The ^{29}Si static NMR spectra (Figure 4.1.b) resolves the problem to some extent. The static spectra of the glasses clearly indicate the presence of Q_4 units in these glasses which are more than the minimum required by stoichiometry; consistent with Stebbins [23] investigation in sodium silicate glasses. The amounts of Q_4 species in these glasses are more than that in sodium silicates because the free energy of mixing is comparatively lower in Li_2O-SiO_2 system [24].

Stoichiometrically the samples with less than 33.3 mol% Li_2O need contain only Q_4 and Q_3 species as is described by Grimmer et al. [16] and Dupree et al. [21] and these are evident from both the static and spinning spectra (Figure 4.1). There is no anisotropy associated with the Q_4 resonance but Q_3 is near axially symmetric. The signal due to Q_4 appears on the top of Q_3's anisotropy broadened lineshape. This provides a means of detecting low amounts of SiO_4 tetrahedra in the material. The presence of Q_2 species is not obvious in these materials.

In order to clarify the presence of the species, the Q_3 and Q_2 patterns in LS3 glass were simulated using different

LITHIUM SILICATE

(a) GLASS

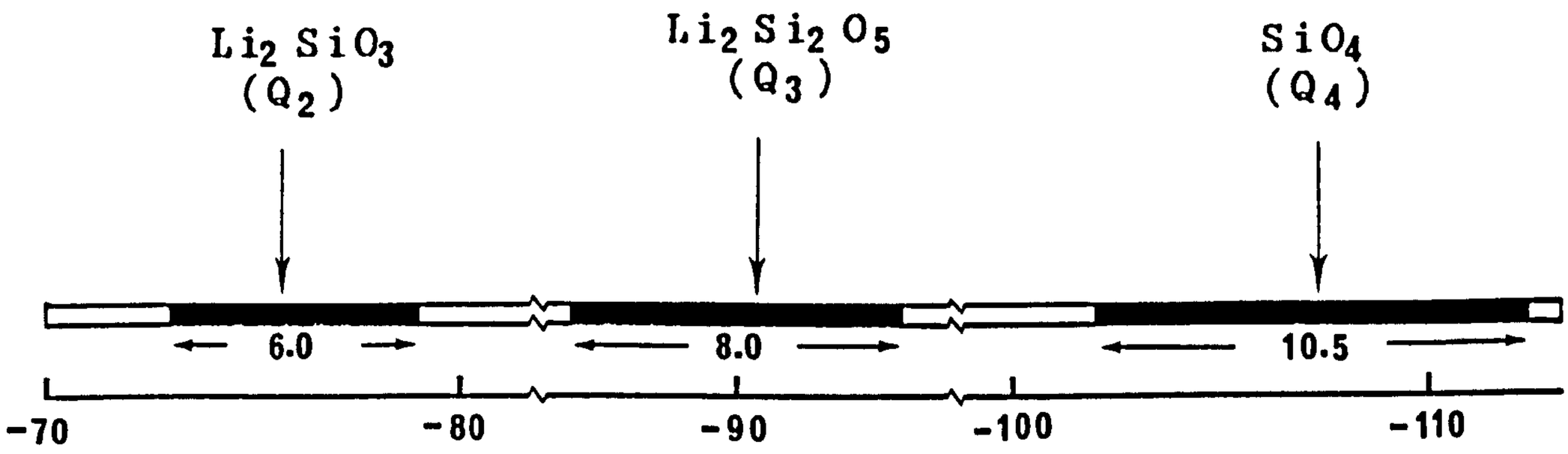

(b) CRYSTALLINE

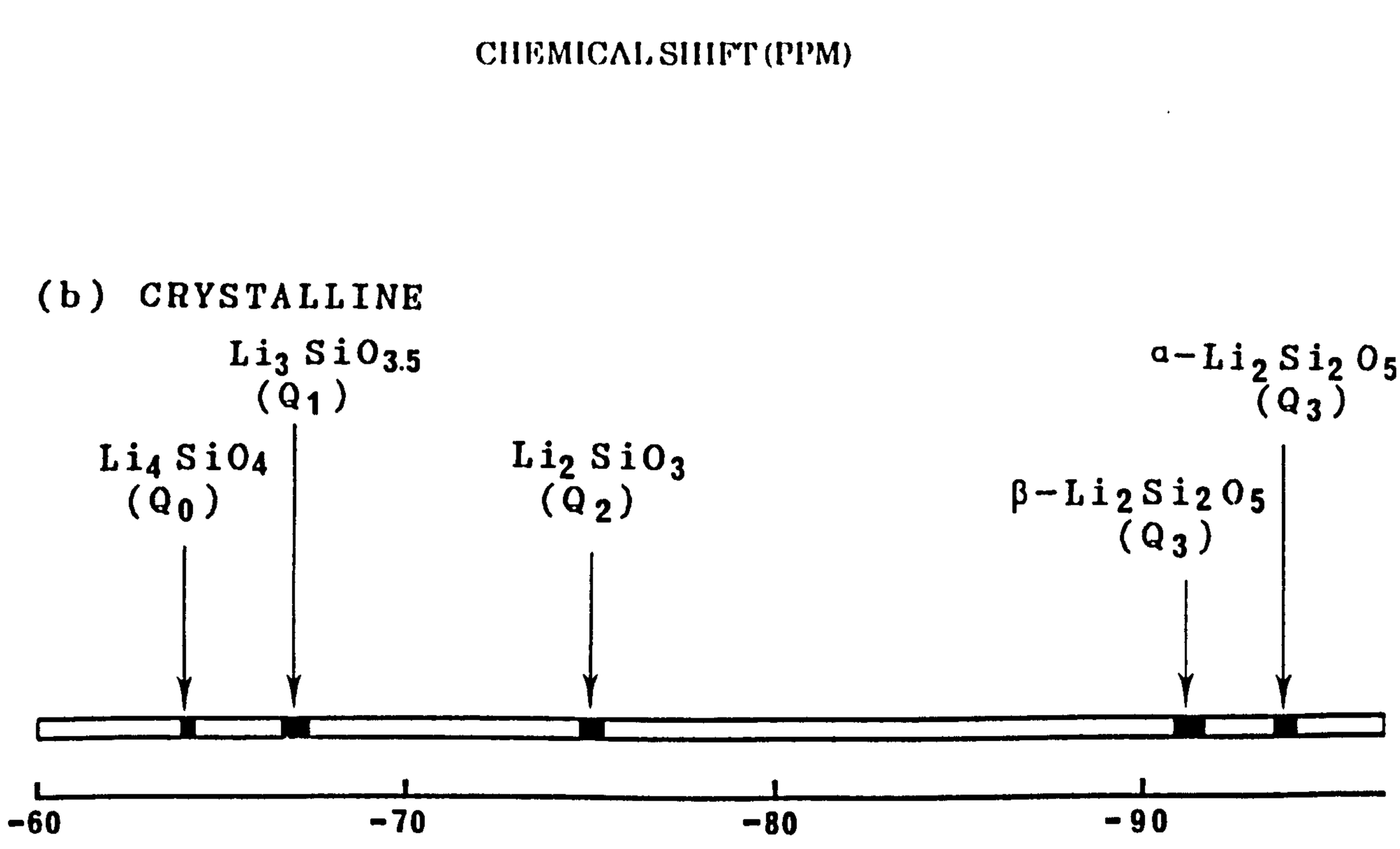

Figure 4.2 Chemical shift(δ) ranges for ^{29}Si in lithium silicate (a) glass and (b) crystalline Q_m species. The data for Q_0 and Q_1 are taken from ref. 14.

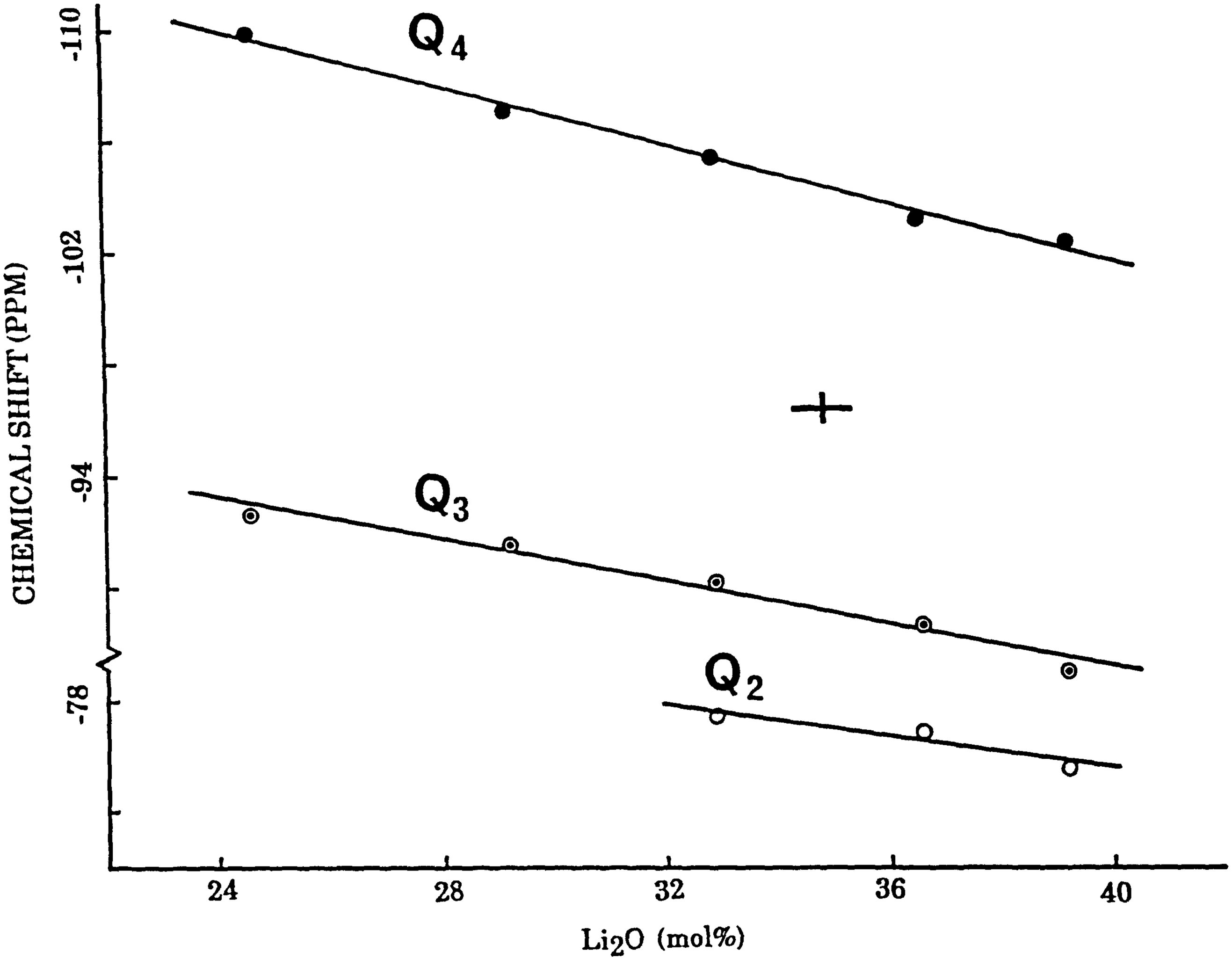

Figure 4.3 Variarion in Q_m chemical shift as a function of Li_2O content in the lithium silicate glasses.

anisotropic range, $\Delta\sigma$, and asymmetry parameter, η . As the anisotropic range in alkali silicate glass and crystal does not vary too much [23], the $\Delta\sigma$ value for Q_2 was initially estimated from the spinning sidebands of crystalline Q_2 using the method described by Herzfeld and Berger [25]. A Gaussian was fitted to Q_4 resonance and the lineshapes were normalised by assuming the area of (total Q_4 - Q_4 obtained by stoichiometry) = Q_2. All the lineshapes were fitted to experimental LS3 glass powder pattern and are shown in Figure (4.4) for optimum fit. Unlike LS3, a good fit to the experimental envelope of LS1 and LS2 can be obtained using the Q_3 and Q_4 powder lineshapes. The chemical shift tensors for the Q_3 species were found to be $\sigma_{xx} = -41\pm3$, $\sigma_{yy} = -70\pm3$, $\sigma_{zz} = -160\pm12$ PPM and those for Q_2 species were $\sigma_{xx} = -26\pm8$, $\sigma_{yy} = -63\pm6$ and $\sigma_{zz} = -133\pm10$ PPM. The $|\Delta\sigma|$ and η values for the Q_3 are 105 $\pm$ 12 PPM and 0.4 $\pm$ 0.1 respectively and those for the Q_2 are 89 $\pm$ 11 and 0.6 $\pm$ 0.2 respectively. The presence of the species for LS4 and LS5 can also be revealed by fitting normalised simulated Q_2, Q_3 and Q_4 lineshapes. The expanded spinning spectra of LS4 and LS5 also reveal the presence of Q_2 species in the materials.

The amounts of Q_4 in LS3-LS5 glasses are 10.2, 5.3 and 3.4%. ($\pm$1.0) respectively. By fitting an uncertain gaussian to the tail of the spinning spectra, such small amounts of unresolved Q_4 can only be estimated. Analysed composition of the respective glasses are 32.6, 36.8 and 39.2 mol% respectively. Therefore according to stoichiometry the LS3 can have some Q_4 units but this is more than the required stoichiometry.

The average percentages of composition obtained by

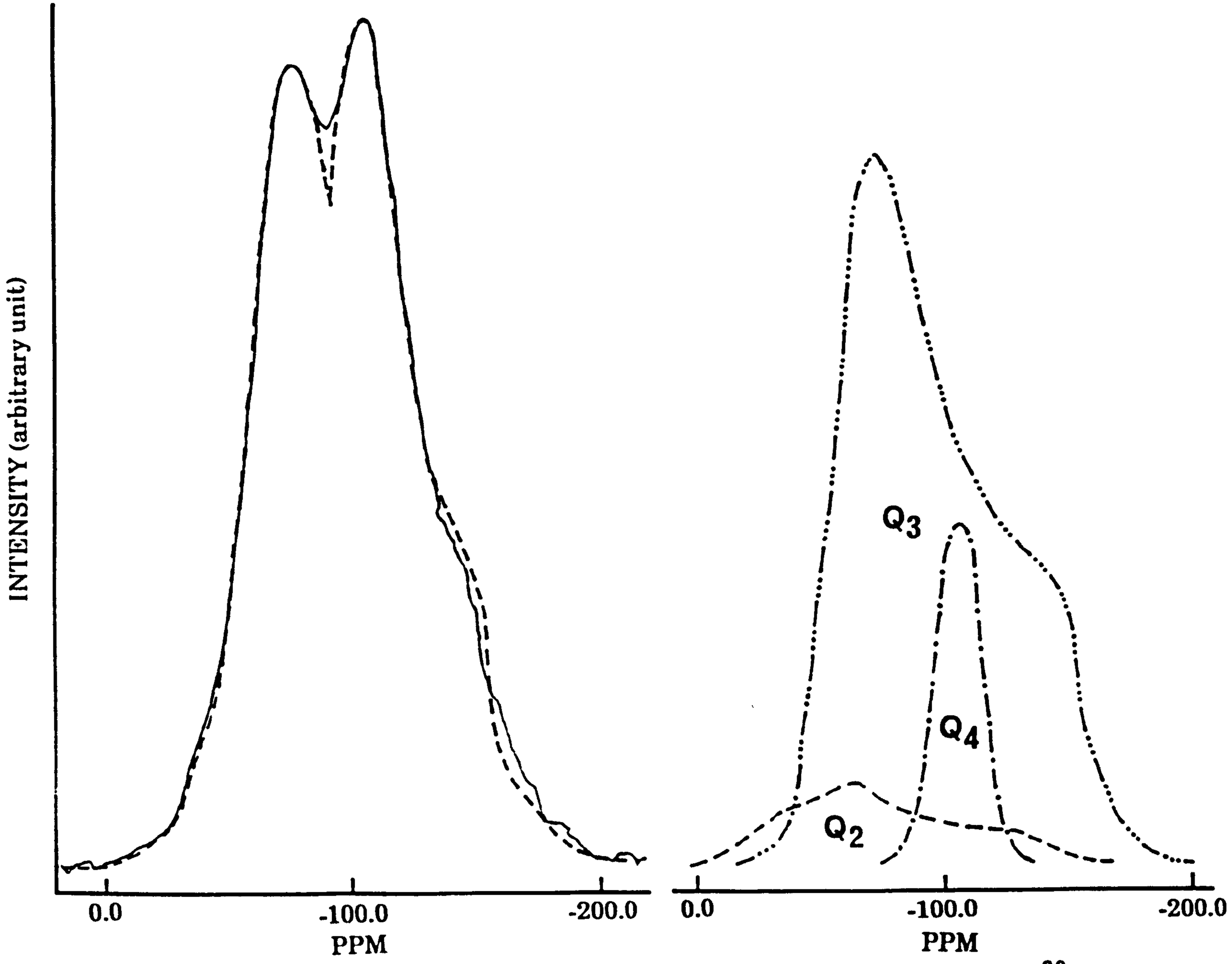

Figure 4.4 Computer fitting(- - - -) of the observed ^{29}Si spectrum from glass LS3(———) to a combination of Q_3(—·····—), Q_2(— — —) and Q_4(—·—·—).

integrating the area of the fitted lineshapes to the static spectra and by deconvoluting the spinning spectra are summarized in Table 4.1. The variation of composition with Li_2O content (mol%) is shown in Figure (4.5). The extrapolation of Q_2 concentration may indicate that the glasses containing more than 29 mol% Li_2O may contain Q_2 species. Thus the glasses with less than 30 mol% Li_2O are consistent with the constrained random (binary distribution) [21] model. From Figure (4.5) it can be inferred that the amount of Q_3 reaches a maximum when the lithium concentration is ~31 mol%.

4.2.2 ^7Li NMR

The biological and industrial applications of lithium have led to the NMR study of this element [26-32]. Most of these studies are concerned with the lithium ion motion, spin-spin and spin-lattice relaxation time at different temperatures. NMR investigation of ^7Li in lithium silicate system was first done by Gobel et al. [30] which was also concerned with T_1 relaxation measurements. In this section MAS and static NMR OF ^7Li in lithium silicates is presented with the hope of understanding the local environment of lithium in this system.

The magnitude of the Sternheimer antishielding factor for ^7Li is comparatively low (0.25 for Li^+ whereas 5.25, 19.96, 47.66 for Na^+, K^+, Rb^+ respectively) [32] and the quadrupole moment is small. Therefore, in principle, ^7Li spectra are dominated by the first order quadrupolar interaction and MAS NMR should provide high resolution spectra. The spinning and static ^7Li spectra of LS1, LS3 and

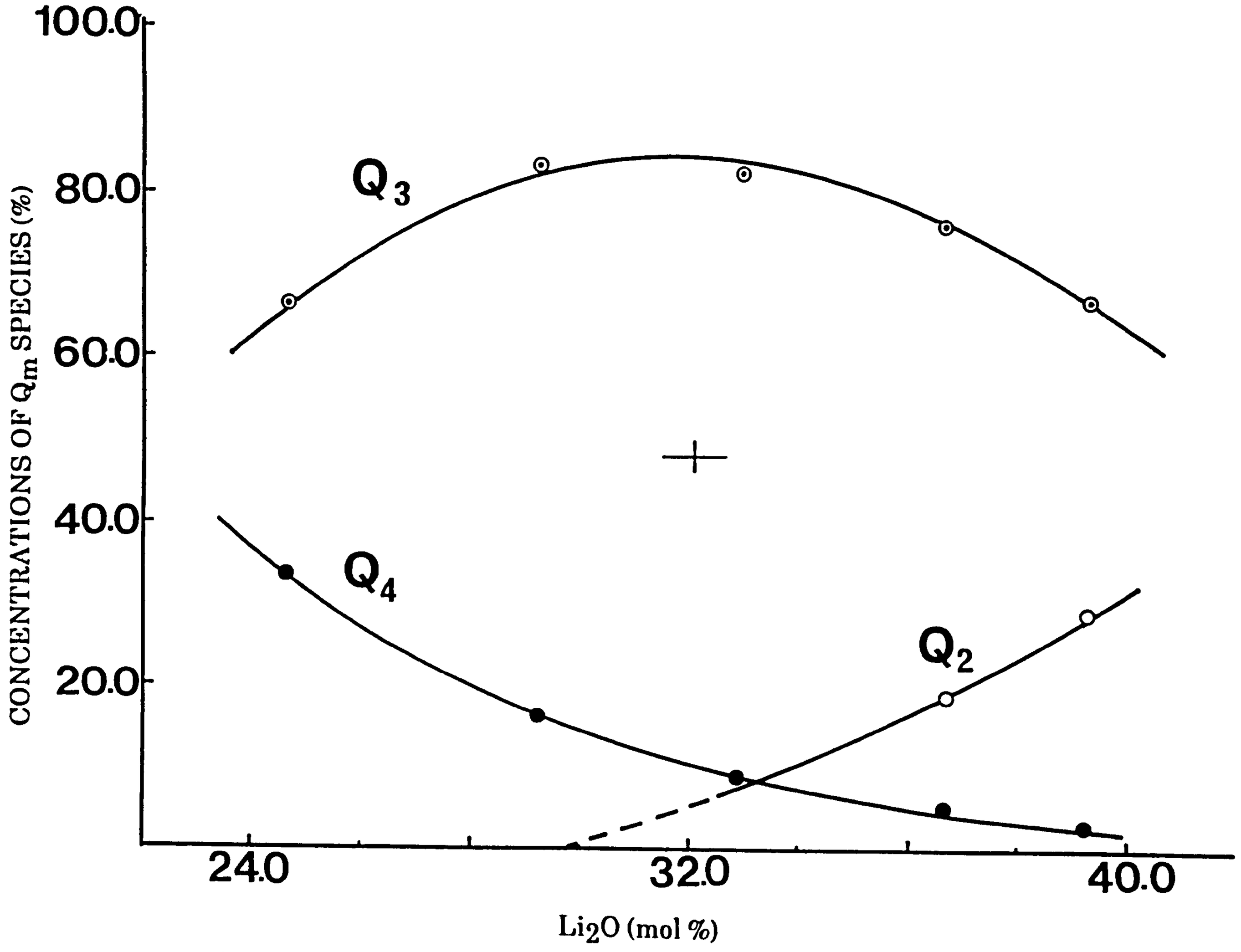

Figure 4.5 Variation in concentration of Q_m species as a function of Li_2O content.

LS5 are shown in Figure (4.6) and the spectral parameters are presented in Table (4.2). In LS1, lithium environment is $Si(OSi)_3\ O^-Li^+$ but in LS3 and in LS5 the lithium environments are $Si(OSi)_3O^-Li^+$ and $Si(OSi)_2.\ 2(O^-Li^+)$. Unfortunately ^7Li has a very small range of resonance frequences (~ 4 PPM) [26] and the MAS NMR spectra cannot distinguish such a little change of lithium environment in this system. However, a little change might be expected because of different numbers of lithium per silicon in the systems. The linewidth of ^7Li spectra in LS3 and LS5 are wider than that of LS1. The peak positions of LS3 and LS5 virtually show no difference with respect to LS1 (Figure 4.6).

TABLE NO.4.2 SPECTRAL PARAMETERS FOR ^7Li IN CONVENTIONALLY PREPARED LITHIUM SILICATE GLASSES

Sample	Condition	Peak position (PPM) ± 0.2	FWHM (PPM) ±0.5	Reduction factor due to MAS
LS1	static*	0.1	34.8	7.7
	MAS	0.7	4.5	
LS3	static	0.1	38.2	8.5
	MAS	0.6	4.5	
LS5	static	0.0	40.0	6.9
	MAS	0.6	5.8	

* Error in peak position is ±0.5

4.3 LITHIUM SILICATE GLASS CERAMICS

4.3.1 ^{29}Si NMR

Following Schramm et al.'s [14] first investigation of partially crystallised Li_2O-SiO_2 system by MAS NMR, crystalline lithium disilicate was studied by Rao et al. [17].

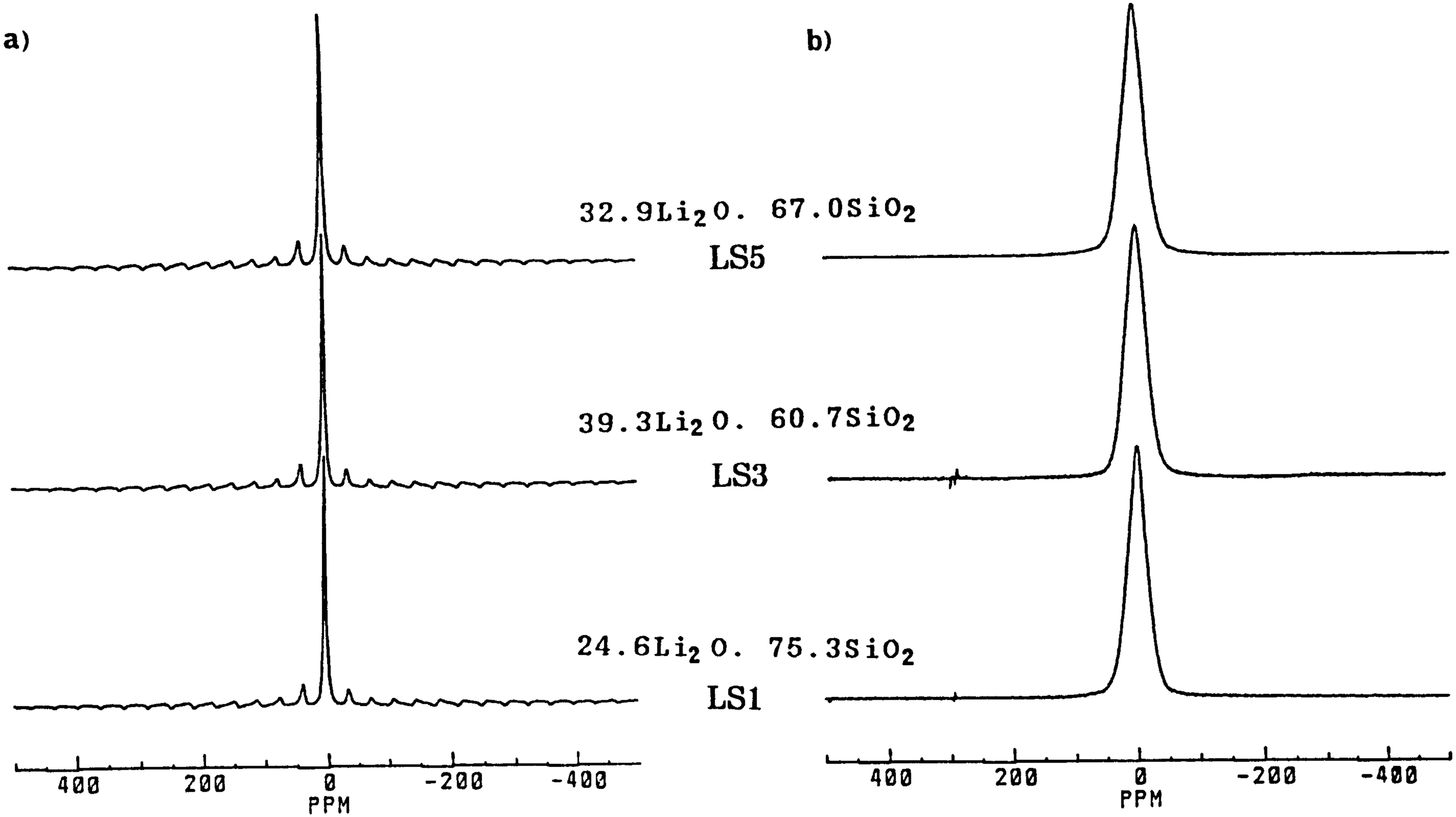

Figure 4.6 ^{7}Li spectra of Li_2O-SiO_2 base glasses (a) spinning (b)static. Analysed compositions are indicated in the diagram.

But the interim state between glass and crystal, i.e. the successive change with heat treatment using MAS NMR has not been made. In this section a systematic study, starting from base glass to its crystalline form, is presented.

The ^{29}Si spectra of lithium silicate system, heat treated at different temperatures are shown in Figure (4.7). The isotropic lines are indicated as I_0 and the spinning sidebands as SS in the figure. The chemical shifts and FWHM as a function of heat treatment are presented in Table (4.3). The resonance position varies with heat treatment indicating a change of average local environment of the ^{29}Si which might be due to change of bond angle, bond length etc. In order to understand this change a wide range of heat treatments was given to the lithium disilicate glass (LS3). A change of resonance position from -90 PPM (for glass) to -94 PPM (for crystal) was observed. The FWHM is considerably narrowed in the crystalline material. As the crystallinity depends upon the heat treatment temperature and time provided that the temperature is below liquidus and above glass transition temperature the heat treatment on LS3 was carried out for different times. The plots of Q_3, Q_4 chemical shifts (CS) and the Q_3 full width at half maximum (FWHM) as a function of heat treatments are shown in Figure (4.8). It appears from high resolution measurements that the local environment of the ^{29}Si in the glasses is almost unchanged below glass transition temperature. These measurements provide evidence that the configuration does not change until well below T_g which have been assumed for a long time [33]. Above the T_g the chemical shift and FWHM change with time and temperature as shown in Figure (4.8) because of the change of local environment and

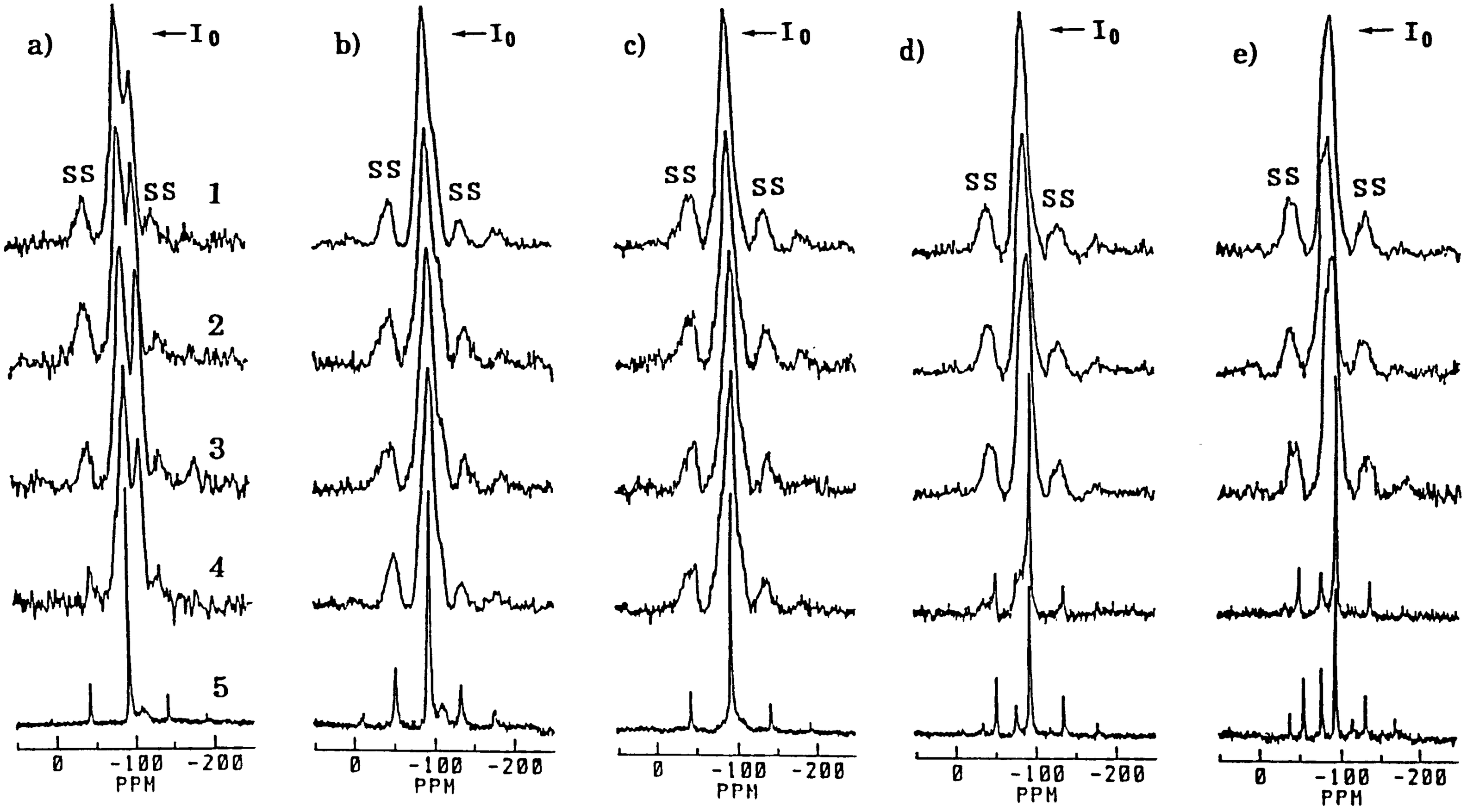

Figure 4.7 ^{29}Si spectra of lithium silicate glasses (a) LS1 (b) LS2 (c) LS3 (d) LS4 and (e) LS5 after 6 hours heat treatment (1 = as cast, 2 = 425 °C, 3 = 475 °C 4 = 525 °C, 5 = 575 °C).

TABLE 4.3 SPECTRAL PARAMETERS AND COMPOSITION OF LITHIUM SILICATE GLASS CERAMICS

Sample	Heat treatment T°C/th	^{29}Si spectral paramaters (PPM) ± 0.5					
		Q_4		Q_3		Q_2^+	
		CS	FWHM	CS	FWHM	CS	FWHM
LS1	425/6	-109.8	12.9	-92.7	15.0	-	-
	475/6	-111.2	12.7	-93.3	14.0	-	-
	525/6	-111.5	12.3	-93.4	13.1	-	-
	575/6	-111.6	12.3	-93.4	1.7		
LS2	425/6	-107.2	11.9	-91.6	15.3	-	-
	475/6	-109.2	12.0	-92.5	14.9	-	-
	525/6	-109.3	11.2	-93.2	14.5	-	-
	575/6	-109.3	11.3	-94.0	3.0	-	-
LS3	250/6	-105.6	12.5	-90.0	16.9	-77.1	7.9
	250/168	-106.0	12.1	-90.0	16.7	-77.4	8.0
	425/6	-105.3	11.9	-90.3	16.5	-77.2	7.8
	425/168	-105.0	12.0	-91.2	15.8	-76.9	7.8
	475/6	-105.1	12.2	-91.8	16.0	-77.0	7.9
	475/168	-105.5	12.4	-92.9	15.9	-76.0	8.1
	525/6	-105.7	12.0	-92.7	15.6	-76.5	7.8
	525/168	-	-	-93.2	4.0	-	-
	575/6	-	-	-93.2	2.0	-	-
	626/6	-	-	-93.4	1.8	-	-
	725/6	-	-	-92.0, -93.7	1.7	-	-
LS4	425/6	-103.2	11.0	-89.0	15.1	-76.5	8.3
	475/6	-103.0	10.8	-91.3	15.0	-75.9	8.0
	525/6	-	-	-94.2	2.0	-75.1	3.0
	575/6	-	-	-94.2	1.7	-75.0	2.5
LS5	425/6	-102.0	10.5	-87.8	14.0	-75.4	10.0
	475/6	-102.1	10.3	-90.2	12.5	-75.0	8.3
	525/6	-	-	-94.3	2.0	-74.5	2.0
	575/6	-	-	-94.2	1.5	-74.9	1.5

+ The spectral parameters for Q_2 in LS3 are assigned tentatively. Error in those measurements is ± 1.0

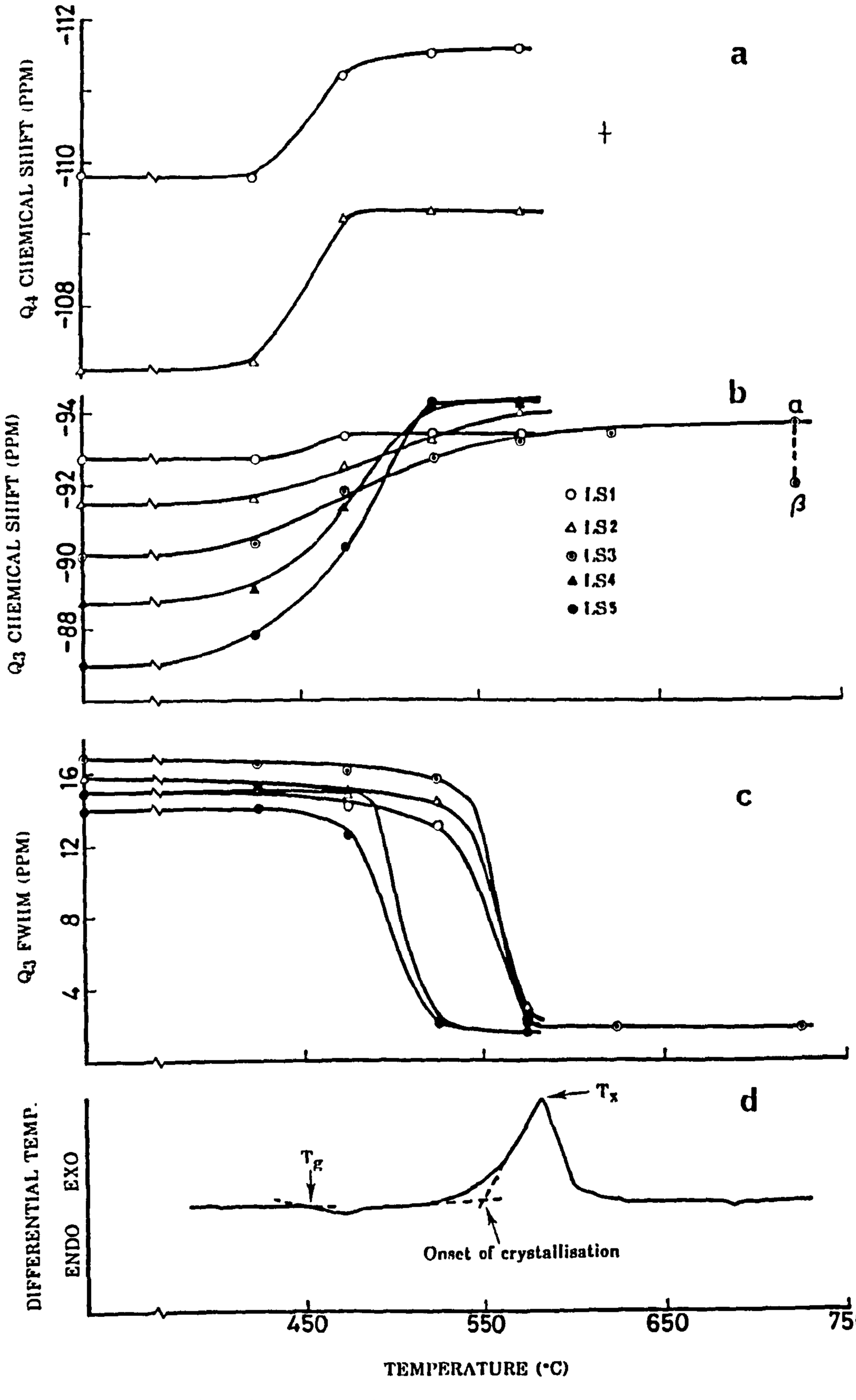

Figure 4.8 Variation in (a) Q_4 chemical shift (b) Q_3 chemical shift and (c) Q_3 full width at half maximum as a function of heat treatment temperatures for 6 hours and in comparison with (d) the DTA curve for the glass LS3.

the entropy in the material. So it may be said that the FWHM is a measure of the randomness of atomic arrangements, i.e. a measure of the configurational entropy of the system.

A closer look at the MAS NMR spectrum of crystalline lithium disilicate shows an asymmetric lineshape (Figure 4.9). Therefore two resonances can easily be fitted to the spectrum as shown in the Figure. The chemical shifts were found to be -92.0 and -93.7 PPM. The areas under these resonances were found to be 29.7 and 70.3% respectively. XRD pattern also gives an evidence of the formation of two polymorphs in the sample (see 4.3.3). Although the resolution of the Bruker MSL-360 spectrometer is about 0.1 PPM, the two lines which correspond to two different polymorphs are not well resolved, indicating that the two type of silicon environments are not very different from each other.

Comparison of the glass and crystalline static spectra (Figures 4.4 and 4.10) of lithium disilicate clearly reveal the absence of Q_4 species in the latter and therefore restructuring $Q_4+Q_2 \longrightarrow 2Q_3$ must occur during devitrification. The reaction $Li_2O+2Q_4 \rightarrow 2Q_3$ is possible only when excess Li^+ occupies the holes in the glass structure. This is unlikely and the disproportionation $Q_4+Q_2=2Q_3$ must be responsible for the disappearance of the Q_4 resonance from the near axially Q_3 powder lineshape.

As the spinning spectrum of crystalline LS3 (Figure 4.9) shows the presence of two polymorphs, axially symmetric ($\sigma_{xx} = \sigma_{yy}$) powder patterns for each of the polymorphs can be fitted to the experimental powder lineshape as shown in Figure (4.10). The percentage of composition was obtained from the spinning spectra as discussed earlier. The principal

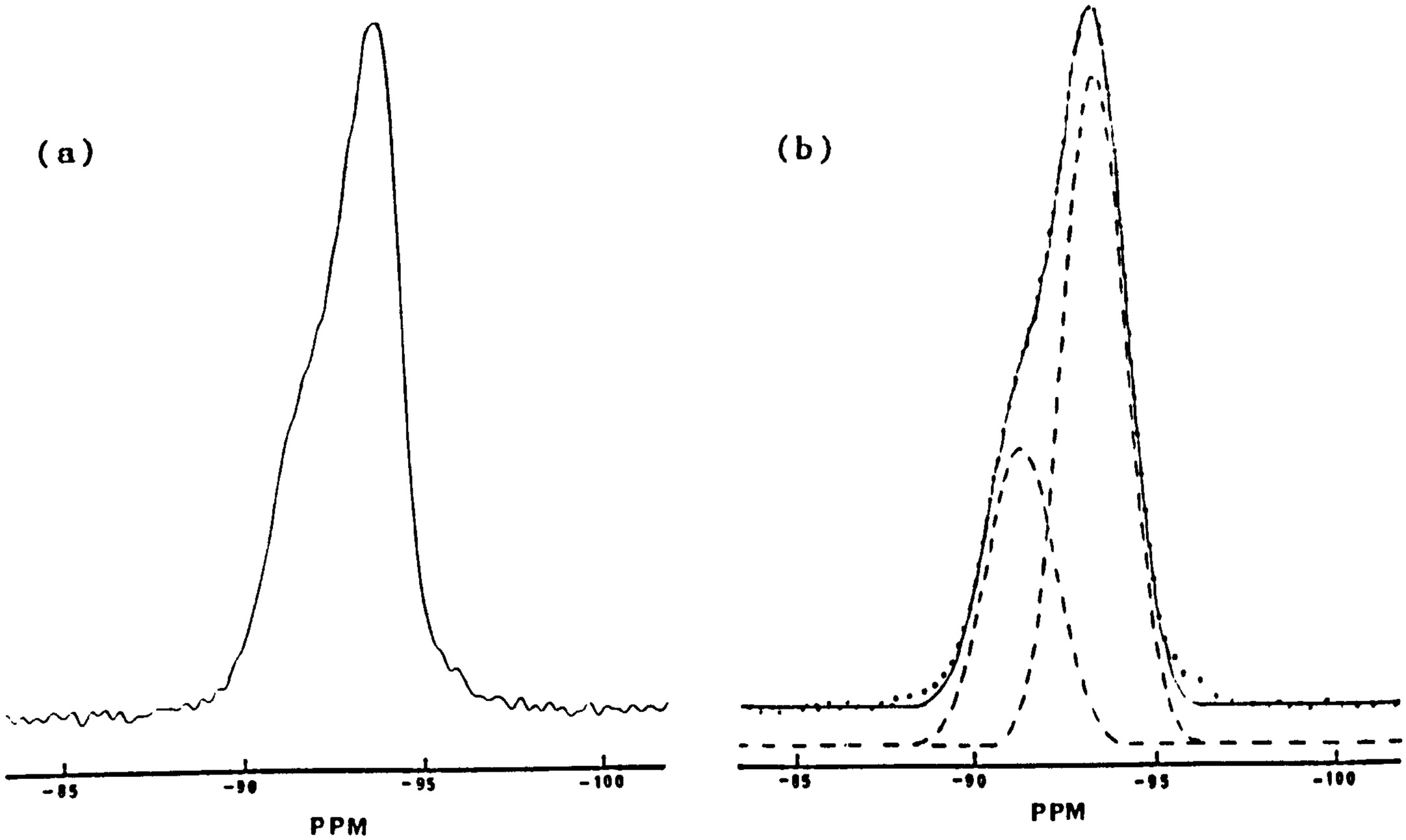

Figure 4.9 (a) ^{29}Si MAS spectrum of crystalline LS3. (b) Computer fitting of the observed α- and β- $Li_2Si_2O_5$ polymorphs in (a). Dots represent exterimental points.

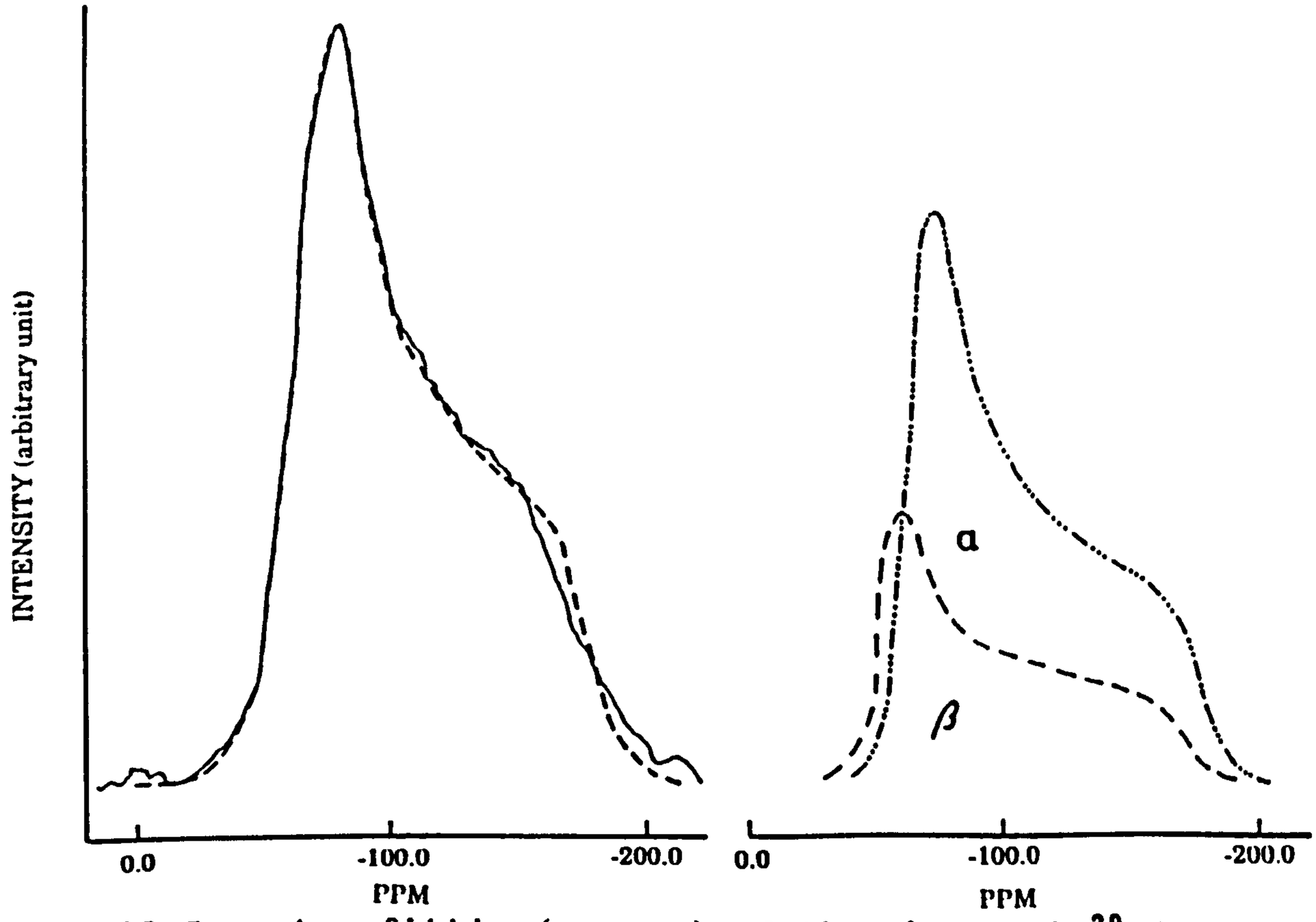

Figure 4.10 Computer fitting(— — —) of the observed ^{29}Si spectrum (static) from crystalline LS3 to a combination of α-$Li_2Si_2O_5$ (—···—) and β-$Li_2Si_2O_5$ (— — —).

components of the chemical shift tensor were found to be σ_{xx} = σ_{yy} = -57±5, σ_{zz} = -160±8 PPM and σ_{xx} = σ_{yy} = -59±5, σ_{zz} = -163±8 PPM respectively. The anisotropic range is almost the same as glass spectra. The isotropic values corresponding to the σ_{ii} (i= x,y,z) are -91.7 and -93.7 respectively and are consistent with the spinning spectra. The lower η value in the crystalline material indicates that the ^{29}Si environment is more symmetric than in the respective glass. The experimental envelope of the crystalline LS3 powder pattern can also be fitted to a single Q_3 powder pattern with σ_{xx}= -53±5, σ_{yy} = -67 ±3 and σ_{zz} = -164±8 PPM, which give η=0.26. Therefore, it is worth mentioning that fitting one Q_3 pattern to the crystalline spectrum would give the wrong η ,i.e. incorrect information about the symmetry around the ^{29}Si. Once the Q_4 species disproportionates from > 32 mol% lithia containing samples, the structure does not change even on long devitrification.

The spectra for the LS1 glass and its heat treated (475°C/6h) form (Figure 4.7.a.3) have been shown to exhibit different intensity distributions for the Q_3 and Q_4 species. The spectra were collected under the same condition and therefore this is due to the change of T_1 relaxation time because of heat treatment. Thus one may infer that some changes, possibly glass-in-glass phase separation, has occured at this temperature. Relaxation time in phase separated material become enormously long and in order to prevent saturation, crystalline LS1 was run with 1 μs(π/12) pulse and 3000s delay between the pulses. The effect of phase separation will be discussed further in chapter 7.

4.3.2 ^{7}Li NMR

The ^{7}Li spectra for crystalline glasses (LS1, LS3 and LS5) are shown in Figure (4.11). As the effect of quadrupole moment is small, the satellite, i.e. $\pm$ 3/2 $\longleftrightarrow$ $\pm$ ½ transitions are also observed in the static spectra (Figure 4.11.b) along with +½ $\longleftrightarrow$ -½ transition. The dipolar interaction is dominant in the ^{7}Li spectra.

The width and shape of the spectra depend on the magnetic interactions among the neighbouring nuclei [34,35]. When dipolar interaction occurs between pairs of spins, the static lineshape is a Pake doublet [34] shown in Figure (4.11.b) for Li in crystal phase. A simulation of this doublet for the sample LS3 with additional line broadening is shown in Fig. 4.11.c. The spinning ^{7}Li spectra have ca lorentzian lineshape for the centre band (Figure 4.11.a). The $\pm$ 3/2 $\longleftrightarrow$ $\pm$ ½ transitions are broken up and separated by the rotational frequency.

The spectral parameters, quadrupolar frequency (ν_Q) obtained from the distance between two satellite transitions, and quadrupole coupling constant are presented in Table (4.4).

TABLE NO. 4.4 ^{7}Li SPECTRAL PARAMETERS IN LITHIUM SILICATE GLASS-CERAMICS

Sample (crystalline)	Amounts of Li_2O (mol%) $\pm$0.2	Condition	Peak position (PPM) $\pm$0.2	FWHM (PPM) $\pm$0.5	Reduction factor due to MAS	Quadrupole frequency ν_Q (MHz) $\pm$0.003	Quadrupole coupling constant (e^2qQ/h) (MHz) $\pm$0.006	Level of splitting (Hz) $\pm$300
LS1	24.6	static MAS	- 0.6	58.9 8.5	6.9 -	0.043 -	0.086 -	4542
LS3	32.9	static MAS	- 0.6	59.9 8.5	7.0 -	0.042 -	0.084 -	4500
LS5	39.3	static MAS	- 0.7	60.0 8.0	7.5 -	0.042 -	0.084 -	4192

4.3.3 DTA AND XRD

Although numerous studies [2-11] have already been made on lithium silicates, some work on the system used for NMR investigation have been carried out using DTA and XRD to make

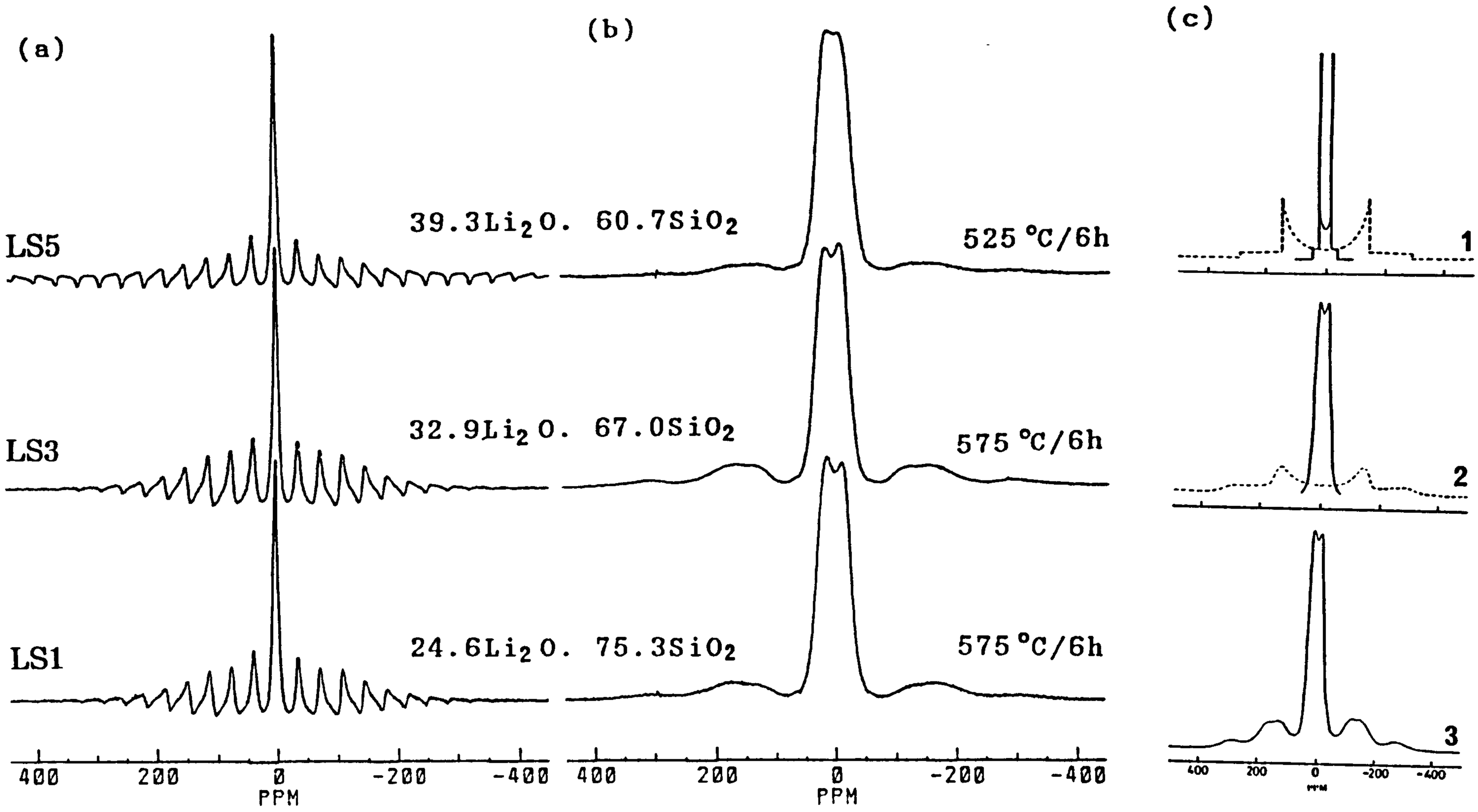

Figure 4.11 ^{7}Li spectra of heat treated lithium silicate glasses (a) spinning (b) static. (c) 1. A simulation of the $+1/2 \longleftrightarrow -1/2$ and $\pm 3/2 \longleftrightarrow \pm 1/2$ transitions of ^{7}Li in crystalline LS3, 2. with 2500 Hz dipolar broadening and 3. the observed spectrum.

a comparison with NMR results. The glass transformation temperature, T_g, liquidus temperature, T_{ls} for the samples LS1-LS5 obtained from DTA are presented in Table (4.5). The results are consistent with previous workers [7,8]. XRD patterns of the devitrified glasses are also consistent with previous workers [7,8].

The T_g decreases with the increase of Li_2O content because of the decrease of SiO_4 tetrahedra. The onset of crystallisation and the maximum crystallisation temperature in LS3 were found to be 540 $\pm$ 5 and 590 $\pm$ 2°C respectively (Figure 4.8.d). XRD of LS3 heat treated below 475°C/6h showed no crystallinity in the material but above 475°C/6h showed lithium disilicate peak on the top of x-ray amorphous halo. However for the heat treatment at 475°C/168h crystalline $Li_2Si_2O_5$ was also observed. XRD of crystallised LS3 gave a pattern consistent with two different polymorphs, one is the low temperature form and the other one is the high temperature form [12,13]. Presence of these two polymorphs also confirm the presence of two resonances in the MAS NMR spectrum (Figure 4.9). Both the polymorphs are known to be orthorhombic with slightly different lattice constants. However information about the local order of the nuclei, e.g. Si-O-Si or Si-O-Li bond angle, bond length are not known. Single crystal study of lithium silicate showed only one monoclinic form with pseudo orthorhombic structure [36] with Si-O-Si mean bond angle 137.3°. The ratio of the amounts of two polymorphs obtained from x-ray study is 59.6 : 40.4 which is slightly different from the MAS NMR value (70.3 : 29.7).

TABLE 4.5 DATA FOR GLASS TRANSITION TEMPERATURE, T_g, CRYSTALLISATION TEMPERATURE, T_x, AND LIQUIDUS TEMPERATURE, T_{ls} IN LITHIUM SILICATE GLASSES

Sample	Glass transition temperature, T_g	Crystallisation temperature, T_x	Liquidus temperature, Tls
	(^oC) ± 3	(^oC) ± 2	(^oC) ± 2
LS1	480	623	1061
LS2	461	601	1050
LS3	452	590	1042
LS4	446	581	1039
LS5	441	574	1040

4.4 DISCUSSION OF THE CONVENTIONALLY PREPARED LITHIUM SILICATE GLASS AND GLASS CERAMICS RESULTS

4.4.1 ^{29}Si SPECTRA

The structure of lithium silicate depends upon the concentration of Li_2O, in SiO_4 tetrahedra in agreement with previous workers [14-18]. The constrained random model [21] seems to be applicable to < 30 mol% Li_2O containing glasses. The glasses with > 30 mol% Li_2O contain Q_2, Q_3 and Q_4 species (Figure 4.5) which are more than the stoichiometric requirement.

In Li_2O-SiO_2 system, the average distance between two magnetic silicons is 10.2 Å and therefore the effect of homonuclear dipolar interaction is small because the dipolar interaction is invesely proportional to the cube of the distance between two nuclei. Dipolar heteronuclear (Li-Si)

interaction may also be considered as small. Therefore the chemical shift interaction is the primary source of broadening in the ^{29}Si spectra. The line width in glass for Q_2 is 9 PPM whereas that in Q_3 and Q_4 is 16 and 12 PPM respectively. This indicates that Q_2 environment is more ordered than Q_3 and Q_4 species.

The plot (Figure 4.5) clearly shows that the percentage of Q_4 decreases and that of Q_3 increases with increasing Li_2O. The amount of Q_3 goes through a maximum at ~31 mol% Li_2O and then decreases with further increase of Li_2O. The formation of Q_2 leaving some Q_4 in LS3-LS5 may be due to clustering tendency of lithium atoms [37,38]. The amount of Q_2 increases with increasing Li_2O content and the maximum of that can be achieved at 50 mol%. But this is beyond the glass forming region [1] and the sample made with 50 mol% Li_2O would be readily crystallised as observed by Schramm et al. [14].

The chemical shift of Q_m species in Li_2O-SiO_2 system varies with Li_2O content, e.g. the range of chemical shift for Q_4 unit is -102 to -112 PPM and that for Q_3 is -86 to -94 PPM depending upon the concentration of Li_2O, consistent with other workers [14-18]. This indicates that lower amount of Q_m may easily be influenced by higher amount of Q_{m-1} ($0 \leqslant m \leqslant 4$) or vice versa. As the maximum concentration of Q_3 may occur at 31 mol% Li_2O containing glass, the chemical shift for Q_3 in the vicinity of this level of Li_2O will be less influenced by other species. The Q_3 chemical shift in LS3 glass (32.9 mol% Li_2O) is -90.0 ± 0.5 PPM; whereas that for crystalline phase is -93.8 ± 0.2 PPM. This dissimilarity in chemical shift between glass and crystalline lithium disilicate suggests that the local electronic density of silicon in glass

and crystalline phases are different.

Calculation of the chemical shift anisotropy, $|\Delta\sigma| = |\sigma_{zz} - \frac{1}{2}(\sigma_{xx} + \sigma_{yy})|$ is another means of understanding the electronic environment around the investigated nuclei [39, 40]. Similar $|\Delta\sigma|$ indicates almost the same electronic environment around the silicon in glass and crystalline Si $(OSi)_3\ O^-Li^+$. The axially symmetric lineshape for crystalline Q_3 (Figure 4.10) represents three Si-[bO] bond distances and three Si-O-Si bond angles are close to each other [39]. However crystallographic study of $Li_2Si_2O_5$ shows two Si-O-Si bond angles are 128^o but the other one is 156^o [36]. This large deviation of bond angle suggests that crystallographic structure has to be refined. Similar inconsistency is also found by several authors in different systems [41]. The contribution to σ_{zz} could be dominated by the Si-O-Li bond angle which is 83^o [36].

If the distribution of Q_m species does not change during devitrification, the amounts of the species will be the same in glass and in crystal. The experimental (Q_4/Q_3) ratio in LS1 glass is 0.51 $\pm$ 0.05 and that in crystal is 0.50 $\pm$ 0.05. The calculated value for them is 0.53 $\pm$ 0.05. Therefore these three values are in good agreement with each other and it gives an evidence that the distribution of Q_m species follow the constrained random model [21] in the neighbourhood of 25 mol% Li_2O containing lithium silicate glasses.

Disappearance of Q_4 and formation of Q_3 in LS3 glass due to devitrification suggests that Q_4 must have reacted with the same amount of Q_2. Therefore during devitrification the reaction of $Q_4+Q_2=2Q_3$ occurs and only an axially symmetric lineshape due to Q_3 species is observed (Figures 4.4 and

4.10). However, the disproportionation observed in high lithia containing glasses (LS4, LS5) is somewhat different from LS3. The crystalline spectra of both the LS4 and LS5 reveal the presence of Q_2 in the material (Figures 4.7.d and 4.7.e). During devitrification Q_4 reacts with a fraction of Q_2, Δp, where p is the concentration of Q_2,which forms $2\Delta pQ_3$ leaving the rest of Q_2 (p- Δp) and total Q_3 (1-p-q + 2 Δp) intact throughout further crystallisation, where q is the amount of Q_4. Infact in crystalline LS4 and LS5 q=0 and the total amount of Q_3 becomes (1-p+2 Δp). In crystalline LS5 the experimental (Q_3/Q_2) = 2.3 $\pm$ 0.3 is consistent with the calculated value (2.4 $\pm$ 0.4).

A sample of similar composition to LS5 has also been investigated by Schramm et al. [14] who have attributed the disproportionation of the form $2Q_3 \longrightarrow Q_2+Q_4$ due to devitrification. Early nucleation, i.e. nucleation during quenching from the melt could change the route of crystallisation [42]. Dupree and Holland [43] stated that the early nuclei, as $Li_2O.SiO_2$ (Q_2) in this case, could form at a faster rate because of Li^+ diffusion to this site which reduces the growth of $Li_2O.2SiO_2$ (Q_3) and leaves excess silicon as SiO_4 tetrahedra. Q_2 has a tendency to crystallise readily because of its lower activation energy and relatively narrow full width at half maximum. Therefore Li^+ ion from Q_3 site preferentially occupies Q_2 site and hence the area under Q_2 and Q_4 resonances increases. Such a disproportionation was not observed in this study, possibly due to absence of required level of early nucleation in the glass to change the devitrification route.

The asymmetric lineshape in crystalline LS3 (Figure 4.9)

indicate the presence of two polymorphs with only a small difference in local order consistent with x-ray studies [13]. The information about the Si-O-Si bond angle and the bond length may be difficult to obtain because of such a small change in local order. The inconsistency between the amounts of polymorphs obtained from the XRD and NMR may be due to the difference in sensitivity of the two techniques. In this regard it may be said that the amounts obtained from NMR measurements are more reliable. Comparison of the DTA trace with the plots of chemical shift and FWHM as a function of heat treatment (Figure 4.8) clearly show the structural change within the same range of temperature. The maximum rate of change of FWHM with heat treatment may correspond to the onset of crystallisation (540^{o}c).

In LS1 (24.6 mol% Li_2O) the chemical shift changes from -109.8 to -111.6 PPM whereas that in LS2 (29.2 mol% Li_2O) changes from -107.2 to -109.3 PPM due to heat treatment (Figure 4.8.a). This may indicate that the Si-O-Si mean bond angles and bond lengths in the Q_4 environments in these materials are different.

The range of ^{29}Si chemical shift difference between glass and crystalline Q_2 species in lithium silicate is 3 PPM but that in Q_3 is 8 PPM. Therefore it can be concluded that the distribution of local environment of Q_2 is almost independent of large scale clustering leading to glass-in-glass phase separation but that in Q_3 is not. It can be concluded that in lithium silicate glass and crystals, like Na_2O-SiO_2 system [21], silicon environment of Q_m species does not change and the site symmetry varies between glass and crystal; but the variation is different from one type of Q_m

species to the other. However, only a small change was observed between glass and phase separated Q_2 and Q_3 in a Raman study from which Matson et al. [11] predicted no alteration of local order in both the Q_2 and Q_3 due to heat treatment. This discrepancy between MAS NMR and Raman may be due to which is sensitive to local order rather than bond vibration.

4.4.2 ^{7}Li SPECTRA

The ^{7}Li spectra of crystalline materials are more informative than those of the glasses. The reduction factor due to MAS (~ 6-8) in both the glass and crystal is a representation of the presence of strong dipolar interaction between two spins. The same quadrupolar coupling constant in all the crystalline materials gives roughly the same type of quadrupolar interaction.

The central $+\frac{1}{2} \longleftrightarrow -\frac{1}{2}$ transition of ^{7}Li is not broadened by the first order quadrupolar interaction and it behaves as a spin half nuclei when the second order quadrupolar interaction is negligible [44]. Therefore Pake doublet first observed for ^{1}H - ^{1}H interaction in H_2O molecule [34] can also be seen for ^{7}Li when two lithium ions are close to each other. The calculation of the ^{1}H - ^{1}H separation using equ. (2.40) is possible but such an expression for I = 3/2 does not exist in the literature.

The MAS ^{7}Li spectra (Fig. 4.11.b) show single resonance in all the materials. Moreover the ^{7}Li static spectrum of a single phase $Li_2Si_2O_5$ also showed virtually the same doublet. Thus the splitting of the doublets is not due to two lithium sites or two different polymorphs of $Li_2Si_2O_5$ in the

crystalline samples (LS1, LS3, LS5). The formation of Li pairs is therefore unsuspected and has not been reported anywhere in the crystallographic studies of $Li_2Si_2O_5$ polymorphs [4,12,13,36].

The level of splitting in LS1 and LS3 is almost the same because of the presence of Q_3 species only but that in LS5 decreases due to a range of interactions arising from lithiums in Q_2 and Q_3 environments. In crystalline material Q_2 separates from the Q_3 phase and also due to formation of different polymorphs of Q_3 the ^7Li resonances are expected to be different. But because of small chemical shift range broader lineshapes rather than distinct peaks are observed.

4.5 SOL-GEL PREPARED LITHIUM SILICATE GLASSES

4.5.1 ^{29}Si NMR

The ^{29}Si spectra of sol-gel prepared lithium silicate glasses (LSG1-LSG3) and their compositions are shown in Figure (4.12) [45]. The spectral parameters and the amounts of the respective species obtained by deconvoluting the spectra using the computer fitting programme are presented in Table (4.6).

TABLE 4.6 ^{29}Si NMR SPECTRAL PARAMETERS OF SOL-GEL PREPARED LITHIUM SILICATE GLASSES

Sample	Amounts of Li_2O* (mol %)	Spectral parameters (PPM) ± 0.5				Amounts of (%)±4%	
		Q_4		Q_3		Q_4	Q_3
		CS	FWHM	CS	FWHM		
LSG1	10.0	-110.0	11.0	-100.6	8.7	80.2	19.8
LSG2	25.0	-110.0	11.2	-100.6	9.7	64.3	35.7
LSG3	33.3	-112.0	11.6	-100.5	14.9	38.8	61.2

* nominal composition

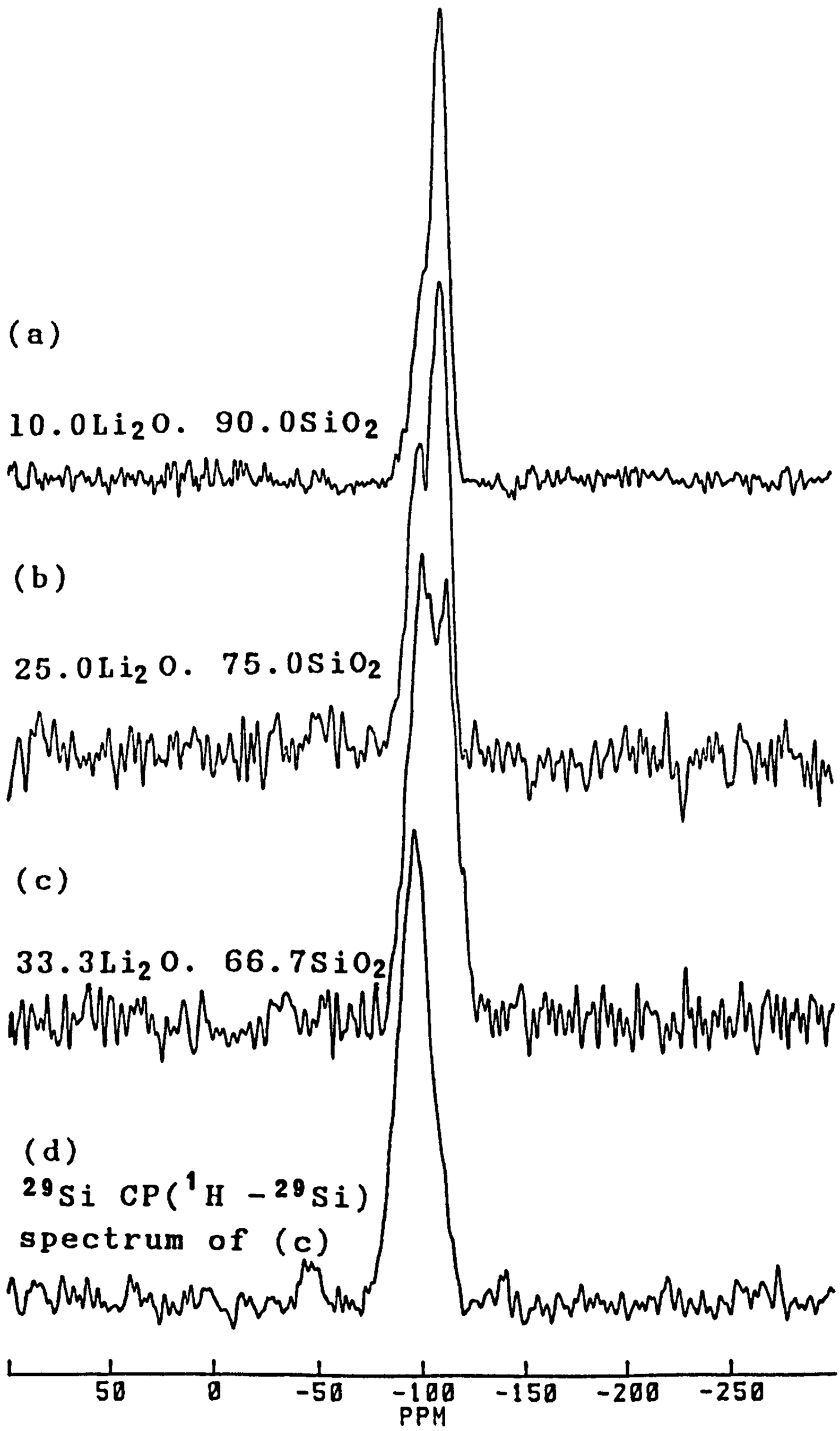

Figure 4.12 ^{29}Si MAS spectra of sol-gel prepared lithium silicate glasses.

The spectra show two peaks, one at -100·6 PPM and the other one within -110·0 to -112·0 PPM range. The relative amount of Q_4 in the glasses decreases with the increase of Li_2O content. But there is no peak observed corresponding to the silicon environment $Si(OSi)_3OLi$ expected at -90·0 PPM. As the protons present in silicon glass allow the technique of cross-polarisation to be used [46], a spectrum of ^{29}Si in LSG3 was collected with 2.5 ms contact time between the proton and the ^{29}Si spins [47]. The pulse repetition rate and the length of the pulse were 10 s and 5.75 μs respectively. The protons transfer polarisation to the nearby silicons and produce an enhanced signal as shown in Figure (4.12.d) with respect to those silicons further from protons. Here the transfer of polarisation was most to the $^{29}Si(OSi)_3OH$ and the signal from $Si(OSi)_4$ is not visible. Longer contact time would transfer less polarisation to the Si in $Si(OSi)_3OH$ and hence Q_4 could become relatively more evident but this was not carried out.

4.5.2 ^7Li NMR

The ^7Li spectra of the glasses, as shown in Figure (4.13), look similar to that of conventionally prepared lithium silicate glasses and little information can be obtained from the spectra.

4.5.3 ^1H NMR

The interaction of H_2O with catalysts, minerals, glasses, etc. could change the properties of these materials. However, not much of the attention have been given on the high resolution proton NMR in minerals and biologically relevant materials [48-49]. Recently Eckert et al. [50] and Dupree et

al. [51] have revealed structural information via proton NMR in silicate glasses. In this section ^1H NMR in sol-gel prepared lithium silicate glasses is presented.

^1H spectra of LSG1-LSG3 are shown in Figure (4.14) and the spectral parameters are recorded in Table (4.7). The resonances in all the glasses consist of partially overlapping two lines, one at +2.2 and the other one, relatively broader at +4.8 PPM. There could be some molecular water although the samples were dried at 400°C/25h. In order to compare the spectra, proton spectrum in $LiOH.H_2O$ is also shown in the Figure (4.14.d). The shift for proton in $LiOH.H_2O$ are +2.2 and +6.5 PPM (Table 4.6). The peak at +6.5 PPM is due to structural H_2O [48] and therefore the peak at +2.2 PPM could be due to ^1H in LiOH. The relatively narrow peak at 6.5 PPM is almost twice the intensity of the other peak (+2.2 PPM). This also provides an evidence in favour of the assignment because H_2O molecule contains two protons but that for LiOH is only one. Thus the peak at +2.2 PPM in the glasses could be assigned to ^1H in LiOH environment. So, the other resonance (+4.8 PPM) is most likely due to proton in $Si(OSi)_3OH$ surrounding.

TABLE 4.7 DATA FOR ^1H NMR IN SOL-GEL GLASSES

Sample	Spectral Parameters (PPM)			
	CS (± 0.2)	FWHM (± 0.4)	CS (± 0.2)	FWHM (±0.4)
LSG1	+ 4.7	1.3	2.2	1.5
LSG2	+ 4.8	3.1	2.2	1.6
LSG3	+ 4.9	4.8	2.3	1.5
$LiOH.H_2O$	+ 6.5	0.5 ± 0.2	2.2	1.5

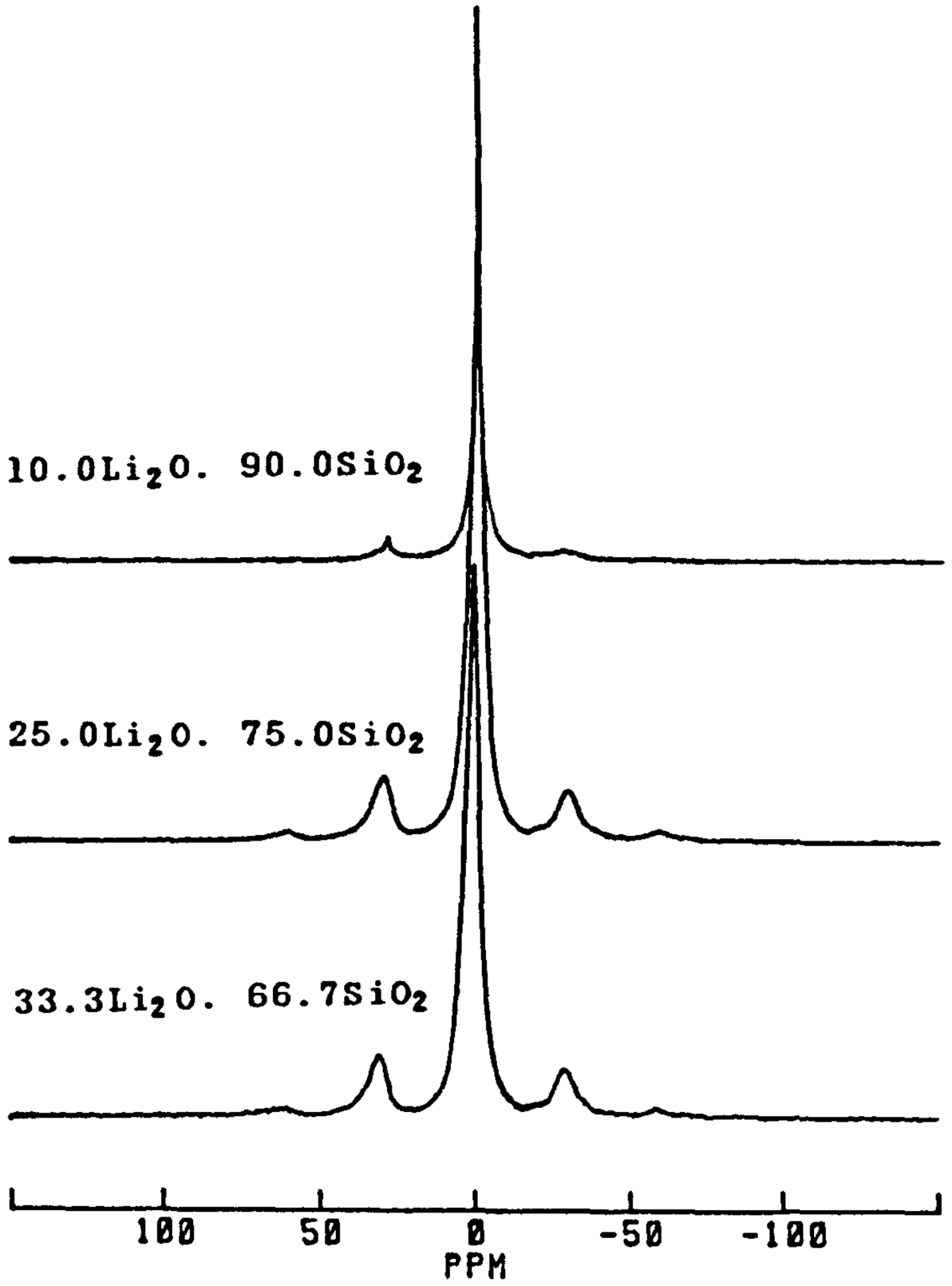

Figure 4.13 ^{7}Li spectra of sol-gel prepared lithium silicate glasses.

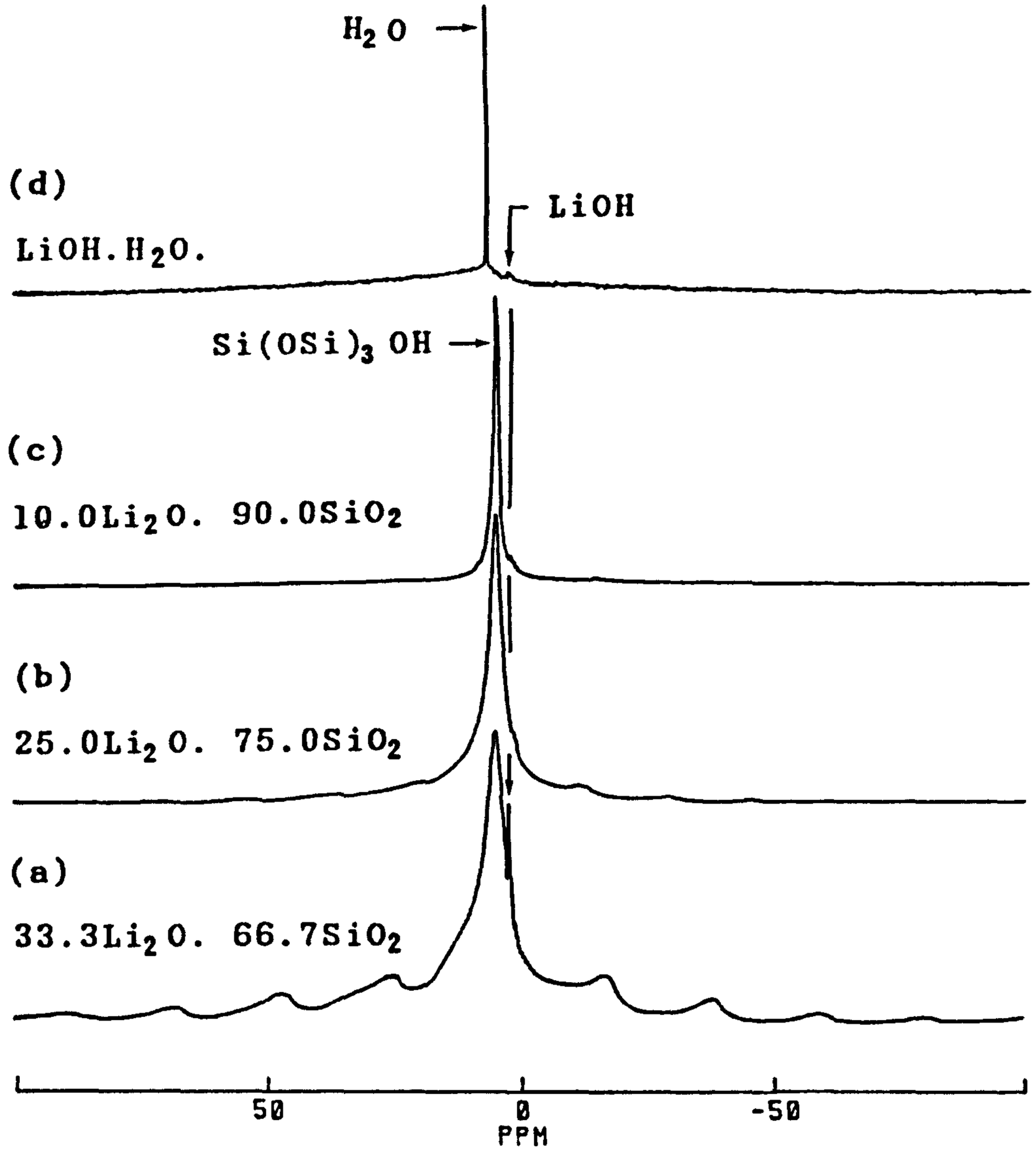

Figure 4.14 ^{1}H spectra of sol-gel prepared (a) $33.3Li_2O.2SiO_2$ (b) $25.0Li_2O.75.0SiO_2$ (c) $10.0Li_2O.90.0SiO_2$ glasses and (d) $LiOH.H_2O$.

4.6 DISCUSSION OF THE RESULTS OF SOL-GEL PREPARED LITHIUM SILICATE GLASSES

The ^{29}Si peak position -100.6 PPM (Table 4.6) is different from the normal (conventionally prepared $Li_2Si_2O_5$) Q_3 (-90.0 PPM) resonance. Maciel and Sindrof [52] observed the resonance for $Si(OSi)_3OH$ at -99.8 PPM in silica gel, Farnan et al. [46] and Aujla et al. [53,54] reported the shift -100.5 PPM for that species in hydrous silica glass. Therefore the ^{29}Si shift in these glasses at -100.6 PPM can be assigned to Q_3 species where the nbo is bonded to ^1H. The ^{29}Si resonance in anhydrous vitreous silicon ranges from -110.0 to -112.5 PPM [55-58]. This range of chemical shift mainly depends upon the method of preparation. The shifts in the glasses are within the range of anhydrous vitreous silica and are due to the $Si(OSi)_4$ (Q_4) unit.

The sources of hydrogen are presumably due to the breakdown of starting materials, e.g. $LiOC_3H_7$, $Si(OCH_3)4$, CH_3OH, H_2O, HNO_3 etc. and the hydrogen seems to play an important role in the glass structure. The electronegativities for ^1H and Li are 2.15 and 0.95 respectively. Therefore H^+ is more likely to form bond with [nbo]. It can be inferred from the ^{29}Si shift (-100.6 PPM) that ^1H does indeed bond with the network former Si^{4+} via oxygen. The ratio (Q_4/Q_3) for LSG1 is comparable with the binary model [21] but that for LSG2 and LSG3 is not. The transfer of polarisation to the silicon confirms the presence of OH^- ions as $Si(OSi)_3OH$ in the samples LSG1-LSG3. The presence of $Si(OSi)_2 2OH$ may be ignored because no evidence of peak around -90 to -93 PPM is observed from the spectrum (Figure 4.12.d).

With the increase of Li^+ in the glasses the area under the proton resonance at +2.2 PPM increases. This may indicate the increase of LiOH environment with Li^+ content. Molecular water, if present, might have an effect on the resonances but direct prediction is not possible from the spectra. The assignment of the peak (^1H) at +4.8 PPM due to $Si(OSi)_3OH$ is resonable because the ^{29}Si chemical shifts in these materials correspond to Si in $Si(OSi)_3OH$ environment. Therefore it can be concluded that Li^+ occupies the holes in the glass structure as LiOH and ^1H acts as a modifier in the sol-gel prepared lithium silicate glasses.

REFERENCES

1. P.W. McMillan, Glass Ceramics, Academic Press, 2nd Edn., London, 1979.

2. J.W. Cahn and R.J. Charles, Phys. Chem. Glasses, 6(5), 181 (1965).

3. F. Liebau, Z. Naturf. B, 15, 467 (1960).

4. K.F. Hesse, Acta crystallogr. B, 33, 901 (1972).

5. H. Vollenkle, A. Wittmann and H. Novotny, Montash. f. Chem., 99, 1360 (1968).

6. H. Vollenkle, A. Wittmann and H. Novotny, Montash, f. Chem., 100, 295 (1969).

7. M. Ito, T. Sakaino and T. Moriya, Bull. Tokyo Inst. Techn., 88, 127 (1968).

8. P.F. James, Phys. Chem. Glasses, 15(4), 95 (1974).

9. G. Roed, N.H. Christensen and J. Middelboe, Am. Ceram. Soc. Bull., 55(8), 722 (1976).

10. D.M. Sanders, W.B. Person and L.L. Hench, Appl. Spectrose., 28, 247 (1974).

11. D.W. Matson, S.K. Sharma and J.A. Philpotts, J. Non Crystalline Solids, 58, 323 (1983).

12. G. Donnay and J.D.H. Donnay, Am. Miner., 38, 163 (1953).

13. A.M. Kalinina. Inorg. Mat., 6, 796 (1970).

14. C.M. Schramm, B.W.H.S. de Jong and V.E. Parzialy, J. Am. Chem. Soc., 106, 4396 (1984).

15. U. Selvaray, K.J. Rao, C.N.R. Rao, J. Klinowski and J.M. Thomas, Chem. Phys. Lett., 114(1), 24 (1985).

16. A.R. Grimmer, M. Magi, M. Hahnert, H. Slade, A. Samoson, W. Wieker and E. Lippman, Phys. Chem. Glasses., 25(4), 105 (1984).

17. C.N.R. Rao, J.M. Thomas, J. Klinowski, U. Selvaraj, K.J. Rao, G.R. Milward and S. Ramdas, Angen. Chem., 24(1), 61 (1985).

18. J.B. Murdoch, J.F. Stebbins and I.S.E. Carmichael, Am. Miner., 70, 332 (1985).

19. L.F. Gladden, T.A. Carpenter, J. Klinowski and S.R. Elliot, J. Magn. Reson., 66, 93 (1986).

20. R. Dupree, D. Holland and D.S. Williams, Journal De Physique, Colloque C8, Supplement au no.12, Tome 46, 1985.

21. R. Dupree, D. Holland, P.W. McMillan and R.F. Pettifer, J. Non-cryst. solids, 68, 399 (1984).

22. R. Dupree, D. Holland and D.S. Williams, J. Non-cryst. Solids, 81, 185 (1986).

23. J.F. Stebbins, Nature, 330, 465 (1987).

24. R.J. Charles, J. Am. Chem. Soc., 52 (12), 631 (1967).

25. J. Herzfeld and A.K. Berger, J. Chem. Phys., 73(12), 6021 (1980).

26. B. Lindman and S. Forsen, The alkali metals; NMR and the Periodic Table. Edited by R.K. Harris and B.E. Mann, Academic Press, P.129 (1978).

27. P. Laszlo, The Alkali Metals : The Multinuclear Approach to NMR Spectroscopy, edited by J.B. Lambert and F.G. Riddel, D. Riddel Publishing Company, P.261, 1982.

28. D.M. Follstaidt and R.M. Biefeld, Phys. Rev. B, 18(11), 5928 (1978).

29. T. Asai and S. Kawai, Solid State Commun., 36, 891 (1980).

30. E. Gobel, W. Muller-Warmth, H. Olyschlager and H. Dutz., J. Magn. Reson., 36, 371 (1970).

31. D.M. Follstaedt and P.M. Richards, Phys. Rev. Lett., 37 (23), 1571 (1976).

32. P.C. Schmidt, K.D. Sen, T.P. Das and A. Weiss, Phys. Rev. B, 22, 4167 (1980).

33. S.W. Kennedy, Encyclopedic Dictionary of Physics, Pergamon Press, Ed. J. Thewlis, P.476, 1961.

34. G.E. Pake, J. Chem. Phys., 16, 327 (1948).

35. J.H. Van Vleck, Phys. Rev., 74, 1168 (1948).

36. F. Liebau, Acta. Cryst., 14, 389 (1961).

37. B.W.H.S. de Jong, Nature, 330, 422 (1987).

38. M. Tomozawa, Phys. Chem. Glasses, 13(6), 161 (1972).

39. E. Schneider, J.F. Stebbins and A. Pines, J. Non-cryst. Solids, 89, 371 (1987).

40. R. Dupree, Int. Conference in East Germany, 1988, to be published.

41. K. Mitteilung, A.-R. Grimmer, F.V. Lampe, M. Magi and E. Lippmaa, Mon. Chem., 114, 1053 (1983).

42. T.P. Seward, III, Metastable phase diagrams and their application to glass forming ceramic systems, in

Phase Diagrams. Edited by A.M. Alper, Vol.6-I, P.299, Academic Press, 1970.

43. R. Dupree, D. Holland, in New Horizons in glass and glass-ceramics, Ed. M.H. Lewis, Chapman and Hall (1988).

44. G.L. Turner, R.J. Kirkpatrick, S.H. Risbud and E. Oldfield, Am. Ceram. Soc. Bull., 66(4), 656 (1987).

45. The sol-gel prepared lithium silicate samples were kindly supplied by Dr. A. H. Chen and Dr. P.F. James, University of Sheffield.

46. I. Farnan, S.C. Kohn, and R. Dupree, Geochim. Cosmochim. Acta., 51, 2869 (1987).

47. This spectrum was collected in collaboration with Dr. M.E. Smith. Dept. of Physics, Univ. of Warwick.

48. J.P. Yesinowski and H. Eckert, J. Am. Chem. Soc., 109, 6274 (1987).

49. J.P. Yesinowski, H. Eckert and R. Rossman, J. Am. Chem. Soc., 110, 1367 (1988).

50. H. Eckert, J.P. Yesinowski, Lynn A. Silver and E.M. Stolper, J. Phys. Chem., 92, 2055 (1988).

51. R. Dupree, S. Kohn, M.E. Smith, Abs.NO. V12 A-04, EOS, Vol.69, 504 (1988).

52. G.E. Maciel and D.W. Sindorf, J. Am. Chem. Soc., 102, 7606 (1980).

53. R. Aujla, R. Dupree, I. Farnan and D. Holland, 2nd International Conference on the Effects of Models of Formation of the Structure of Glass, Nashvile, U.S.A. Vol.2, June 8-12, 1987.

54. R. Aujla, R. Dupree, I. Farnan and D. Holland, The Physics and Technology of amorphous silica, France, June 29 - July 3, Plenun Press (1987).

55. R. Dupree and R.F. Pettifer, Nature, 308, 523 (1984).

56. R.J. Kirkpatrick, T. Dunn, S. Schramm, K.A. Smith, R. Oestrike and G. Turner, A Review in Structure and Bonding in Non-crystalline Solids (Eds. G.E. Walrafen and A.G. Revesz) Plenun Press, New York, 303 (1986).

57. L.F. Gladden, T.A. Carpenter and S.R. Elliott, Phill. Mag. B53, L81 (1986).

58. R.A.B. Devine, R. Dupree, I. Farnan and J.J. Cappni, Phys. Rev., B35, 2560 91987).

CHAPTER 5

SODIUM SILICATE SYSTEM

5.1 INTRODUCTION

The sodium silicate glass structure has been examined by several techniques; e.g. infrared, radial distribution functions obtained from XRD, XPS, Raman spectroscopy etc. [1-5]. These show limited success in determining local structure or concentration of species in the quenched glasses. Infrared spectra [1] of sodium silicate glass reveal absorption bands due to bridging oxygens [bo] and non-bridging oxygens [nbo]. Comparison of the calculated and experimental radial distribution function [2,3] shows similar local order of the network former in glasses and their crystalline analogues. The presence of [nbo] has also been shown by XPS [4]. However none of these measurements have presented successful quantitative data about the particular Q_m species present in these glasses.

This system is of interest in the study of the kinetics of nucleation and crystallisation [6-9]. High resolution electron microscopy (HREM) has been used by several workers to determine these characteristics. Base glasses can be inhomogeneous after quenching from a high temperature melt even though they appear clear. Sub-microscopic inhomogeneity can be detected by using HREM [6]. However the resolution of the technique (~ 15 Å) prevents determination of early nucleation and hence microphase separation [10-13].

^{29}Si NMR has been shown to be sensitive to the local electronic environment of silicon in silicate glasses and minerals [14-32] and the structure of sodium silicate has also been investigated by several authors using NMR [14,15,31]. Incorporation of paramagnetic centres has been shown to

facilitate the NMR experiments of the glass system by reducing the spin-lattice relaxation time [14,15]. However a systematic study on the system as a function of impurity concentration is yet to be made. There are several crystallographically non-equivalent structures, such as α , β , γ etc., of sodium disilicates which can be produced by judicious choice of heat treatment [33]. In this chapter the effect of paramagnetic impurity and the effect of systematic heat treatments on the $Na_2O.2SiO_2$ glasses are presented via MAS NMR, NMR and DTA.

5.2 THE EFFECT OF PARAMAGNETIC IMPURITY

The presence of paramagnetic impurities induces line shifts and nuclear spin relaxation because of the space varying magnetic field produced by the impurity moment [34-41]. The paramagnetic centres change the chemical shift and reduce spin-lattice relaxation time [39-41]. The impurity moment has also a significant effect on the line shape. The change of ^{29}Si relaxation time due to incorporation of paramagnetic impurities has been reported qualitatively by several authors [14,15,18,19,24,25] but the change of full width at half maximum (FWHM) and chemical shift (CS) has not been reported. Thus a quantitative measurement of the ^{29}Si nuclear properties and relative crystallisation in sodium disilicate glasses with varying amounts of MnO are the theme of this section.

5.2.1 ^{29}Si NMR

The ^{29}Si spectra of $Na_2O.2SiO_2.xMnO$ (x=0, 0.05, 0.1, 0.2, 0.4 and 0.8%; NS1-NS6) are shown in Figure (5.1). For

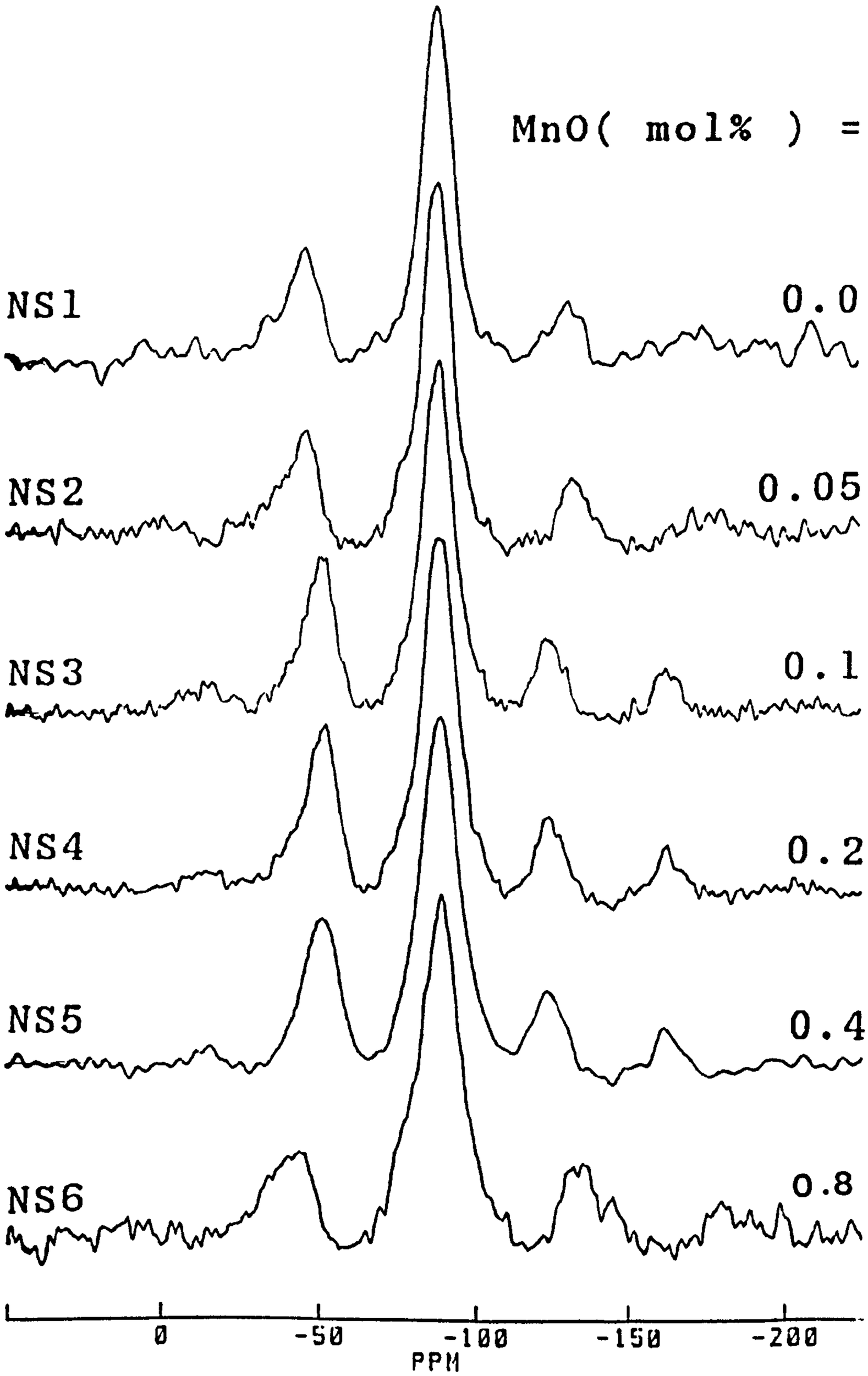

Figure 5.1 ^{29}Si spectra of $Na_2O.2SiO_2$ glasses with varying amounts of MnO.

alkali ions the chemical shift moves to a lower frequency, i.e. more shielded [39-41] and a similar effect is observed in the case of ^{29}Si.

Semilogarithmic plots of recovered magnetisation versus relaxation delay of the samples NS1, NS3-NS6 are shown in Figure 5.2 and the effect of paramagnetic centres on the relaxation rate is shown in Figure (5.3). The relaxation rate is changing roughly linearly, i.e. a steep drop in T_1 for low concentration of Mn^{2+}. The rate of decrease is reduced for higher levels of Mn^{2+}. Although the sample NS1 does not contain MnO but it does contain some impurities, e.g. Fe_2O_3 - 11 PPM, Al_2O_3 - 162 PPM, which could reduce the relaxation time. Thus the straight line of Figure 5.3 is not expected to be passed through the origin. The gradient ($\Delta T^{-1}/\Delta C$), where C is the concentration of MnO, gives 0.66 $s^{-1}/\%$. The spectral parameters and the T_1 relaxation times are summarised in Table 5.1. The variation of FWHM and chemical shift as a function of MnO content is shown in Figure 5.4.

5.2.2 DTA

The presence of any impurity, e.g. paramagnetic centres, in a glass melt may influence nucleation [33] and hence enhance phase separation, crystallisation etc. In order to observe the relative rate of crystallisation due to varying amounts of MnO in $Na_2O.2SiO_2$ DTA experiments were carried out. The glass transition temperature, T_g, crystallisation temperature, T_x, and the liquidus temperature, T_{ls} are recorded in Table (5.1). The T_g, T_x and T_{ls} do not change very much due to addition of impurity (MnO) in the system but the rate of crystallisation increases with the impurity

TABLE NO.5.1 Spectral Parameters, relaxation times, T_g, T_x and T_{ls} of $Na_2O.2SiO_2.XMnO$

Sample	Level of MnO (mol%)	Chemical Shift (PPM) ±0.5	FWHM (PPM) ±0.5	T_1 relaxation time (s)	Relaxation rate (s^{-1}) x10^{-2}	Glass transition temperature 'T_g' (^oC) ±5	Crystallisation temperature T_x (oC) ±2	liquidus temperature T_{ls} (^oC) ±2
NS1	0.0	-88.8	10.5	112.0±9.8	0.90±0.08	457	643	890
NS2	0.05	-88.8	10.6	-	-			
NS3	0.1	-89.0	11.5	21.0±2.2	4.81±0.5	453	639	887
NS4	0.2	-89.2	12.5	8.0±1.0	12.7±1.6	459	643	888
NS5	0.4	-89.4	14.0	4.0±0.3	25.1±1.9	451	638	884
NS6	0.8	-89.9	15.0	1.76±0.2	56.8±6.3	456	640	889

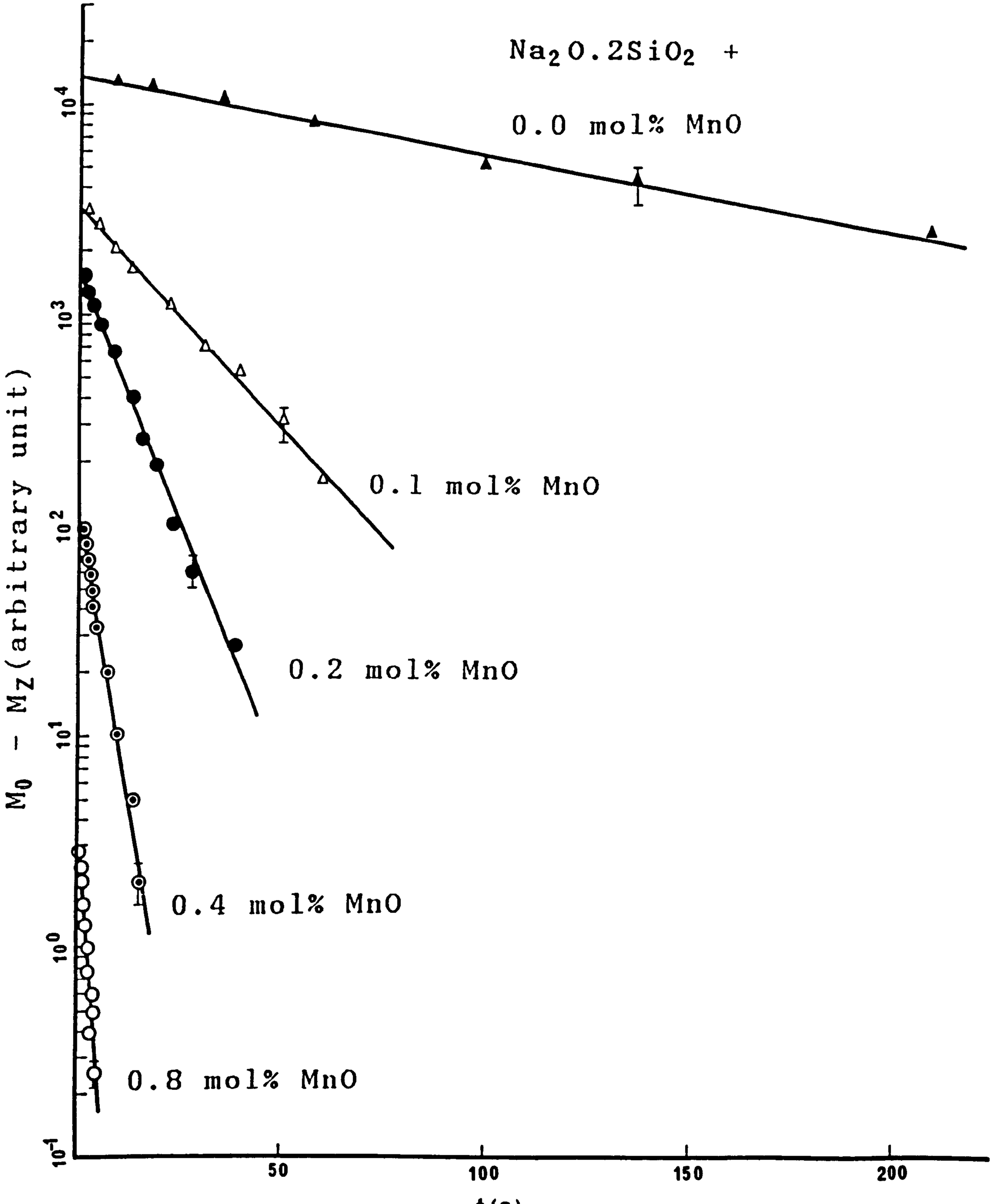

Figure 5.2 ^{29}Si relaxation decay of sodium disilicates with different amounts of MnO. In order to prevent overlapping (M_0 - M_Z) of each plot is shifted.

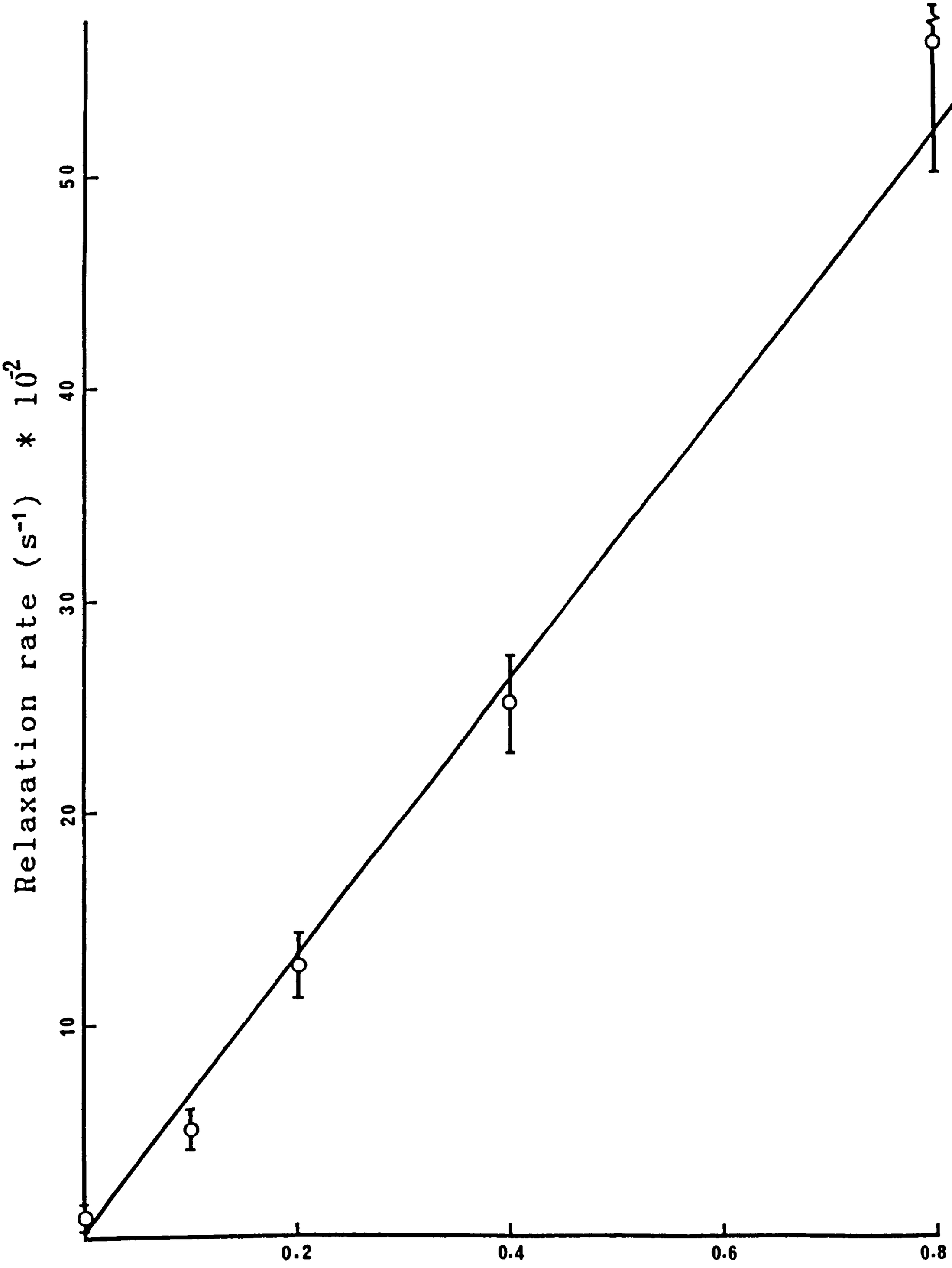

Figure 5.3 ^{29}Si relaxation rate as a function of MnO content in sodium disilicate base glasses.

concentration >0.2 mol%. An example of this is shown in Figure (5.5). Exactly the same pair of crucibles and the same amounts of samples were taken for the measurements. Therefore the relatively large area under the exothermic peak must represent the higher crystallisation rate.

According to Williamson and Glasser [33] the transformation of α_{III} phase occur at 678 and 707 ^{o}C. But the two peaks found in this case are at 695 and 723 ^{o}C. The peaks due to γ-$Na_2Si_2O_5$ transformation occur at 560, 575 and 595 ^{o}C and those for $\gamma + \delta$ -$Na_2Si_2O_5$ occur at 580 and 595^{o}C. Therefore the observed peaks are close to α_{III} - $Na_2Si_2O_5$ and it may be said that α_{III} - $Na_2Si_2O_5$ transformation occurs during the heating cycle of DTA experiments (Figure 5.5).

5.3 THE EFFECT OF DEVITRIFICATION

The MAS NMR spectra of species in glasses with very small structural differences are indistinguishable from each other since the chemical shift difference is much less than the linewidth. Therefore only an average electronic environment of a particular species is observable in glass. For example, ^{29}Si spectra of $Na_2O.2SiO_2$ glasses (Figure 5.1) are not very informative as to how and where the Na^+ ion is situated because of the range of sites of the species. In ordered material it would be expected that MAS NMR spectra should provide well resolved lines corresponding to different positions of the next nearest neighbour (nnn). The purpose of this section is to show the sensitivity of MAS NMR to the local environment of the ^{29}Si in sodium disilicate by judicious choice of heat treatments.

Glass ceramics of $Na_2O.2SiO_2$ were produced by controlled

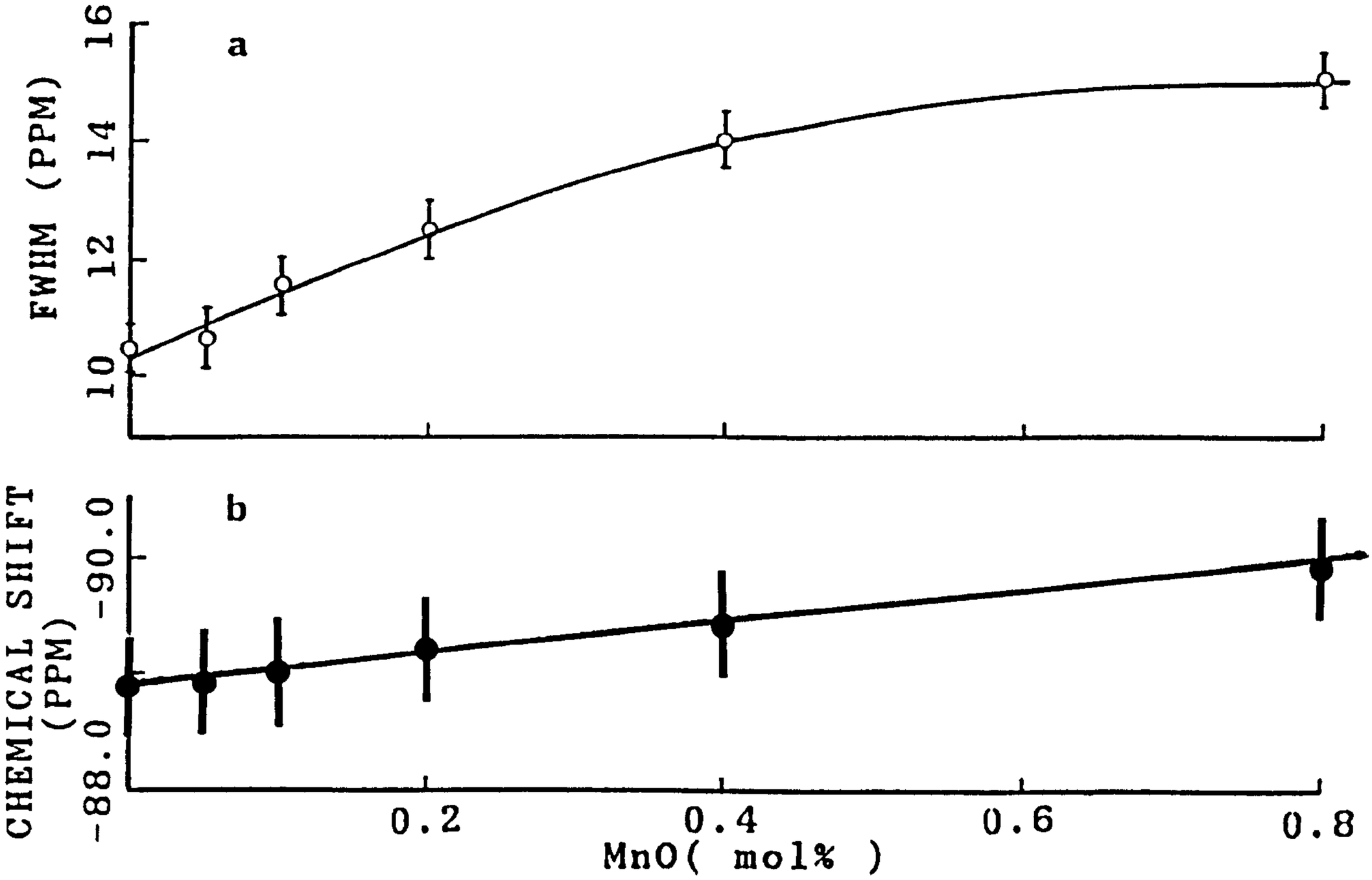

Figure 5.4 Variation of (a) full width at half maximum(FWHM) and chemical shift(CS) with MnO content in sodium disilicate base glasses.

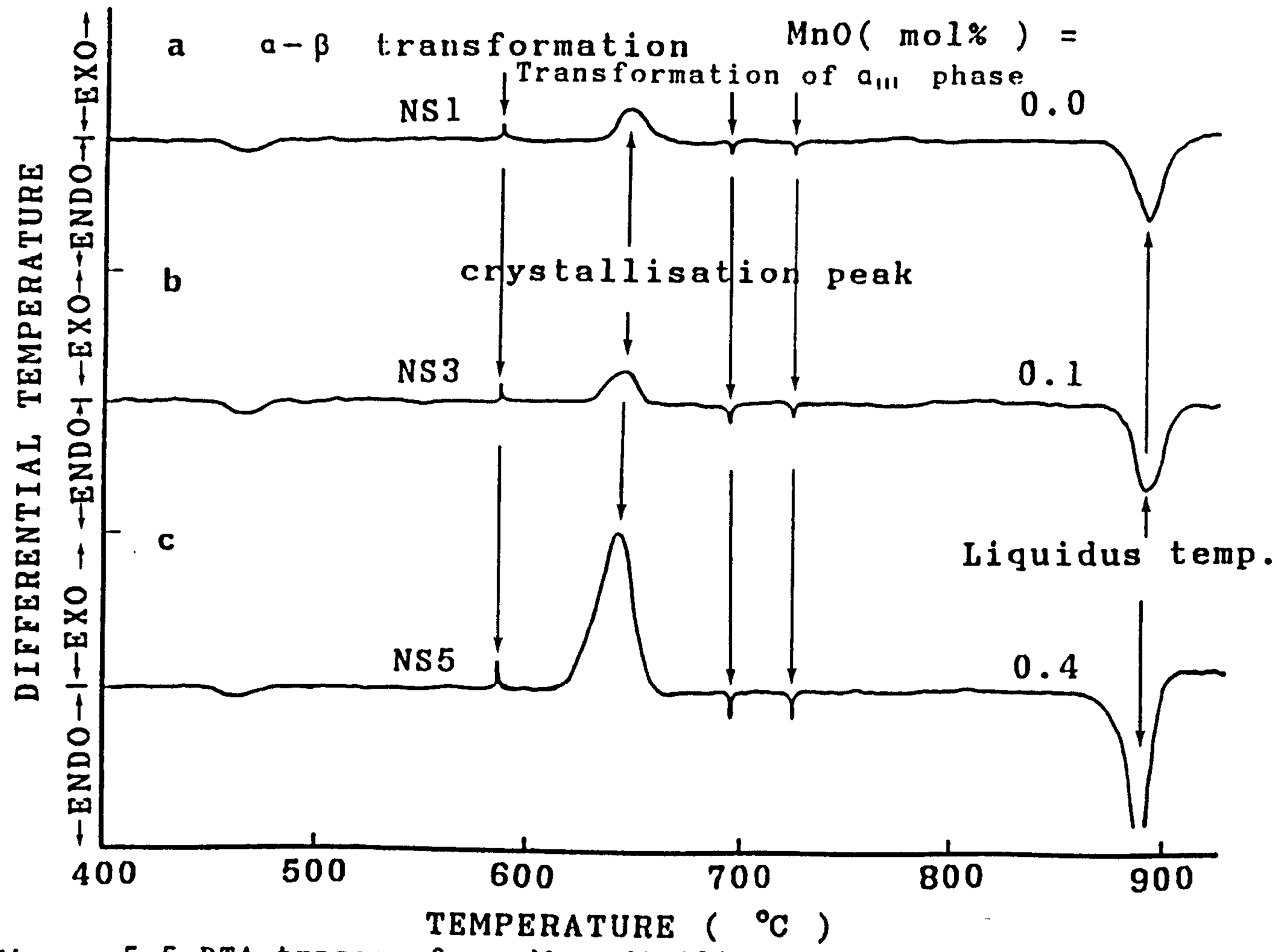

Figure 5.5 DTA traces of sodium disilicate glasses with (a) no MnO (b) 0.1 mol% MnO and (c) 0.4 mol% MnO. Peak heights are normalised.

heat treatment of the glass under normal atmospheric pressure. Sodium disilicate glass can be crystallised to yield six polymorphs at one bar pressure depending on temperature and time of heat treatments [33]. A set of heat treatment temperatures was chosen to produce different polymorphs. The ^{29}Si spectra of the respective products are shown in Figure (5.6). Their chemical shifts and the Si-O-Si mean bond angles are given in Table 5.2.

Like lithium disilicate (Chapter 4), the sodium disilicate glass contains Q_3 and a small percentage of Q_4 and Q_2 species (Figure 5.7.a) whilst the crystal contains only Q_3 species. The ^{29}Si static spectrum of crystalline $Na_2O.2SiO_2$ (Figure 5.7.b) is a representation of an axially symmetric powder pattern from which it is not possible to infer the number of polymorphs formed during devitrification. But in the case of MAS NMR spectra (Figure 5.7.c) narrowed spectra due to the formation of α, β and a mixture of γ and δ phases at $625^oC/12h$ are observed. The mixture of γ and δ phases at that particular temperature was noted by Williamson and Glasser [33]. According to their investigation the subtraction of the δ phase XRD pattern from the composite pattern of $\gamma + \delta$ phase yielded the XRD trace of γ phase.

An attempt to correlate the chemical shift with $\overline{\sec \alpha'}$, where α' = Si-O-Si bond angle, is made in a different way from previous workers [30]. They used a correlation derived by Smith and Blackwell [42] for silica polymorphs to correlate Q_2, Q_3 and Q_4 structural units. In alkali silicates, the isotropic chemical shift values of Q_2, Q_3 and Q_4 are within -77 ± 2, -90 ± 4 and -105 ± 7 PPM respectively. Chemical shift and bond angle depend upon the number of [bo] and [nbo]. Thus the

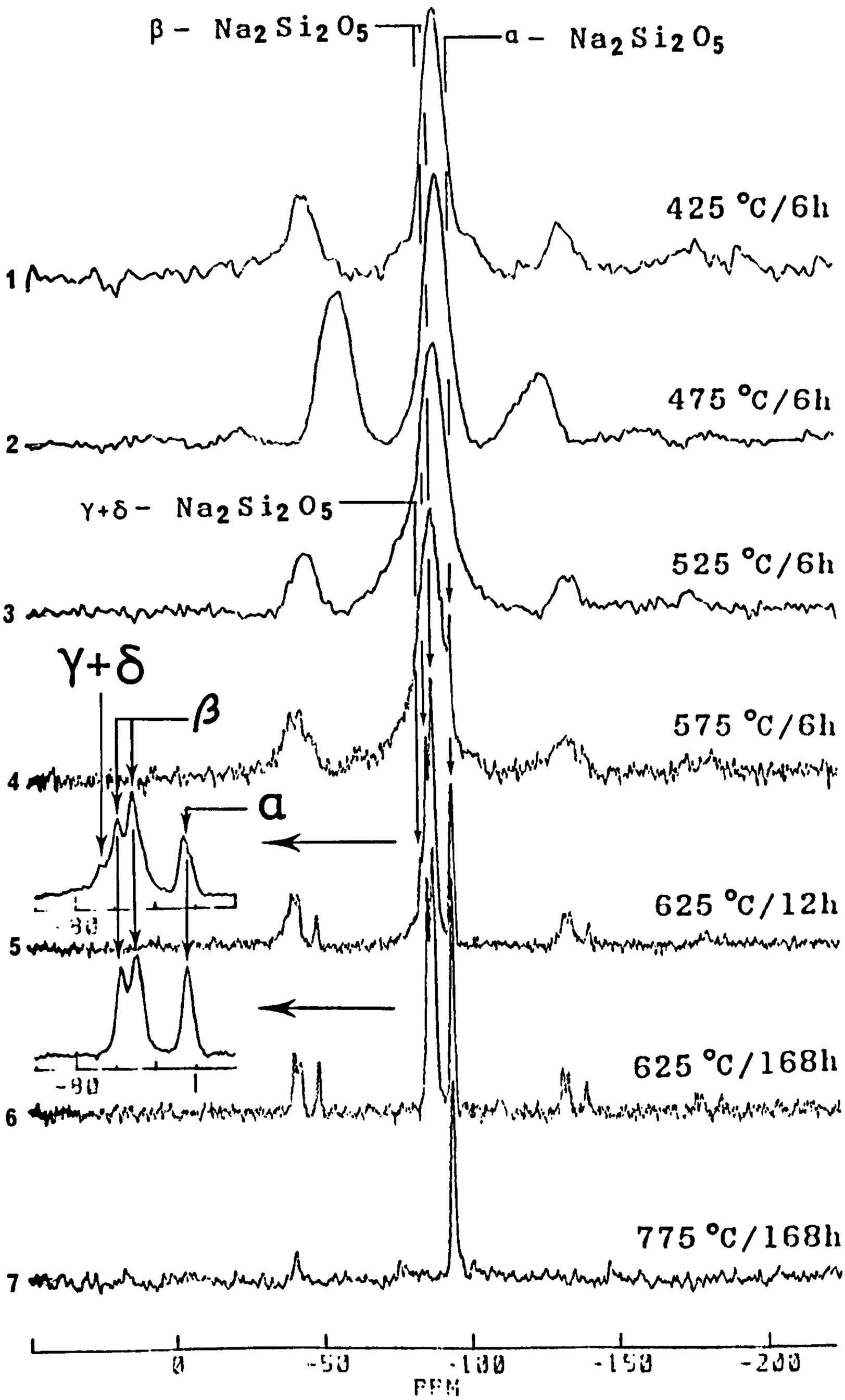

Figure 5.6 ^{29}Si spectra of heat treated sodium disilicate glasses.

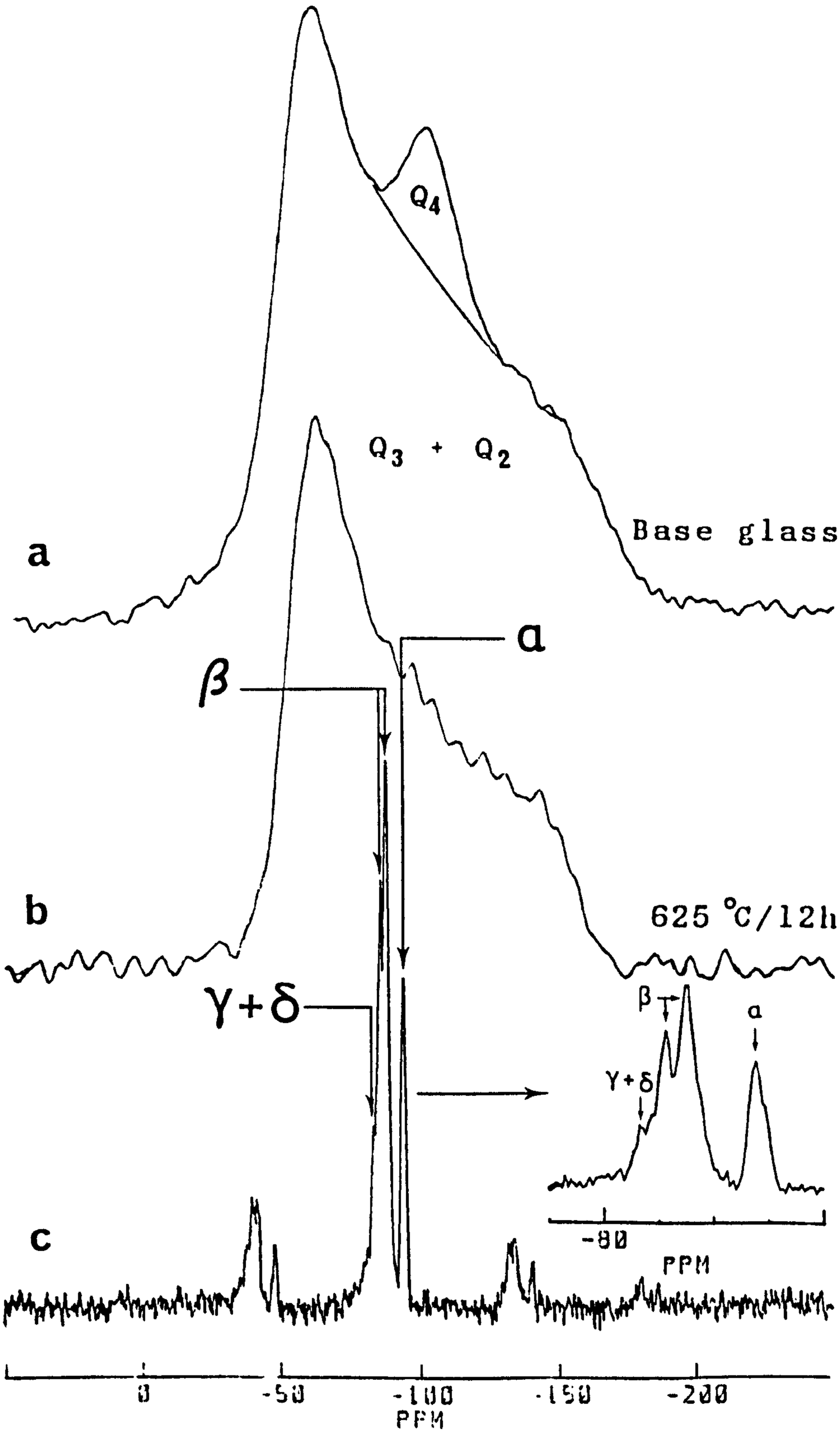

Figure 5.7 ^{29}Si static spectra of sodium disilicate (a) base glass (b) crystalline. (c) ^{29}Si MAS spectra of (b) and inset is an extended form of centre band.

TABLE NO. 5.2 Spectral parameters and Si-O-Si mean bond angle of $Na_2Si_2O_5$ polymorphs

Polymorph	Chemical shift (PPM) ± 0.2	FWHM (PPM) ± 0.2	Si-O-Si mean bond angle (°)
α	-93.6	1.4	149.5
β	-87.4	1.8	136.8
	-85.6	1.4	135.1
γ+δ	-83.8	-	+
γ*	-86.0	-	+
δ*	-90.0	-	+

* Obtained from page 183 and 184

\+ Not known

correlation used for Q_4 tetrahedra [42] may not be used for Q_3 and Q_2 units [43]. The Si-O-Si bond angles for α - and β - $Na_2Si_2O_5$ are known [44,45] but those of γ and δ are unknown. Figure (5.8.a) shows the plot of ^{29}Si chemical shift against the sec α' for the polymorphs. A straight line is drawn with some uncertainty because of only three points and the correlation is found to be

$$\delta = -132.5 - 33.3 \ \overline{\sec \alpha'} \qquad \ldots \qquad \ldots \qquad (5.1)$$

where δ is the chemical shift. Figure 5.8.b shows the variation of chemical shift for a certain range of α' .

5.4 ^{23}Na NMR IN SODIUM DISILICATE GLASS AND GLASS-CERAMICS

Dupree et al. [14] first carried out ^{23}Na MAS NMR in sodium silicate glasses and glass-ceramics. The results presented in this section on $Na_2Si_2O_5$ are consistent with Dupree et al. [14] but extend to a more systematic study of how the sodium environment changes with successive heat treatments.

The ^{23}Na spectra of $Na_2Si_2O_5$ glass and samples heat treated at different temperatures and times are shown in Figure (5.9). The spinning spectra of the glasses are almost gaussian lineshapes flanked by spinning sidebands. The static spectra of glasses are also gaussian lineshape. The satellite transitions corresponding to $\pm 3/2 \longleftrightarrow \pm 1/2$ are not observed because of a large electric field gradient which wipes out the higher order transition. A change in the ^{23}Na lineshape in glass is observed (Figure 5.9) with successive heat treatment. The spectra for crystalline materials represent the second order quadrupolar effect at the site of the sodium nucleus.

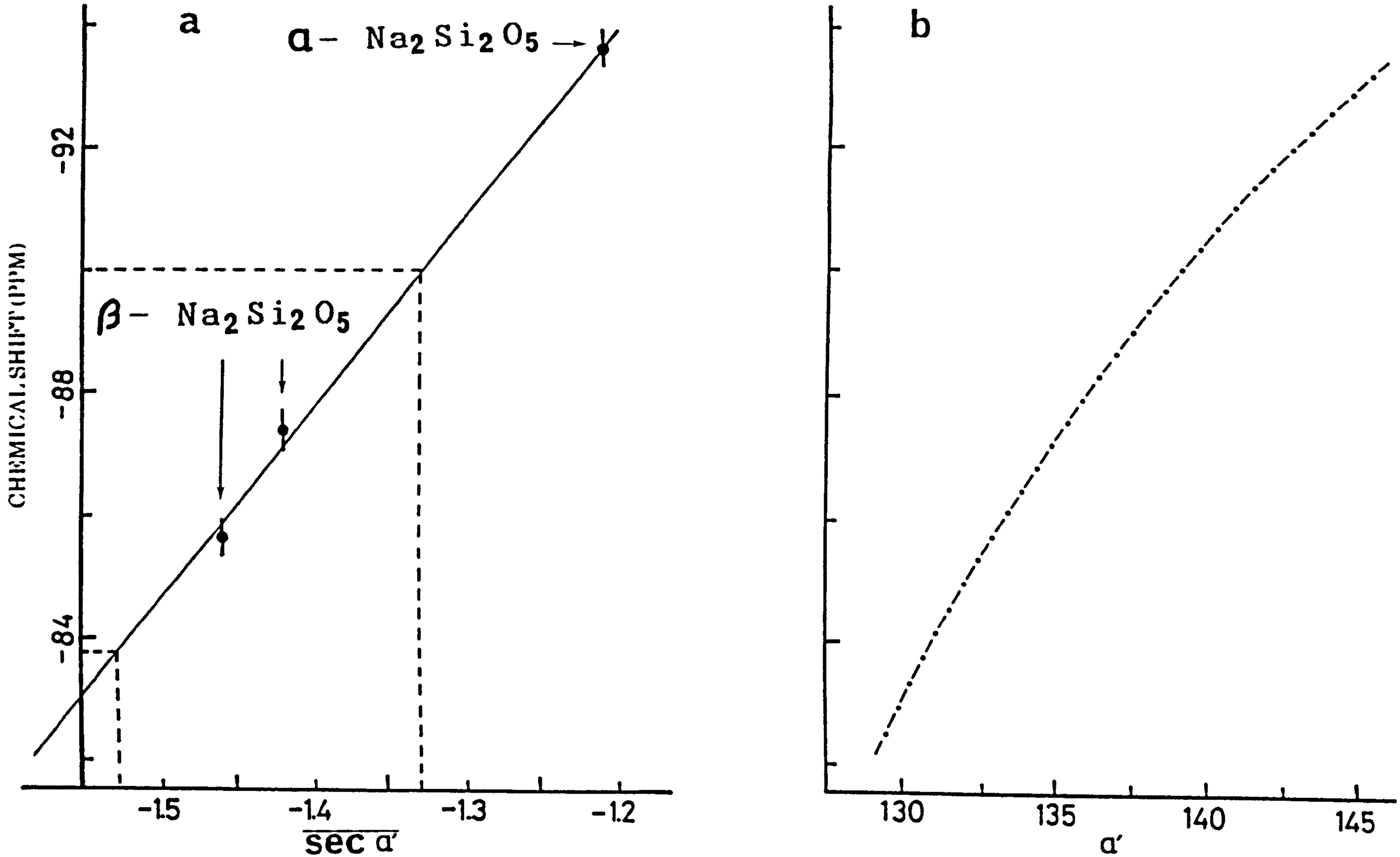

Figure 5.8 Variation of the ^{29}Si chemical shift with (a) mean sec α' and (b) α' , where α' = Si - O - Si bond angle.

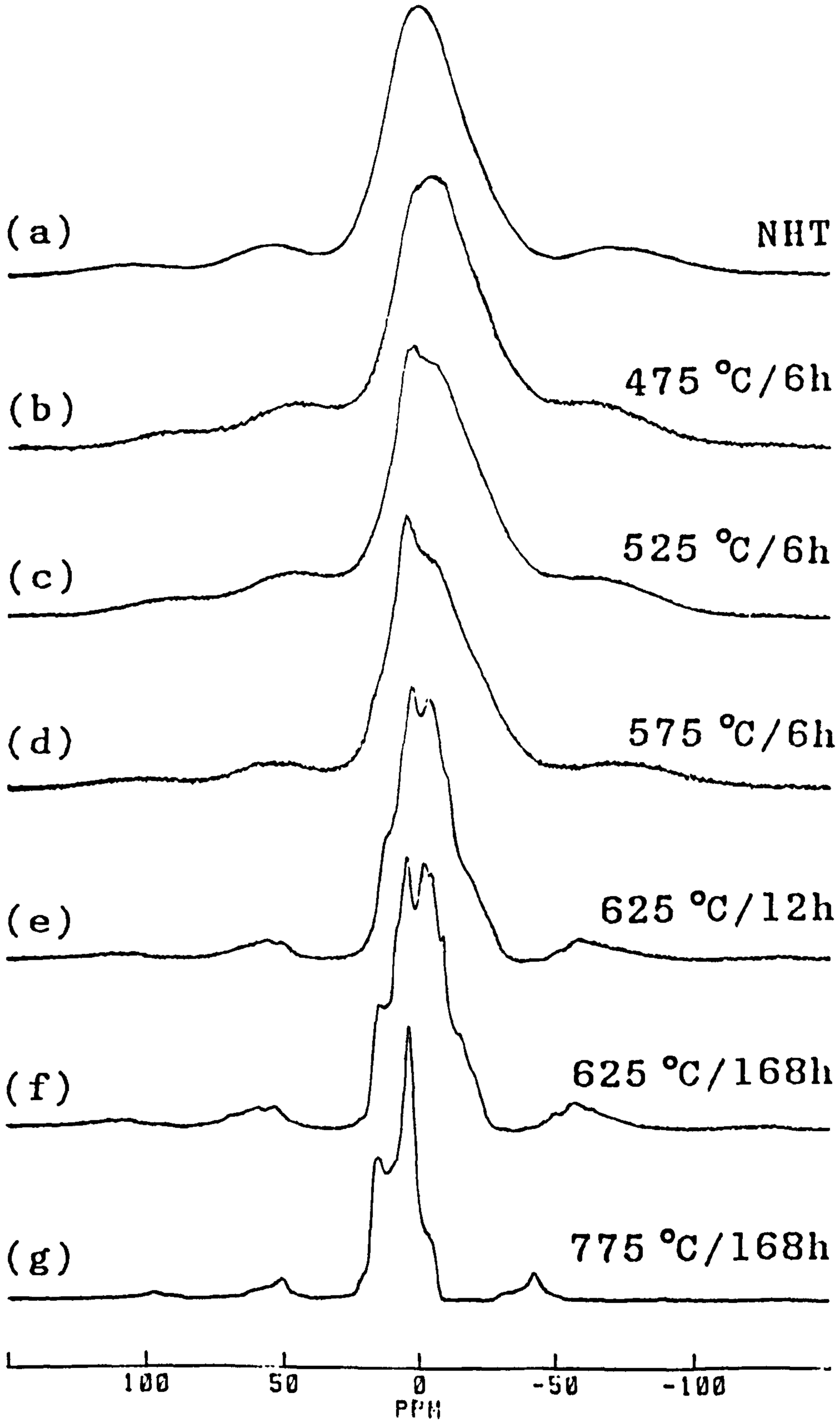

Figure 5.9 ^{23}Na spectra of $Na_2Si_2O_5$ glass and glass ceramics.

The peak position corresponding to glass spectrum is +0.7 PPM, consistent with Dupree et al. [14]. The observed change in resonance frequency and in lineshapes between glass and crystalline spectra indicate the change of ^{23}Na environment because of heat treatment. This effect has also been observed by Dupree et al. [14] in Na_2O-SiO_2 system. The spectra are narrowed by a factor of 4-5 due to spinning at the magic angle.

An attempt has been made to simulate the spectra using different η values to calculate the electric field gradient at the site of sodium nucleus but the presence of more than one polymorph creates a problem for simulation. Although the ^{29}Si spectrum of $Na_2O.2SiO_2$ heat treated at 775°C/168h shows a single resonance (Figure 5.6.7), XRD powder pattern of the sample is consistent with α_I and α_{II} forms of the α-$Na_2Si_2O_5$ family. This therefore gives rise to two peaks with dissimilar intensity (Figure 5.9.g) in the ^{23}Na spectra of the sample and this makes simulation inaccurate. The local symmetry of sodium does not seem to be very different from the powder diffraction studies of α_I and α_{II} - $Na_2Si_2O_5$ polymorphs [33]. Single crystal studies of these two polymorphs are not available to date and it is not possible to calculate the values of the asymmetry parameters for the sodium sites of the polymorphs. Despite this complication an estimate of quadrupolar coupling constant (e^2qQ/h) of 1.7 $\pm$ 0.2 MHz can be made from the peak positions by assuming the asymmetry parameter, η =0. Static ^{23}Na NMR with 2.5MHz spectral width did not show any higher order transitions.

5.5 DISCUSSION

5.5.1 PARAMAGNETIC IMPURITIES

Impurities are unavoidable constituents in the glass system. The presence of paramagnetic impurities in the diamagnetic solids change the magnetic properties of the constituent elements. The large impurity moment may have an influence on the linewidth and on the chemical shift.

The alkali to silicon ratio is constant for all the samples and it would be expected that the amounts (%) of Q_4 and Q_2 may be the same in all the materials. Therefore the Q_3 chemical shift is relatively unaffected by the connections $Q_3 \longleftrightarrow Q_4$ and $Q_2 \longleftrightarrow Q_3$. The apparent change in the ^{29}Si linewidths and chemical shifts with the increase of paramagnetic centres is due to modification of the local field in the vicinity of ^{29}Si [37].

The magnetisation M due to the presence of paramagnetic centres is given by [46]

$$M \sim N \frac{g^2 \mu^2}{3} \frac{S(S+1)}{kT} B_0 \quad \ldots \quad \ldots \quad (5.2)$$

where N is the number of impurity ions per unit volume, g is the Lande g-factor, μ is the Bohr magneton, S is the spin of manganese, k is the Boltzmann constant and T is the temperature. All the terms on the right hand side of equ. (5.2), except N, are constant. The value of N for 0.1 mol% MnO in $Na_2O.2SiO_2$ is 7.87×10^{26} m^{-3} and that for 0.8 mol% MnO is 6.3×10^{27} m^{-3}, i.e. M increases linearly with N. Moreover the field varies as $1/r^3$, i.e. the silicons at different distances see different fields. Thus the ^{29}Si in the neighbourhood of paramagnetic centres sees a large field

in comparison to its average local field. Therefore the nearby silicons do not contribute to the NMR signal, i.e. within a radius 'b' there will be no spin diffusion [35]. This large space varying magnetic field may be the cause of relatively wider linewidth and more shielded chemical shift. Increased addition of MnO will ultimately wipe out the ^{29}Si signal.

The overall process involves the rate at which spins can diffuse energy to the paramagnetic centres and the rate at which the magnetic centres equilibrate spins in their neighbourhood [36-38]. For both fast and slow diffusion limits several authors have shown that the relaxation rate is proportional to the concentration of the impurity ion (see section 2.6).. Figure (5.2) shows the marked change of relaxation time and Figure (5.3) clearly shows that the relaxation rate is proportional, within the experimental error, to the impurity concentration as expected.

Impurities enhance nucleation, phase separation,

crystallisation etc. and hence change the glass properties [47]. Paramagnetic impurities may also have a profound effect in this respect. Addition of paramagnetic impurity upto 0.8 mol% is not reflected in any appreciable change of T_g, T_x and T_{ls} (Table 5.1). This suggests that MnO is not chemically bonded to the network.

The area under the crystallisation peak for the samples NS1 (0.0 mol% MnO) and NS3 (0.1 mol% MnO) are almost the same but that for NS5 (0.4 mol% MnO) is larger. This indicates that upto 0.1 mol% MnO the rate of crystallisation does not change appreciably. Therefore it can be concluded that up to 0.1 mol% MnO can be added to facilitate the NMR experiments for structural investigation in alkali silicate glasses. The impurity MnO may act as nucleating agent, i.e. higher the impurity concentration higher the nucleation centres and hence the comparatively large crystallisation peak in Figure 5.5.c. Therefore by adding a precise amount of MnO the crystallisation property of the silicate matrix may be tailored to the desired level.

5.5.2 DEVITRIFICATION OF $Na_2Si_2O_5$

There are six polymorphs, α_I, α_{II}, α_{III}, β , γ and δ , of $Na_2Si_2O_5$ known to exist at low pressure (1 bar) [33]. The non equivalent crystalline sites begin to appear for heat treatment 575°C/6h. The crystallisation products in $Na_2O.2SiO_2$ heat treated at 625°C/12h are α_I, α_{II}, β and $\gamma + \delta$ phases. The individual mean bond angle and bond lengths for the α -$Na_2Si_2O_5$ group are unknown and from MAS NMR only one peak at -93.5 PPM corresponding to this group is observed. It may be said that the local order of silicons in the α-group is

essentialy the same but in long range order they are different. The effect of sodium site symmetry on silicons of the group is difficult to interpret from the ^{23}Na spectrum (Figure 5.9.e) because this material contains a variety of polymorphs in which sodiums local order are impossible to distinguish. However the little shoulders (Figure 5.6.5; enlarged scale of 625°C/12h) on the peak at -93.5 PPM may be due to the members of α-$Na_2Si_2O_5$ family.

XRD data [45] show that β-$Na_2Si_2O_5$ does have two different silicon sites and this is confirmed by two well resolved ^{29}Si resonances at -87.5 and -85.7 PPM. This resolution may also be enhanced by the different coordinations of sodium, one is octahedral and the other one is trigonal biprism, as nnn of the two silicons.

The mixture $\gamma + \delta$ phase is unstable [33, 48] and only α- and β -$Na_2Si_2O_5$ are observed for the heat treatment 625°C/168h. All the $\gamma + \delta$ phase is converted to β phase which is evident from the Figure (5.6.6). The β -$Na_2Si_2O_5$ is also unstable [33,48] and when the sample was heat treated at 775°C/168h, all the β -$Na_2Si_2O_5$ is converted to α_I- and α_{II} - $Na_2Si_2O_5$. This is confirmed by XRD and the resonance position corresponding to this phase is observed at -93.6 PPM which is close enough to the previously assigned peak (-93.5 PPM) for α_I- and α_{II} - $Na_2Si_2O_5$.

According to Smith et al. [49] and Brown et al. [50] the <Si-O> bond distance changes from 1.61 Å to 1.64 Å as the various Q_m ($0 \leqslant m \leqslant 4$) species grow in the glass system from Q_4 to Q_0 due to addition of alkali metal oxide. Chemical shift is a function of bond distance and bond angles [51,52] and the former increases with the decrease of the latter [53]. These

facts suggest the validity of equ. (5.1) and therefore Si-O-Si mean bond angle for the species of unknown structure may be determined. Using equ. (5.1) the mean bond angle for Y + δ and δ phases are estimated to be 132.7 and 141.3° respectively. Thus NMR provides an estimate of mean bond angle where the single crystal study is not available.

Despite the complicated lineshapes of ^{23}Na spectra some structural information can also be obtained from the $+\frac{1}{2} \leftrightarrow -\frac{1}{2}$ transition. For half integral spin, the central transition can be expressed as a linear combination of three functions of which the powder average is zero [54]. The MAS NMR ^{23}Na spectra for $\eta = 0$ may therefore be obtained with three singularities for which the sodium in the material under investigation has crystallographically single environment. However with the change of η, the number of singularities changes. Behrens and Schnabel [55] have shown that the shape of the central line may exhibit four singularities for $0.50 \leqslant \eta \leqslant 0.75$. But all these derivations are for single phase material which is not achieved by the heat treatments carried out in this work.

The ^{23}Na spectrum of $Na_2Si_2O_5$ heat treated at 775°C/168h (Figure 5.9.g) is a representation of two sodium environments in α_I- and α_{II}-Na_2Si_2O5. The dissimilarity in peak intensity indicates that the sodium sites are slightly different in these two polymorphs. The wiping out of $\pm$ 3/2 $\rightarrow \pm\frac{1}{2}$ transitions suggests that the e^2qQ/h could be 1.7 MHz as estimated from the spectrum. A comparison of Figure 5.9.g with 5.9.f indicates that the two highest peaks are at the same place. Thus it may be said that there is an environment with $\eta = 0$ in the $Na_2Si_2O_5$ heat treated at 625°C/168h. The

^{23}Na MAS NMR at two different fields may provide a way to estimate these parameters more accurately.

REFERENCES

1. R. Hanna and G.J. Su., J. Am. Ceram. Soc., 47, 597 (1964).

2. J.S. Jen and M.R. Kalinowski, J. Non-Cryst. Solids, 38/39, 21 (1980).

3. I. Yasui, H. Hasegawa and M. Imaoka, Phys. Chem. Glasses, 24 (3), 65 (1983).

4. I. Yasui, H. Hasegawa and M. Imaoka, Phys. Chem. Glasses, 24 (3), 72 (1983).

5. D.W. Matson, S.K. Sharma and J.A. Philpotts, J. Non-Cryst. Solids, 58, 323 (1983).

6. W. Vogel and K. Gerth, Symposium on Nucleation and Crystallisation in Glasses and Melts, Am. Ceramic Society, 1962, p.21.

7. J.W. Catin and R.J. Charles, Phys. Chem. Glasses, 6 (5), 181 (1965).

8. D.I.H. Atkinson, P.W. McMillan, J. Mat. Sc., 11, 989 (1976).

9. P.F. James, J. Non-Cryst. Solids, 73, 517 (1985).

10. R.J. Charles, J. Am. Ceram. Soc., 46 (5), 235 (1963).

11. R.J. Charles, J. Am. Ceram. Soc., 50 (12), 631 (1967).

12. R.E. Tickle, Phys. Chem. Glasses, 8, 101 (1967).

13. K. Hughes and J.O. Isard in Physics and Electrolytes, Vol.1. Ed. J.H. Haladik, 1972, Academic Press, London, P.351.

14. R. Dupree, D. Holland, P.W. McMillan and R.F. Pettifer, J. Non-Cryst. Solids, 68, 399 (1984).

15. R. Dupree, D. Holland and D.S. Williams, J. De Physique, Colloque C8, Supplement au no.12, Tome 46, C8-119 (1985).

16. K.A. Smith, R.J. Kirkpatrick, E. Oldfield and D.M. Henderson, Am. Miner., 68, 1206 (1983).

17. J.B. Murdoch, J.F. Stebbins and I.S.E. Carmichael, Am. Miner.,70, 332 (1985).

18. R. Dupree, N. Ford, D. Holland, Phys. Chem. Glasses, 28 (2), 78 (1987).

19. R. Dupree, D. Holland and D.S. Williams, J. Non-Cryst. Solids, 81, 185 (1986).

20. T.L. Weeding, B.W.H.S. de Jong, W.S. Veeman, B.G. Aitken Nature, 318, 353 (1985).

21. E. Schneider, J.F. Stebbins and A. Pines, J. Non-Cryst. Solids, 89, 371 (1987).

22. C.M. Schramm, B.W.H.S. de Jong and V.E. Parziale, J. Am. Chem. Soc., 106, 4396 (1984).

23. A.-R. Grimmer and W. Muller, Montash Chem., 117, 799 (1986).

24. R. Dupree, D. Holland and M.G. Mortuza, Nature, 328, 416 (1987).

25. R. Dupree, D. Holland and M.G. Mortuza, Phys. Chem. Glasses, 29 (1), 18(1988).

26. R. Dupree, R.F. Pettifer, Nature, 308, 523 (1984).

27. R.A.B. Devine, R. Dupree, I. Farnan and J.J. Capponi, Phys. Rev., B35, 2560 (1987).

28. J.F. Stebbins, Nature, 330, 465 (1987).

29. I. Farnan, S.C. Kohn and R. Dupree, Geochim. Cosmochim. Acta., 51, 2869 (1987).

30. U. Selvaraj, K.J. Rao, C.N.R. Rao, J. Klinowski and J.M. Thomas, 114 (1), 24 (1984).

31. A.R. Grimmer, M. Magi, H. Hahnert, H. Stade, A. Samoson, W. Wicker and E. Lippmaa, Phys. Chem. Glasses, 25 (4), 105 (1984).

32. R. Dupree, D. Holland, in New Horizons in Glass and Glass-ceramics, Ed. M.H. Lewis, Chapman and Hall (1988)

33. J. Williamson and F.P. Glasser, Phys. Chem. Glasses, 7 (4), 127 (1966).

34. N. Bloembergen, Physica, XV (3-4), 386 (1949).

35. P.-G. de Gennes, J. Phys. Chem. Solids, 7, 345 (1958).

36. H.E. Blumberg, Phys. Rev., 119 (1), 79 (1960).

37. H.E. Rorschach Jr., Physica, 30, 38 (1964).

38. H. Kessemeier and R.E. Norberg, Phys. Rev., 155 (2), 321 (1967).

39. E.A. Nikoforov and A.A. Popel, J. Struc. Chem. USSR,11, 1043 (1970).

40. G.M. Gusakov, I.I. Evdokimov and R.K. Mazitov, J. Struc. Chem., USSR, 12, 642 (1971).

41. G.M. Gusakov, I.I. Evdokimov and R.K. Mazitov, J. Struc. Chem., USSR, 12, 531 (1971).

42. J.V. Smith and C.S. Blackwell, Nature, 303, 223 (1983).

43. G. Engelhardt and D. Michel, High-Resolution Solid State NMR of Silicates and Zeolites, John Wiley, P.195 (1988).

44. A.K. Pant and D.W.J. Cruickshank, Acta. Cryst., B24, 13 (1968).

45. A.K. Pant, Acta. Cryst., B24, 1077 (1968).

46. N.W. Ashcroft and N.D. Mermin, Solid State Physics, Holt-Saunder International Editions, 1981, P.656.

47. P.W. McMillan, Glass Ceramics, Academic Press, 2nd Edn. London, 1979.

48. J.D.H. Donnay, Am. Mineral., 38, 163 (1953).

49. J.V. Smith and S.W. Baily, Acta. Cryst., 16, 801 (1963).

50. G.E. Brown and G.V. Gibbs., Am. Miner., 55, 1587 (1970).

51. A.-R. Grimmer, Chem. Phys. Lett., 119 (5), 416 (1985).

52. A.-R. Grimmer, R. Radeglia, Chem. Phys. Lett., 106 (4), 262 (1984).

53. W.H. Baur and T. Ohta, Acta Crystallogr., B 38,390 (1982).

54. F. Lefebvre, J.-P. Amoureux, C. Farnandez and E.G. Derouane, J. Chem. Phys., 86 (11),, 6070 (1987).

55. H.-J. Behrens and B. Schnabel, Physica, 114B, 185 (1982).

CHAPTER 6

EFFECT OF PHOSPHORUS IN ALKALI DISILICATE SYSTEM

6.1 INTRODUCTION

The aim of the glass ceramist is to produce crystalline materials by controlled crystallisation using a judicious choice of heat treatments [1]. Mechanical and electrical properties of glass ceramics depend upon the size of the microstructure formed during crystallisation and the objectives include the attainment of a fine grained microstructure that will confer appreciable mechanical properties [1]. This desired microstructure in most glass ceramics is markedly dependent on causing a high nucleation rate within the glasses which can be achieved by adding a suitable nucleating agent in the glass melt [1].

Phosphorus pentoxide (P_2O_5) is one of the best nucleating agents that enhances the rate of nucleation in alkali silicates [1,2-14]. Numerous studies [2-17] have already been carried out on the effect of P_2O_5 addition in alkali silicates. There has been considerable speculation about the physical and chemical processes that occur during conversion from glass to glass ceramics by means of heat treatment. Controversy still exists over the exact kinetics of nucleation, crystallisation, phase separation, etc. in P_2O_5 containing alkali silicate, henceforth referred to as alkali phosphosilicate, glasses. TEM study of partially crystallised lithium phosphosilicate glasses [13] of compositions $30Li_2O.69SiO_2.1P_2O_5$ and $31.5Li_2O.67.5SiO_2.1P_2O_5$ has led to five models of phase separation. In those models James and McMillan [13] predicted the presence of $Li_2Si_2O_5$ and SiO_2 crystal with the possible formation of crystalline Li_3PO_4, $Li_4P_2O_7$, $LiPO_3$, P_2O_5 and the presence of P_2O_5 in the

precipitated silica. In the partially crystallised state the volume fractions of those compounds were so small that they could not be identified by using XRD. In a further study [14] of the same composition the authors did observe lithium disilicate crystals along with crystals of either different composition or different structure which they assumed to be phosphates.

Harper and McMillan [5] reported a considerable change (300 times greater) of nucleation density due to replacement of 1 mol% SiO_2 by the same amount of P_2O_5 in $30Li_2O.70SiO_2$ glass. Later Hing and McMillan [7] revealed that the nucleation density can be made 10^6 times higher by choosing the optimum nucleation temperature in the same P_2O_5 containing sample. Recently the researchers at Sandia National Laboratory [18] have found Li_3PO_4 in a highly crystalline Li_2O-SiO_2-P_2O_5 system and predict the growth of other phases epitaxially on the top of Li_3PO_4 crystals. This nucleating property of phosphorus, even in small amounts, must reflect the effect of its presence on the local structure in the glass. However to date there is little structural information available because of poor sensitivity of the techniques, e.g. XRD, TEM, SEM , to the random long range order of the network formers. Several questions arise about the environment of network formers Si^{4+}, P^{5+}, etc. in the alkali phosphosilicate system. (i) Does P^{5+} go into the Si^{4+} network? (ii) Does p^{5+} form the same environment in all the alkali phosphosilicate system? (iii) How does Si^{4+} behave due to addition of P^{5+}? (iv) What happens to the modifier oxide, R_2O (R = Li, Na, K)? (v) How does P^{5+} enhance phase separation in alkali silicates? etc. In order to answer some

of these questions the identification of Si^{4+}, P^{5+} local environments has been raised by several authors [19-21] in the sodium phosphosilicate system using vibrational spectroscopy. Raman spectroscopic data [20] on sodium silicate glasses have been interpreted as indicating the presence in these glasses of a phosphate unit similar to that found in sodium orthophosphate (Na_3PO_4), i.e. monomer followed for concentrations of P_2O_5 greater than 5 mol% by units similar to those found in sodium pyrophosphate ($Na_4P_2O_7$), i.e. dimers. All the monomer, dimer and chain phosphate ($NaPO_3$) are present in high P_2O_5 containing glasses [20], but the relative proportions of these units could not be determined. Infrared and Raman spectroscopic data also suggests the presence of a structural unit containing Si-O-P bonding in high P_2O_5 containing glasses [19,20]. These studies [13,14,19-21] lead to the alkali phosphosilicate glass structure as

Initial crystalline components → Final glass product

$$R_2O + SiO_2 + P_2O_5 \longrightarrow R_2Si_2O_5 + SiO_2 + \begin{cases} (1)\ R_3PO_4 \\ (2)\ R_4P_2O_7 \\ (3)\ RPO_3 \\ (4)\ P_2O_5 \\ (5)\ SiO_2{+}P_2O_5{\rightarrow}Si\text{-}O\text{-}P \end{cases} \quad ...(6.1)$$

The first two, (3) and (5) of the final glass product may form a 3- dimensional network but the rest remain as an isolated unit. Among the five possibilities, along with $R_2Si_2O_5$ and SiO_2, how many of these form at what level of P_2O_5 in which kind of alkali content are not very clear. Formation of Si-O-P bonds suggest the formation of $Si_3(PO_4)_4$, SiP_2O_7 and $Si_5O(PO_4)_6$. The silicons in $Si_3(PO_4)_4$ and SiP_2O_7 are 6-coordinated but those in the $Si_5O(PO_4)_6$ are 4- and 6-

coordinated [22,23]. Crystallographically 5- coordinated silicon does not exist in inorganic materials [22]. Therefore this information leads to further questions : (i) does the silicon coordination change from its original four to any other numbers? (ii) what happens in the case of potassium and lithium silicates? All these questions are yet to be answered.

MAS NMR must reflect some idea of the local order of Si^{4+} and P^{5+} in the alkaliphosphosilicate system from which direct quantitative information about the nearest neighbour and next nearest neighbour environment of the nucleus can be obtained. However, the interpretation of ^{31}P signals can be difficult because of overlapping spinning sidebands due to the large chemical shift anisotropy and strong homonuclear dipolar coupling [24]. This can be overcome by spinning the sample at a rate higher than the dipolar interaction which could be 5kHz. In this chapter all the questions raised previously are answered by applying MAS NMR spectroscopy to alkali phosphosilicate glasses. A model to calculate the relative amounts of the structural units and the first observation of the change of Si^{4+} coordination to Si^{6+} in glasses are also presented. Some effort is also made to predict the change of silicon coordination by using infrared spectrophotometry.

Raman and X-ray scattering studies [25,26] of Na_2O-Al_2O_3-SiO_2 can provide general information about the nature of tetrahedral polymerisation in the glasses. These methods reveal little about the local order of Na. The change of Al^{3+} coordination is not observable through Raman scattering, XANES and EXAFS studies of the system [23,25,26]. However, Raman investigation of Na_2O-Al_2O_3-SiO_2-P_2O_5 glasses [28] can predict

the change of Al^{3+} coordination but cannot provide any evidence of silicophosphate formation. In this chapter the coordination of aluminium is determined and the change from 4- to 6- coordination due to a change of the amounts of phosphorus in the high phosphorus containing samples are presented. An attempt is also made to interpret the sodium environment by using ^{23}Na NMR.

The glass structure in the vicinity of transition region changes with cooling or heating rate which also reflect the change of physical and chemical properties [29-31]. The structural state of the glass can be represented by a temperature, generally called fictive temperature, T_f [29-33]. The change of glass structure depending upon the variation of cooling rate can be easily measured by MAS NMR and a correlation is presented between the structural relaxation and the T_f.

6.2 THE ROLE OF SMALL AMOUNTS OF P_2O_5

The influence of the addition of small amounts (1-8 mol%) of P_2O_5 in the alkali disilicate glass structure is the theme of this section. In addition to a glass there are four cystalline forms of P_2O_5 [34-38], including a high pressure form [34]. The arrangements of PO_4 tetrahedra, stable at atmospheric pressure, are different [34,35] and the ^{31}P chemical shifts are observed at -46.5, -47.0, -57.9 and -61.2 PPM [39]. However, in the P_2O_5 glass these differences are not distinguishable and only one ^{31}P resonance at -54.9 PPM is observed [39]. Here the reaction of this P_2O_5 with different R^+ (R=Li, Na, K) metal ions, which could be observed from the different-from-aforesaid chemical shifts, in the binary alkali

disilicate and the local order of Si^{4+}, P^{5+} and Na^{+} in the system are presented.

6.2.1 LITHIUM DISILICATE

6.2.1.1 ^{29}Si NMR IN BASE GLASSES

The spectra for ^{29}Si in the lithium disilicate compositional range (LSP1, LSP2 and LSP4(a)) with different amounts of P_2O_5 are shown in Figure (6.1). The spectra generally consist of two overlapping isotropic peaks (I_0), one corresponding to Q_4 [40-45] as a spherically symmetric unit, has no spinning sidebands and the other corresponding to Q_3, near axially symmetric and therefore associated with spinning sidebands (SS). Visual examination of the spectra shows that the Q_4 resonance increases in intensity as the amount of P_2O_5 increases. A least squares fit of the spectra to two gaussians was carried out to obtain the chemical shifts, full width at half maximum and area under the respective species. These data are summarised in table (6.1) together with the observed (Q_4/Q_3) ratio. The chemical shift for both Q_4 and Q_3 becomes more negative as the concentration of P_2O_5 increases. The FWHM of the Q_4 resonance also increases by amounts greater than the experimental error.

6.2.1.2 ^{29}Si NMR IN HEAT TREATED GLASSES

The ^{29}Si spectra of the glasses LSP1 and LSP4(a) as a function of heat treatment are shown in Figures 6.1.b and 6.1.c respectively. The chemical shifts of the Q_3 and Q_4 species in LSP1 change with heat treatment and approach the value similar to their crystalline form. The sample LSP4(a) was

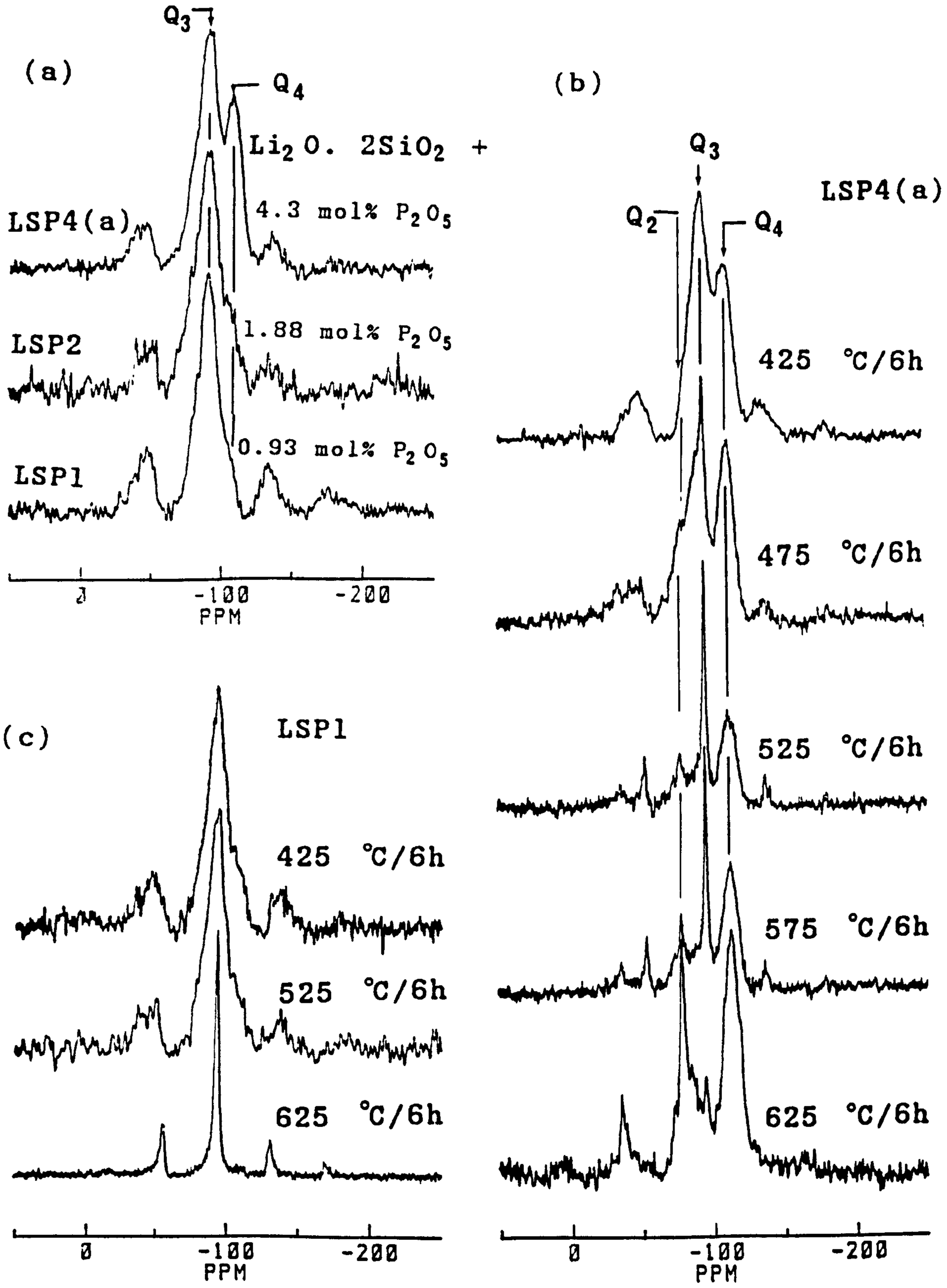

Figure 6.1 ^{29}Si spectra of lithium phosphosilicate (a) base glasses, (b) LSP1 and (c) LSP4(a) heat treated at various temperatures.

initially phase separated and the chemical shifts of the species do not change with heat treatment. However the FWHM in all the samples changes with heat treatments and are summarised in Table (6.1).

The striking differences between the two sets of spectra (Figure 6.1.b and 6.1.c) are the formation of Q_2 units along with Q_3 and Q_4 species in LSP4(a) due to heat treatments. There is no evidence of formation of Q_2 in LSP1 because of devitrification and the relative amounts of Q_3 and Q_4 remain almost constant. The amounts of Q_2 and Q_4 in LSP4(a) glass ceramics increases and that of Q_3 decreases as a result of disproportionation $2Q_3 \longrightarrow Q_2 + Q_4$. The rate of disproportionation increases with the increase of heat treatment temperature. This could be equally true if the sample is held at a particular temperature, which is high enough to disproportionate Q_3, for a different length of time.

6.2.1.3 ^{31}P NMR

The spectra for ^{31}P in the lithium disilicates (LSP1, LSP2 and LSP4(a) are shown in Figure (6.2). Only one phosphorus site is observed for all phosphorus concentrations, with a chemical shift of ~10 PPM. Comparison of the peak position (10 PPM) with crystalline material [46,47] suggests that the environment of phosphorus is like Li_3PO_4.

The ^{31}P spectra of heat treated LSP1 and LSP4(a) are shown in Figures (6.2.b and 6.2.c) respectively. From the single peak in both the glass and glass ceramic, it can be inferred that the ^{31}P environment does not change due to heat treatment. The relatively narrow line in the heat treated material represents the crystallinity of Li_3PO_4 units. The

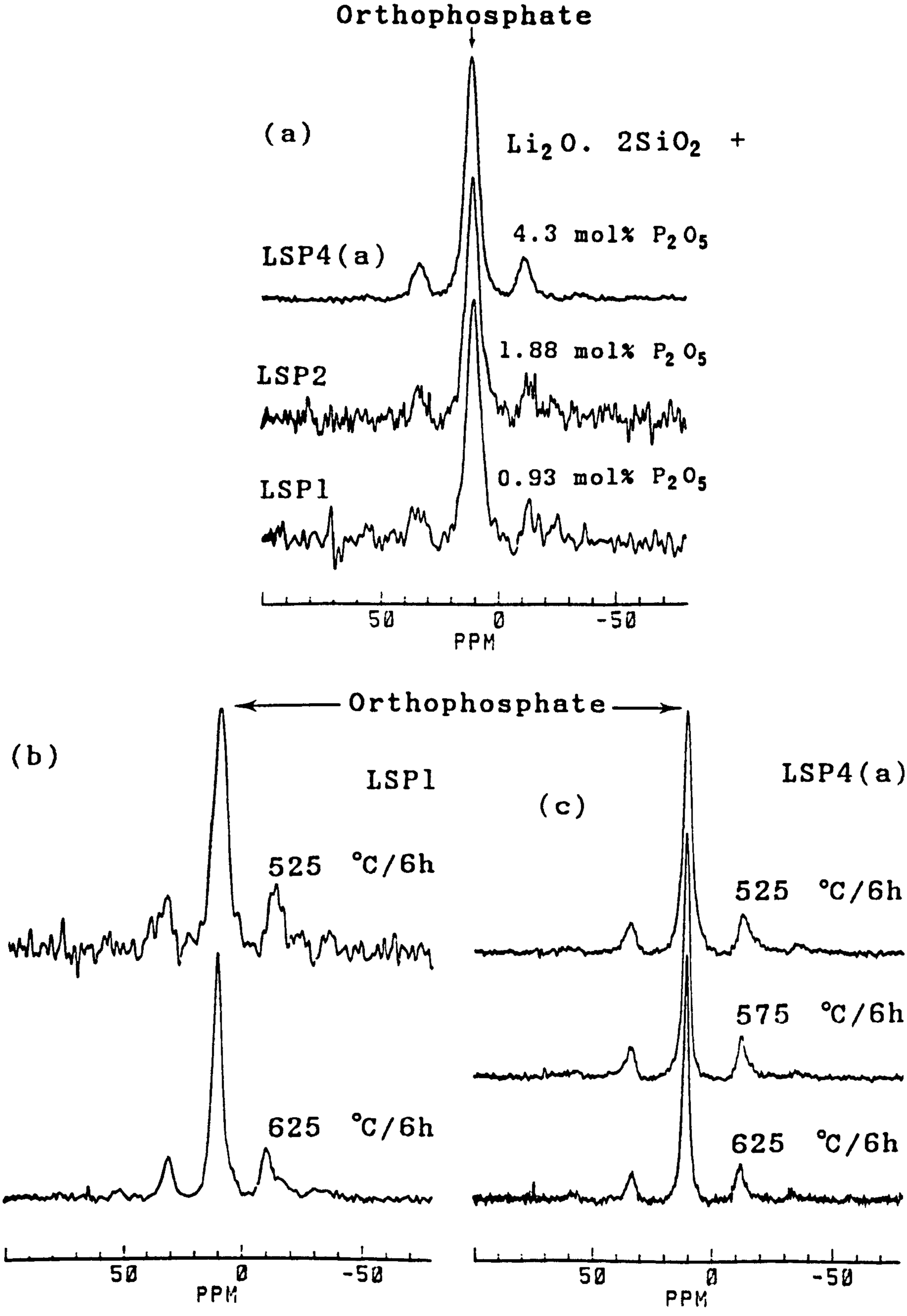

Figure 6.2 ^{31}P spectra of lithium phosphosilicate glass and glass ceramics. (a) Base glasses. (b) LSP1 and (c) LSP4(a) heat treated at various temperatures.

TABLE NO.6.1 ^{29}Si AND ^{31}P MAS NMR DATA FOR LITHIUM PHOSPHOSILICATE GLASSES AND GLASS-CERAMICS

Sample	Amounts of P_2O_5 (mol%)±2%	Heat treatment T°C/th	^{29}Si chemical shifts (CS) parameters (PPM)						^{31}P CS parameters (PPM) ± 0.5		Values of the $\frac{Q_4}{Q_3}$ ratio	
			Q_4 ± 0.5		Q_3 ±0.5		Q_2 ±0.5				Theoretical ±0.05	Experimental ±0.05
			CS	FWHM	CS	FWHM	CS	FWHM	CS	FWHM		
LSP1	0.93	NHT*	-108.0	7.2	-91.6	18.6	-	-	+9.7	7.0	0.14	0.08
LSP2	1.88	NHT	-109.1	10.1	-92.5	18.6	-	-	+9.7	7.0	0.26	0.22
LSP4(a)	4.30	NHT	-111.4	12.4	-93.6	18.8	-	-	+10.4	7.0	0.73	0.36
LSP1		425/6	-108.7	8.5	-92.3	16.1	-	-	+10.0	7.0	0.14	0.10
		475/6	-108.3	9.6	-92.5	14.5	-	-	-	-	-	-
		525/6	-110.2	10.4	-93.2	14.0	-	-	-	-	-	-
		575/6	-110.6	12.1	-93.6	4.0	-	-	+10.1	3.0	0.14	0.07
LSP4(a)		425/6	-111.3	12.5	-93.7	18.5	-	-	-	-	-	-
		475/6	-111.8	13.2	-94.4	10.0	-77.9	9.8	+10.4	4.5	-	-
		525/6	-111.7	13.0	-94.5	3.2	-76.4	9.6	+10.5	5.0	-	-
		575/6	-112.3	12.1	-94.7	2.7	-76.8	5.9	+10.4	3.2	-	-

* No heat treatment

chemical shifts and FWHM are presented in Table (6.1). Only one or possibly two pairs of SS due to spinning the sample at 3.3 kHz represent the small anisotropy associated with phosphorus in the material. Calculation of the anisotropic range using the method of Herzfield and Berger [48] shows 45±5 PPM which is consistent with the spectra.

6.2.1.4 ^{7}Li NMR

The ^{7}Li spectra of lithium phosphosilicate glasses and glass-ceramics are shown in Figure (6.3). The glass spectra are almost indistinguishable from the ^{7}Li spectra of LS3 glass (Figure 4.6). The Pake doublet as observed in LS3 crystal (Figure 4.11.b) is not noticeable in lithium phosphosilicate crystalline materials.

6.2.2 SODIUM DISILICATE

In this section sodium disilicates with varying amounts (1-8 mol%) of P_2O_5 studied using MAS NMR to identify changes the sodium phosphosilicate glass structure. The results presented here agree in part with infrared and Raman data [19,20]. The MAS NMR data show that the rates of nucleation, phase separation and crystallisation are comparatively lower in sodium phosphosilicates than in the lithium phosphosilicate system. The structural information obtained from ^{29}Si and ^{31}P NMR possibly explains the root cause of low nucleation and hence low crystallisation rate in the system. The ^{23}Na NMR is also presented in this section.

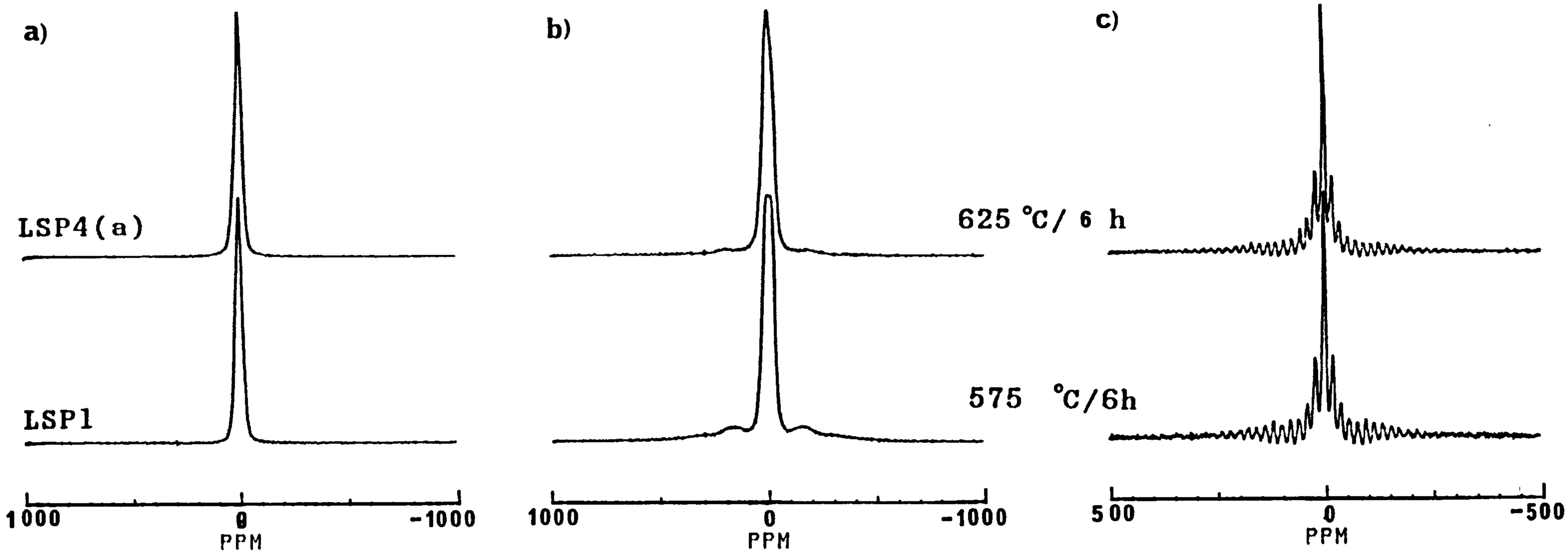

Figure 6.3 ^{7}Li spectra of lithium phosphosilicate glasses (a) glass(static) (b) crystalline (static) (c) crystalline (spinning).

6.2.2.1 ^{29}Si NMR IN $Na_2O.2SiO_2$-P_2O_5 BASE GLASSES :

The ^{29}Si spectra of sodium phosphosilicate glasses (NSP1-NSP5) are shown in Figure (6.4). Like the lithium phosphosilicate system, the spectra are also a combination of overlapped Q_3 and Q_4 resonances. However, the amounts of Q_4, either by visual examination or by deconvoluting the spectra, are less in comparison to the $Li_2O.2SiO_2$-P_2O_5 system. But the general trend of the increase of Q_4 units with the increase of P_2O_5 content remains the same. The spectral parameters and the ratio of the two species (Q_4/Q_3) are summarised in Table (6.2).

6.2.2.2 ^{29}Si NMR IN $Na_2O.2SiO_2$-P_2O_5 GLASS CERAMICS

The ^{29}Si spectra of heat treated NSP1-NSP3 are shown in Figure (6.5.a, .b and .c) respectively. The evidence of disproportionation of Q_3 unit and the formation of Q_2 and Q_4 due to heat treatment is not observed for 1-4 mol% P_2O_5 containing samples. The single wide (-11 PPM) Q_3 resonance observed in the glasses splits up into two narrow lines in the heat treated materials, one at -94 PPM and the other one at -90 PPM, representing the formation of two sodium disilicate polymorphs. XRD patterns of the crystallised samples are consistent with α- and δ- $Na_2Si_2O_5$ phases. In addition to these phases a small amount of γ- $Na_2Si_2O_5$ and SiO_2 are also observed in NSP2 and only SiO_2 in NSP3 crystals (Figure 6.5).

As it has been found that [see Chapter 5] the peak at -94 PPM is due to α- $Na_2Si_2O_5$, the other peak at -90 PPM could be a characteristic of δ - $Na_2Si_2O_5$. The peak at -110 PPM is due to the formation of SiO_4 tetrahedra. A closer look at

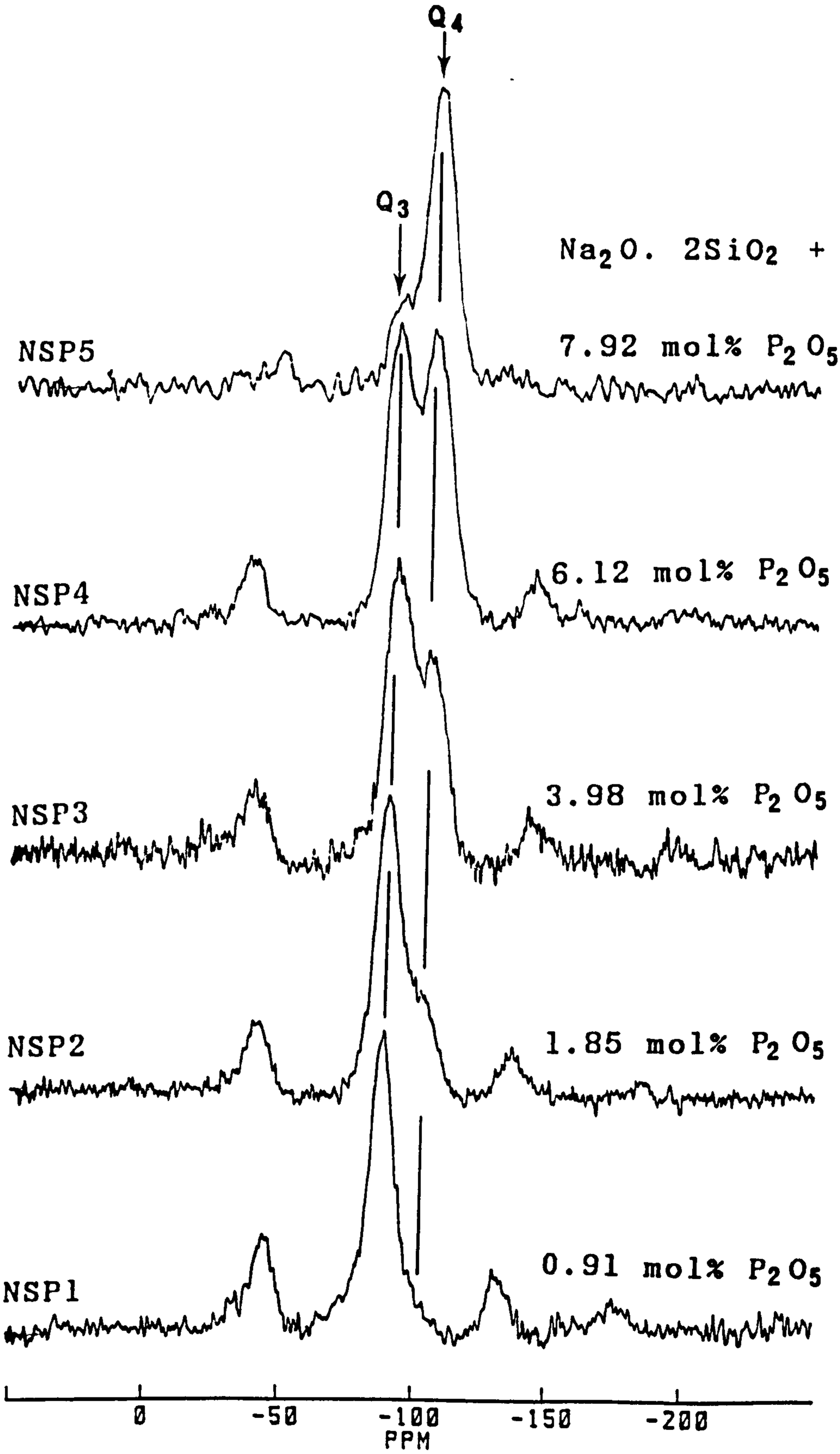

Figure 6.4 ^{29}Si spectra of sodium phosphosilicate glasses.

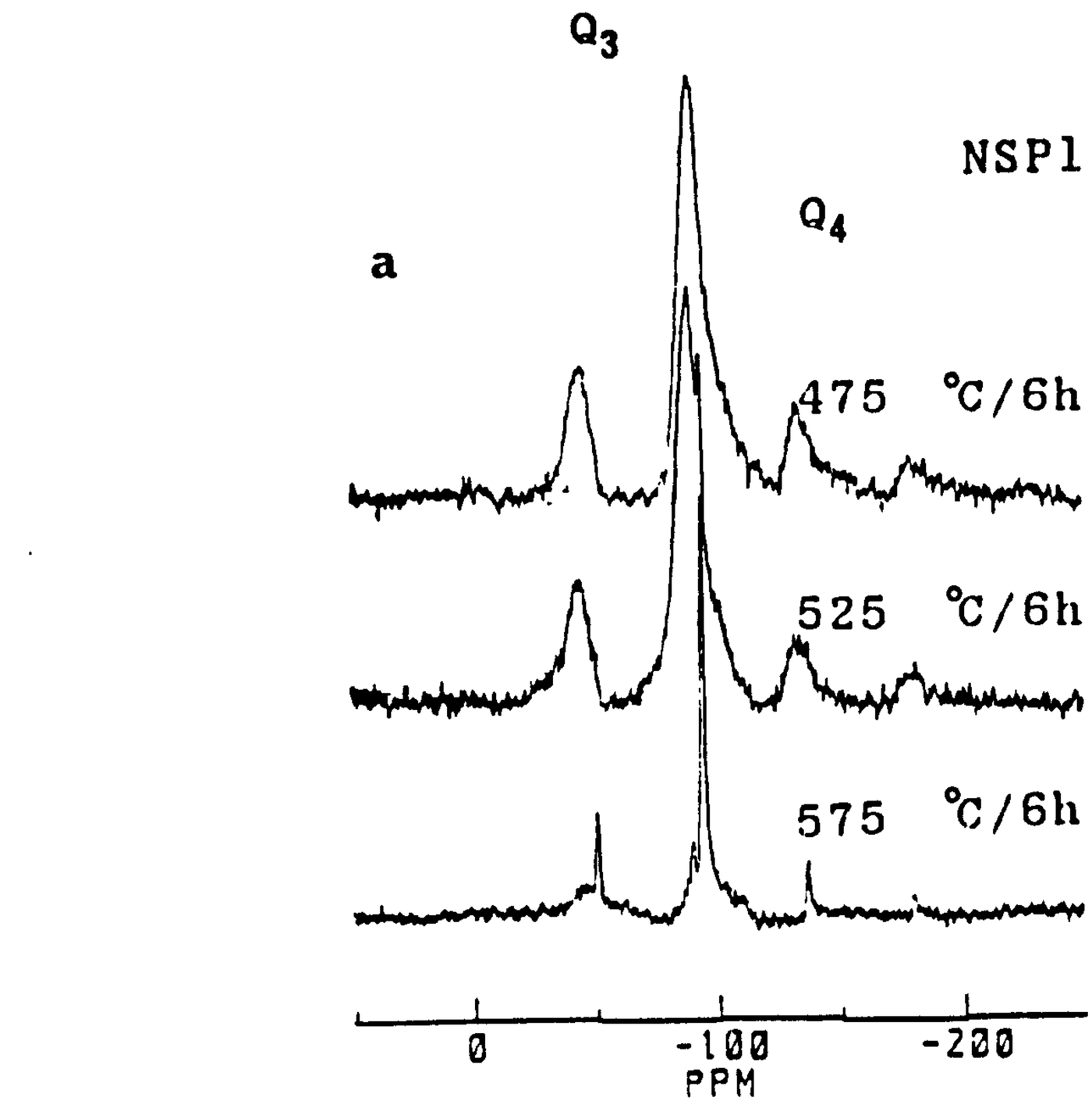

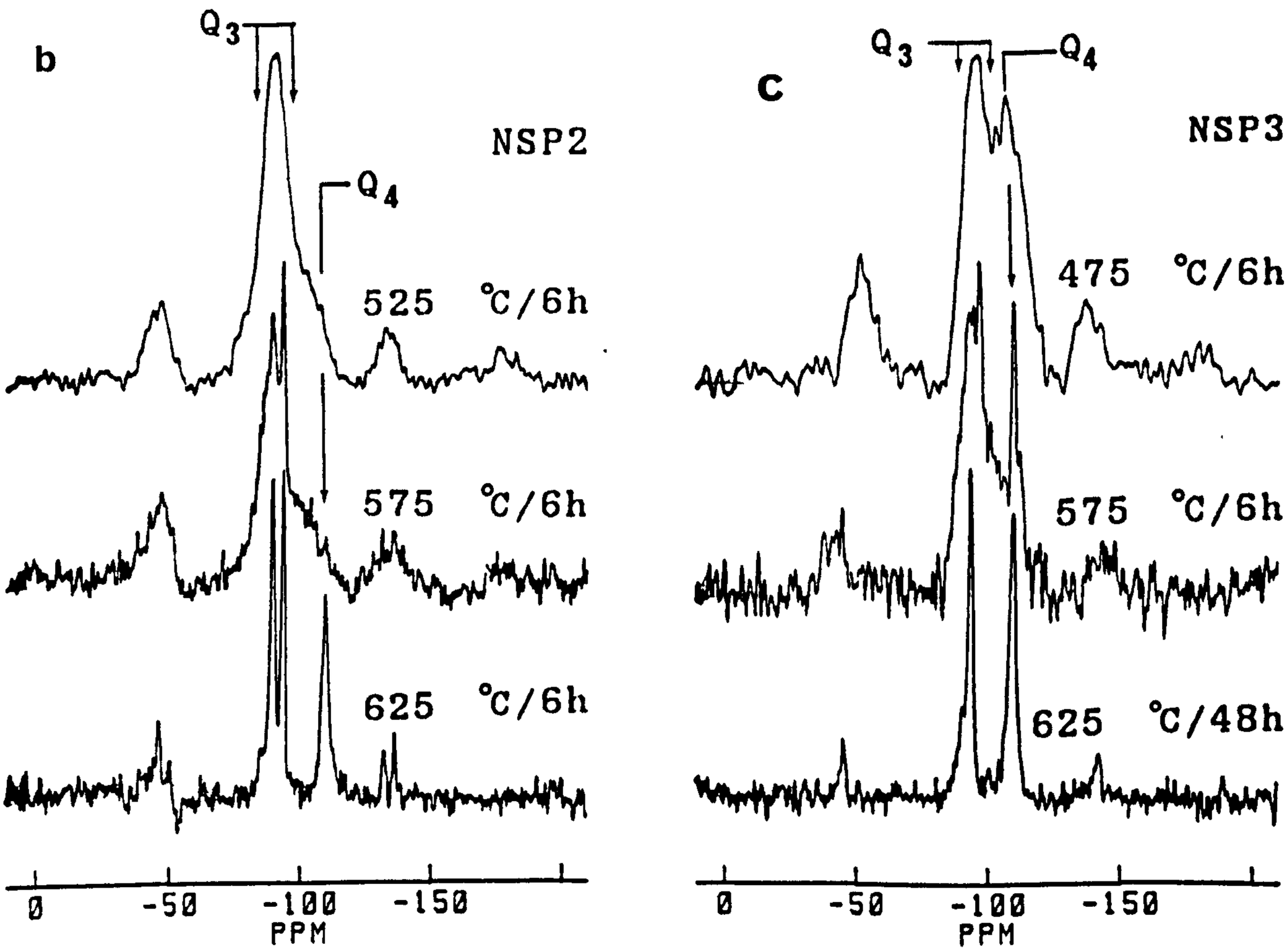

Figure 6.5 ^{29}Si spectra of heat treated sodium phosphosilicate glasses.

TABLE NO. 6.2 ^{29}Si COMPOSITION AND SPECTRAL PROPERTIES OF SODIUM PHOSPHOSILICATE GLASSES AND GLASS-CERAMICS

Sample	Amounts of P_2O_5 (mol%) ±2%	Heat treatment T^oC/th	^{29}Si chemical shift parameters (PPM)				Values of the $\frac{Q_4}{Q_3}$ ratio	
			Q_4 ±0.5		Q_3 ±0.5		Theoretical ±0.05	Experimental ±0.05
			CS	FWHM	CS	FWHM		
NSP1	0.91	NHT	-103.6	10.1	-88.6	12.5	0.12	0.08
NSP2	1.85	NHT	-105.1	10.0	-90.5	12.8	0.19	0.17
NSP3	3.98	NHT	-106.6	11.1	-93.5	12.9	0.39	0.38
NSP4	6.12	NHT	-107.5	12.0	-93.4	12.6	0.99±0.1	0.78±0.1
NSP5	7.92	NHT	-108.9	12.6	-94.1	12.1	3.35±0.5	2.28±0.5
NSP1		475/6	-104.2	10.8	-89.9	11.0		
		525/6	-104.8	11.3	-93.8,-89.1	3.5,8.3		
		575/6	-109.6	12.5	-94.0,-90.2	1.7,3.0		
NSP2		525/6	-106.7	12.0	-90.4	12.2		
		575/6	-110.5	12.3	-94.0,-90.2	3.6,5.2		
		625/6	-110.0	2.4	-93.9,-89.9	1.9,2.0		0.34
NSP3		475/6	-106.8	11.2	-93.4	12.8		
		525/6	-107.0	10.8	-94.0	12.4		
		575/6	-110.4	2.8	-94.0,-90.0	1.8,6.4		
		625/48	-110.6	2.9	-93.9,-90.1	1.8,4.1		0.80±0.1

the MAS NMR spectrum of NSP2 heat treated at 625°C/6h clearly shows a shoulder at -86 PPM. This shift could be assigned to γ - $Na_2Si_2O_5$. The other polymorph, β - $Na_2Si_2O_5$, may not form in this material. All the spectral parameters and the composition formed during heat treatment are also given in Table (6.2).

the experimental Q_4/Q_3 ratios in NSP2 and NSP3 glasses are 0.17 ± 0.05 and 0.38 ± 0.05 respectively. However, the ratio in the heat treated glasses apparently increases with heat treatment and finally the ratios become 0.34 ± 0.05 and 0.80 ± 0.1 respectively. For both the cases $(Q_4/Q_3)_{crystal} > (Q_4/Q_3)_{glass}$ and therefore it indicates the polymerisation of SiO_4 tetrahedra. This could only happen if the alkali metal ion dissociates from the Q_3 species due to heat treatment.

6.2.2.3 ^{31}P NMR IN BASE AND HEAT TREATED GLASSES

The spectra for ^{31}P NMR in the sodium phosphosilicate glasses (NSP1-NSP5) are shown in Figure (6.6.a). For this system two distinct sites with chemical shifts of 15.0 and 2.5 PPM are found. As the concentration of P_2O_5 is increased, the latter resonance increases in intensity at the expense of the former up to 4 mol% and then the former increases at the expense of the latter up to 8 mol% P_2O_5. Comparison with the chemical shift data for crystalline materials [46, 49-51] suggests that the higher chemical shift (~ +15 PPM) is in a site very similar to the sodium orthoposphate, the monomer Na_3PO_4 + 13.7 PPM. The phosphorus nuclei with the smaller chemical shift at +2.5 PPM can be assigned to an environment like sodium pyrophosphate, the

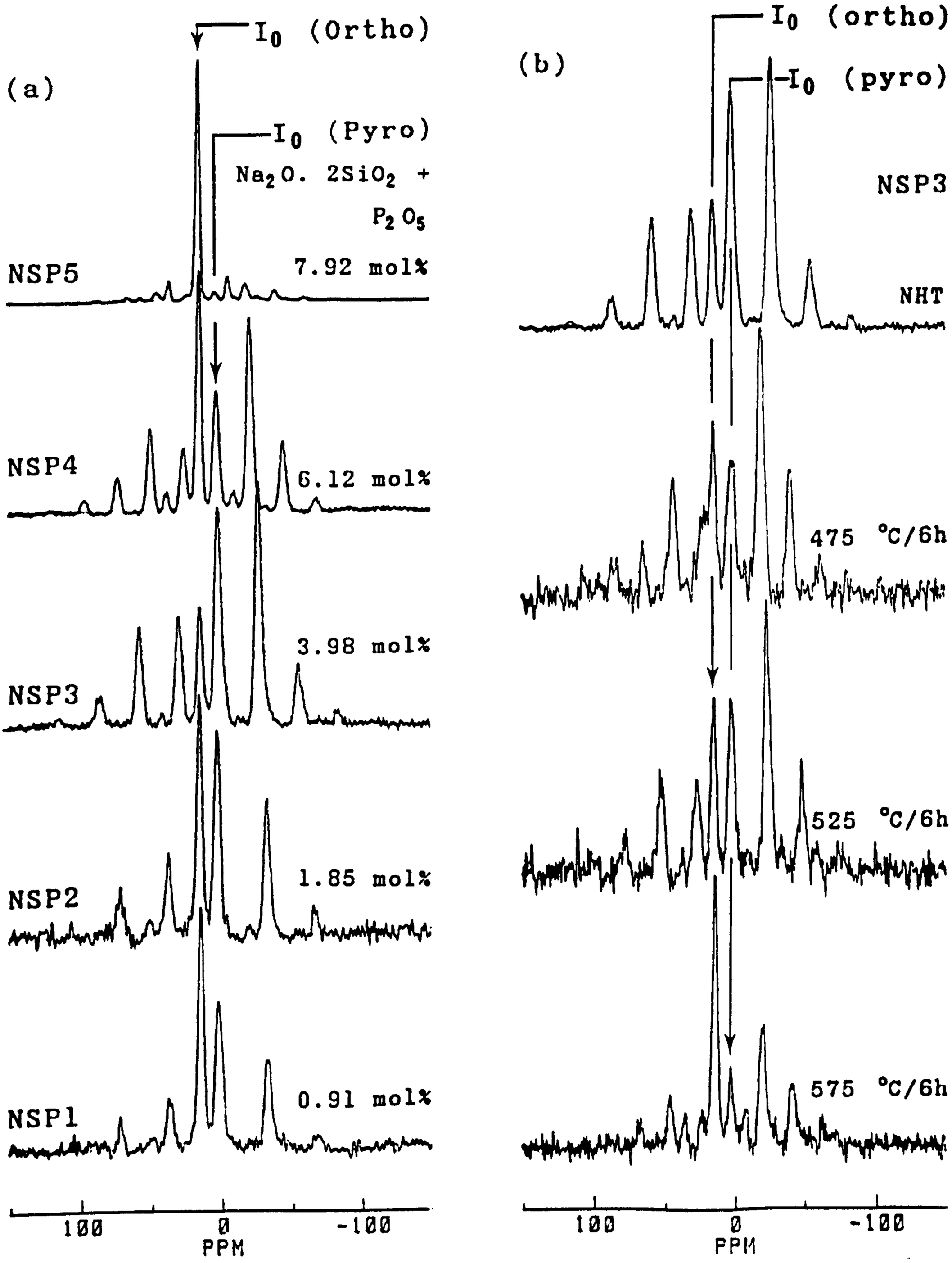

Figure 6.6 ^{31}P spectra of (a) sodium phosphosilicate base glasses (b) NSP3 heat treated at various temperatures. The isotropic peaks are marked as I and the rests are spinning sidebands(SS)

dimer $Na_4P_2O_7$ at 2.4 PPM. The anisotropy, $|\Delta\sigma|$, associated with phosphorus in Na_3PO_4 is small, ~ 50 PPM, but that in $Na_4P_2O_7$ is comparatively large, $|\Delta\sigma|$ ~ 125 PPM. These ranges of anisotropy can also be declared from the number of spinning sidebands of the isotropic lineshapes of Na_3PO_4 and $Na_4P_2O_7$. The relative amounts of phosphorus in different sites can be obtained by summing the intensities of all peaks arising from the individual resonances (I_0 + all SS for each resonance), and deconvoluting where overlapping occurs. The plots of the concentrations of Na_3PO_4 and $Na_4P_2O_7$ as a function of analysed P_2O_5 concentration in NSP1-NSP5 glasses are shown in Figure (6.7).

On heating the sodium disilicate glass containing 4 mol% (NSP3) P_2O_5 the pyrophosphate dimer dissociates to some extent and forms the monomer Na_3PO_4. The ^{31}P spectra as a function of heat treatment in NSP3 glass are shown in Figure (6.6.b). In the MAS NMR spectra, the crystallinity is followed by a narrow lineshape and is also clear from the Figure. The isotropic chemical shifts, FWHM and the relative amounts of each phosphorus site in the various glasses together with the chemical shift anisotropy of each site, determined from the spinning sideband intensity [48], are summarised in Table (6.3).

6.2.2.4 ^{23}Na NMR

In the case of ^{23}Na NMR in NSP1-NSP5 only the $+\frac{1}{2} \longleftrightarrow -\frac{1}{2}$ transition is observed and the spectra are shown in Figure (6.8). As the first order frequency shift for this transition is zero, the wide gaussian lineshapes could represent the random distribution of sodium atoms and the second order quadrupolar

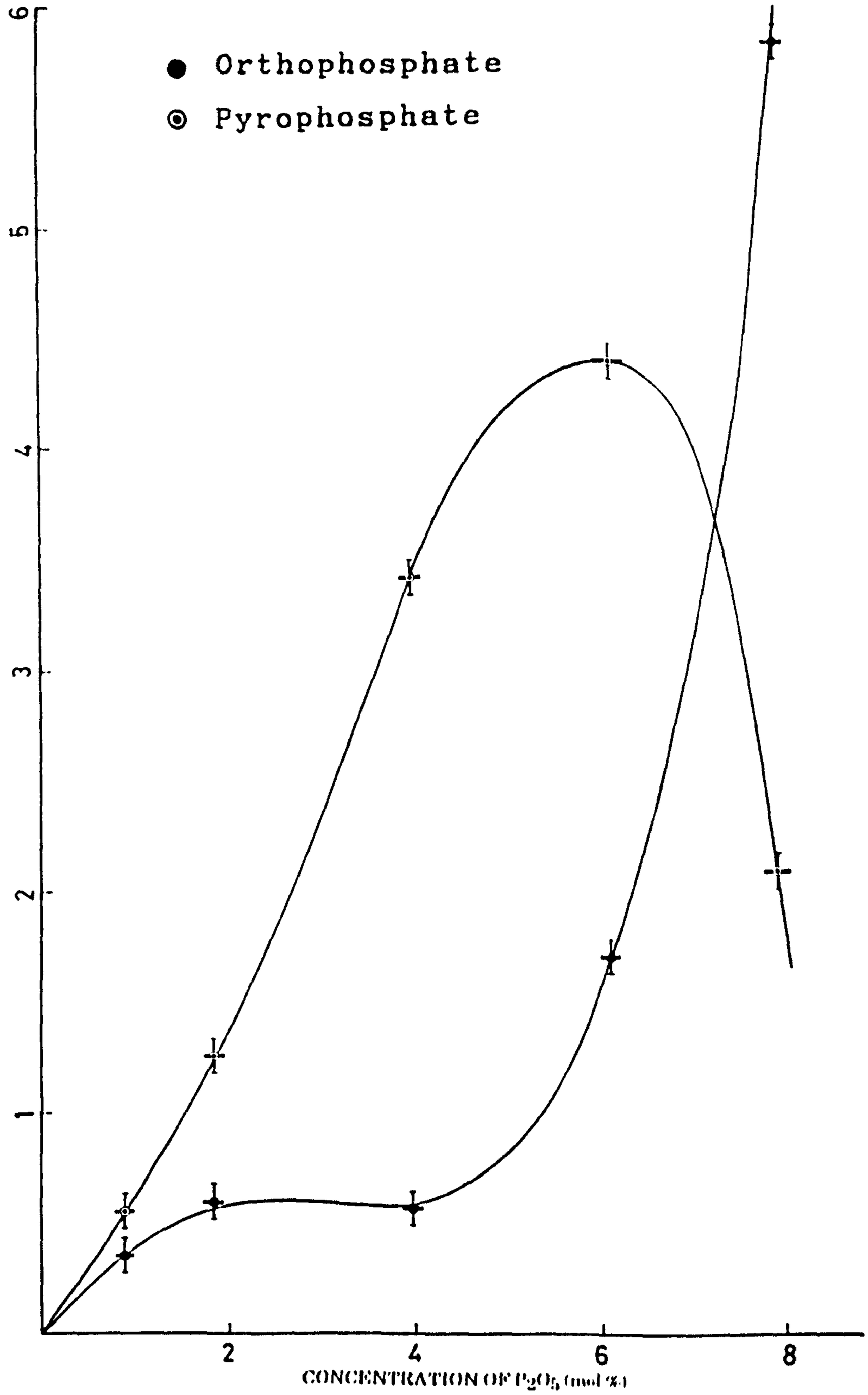

Figure 6.7 Formation of orthophosphate and pyrophosphate in sodium disilicate base glasses with 1 - 8 mol% P_2O_5.

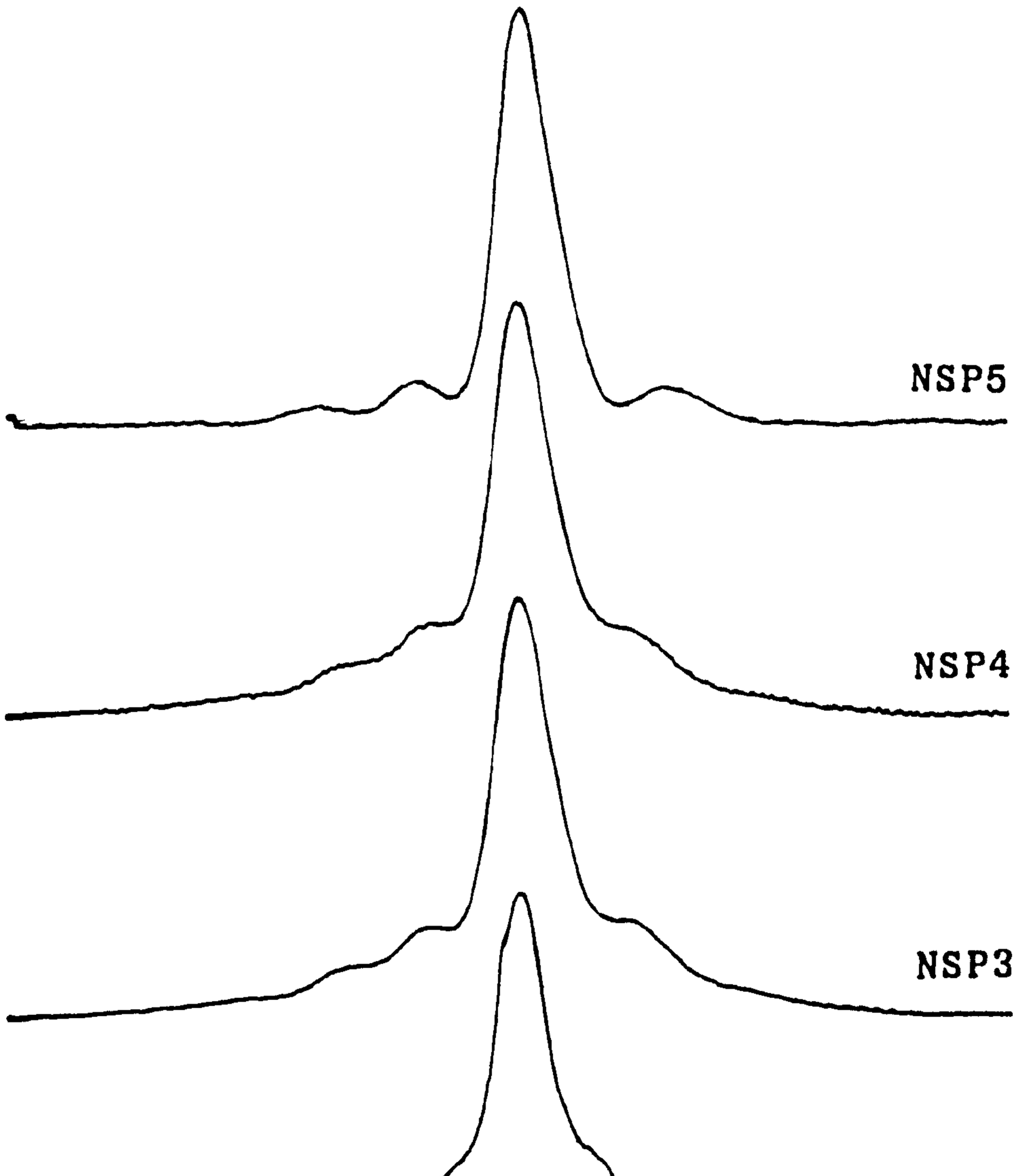

Figure 6.8 ^{23}Na spectra of sodium phosphosilicate glasses.

TABLE No.6.3 ^{31}P AND ^{23}Na MAS NMR SPECTRAL PARAMETERS AND COMPOSITIONS OF THE PHOSPHATE GROUPS IN SODIUM PHOSPHOSILICATE GLASSES AND GLASS-CERAMICS

Sample	Heat treatment	^{31}P Chemical Shift Parameters (PPM) ±0.5						Values of the fractional content		^{23}Na spectral parameters (PPM) ±1.0	
		Like orthoposphate			Like pyrophosphate			orthophos-phate (m)	Pyro-phosphate (n)		
	T^oc/th	CS	FWHM	$\lvert\Delta\sigma\rvert$ ±5.0	CS	FWHM	$\lvert\Delta\sigma\rvert$ ±5.0			Peak position	FWHM
NSP1	NHT*	+14.7	4.5	46	+2.0	6.0	125	0.36	0.64	-2.14	28.0
NSP2	NHT	+15.6	4.5	48	+2.8	6.0	123	0.29	0.71	-5.3	34.0
NSP3	NHT	+15.7	4.5	47	+2.5	6.0	126	0.11	0.89	-6.6	34.4
NSP4	NHT	+15.5	4.5	50	+2.6	6.0	128	0.30	0.70	-7.9	33.0
NSP5	NHT	+14.9	4.5	52	+2.4	6.0	124	0.76	0.24	-9.8	31.6
NSP3	475/6	+15.1	4.5		+2.3	6.0		0.17	0.83		
	525/6	+15.0	4.5		+2.6	6.0		0.20	0.80		
	575/6	+14.8	4.0		+2.8	5.5		0.41	0.59		

* NHT - No heat treatment

interaction. The dipolar coupling between Na and P, which is not solely (3 $Cos^2\theta$ -1) dependent [52], may also cause spectral broadening. Non-existence of the second order quadrupolar lineshape indicates that the quadrupolar interaction is small in comparison to chemical shift dispersion. The peak positions and FWHM are presented in Table (6.3).

6.2.3 POTASSIUM DISILICATE

The ^{29}Si and ^{31}P results of $K_2O.2SiO_2$-P_2O_5 are very similar to those of the $Na_2O.2SiO_2$-P_2O_5 system and are presented in brief in this section.

6.2.3.1 ^{29}Si NMR

Like sodium phosphosilicates, the ^{29}Si spectra in $K_2O.2SiO_2$-P_2O_5 also consist of Q_3 and Q_4 species and are shown in Figure (6.9.a). However the amounts of Q_4 are less in comparison with the $Li_2O.2SiO_2$-P_2O_5 and $Na_2O.2SiO_2$-P_2O_5 systems. The spectral parameters and the amounts of the species are summarised in Table (6.4).

6.2.3.2 ^{31}P NMR

The spectra for ^{31}P in the potassium disilicate with varying amounts (1-4 mol%) of P_2O_5 are illustrated in Figure (6.9.b). There are two distinct phosphorus sites, one at ~13 PPM and the other one at ~1.5 PPM. The phosphorus environment in the former is characteristic of K_3PO_4 and the latter is like $K_4P_2O_7$ [46,51,53]. Like $Na_2O.2SiO_2$ with 1-4 mol% P_2O_5, the amount of phosphorus with a chemical shift of 1.5 PPM increases at the expense of that with a chemical shift

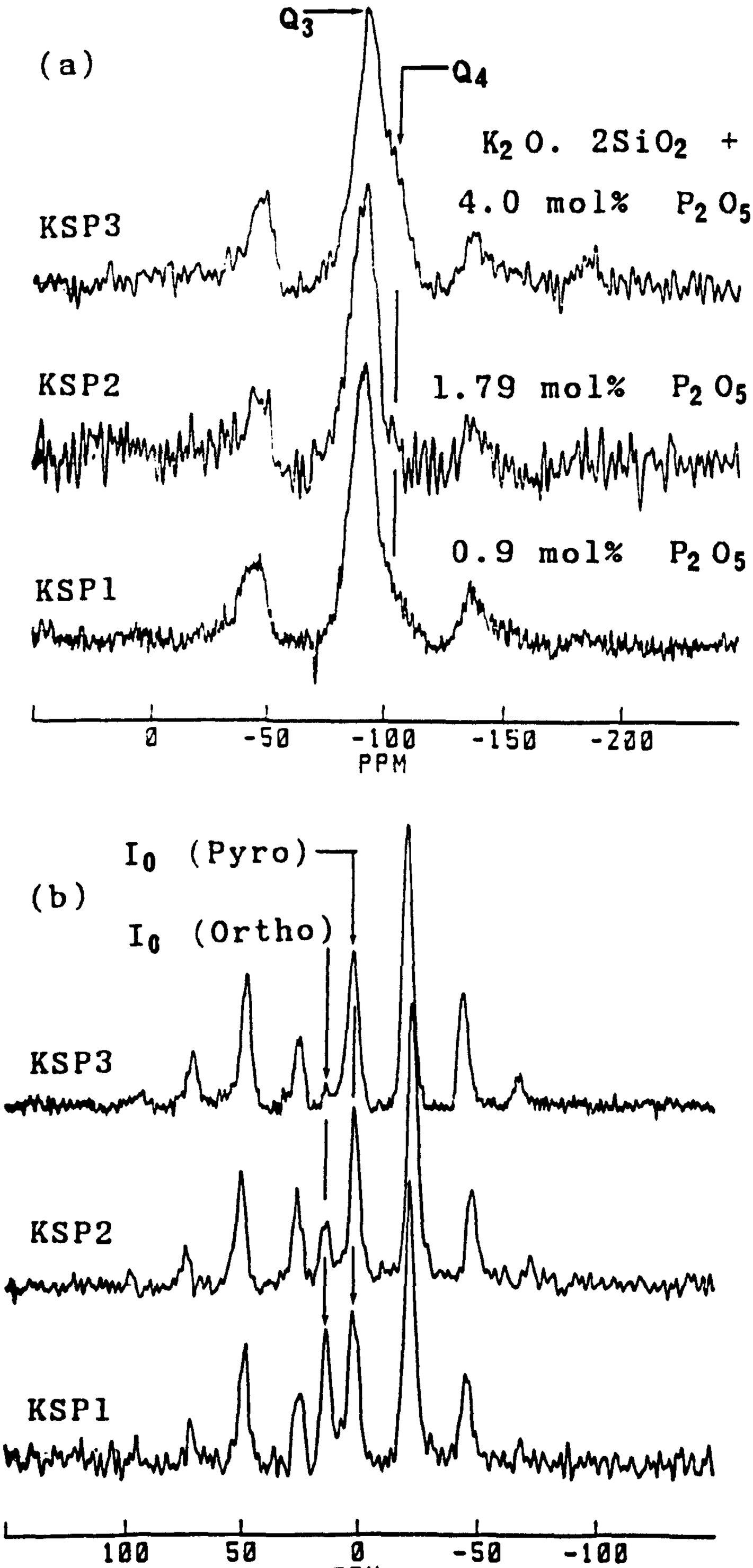

Figure 6.9 (a) ^{29}Si and (b) ^{31}P spectra of potassium phosphosilicate glasses. All the isotropic peaks are assigned according to their respective environments. The other peaks are spinning sidebands.

TABLE NO. 6.4 ^{29}Si AND ^{31}P SPECTRAL CHARACTERISTICS AND COMPOSITIONS OF THE SILICATE AND PHOSPHATE GROUPS IN POTASSIUM PHOSPHOSILICATE GLASSES

Sample (base glass)	Amounts of P_2O_5 (mol%) ±2%	^{29}Si spectral parameters (PPM) ±0.5				^{31}P spectral parameters (PPM) ±0.5						Values of the fractional content ±0.05		Values of the (Q_4/Q_3 ratio ±0.05	
		Q_4		Q_3		Like orthophosphate			Like pyrophosphate						
		CS	FWHM	CS	FWHM	CS	FWHM	|Δσ|	CS	FWHM	|Δσ| ±5	ortho-phosphate (m)	Pyro-phospate (n)	Theoretical	Experimental
KSP1	0.90	-104.1	10.0	-91.8	12.0	+13.4	6.0	*	+2.2	4.5	126	0.15	0.85	0.11	0.08
KSP2	1.79	-104.9	10.1	-92.0	12.3	+13.0	6.0	*	+1.2	4.5	120	0.10	0.90	0.17	0.15
KSP3	4.01	-106.7	12.0	-92.2	12.2	+12.8	5.8	*	+1.2	5.0	127	0.04	0.96	0.37	0.33

* Side band intensities are small to measure.

of ~13 PPM as the phosphorus content increases. The anisotropy associated with phosphorus in K_3PO_4 is very small but comparatively large, $|\Delta\sigma|$ ~ 125 PPM, in $K_4P_2O_7$ consistent with other workers [46,51,53]. The chemical shift, FWHM and relative amounts of the different phosphorus units are presented in Table (6.4).

6.2.4 DISCUSSION

For a simple binary system $R_2O:SiO_2$ of ratio of 1:2, the major species present in the sample is the Q_3 unit [40-45]. However Q_2 and Q_4 species also form in the alkali disilicate compositional range (see Chapter 4). The situation is somewhat different on addition of P_2O_5, even 1.0 mol%, to the $R_2O.2SiO_2$ (R=Li, Na,K) glass system. A more prominent Q_4 resonance is observed along with a Q_3 resonance and the former increases at the expense of the latter due to increase of P_2O_5 in all the alkaliphosphosilicates.

As predicted in section (6.2.1 - .3) that P_2O_5 reacts with alkali metal ion and forms Li_3PO_4 in lithium phosphosilicates, R_3PO_4 and $R_4P_2O_7$ (R=NA,K) in sodium and potassium phosphosilicates, some of the alkali metal ions are scavenged by the phosphorus from the Q_3 site, reducing the effective concentration of alkali in the silicate matrix. In fact the number of oxygen per phosphorus is 2.5 in P_2O_5 but none of them are non-bridging oxygen [nbo]. Therefore in order to form an environment like R_3PO_4, phosphorus has to extract 1.5 oxygen atoms from the Q_3 portion of the glass [16,54]. This results in three additional Q_4 tetrahedra per phosphorus and the polymerisation of SiO_4 units increases with the increase of P_2O_5, resulting in an increase in intensity of

the Q_4 resonance. In addition to nearest neighbour and next nearest neighbour as the chemical shift depends upon the modifier content [45], the observed variation in chemical shift with increasing P_2O_5 content reflects the change in effective modifier content. The polymerisation of the SiO_4 network should move the chemical shift of both the Q_3 and Q_4 resonance as a function of P_2O_5 content towards the more shielded side, i.e. more negative. This is indeed the case, as seen in Tables (6.1 and 6.2).

Comparison of the crystalline static spectra of $Li_2O.2SiO_2.1P_2O_5$ and $Li_2O.2SiO_2$ (Figure 6.10) clearly reveals the presence of SiO_4 tetrahedra in the former. Therefore it can be concluded that Q_2 species may not be present in LSP1 which could accelerate the disproportionation $Q_2 + Q_4 \longrightarrow 2Q_3$ in the glass (LSP1). Alternatively by looking at the ^{29}Si spectra of heat treated $32Li_2O.63SiO_2.4P_2O_5$ (LSP4(a)); Figure 6.1.c) it is clear that Q_3 units convert to Q_2 and Q_4 as a result of aforesaid disproportionation. This indicates the presence of early nucleation of $Li_2O.SiO_2$ (Q_2) in LSP4(a) which could be small in amount to give the well resolved Q_2 lineshape in the base glass (Figure 6.1.a). A close inspection suggests that the shoulder present at -75 PPM could be due to Q_2 species which has become prominent when the sample is heat treated at 475°C/6h (Figure 6.1.c).

In the case of sodium silicates, the association of alkali ions with phosphorus is not so pronounced and extensive dimerisation occurs, in preference to the formation either of further $P-O-R^+$ or Si-O-P bonds. Formation of the dimer, $Na_4P_2O_7$, in addition to the monomer, Na_3PO_4 confirms that the number of Na^+ ions scavenged per phosphorus in sodium

the Q_4 resonance. In addition to nearest neighbour and next nearest neighbour as the chemical shift depends upon the modifier content [45], the observed variation in chemical shift with increasing P_2O_5 content reflects the change in effective modifier content. The polymerisation of the SiO_4 network should move the chemical shift of both the Q_3 and Q_4 resonance as a function of P_2O_5 content towards the more shielded side, i.e. more negative. This is indeed the case, as seen in Tables (6.1 and 6.2).

Comparison of the crystalline static spectra of $Li_2O.2SiO_2.1P_2O_5$ and $Li_2O.2SiO_2$ (Figure 6.10) clearly reveals the presence of SiO_4 tetrahedra in the former. Therefore it can be concluded that Q_2 species may not be present in LSP1 which could accelerate the disproportionation $Q_2 + Q_4 \longrightarrow 2Q_3$ in the glass (LSP1). Alternatively by looking at the ^{29}Si spectra of heat treated $32Li_2O.63SiO_2.4P_2O_5$ (LSP4(a)); Figure 6.1.c) it is clear that Q_3 units convert to Q_2 and Q_4 as a result of aforesaid disproportionation. This indicates the presence of early nucleation of $Li_2O.SiO_2$ (Q_2) in LSP4(a) which could be small in amount to give the well resolved Q_2 lineshape in the base glass (Figure 6.1.a). A close inspection suggests that the shoulder present at -75 PPM could be due to Q_2 species which has become prominent when the sample is heat treated at 475°C/6h (Figure 6.1.c).

In the case of sodium silicates, the association of alkali ions with phosphorus is not so pronounced and extensive dimerisation occurs, in preference to the formation either of further $P-O-R^+$ or $Si-O-P$ bonds. Formation of the dimer, $Na_4P_2O_7$, in addition to the monomer, Na_3PO_4 confirms that the number of Na^+ ions scavenged per phosphorus in sodium

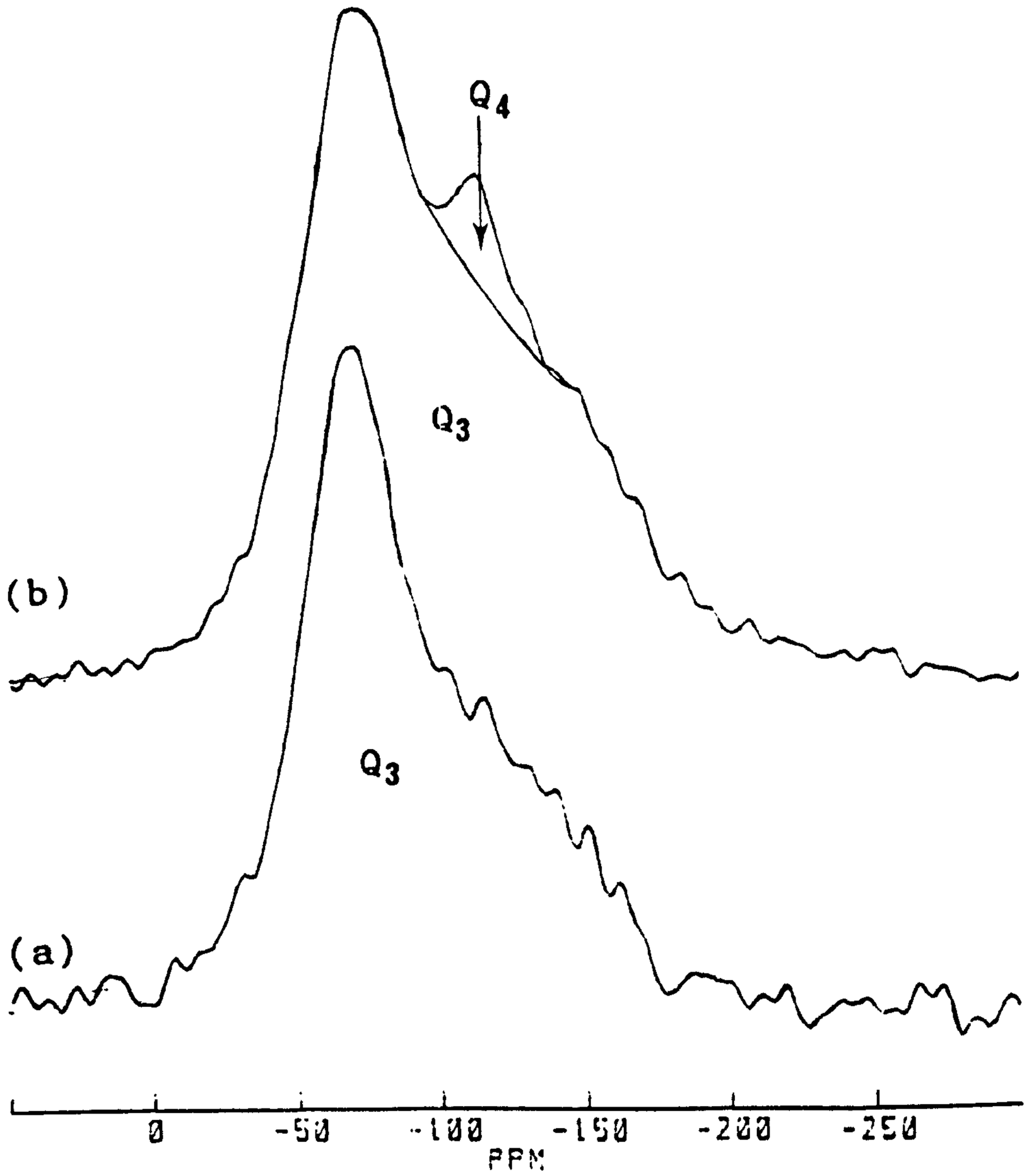

Figure 6.10 A comparison of the crystalline (a) $Li_2O.\ 2SiO_2$ and (b) $Li_2O.\ 2SiO_2.\ 1P_2O_5$ static spectra.

phosphosilicate is less in comparison to that of lithium phosphosilicate where only the monomer forms. Thus the rate of polymerisation of the Q_4 unit in sodium phosphosilicate is comparatively less.

The dimerisation is more evident in $K_2O.2SiO_2$-P_2O_5 and this could be the reason why the Q_4 in potassium phosphosilicate is less than the $Na_2O.2SiO_2$-P_2O_5 glasses. As the formation of dimer and monomer throughout the composition range (1-8 mol%) do not follow any linear relationship (Figure 6.7) the Q_4 resonance may not be expected to grow linearly. This non-linear characteristic will have an effect on the nucleation rate and may find an industrial application where controlled nucleation is required. The sample NSP5 contains 93% phosphorus as Na_3PO_4 and was initially phase separated. The concentrations of K_3PO_4 and $K_4P_2O_7$ in $K_2O.2SiO_2$-P_2O_5 follow the general trend of $Na_2O.2SiO_2$-P_2O_5 system. The change in FWHM for Q_4 in the lithium disilicate glasses may arise from the increasing presence of phase separation in this particular system. Phase separation gives visible opalescence in the glass containing 4 mol% P_2O_5. The large negative shift of Q_4 here (-111.4 PPM) indicates an environment close to that in vitreous silica, whereas in the case of sodium and potassium disilicates the chemical shifts are typical of Q_4 mixed with Q_3.

Heat treatment of the sodium phosphosilicate gives an increase of Na_3PO_4 and a decrease of $Na_4P_2O_7$ (Figure 6.6.b). In order to form the monomer, $(PO_4)^{3-}$, from the dimer, $(P_2O_7)^{4-}$ the latter has to combine with Na_2O and the chemical reaction which could take place can be represented simply by

$$Na_4P_2O_7 + Na_2O \xrightarrow{\Delta} 2\ Na_3PO_4 \qquad \ldots \qquad (6.2)$$

The additional Na_2O can only be obtained by further scavenging of Na^+ ions from the Q_3 sites which creates excess Na_3PO_4 and hence further polymerisation of SiO_4 tetrahedra. This could be the reason why the Q_4/Q_3 ratio increases in crystalline sodium phosphosilicates. This may be equally true in the case of potassium phosphosilicates of the composition range (1-8 mol%) P_2O_5 as well.

The quadrupolar interaction and chemical shift dispersion broaden the ^{23}Na lineshape. Except the apparent change of resonance position with the increase of P_2O_5 content all the spectra look similar to each other. The change of peak position reflects an increased shielding at the site of sodium nucleus due to Na-P coupling.

In the glasses the degree of polymerisation of the silicate matrix depends on the changing alkali: phosphorus ratio, which in orthophosphates is 3:1 and in pyrophosphates 2:1. The ratio of alkali to network former could be considered as $2R_2O/(SiO_2 + 2P_2O_5)$ or the ratio of alkali to phosphorus R_2O/P_2O_5. In the former case the ratio is <1 for all the P_2O_5 concentration and thus, if R^+ were uniformly distributed throughout the network, the association of phosphorus would be very much less than is observed. In the second case, if alkali were completely associated with the phosphorus, then only orthophosphate unit would be observed for all the alkali metals over this concentration range (1-4 mol%) of P_2O_5 and the rate of polymerisation could be higher. This is the case for lithium disilicate glasses and it can therefore be concluded that Li^+ preferentially associates with $(PO_4)^{3-}$ units in the glass to produce an environment like that in crystalline Li_3PO_4. This implies that there is little

interaction between these units and the silicate network, i.e. no Si-O-P linkages occur. This is consistent with thermodynamic [55] and Raman spectroscopic [20,21] data where $(PO_4)^{3-}$ is assumed not to share oxygens with either phosphorus or silicon tetrahedra. This observation of incipient Li_3PO_4 in the lithium silicate glasses substantiates the opinion that P_2O_5 functions as a nucleating agent in these materials by providing Li_3PO_4 nuclei in the base glasses for the epitaxial growth of $Li_2Si_2O_5$ [13,14,18].

The dimerisation in sodium and potassium phosphosilicates deviates the path of direct nucleation, i.e. first some excess monomer form from the dimer and then the nuclei of $R_2Si_2O_5$ (R=Na,K) grow epitaxially on the top of the monomer. This indirect process of nucleation may be the reason why the rate of nucleation is low in the $R_2O.2SiO_2$-P_2O_5 (R=Na,K) system provided that the early nucleation of $R_2O.SiO_2$ does not occur during quenching from the melt. The formation of $R_2O.SiO_2$ may create another complication in the nucleation process. The reason for differing amounts of orthophosphate and pyrophosphate groups is not yet understood but may arise for one or more of the following causes :

a) with increased ionic ratio, steric hindrances may render R_3PO_4 units unstable with respect to $R_4P_2O_7$;

b) in the case of lithium disilicate glasses, the occurence of phase separation may provide one phase with a much higher alkali : phosphorus ratio than expected from the overall composition.

The glasses where the disproportionation

$$2Q_m = Q_{m+1} + Q_{m-1} \quad \cdots \quad \cdots \quad (6.3)$$

does not occur, as in the case of LSP1, NSP1-NSP3, KSP1-KSP3 and probably in LSP2, the binary model of Dupree et al. [41] can be applied to predict the relative amounts of the Q_m species in the case of binary $R_2O.2SiO_2$ (R=Li,Na,K) glasses. As the incorporation of P^{5+} changes the structure of the $R_2O.2SiO_2$ system and the observed increase of Q_4 resonance depends on the degree of association of the alkali metal ions with the phosphorus oxygen units, the theoretical (Q_4/Q_3) ratios can be calculated on the basis of different structural models:

a) Binary glasses, $XR_2O.(1-X)SiO_2 (X < 0.33)$: Here 2X R^+ ions can form Q_3 species and therefore the number of Q_4 resonances is (1-X-2X) = 1-3X.

$$\therefore \frac{Q_4}{Q_3} = \frac{1 - 3X}{2X} \quad \ldots \quad \ldots \quad (6.4)$$

b) Ternary glasses, $XR_2O.\ (1-X-Z)SiO_2.ZP_2O_5$:

i) If all the phosphorus is present as orthophosphate ions $(PO_4)^{3-}$ and associated with R^+ for charge balance, the 2Z phosphorus can scavenge 6Z R^+ from the Q_3 glass matrix. Therefore the number of Q_3 will be reduced from 2X to (2X - 6Z) and the number of Q_4 is

$$\begin{aligned} Q_4 &= 1 - X - Z - (2X - 6Z) \\ &= 1 - 3X + 5Z \end{aligned}$$

$$\therefore \frac{Q4}{Q_3} = \frac{1 - 3X + 5Z}{2X - 6Z} \quad \ldots \quad \ldots \quad \ldots \quad (6.5)$$

ii) If all the phosphorus is present as pyrophosphate $(P_2O_7)^{4-}$, the number of R^+ scavenged is two per phosphorus. Therefore the number of Q_3 = 2X - 4Z and that of Q_4 is (1-3X + 3Z).

$$\therefore \frac{Q_4}{Q_3} = \frac{1 - 3X + 3Z}{2X - 4Z} \quad \ldots \quad \ldots \quad \ldots \quad (6.6)$$

iii) If both orthophosphate and pyrophosphate groups are present, with fractions m and n respectively (m+n=1), i.e. 100m and 100n determine the percentage of $(PO_4)^{3-}$ and $(P_2O_7)^{4-}$ respectively, then 2Z (3m + 2n) alkali ions will be scavenged by the phosphorus in the system. Therefore the ratio Q_4/Q_3 will become

$$\frac{Q_4}{Q_3} = \frac{1 - 3X - Z\,[1 - 2\,(3m + 2n)]}{2X - 2Z\,(3m + 2n)} \quad \ldots \quad (6.7)$$

The above models assume that no Si-O-P bonds are formed, i.e. phosphorus plays no part in forming the network.

The calculated Q_4/Q_3 ratios based on model (b.iii), using values of m and n derived from the observed intensities in the phosphorus spectra are compared with experiment in Tables (6.1 - 6.4). It can be seen that the agreement is good for LSP1, LSP2, NSP1-NSP3 and KSP1 - KSP3 glasses, but for 4 mol% P_2O_5 in the lithium silicates the experimental ratio (0.36) indicates that much less Q_4 is present than predicted by the model. In this glass phase separation may be occurring to such an extent that the shoulder at -75 PPM, characteristic of Q_2 species, appearing in the base glass (Figure 6.1.a) and distorting the resonance lineshape, making the deconvolution inaccurate. Therefore it may be said that the models provide a means of checking the other species which might occur because of phase separation. The models predict the generalised chemical reaction for the lithium and sodium phosphosilicate glasses as :

i) $Li_2O.2SiO_2.ZP2O_5$ (Z = 1-2) :

$pLi_2Si_2O_5 + rP_2O_5 \longrightarrow 6\ rSiO2 + (p - 3r)Li_2Si_2O_5 + 2rLi_3PO_4$ (6.8), i.e. if p mole of $Li_2Si_2O_5$ react with r mole of P_2O_5, that would create the product of the right hand side.

ii) $Na_2O.2SiO_2.Z\ P_2O_5$ (Z = 1-6) :

$$pNa_2Si_2O_5 + rP_2O_5 \rightarrow (6rm + 4rn)SiO_2 + (p - 3rm - 2rn)Na_2Si_2O_5 + 2rm\ Na_3PO_4 + rn\ Na_4P_2O_7 \quad ..(6.9)$$

The expression (6.9) is also valid in the case of potassium disilicate with low amounts of P_2O_5. The value of Z may be higher in this case. On the basis of the results, a schematic diagram of the sodium phosphosilicate glass structure can be drawn as shown in Figure (6.11).

The validity of the expression (6.2) suggests that the models [a, b.(i) - .(iii)] can also be applied to calculate the ratio (Q_4/Q_3) for a partially crystalline material. However, this may not be identical to the experimental value because the rate of crystallisation for a particular heat treatment is not the same [56] for all the species. At a particular heat treatment one species may be more vitreous with respect to the other resulting in the relative variation of FWHM, i.e. area under the respective peaks may change.

The results suggest that $(PO_4)^{3-}$ in lithium disilicate and $(PO_4)^{3-}$, $(P_2O_7)^{4-}$ in sodium and potassium disilicates form almost instantly on addition of P_2O_5. However the ^{31}P studies of phosphorus oxynitride glasses [57] show that the dimerisation occurs due to polymerisation of chain phosphate, $(PO_3^-)_n$. The environment of phosphorus in alkaline earth silicate glasses [54] is like $(PO_4)^{3-}$. In molybdenum- and

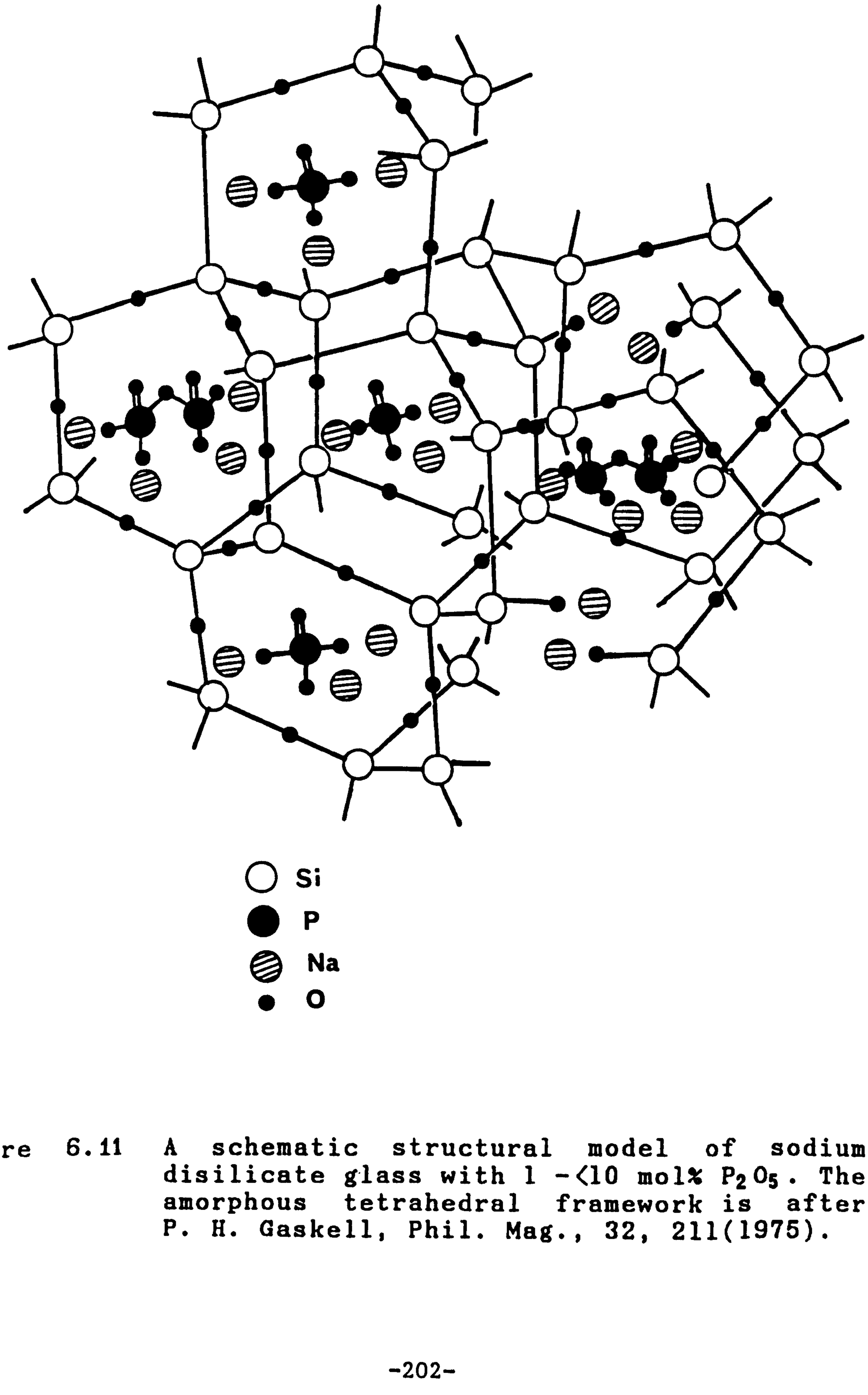

Figure 6.11 A schematic structural model of sodium disilicate glass with 1 -<10 mol% P_2O_5. The amorphous tetrahedral framework is after P. H. Gaskell, Phil. Mag., 32, 211(1975).

vanadium- phosphate glasses, the phosphorus networks consist essentially of chain phosphate [49]. Therefore it can be concluded that the environment of phosphorus is dependent upon the type of investigated material and no definite phosphate model can be predicted. None of these studies show any evidence of Si-O-P bond.

6.3 THE ROLE OF LARGE AMOUNTS OF PHOSPHORUS IN THE SODIUM DISILICATE SYSTEM

Phosphosilicate glasses have applications in glass-to-metal seal industries, particularly to metals of high thermal expansion [58]. But the hygroscopicity of the phosphate glasses makes the seals less durable to some extent. The structure of phosphosilicate glasses are not as clear as binary silicates. The aim of this section is to present the behaviour of SiO_2 and P_2O_5 in the high phosphate containing $Na_2O.2SiO_2$-P_2O_5 system where a number of controversies exist [19-21,24,59].

It has been accepted since 1932 that the building block of silicate glasses consists of silicon tetrahedrally connected to four oxygen atoms [59]. Although the existence of 6-coordinated silicon in a few crystalline materials, such as stishovite, SiP_2O_7, $Si_5O(PO_4)_6$ etc. is known [60-67], the presence of SiO_6 units has not yet been observed experimentally in glasses. Phase diagram of SiO_2-P_2O_5 [68] indicates the presence of SiP_2O_7 crystal when the system contains more than about 27 mol% P_2O_5. However the phase equilibrium diagram of Na_2O-SiO_2-P_2O_5 [69] suggests the formation of sodium silicate, sodium phosphosilicate and silicophosphate crystals for the Na_2O:SiO_2:P_2O_5 ratios 10:7:2,

4:2:1, 5:3:1, 11:6:3 and 14:6:4. These diagrams generally provide a rough estimate of the phases present in glass ceramics. However the presence of the characteristic of silicophosphate environment is not known in glass.

Recent x-ray diffraction and MAS NMR investigations [19,24] of SiO_2-P_2O_5 glasses found only four coordinated silicon although SiP_2O_7 was produced by devitrification. Raman studies [20] of Na_2O-$SiO_2P_2O_5$ glasses were interpreted as indicating the presence of a structural unit containing Si-O-P bonding but otherwise unidentifiable. Here MAS NMR spectroscopy is applied to the system $Na_2O.2SiO_2$:ZP_2O_5 (Z=11-70 mol%) and the first observation of SiO_6 units in the glasses is reported. The coordinations of P^{5+}, Al^{3+} (obtained from the crucible) are also determined. An attempt is also made to obtain information about the Na^+ environment via ^{23}Na NMR.

6.3.1 ^{29}Si NMR

The ^{29}Si spectra in the sodium phosphosilicate glasses (NSP5 - NSP12) are shown in Figure 6.12. The spectral properties of the base glasses obtained from the ^{29}Si resonance with differing phosphorus contents are illustrated in Table (6.5). There are no spinning side bands associated with the isotropic lines of NSP6 - NSP12 glass spectra. The change of ^{29}Si environment due to addition of P_2O_5 is evident from the line shapes.

Addition of 3 mol% P_2O_5 to the 8 mol% P_2O_5 containing $Na_2O.2SiO_2$ sample (NSP5) abruptly changes the ^{29}Si environment. This is obvious from a single resonance at -99 PPM (Figure 6.12.a.2) in NSP6 instead of two partially

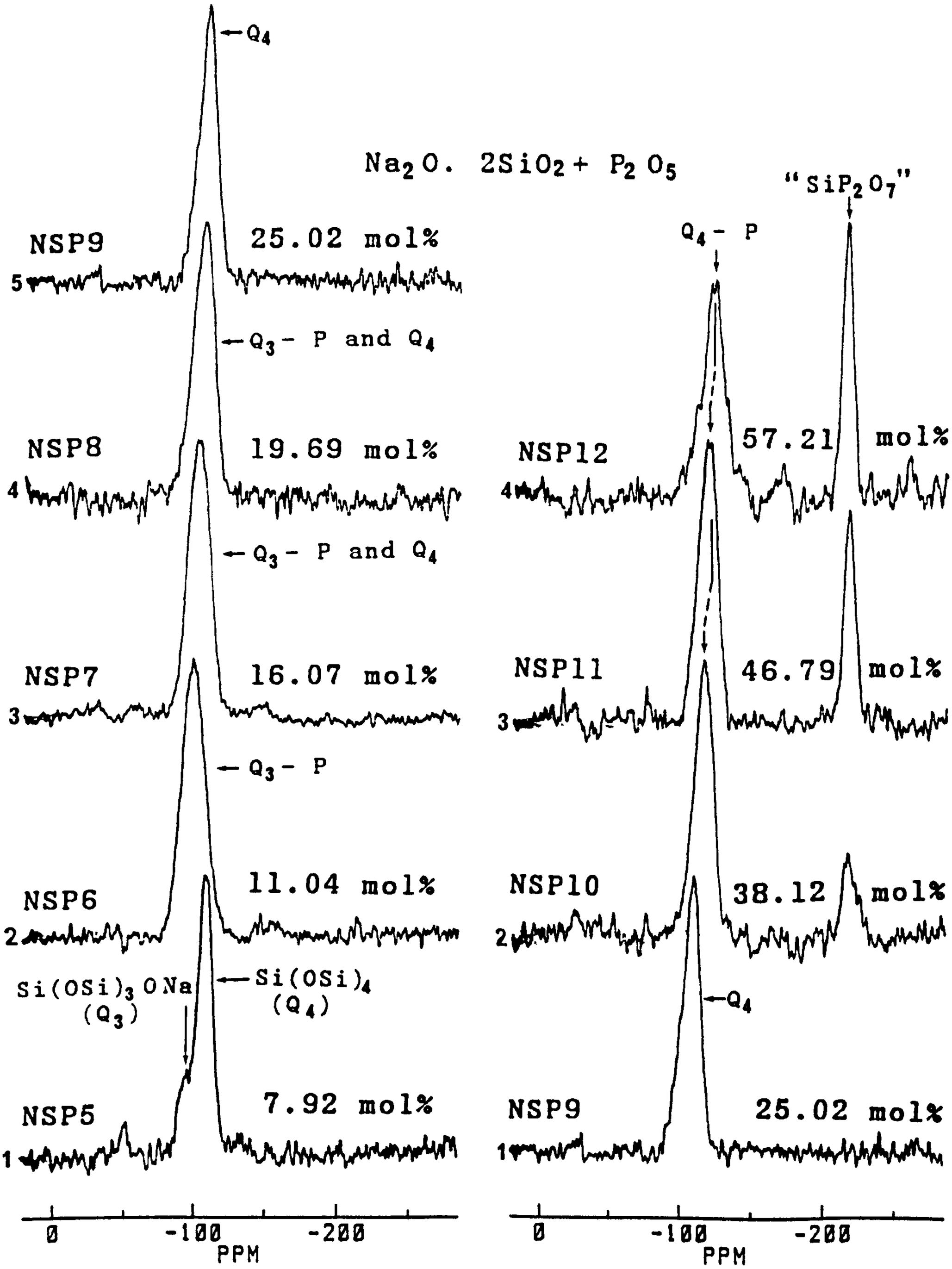

Figure 6.12 ^{29}Si spectra of sodium disilicate base glasses with (a) 8 - 25 mol% P_2O_5 and (b) 25 - 57 mol% P_2O_5.

TABLE NO. 6.5 ^{29}Si SPECTRAL PROPERTIES OF SODIUM DISILICATE BASE GLASSES WITH DIFFERING PHOSPHORUS CONTENTS

Sample	Amounts of P_2O_5 mol%	^{29}Si spectral parameters (PPM) ± 0.5										$\frac{SiO_6}{Q_4\text{-}P}$ ±0.05
		Q_3		Q_3-P+		Q_4		Q_4-P+		SiO_6		
		CS	FWHM	CS	FWHM	CS	FWHM	CS	FWHM	CS	FWHM	
NSP5	7.92	-94.1	12.1	-	-	-108.9	12.6	-	-	-	-	-
NSP6	11.04	-	-	-99.0	18.2	-	-	-	-	-	-	-
NSP7	16.07	-	-	-102.7	18.0	**	**	-	-	-	-	-
NSP8	19.69	-	-	-106.8	21.0	**	**	-	-	-	-	-
NSP9	25.02	-	-	-	-	-109.0	14.0	-	-	-	-	-
NSP10	38.12	-	-	-	-	-	-	-116.6	15.0	-212.6	9.1	0.15
NSP11	46.79	-	-	-	-	-	-	-118.4	15.5	-213.1	9.0	0.44
NSP12	57.21	-	-	-	-	-	-	-119.9	18.0	-212.8	9.0	0.59
NSP13	70.0*	-	-	-	-	-	-	-	-	-	-	-

+ Si - O - P bond between Q species

* Nominal composition

** This species may also present

overlapped peaks at -93 and -108 PPM in NSP5 (Figure 6.12.a.1). The chemical shift values become more negative with the successive addition of P_2O_5, e.g. -103 PPM in NSP7 (16 mol% P_2O_5) and -107 PPM in NSP8 (20 mol% P_2O_5). The ^{29}Si resonance in NSP9 (25 mol% P_2O_5) is at -109 PPM, characteristic of pure Q_4 as in vitreous SiO_2 [45] undiluted by other species. However the MAS spectra obtained from the glasses of > 25 mol% P_2O_5 content are most unusual. When further additions of $P2O_5$ are made (NSP10-NSP12) an additional resonance appears in the silicon spectrum at -213 PPM. The intensity of the peak, relative to that of Q_4, increases with increasing P_2O_5 content. The position of the peak at -213 PPM remains almost constant throughout the differing P_2O_5 concentrations but the peak of "Q_4" silicon resonance shifts from that observed in the 25 mol% P_2O_5 (NSP9) material. It is now found at -116.5 (38%), -118.4 (47%), or -119.9 (57%), P_2O_5. Several authors [24,62,63] have reported the chemical shifts for ^{29}Si when 6-coordinated, as in cubic SiP_2O_7 (-214 PPM) and $Si_5O(PO_4)_6$ (-217 PPM). The peak at -213 PPM is very close to the data of ref. [63] (-213.2, -215.5 PPM). Therefore it can be said that this environment of silicon is very similar to a local order of the silicophosphate, SiP_2O_7, i.e. Si in SiO_6 octahedra. The chemical shift range -99 to -121 PPM lies within the range of SiO_4 tetrahedra [45] and so these peaks are characteristic of silicon in tetrahedral coordination.

6.3.2 ^{31}P NMR

MAS NMR spectra for ^{31}P in the sodium disilicate glasses containing varying amounts of P_2O_5 (NSP5-NSP13) are shown in Figure 6.13. The range of the chemical shifts lies within +16.0 to -41.0 PPM depending on the concentrations of P_2O_5 which covers a variety of phosphorus species [49,50,63]. All the isotropic lines are accompanied by spinning sidebands. Like ^{29}Si resonances in the glasses, the phosphorus sites also vary with P_2O_5 content. The ^{31}P spectral parameters are collected in Table (6.6).

There are two distinct phosphorus sites, one is like pyrophosphate (+2.5 PPM) and the other one is like orthophosphate (+15 PPM) in the sodium disilicate with up to 8 mol% P_2O_5. The phosphorus environment changes suddenly from its two sites to one and resonates at -12.0 PPM when the P_2O_5 concentration is 11 mol%. The phosphorus site appears to be more shielded with the increase of P_2O_5 and resonates at -16 PPM, characteristic of chain phosphate, $(NaPO_3)_n$, due to addition of 25 mol% P_2O_5. Two distinct but partially overlapped lines at -22.9 and -32.7 PPM are found for the 38 mol% P_2O_5 containing sample. The chemical shift for phosphorus in metaphosphate falls within -15 to -27 PPM [49,50] and the former (-22.9 PPM) appears to be like $(NaPO_3)_n$. As the ^{29}Si resonance shows an environment like SiP_2O_7, the other ^{31}P resonance (-32.7 PPM) can be thought of as from an environment like SiP_2O_7. This peak shifts towards the more negative value with the increase of P_2O_5 and finally appears at -40.5 PPM for the 70 mol% P_2O_5 containing sample (NSP13). This change indicates that the peak position

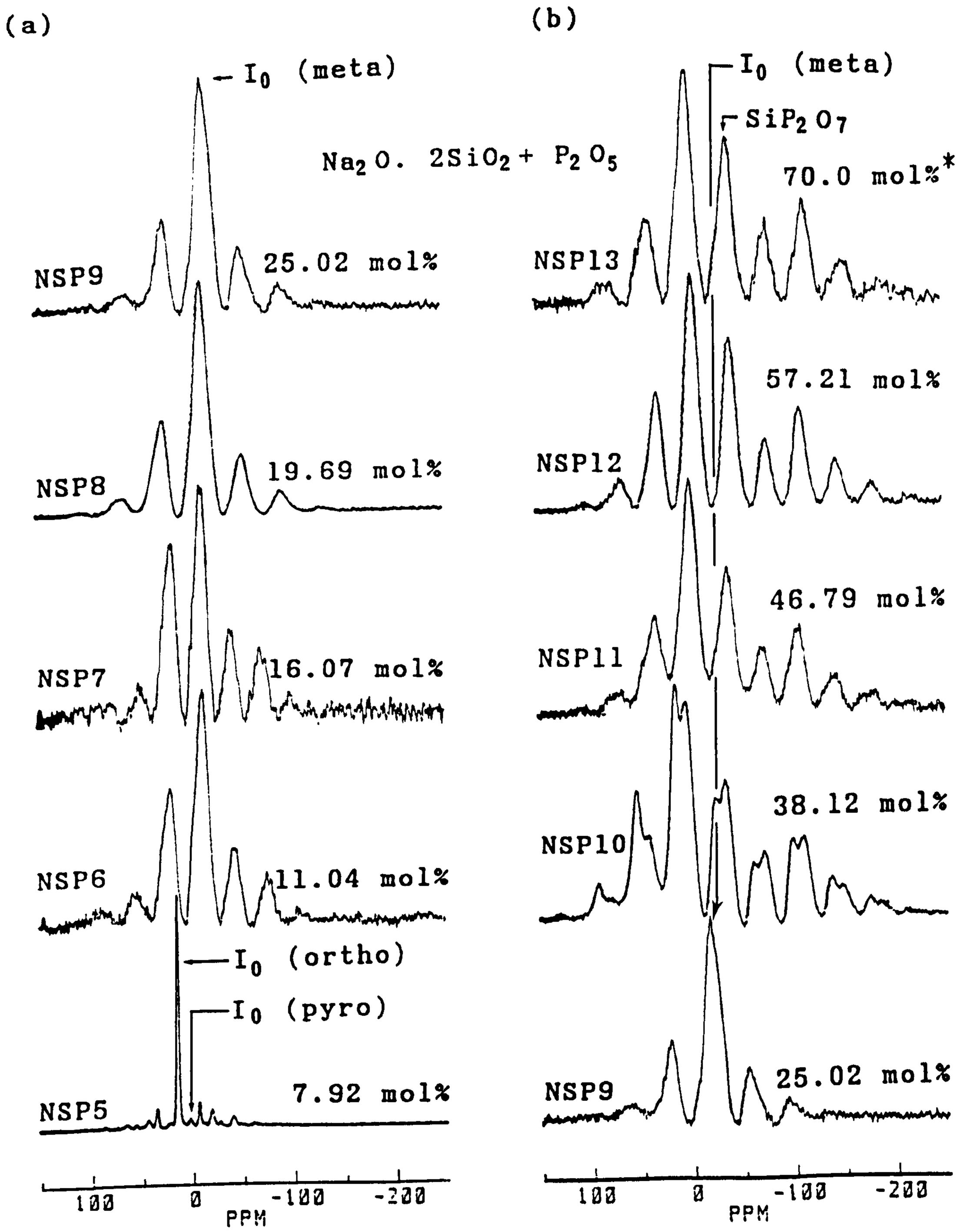

Figure 6.13 ^{31}P spectra of sodium disilicate base glasses with (a) 8-25 mol% P_2O_5 and (b) 25-70 mol% P_2O_5. The Isotropic(I_0) lines are characteristic of respective environments. The other peaks are spinning sidebands.
* Nominal composition.

approaches the reported ^{31}P resonance (-46.4, -47.7, -50.2 and -53.7 PPM) in crystalline SiP_2O_7 [63]. The peak due to $(NaPO_3)_n$ becomes invisible with the increase of P_2O_5, i.e. decrease of Na_2O content in the material. The isotropic lines are very broad (~17 PPM) compared to their crystalline form, 7.0 PPM for $(NaPO_3)_n$ and 8.0 PPM for SiP_2O_7, in the high P_2O_5 glasses. The range of the chemical shift anistropy, $|\Delta\sigma|$, which determines the symmetry of the electron distribution around the investigated nuclei, i.e. ^{31}P, has also been determined using the method of Herzfield and Berger [48]. The values appear to increase with P_2O_5 content but the rate of increase is not linear.

6.3.3 ^{23}Na NMR

Although the ^{23}Na spectra in the glasses as shown in Figure (6.14) are not very informative a little insight can be obtained about the sodium environment in the material. The most interesting feature of the spectra is the fluctuation of Na^+ environment when the silicon switches to Si^{6+} from its original tetrahedral coordination (Si^{4+}). The plot of peak position and FWHM as a function of P_2O_5 content (Figure 6.21) clearly shows the discontinuity between 25.0 and 38.1 mol% P_2O_5 when the SiO_6 units start to build up. The peak position changes almost linearly from +0.7 to -17.5 PPM for the P_2O_5 concentration of 0 to 25 mol%. Following a discontinuity, the ^{23}Na environment starts to become more shielded with the increase of P_2O_5. Low phosphorus containing spectra are relatively wider than the high phosphorus containing spectra and all the spectral parameters are shown in Table (6.6).

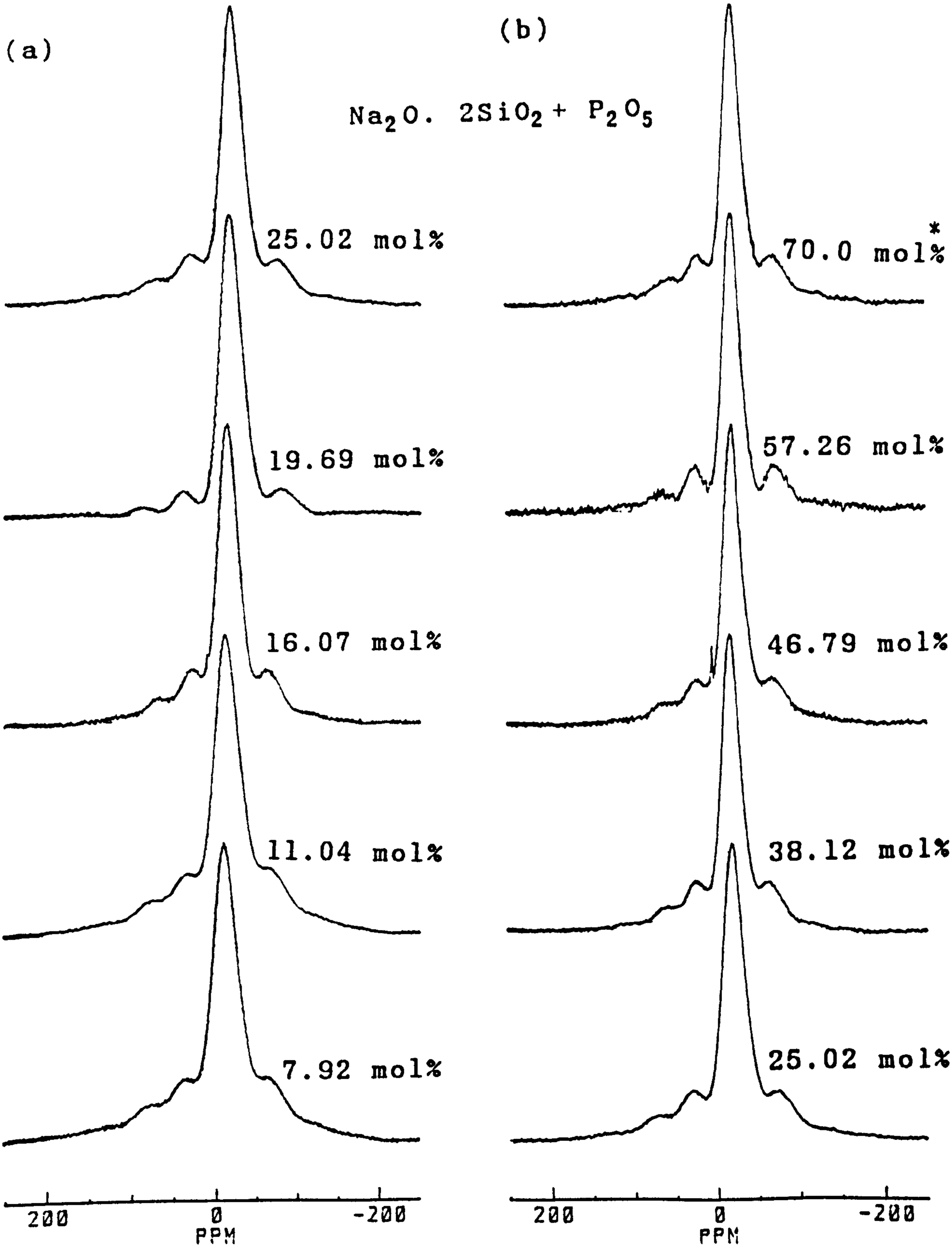

Figure 6.14 ^{23}Na spectra of sodium disilicate base glasses with varying amounts of P_2O_5.
* Nominal composition.

TABLE NO. 6.6 ^{31}P, ^{23}Na AND ^{27}Al SPECTRAL PROPERTIES OF SODIUM PHOSPHOSILICATE GLASSES

Sample	Spectral parameters (PPM) ± 0.5					
	^{31}P(a)		^{23}Na(b)		^{27}Al(c)	
	CS	FWHM	peak position	FWHM	peak position	FWHM
NSP5	+14.9	4.5	-9.8	31.6	-	-
	+2.4	6.0	-	-	-	-
NSP6	-12.0	16.3	-11.2	30.2	+49.2	24.0
NSP7	-12.4	16.3	-13.9	30.0	+45.0	24.4
NSP8	-13.8	16.4	-16.3	31.4	+44.5	22.0
	-	-	-	-	-14.6	16.3
NSP9	-16.0	16.5	-17.5	32.0	+42.5	21.2
	-	-	-	-	-14.4	16.0
NSP10	-22.9	16.0	-14.5	27.2	-17.5	12.4
	-32.7	16.6	-	-	-	-
NSP11	-36.5	17.0	-16.8	26.0	-18.5	12.4
	-	-	+8.0	-	-	-
NSP12	-39.5	17.0	-17.7	26.0	-19.0	12.2
NSP13	-40.0	16.9	-18.3	26.3	-19.3	12.4

(a) CS = 0 for 85% H_3PO_4.

(b) peak position = 0 for 0.1 mol Nacl.

(c) peak position = 0 for 0.1 mol $Al(NO_3)_3$.

6.3.4 ^{27}Al NMR

Figure (6.15) shows the ^{27}Al spectra of the Al^{3+} impurity in the glasses (NSP6-NSP13). The spectra are generally broad because of the quadrupolar electric field gradient. The Al^{3+} environment depends upon the amounts of P_2O_5 added to the system. The peak position between +41 to +52 PPM are roughly within the tetrahedral coordination of Al^{3+} and those between -10 to -17 PPM are approximately within the octahedral coordination. The Al^{3+} coordination changes from tetrahedral to octahedral between 20-35 mol% P_2O_5. The FWHM for the tetrahedral peak changes with the P_2O_5 concentrations but that for octahedra remains constant. The spectral properties are summarised in Table (6.6).

As the ^{27}Al NMR can be considered to quantify the Al^{3+} [70-75], the quantity of Al^{3+} is also estimated from the ^{27}Al signal. α-Al_2O_3 is considered as a standard by assuming that the electric field gradient at the site of Al^{3+} in α-Al_2O_3 is similar to that of the Al^{3+} in the investigated sample. The results are consistent with the atomic absorption and EDX analysis.

6.3.5 EFFECT OF DEVITRIFICATION

6.3.5.1 NMR

Figures 6.16 - 6.19 show the ^{29}Si, ^{31}P, ^{27}Al and ^{23}Na MAS NMR spectra of different heat treated glasses. The spectra for the base glasses are also shown in the figures to allow comparison of the change of different heat treatments.

The ^{29}Si spectra (Figure 6.16.a) for the gradual heat treatment of NSP9 (25 mol% P_2O_5) show the destruction of local

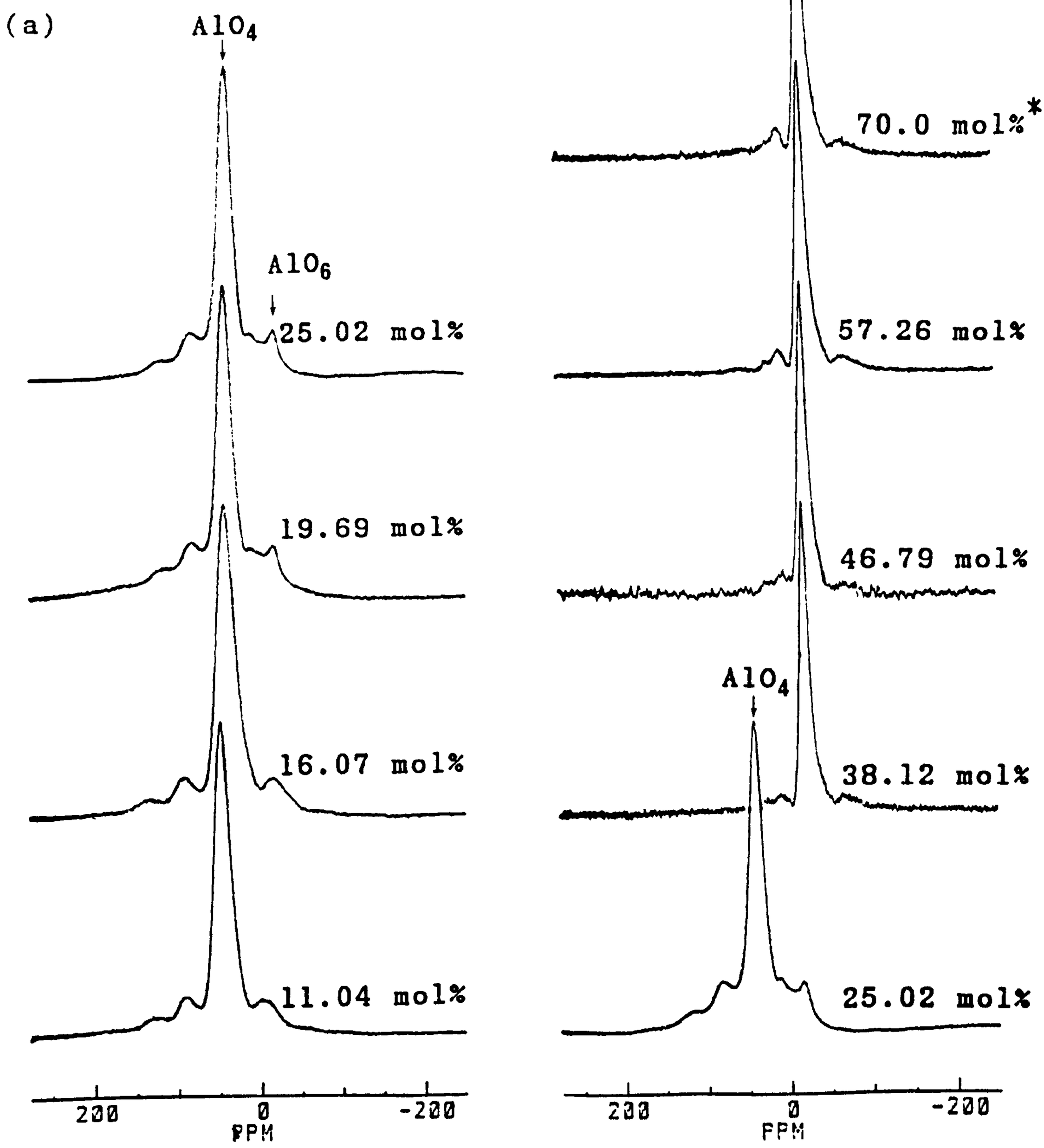

Figure 6.15 ^{27}Al spectra of sodium phosphosilicate glasses. (a) 11 to 25 mol% P_2O_5 and (b) 25 to 70 mol% P_2O_5.
* Nominal composition.

order of the ^{29}Si in SiO_4 tetrahedra. Line asymmetry towards the low field shift followed by partially overlapped resonance covering a range -92 to -104 PPM and a sharp peak at -109 PPM after heat treatment at 725°C/12h are observed. However, the heat treatment effect for the samples containing $[SiO_6]$ octahedra is rather different. The chemical shifts for both the $[SiO_4]$ and $[SiO_6]$ units remain unchanged with heat treatment. For NSP10 (- 38 mol% P_2O_5), the ratio $[SiO_6]/[SiO_4]$ does not change for heat treatment 9-720h (Figure 6.16.b) but that for other samples (NSP11, NSP12) does and is evident from the Figure 6.16.c and 6.16.d. For a particular heat treatment time and temperature the rate of conversion from $[SiO_4]$ to $[SiO_6]$ depends upon the amount of phosphorus added to the system. A spectrum showing the conversion of all the silicons in SiO_4 tetrahredra to SiO_6 octahedra is shown in Figure (6.16.d.3).

The ^{31}P in NSP9 heat treated at 725°C/12h resonates at +5.0, -5.9, -12.6 and -29.4 PPM (Figure 6.17.a). The creation of these various local orders of phosphorus reflects a major change of structure because of devitrification. The peaks at +5.0 and -5.9 PPM could be due to structurally non-equivalent PO_4 tetrahedra in $Na_5P_3O_{10}$ [76] and the peak at -29.4 PPM is a characteristic of phosphorus in $AlPO_4$ [77]. The other peak at -12.6 PPM is close to -15 PPM and may be thought of as an environment like chain phosphate, $(NaPO_3)_n$. The ^{31}P local order does not change in NSP10 whatever the heat treatment condition is (Figure 6.17.b). However in NSP11, the two resonances, one is a characteristic of $(NaPO_3)_n$ (-23 PPM) and the other one may, like SiP_2O_7 (-36 PPM), appear to become more prominent with heat treatment (Figure 6.17.c). But in

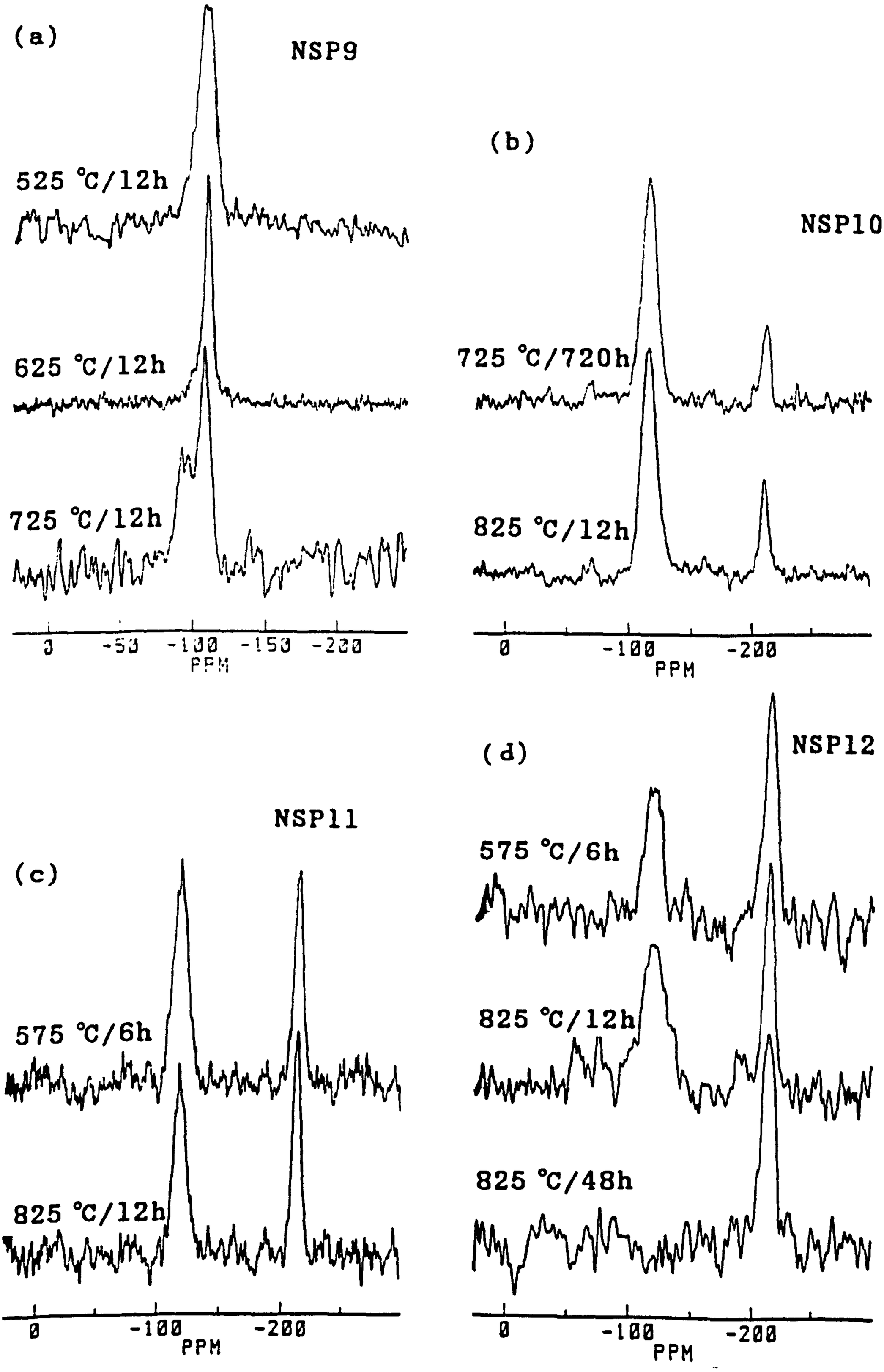

Figure 6.16 ^{29}Si spectra of heat treated high P_2O_5 ($\geq$ 25 mol%) containing sodium disilicate glasses.

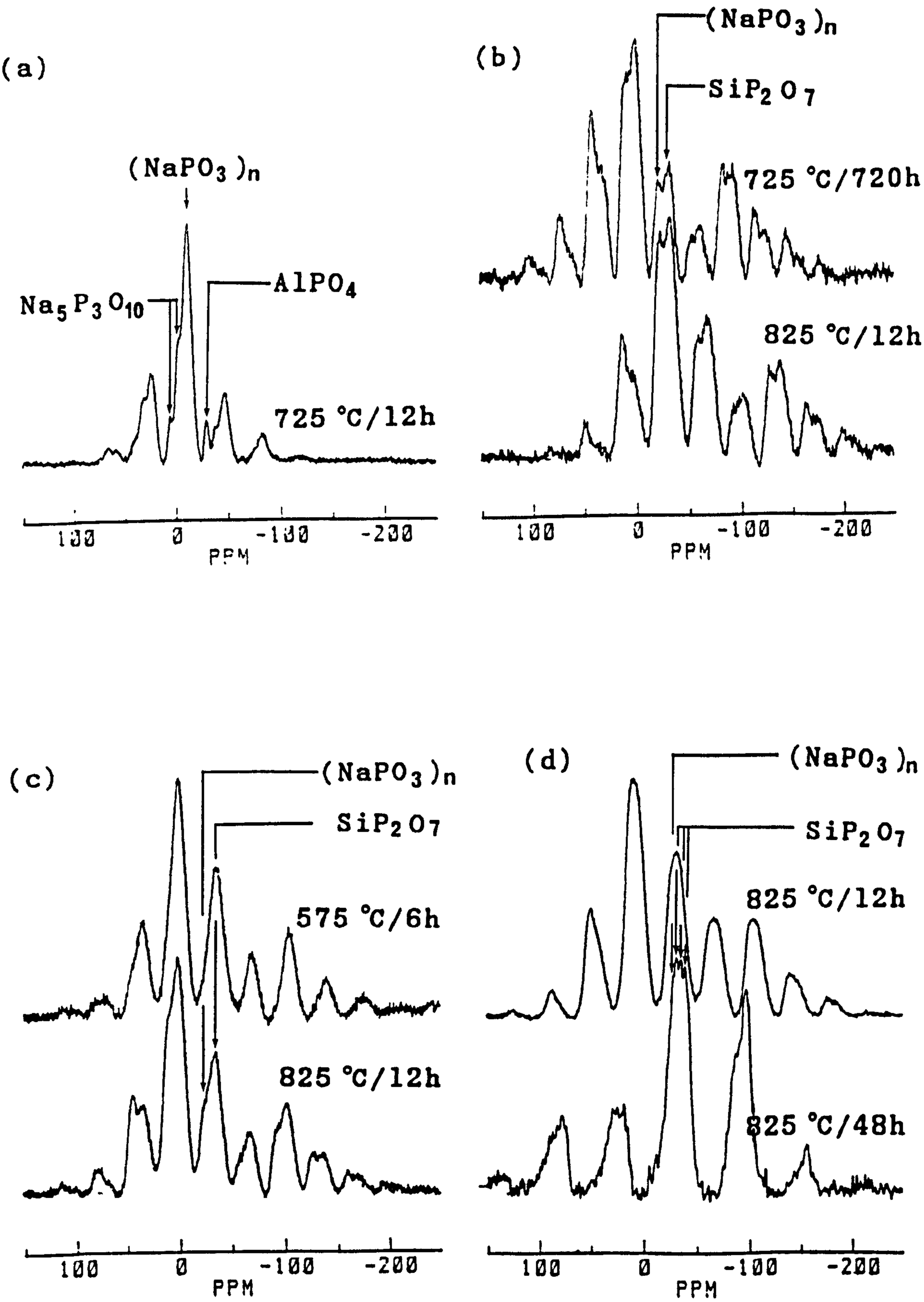

Figure 6.17 ^{31}P spectra of heat treated (a) $Na_2O.2SiO_2.25P_2O_5$ (NSP9), (b) $Na_2O.2SiO_2.38.1P_2O_5$ (NSP10), (c) $Na_2O.2SiO_2.46.8P_2O_5$ (NSP11) and (d) $Na_2O.2SiO_2.57.3P_2O_5$ (NSP12) glasses.

NSP12 such an effect is not observed. The ^{31}P resonance in crystalline NSP12, where all the silicons are present as $[SiO_6]$ octahedra is a broader peak (24 PPM) in comparison to glass (17 PPM) which can encompass metaphosphate and all the three polymorphs of SiP_2O_7. A close inspection of the spectra reveal four small features (-26.4, -30.1, -34.3, -39.0 PPM). These correspond to $NaPO_3$ (-26.4 PPM) and three polymorphs of SiP_2O_7 (-30.1, -34.3, -39.0 PPM). However the reported ^{31}P shifts [63] for different polymorphs are not very close to the observed shifts. The spinning sidebands also reveal the presence of more than one site in the spectrum but the determination of exact number is difficult.

The ^{23}Na spectra (Figure 6.18) are rather featureless and little information has been obtained. The shape of the spectra in glass and heat treated NSP10-NSP12 remains almost the same. The small peak at +4.8 PPM in some of the spectra is an artefact. A change in peak position and shoulders in NSP9 heat treated at 725°C/12h are observed. The shoulders could represent either a quadrupolar effect or three different sodium environments as observed in the sample by ^{31}P NMR (Figure 6.17.a). A small change in FWHM is noticed with heat treatment in all the glasses.

The change of ^{27}Al environment with heat treatment is also clear in the glasses (Figure 6.19). The peak position varies between 0.0 to +4 PPM depending on the degree of devitrification, provided that the next nearest neighbour remains the same. In NSP9 glass the ^{27}Al resonances show both octahedral (-19.0 PPM) and tetrahedral (+42.5 PPM) Al^{3+}. When the sample is devitrified at 725°C/12h, the nearest neighbour and next nearest neighbours remain the same but the resonances

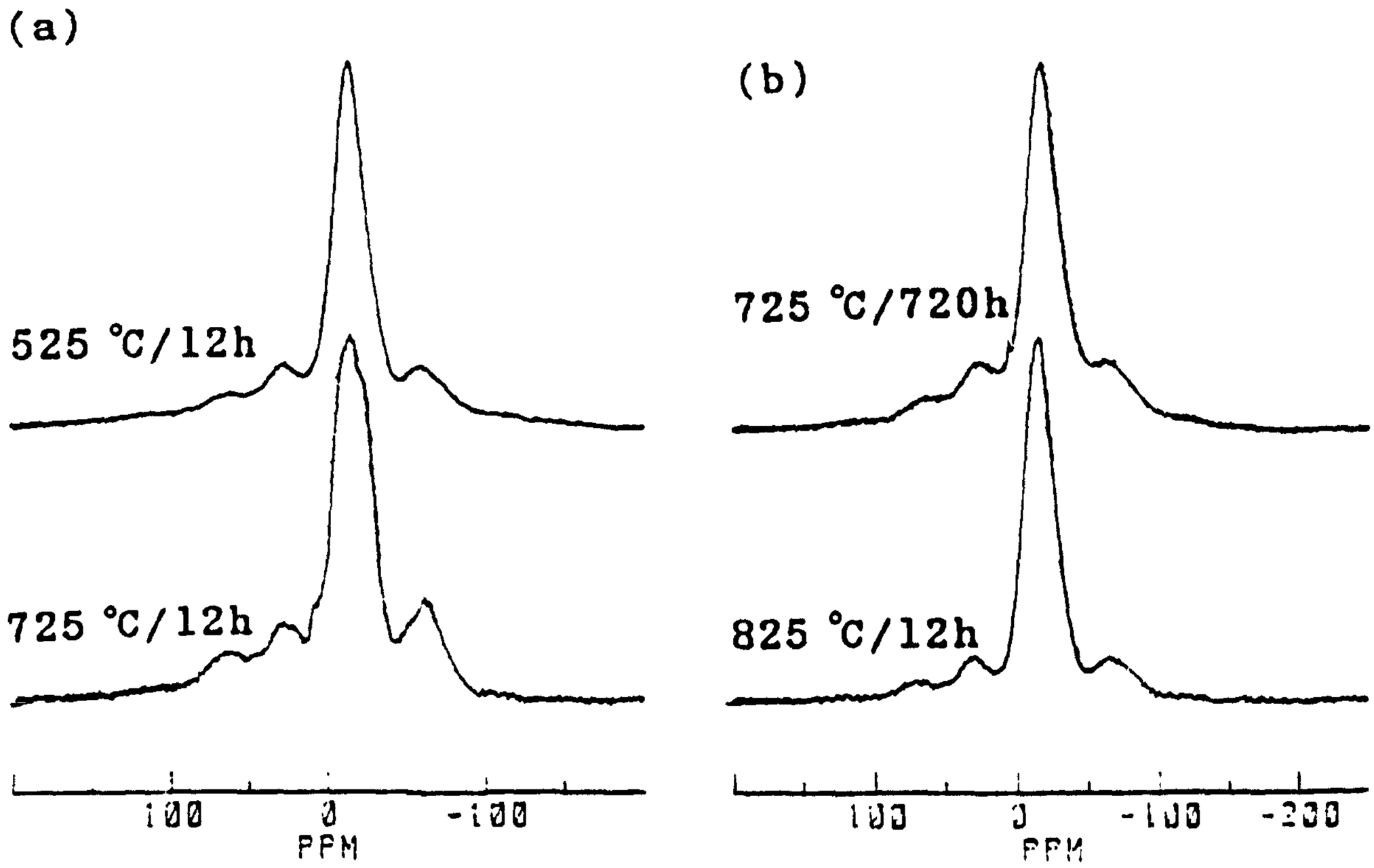

Figure 6.18 ^{23}Na spectra of heat treated (a) $Na_2O.2SiO_2.25P_2O_5$ (NSP9), (b) $Na_2O.2SiO_2.38.1P_2O_5$ (NSP10), (c) $Na_2O.2SiO_2.46.8P_2O_5$ (NSP11) and (d) $Na_2O.2SiO_2.57.3P_2O_5$ (NSP12) glasses.

are observed at -21.4 and -38.7 PPM respectively. The former corresponds to octahedral Al^{3+} with phosphorus as next nearest neighbour and the latter is a characteristic of $AlPO_4$ low-tridymite [77] (Figure 4.19.a). The FWHM of the former remains the same in glass and in crystalline material but for the latter it decreases considerably (by a factor of 5). Comparison of the glass and heat treated ^{27}Al spectra of NSP10 (~38 mol% P_2O_5) clearly reveal no change of peak position (-17.5 $\pm$ 0.5 PPM in glass and -17.6 $\pm$0.5 PPM in heat treated at 675°C/72h) and FWHM (12.0 $\pm$0.5 and 12.2 $\pm$ 0.5 PPM respectively) in the materials (Figure 4.19.b). The sample did not crystallise despite various heat treatments ranging from 575 - 875°C for different time periods, even a month. However the sample containing ~ 47 mol% P_2O_5 (NSP11) crystallises and two peaks at -9.4 and -15.8 PPM, both characteristic of Al^{3+}, are observed (Figure 4.19.c). Such a splitting of the octahedral resonance in NSP12 (~57 mol% P_2O_5) due to heat treatment has not been observed and only one resonance (-19.3 in glass and -17.5 PPM in crystal) in both the glass and crystalline material is found. The crystalline spectrum is about 3 PPM narrower than the glass spectrum.

The spectral properties obtained from ^{29}Si, ^{31}P, ^{27}Al and ^{23}Na for the heat treated NSP9 - NSP12 glasses are presented in Table 6.7.

6.3.5.2 XRD

The sample NSP9 heat treated at 525°C/12h contains crystals of SiO_2, $NaPO_3$ and an amorphous component (~30%) [78]. The other two devitrified products of NSP9 (Table 6.7) are almost fully crystallised (> 90%) and show only the SiO_2

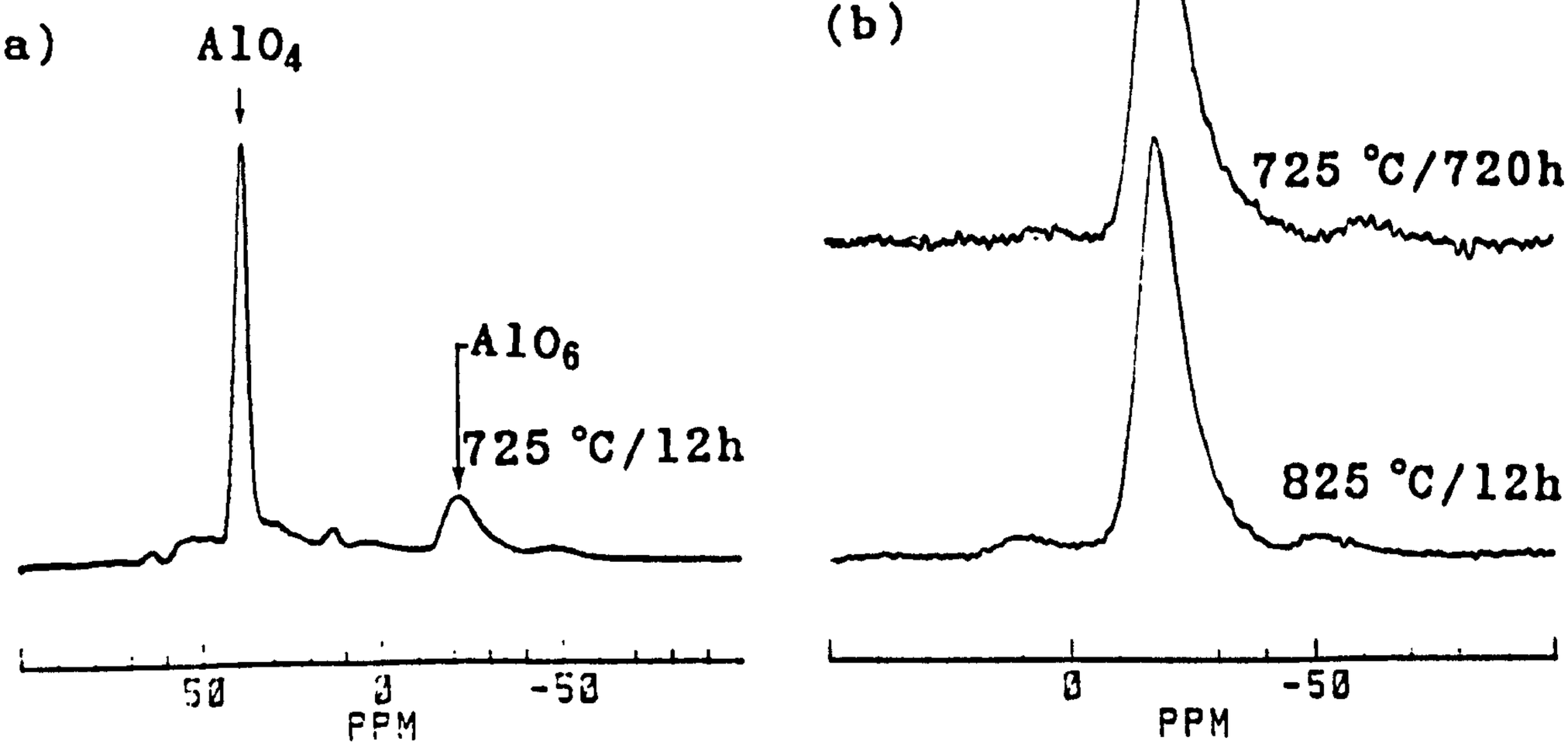

Figure 6.19 Al spectra of heat treated (a) $Na_2O.2SiO_2.25P_2O_5$ (NSP9), (b) $Na_2O.2SiO_2.38.1P_2O_5$ (NSP10), (c) $Na_2O.2SiO_2.46.8P_2O_5$ (NSP11) and (d) $Na_2O.2SiO_2.57.3P_2O_5$ (NSP12) glasses.

TABLE NO. 6.7 SPECTRAL CHARACTERISTICS AND CRYSTALLINE STATE OF SODIUM PHOSPHOSILICATE GLASS-CERAMICS

Sample	Heat treatment $T^{o}C/th$	Spectral Parameters (PPM) ± 0.5								XRD of the glass ceramics
		^{29}Si		^{31}P		^{23}Na		^{27}Al		
		CS	FWHM	CS	FWHM	Peak Position	FWHM	Peak Position	FWHM	
NSP9	525/12	-109.3	15.0							amorphous + crystalline
	625/12	-110.1	5.4			-12.2	24.0			amorphous + crystalline
	725/12	-108.9	10.0	+ 5.0	5.3	-15.1	28.8	+38.7	4.0	amorphous + crystalline
		-92to-102	-	- 5.9	8.8			-21.4	10.0	
				-12.6	11.0					
				-29.4	4.7					
NSP10	725/720	-116.5	13.2	-22.7	15.4	-15.3	22.8	-17.6	12.4	amorphous
		-212.5	8.4	-32.5	15.9	+ 4.8				
	825/12	-116.4	14.0	-23.6	15.0	-14.9	23.4	-17.4	11.6	amorphous
		-212.7	8.0	-32.7	14.5					
NSP11	575/6	-118.5	14.5	-36.2	16.0	-16.2	28.0	-18.3	13.6	amorphous +
		-212.7	9.0							crystalline
	825/12	-118.0	13.4	-24.2	15.9	-16.3	28.0	-9.4	3.5	amorphous +
		-212.9	8.0	-35.2	15.0			-15.8	12.0	crystalline
NSP12	575/6*	-118.8	16.3							amorphous +
		-213.2	9.2							crystalline
	825/12*	-118.5	14.0	-31.1	19.1	-17.6	26.0	-17.9	12.0	amorphous +
		-213.6	10.2			+ 4.6				crystalline
	825/48	-213.8	12.4	-26.4	+	-17.0	25.8	-17.7	10.0	crystalline
				-30.1	+					
				-34.3	+					
				-39.0	+					

* error is ± 1.0 PPM

\+ not measured

and $NaPO_3$ crystalline phases. The XRD patterns of the sample NSP10 heat treated at various temperatures show amorphous haloes. However the diffraction pattern of NSP11 and NSP12 devitrified at different temperatures are surprisingly different (Figure 6.20) although NMR results show similar species in the glasses. In the case of NSP11 the phases SiP_2O_7, $3SiO_2.2P_2O_5$ appear to grow whereas for NSP12 only the SiP_2O_7 phase is observed for all the heat treatments (Figure 6.20).

6.3.6 DISCUSSION

It is well known in a binary alkali silicate that the increase of alkali metal ion in the principal network forming oxide SiO_4 tetrahedra changes the framework, i.e. the structure re-shapes with the number of net extra positive charge is created in the system [40-45]. In addition to Si^{4+} both P^{5+} and Al^{3+} are known to be network formers [1] and the incorporation of either of them in the binary system must introduce a charge imbalance within the structure. The amount of Al_2O_3 remains almost constant (1-3 mol%) and so the ability of Al^{3+} to cause a major structural change may be assumed to be the same throughout the compositional range. The ratio $Na_2O:SiO_2$ = 0.5 for all the glasses but $(Na_2O:SiO_2)$: P_2O_5 is the variable in the system. The P^{5+} is the most electronegative (en) among the network formers (P_{en} = 2.1, Si_{en} = 1.8 and Al_{en} = 1.5) and it should therefore create an enormous change in the structure. The object of this work is to observe this effect in the $Na_2O.2SiO_2.ZP_2O_5$ system.

It has been shown in Section (6.2) that the addition of small amounts (1-8 mol%) of P_2O_5 to the sodium disilicate

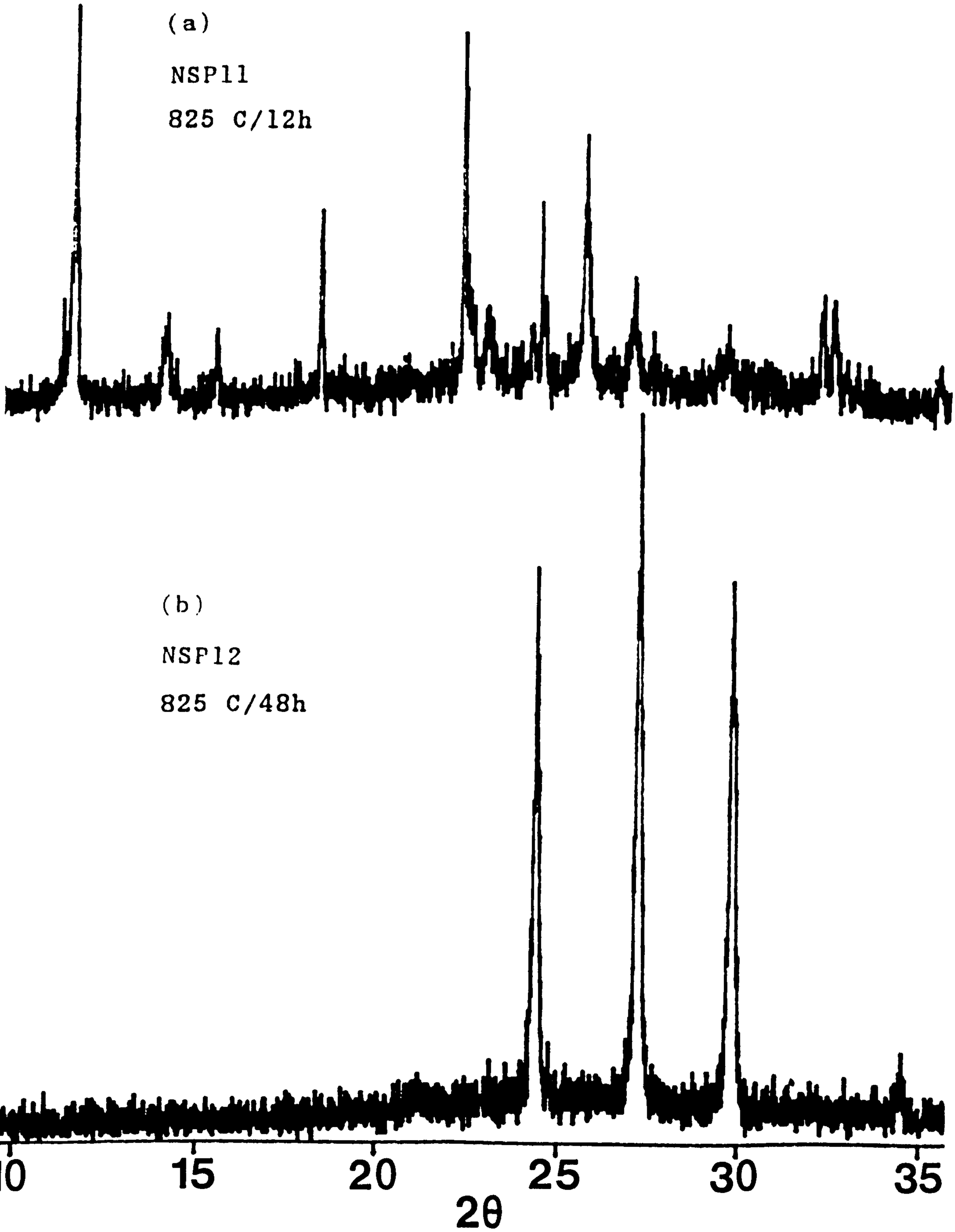

Figure 6.20 X-ray diffraction patterns of heat treated sodium disilicate glasses with (a) 46.78 mol% and (b) 57.26 mol% P_2O_5.

glasses results in the scavenging of modifier cations by phosphorus to give orthophosphate Na_3PO_4 and pyrophosphate $Na_4P_2O_7$, accompanied by polymerisation of the silicate network, i.e. elimination of non-bridging oxygen and conversion of Q_3 $Si(OSi)_3O^-Na^+$ to Q_4 $Si(OSi)_4$ silicons. The formation of Na_3PO_4 and $Na_4P_2O_7$ is not linear with P_2O_5 content (Figure 6.6). It appears that about 75% of the phosphorus forms Na_3PO_4 for 8 mol% P_2O_5. The sample NSP5 contains about 70% Q_4 species and the rest is Q_3 units. Following this trend it is expected that in the vicinity of 10 mol% P_2O_5 all the silicons may appear as Q_4 and all the phosphorus as Na_3PO_4. The monomer Na_3PO_4 may therefore occupy the holes in the three dimensional network of SiO_4 tetrahedra as an isolated unit. The phosphorus thus appears to play no part in the glass network up to 10 mol% P_2O_5. A further addition of P_2O_5 to such a system would cause a charge imbalance and could disrupt the network which might be the case for NSP6 (~ 11 mol% P_2O_5).

The ^{29}Si chemical shift in NSP6 is -99.0 PPM which is intermediate between Q_3 $Si(OSi)_3O^-Na^+$ and Q_4 $Si(OSi)_4$ silicons. The chemical shift for the former in the disilicate compositional range is -89.5 PPM and that for the pure Q_4 is -109.0 PPM [41]. The association of P^{5+} with either Q_3 or Q_4 shifts the resonance position towards more negative values because of the increased electronegativity [54,79]. Therefore the shift at -99.0 PPM could be due to formation of Si-O-P bonds between phosphate and Q_3 species. In order to clarify this the help from ^{31}P spectra is essential.

The arrangements of PO_4^{3-} and PO_3^- are complementary and a switch from one system to another is possible [49].

Therefore addition of an extra 3 mol% P_2O_5 to the NSP5 glass, where most of the P^{5+} local order is like $[PO_4^{3-}\ 3Na^+]$ could result in an environment like $[PO_3^-Na^+]_n$ in NSP6 glass, where n represents the number of units in the chain. There are three Na^+ metal ions per phosphorus in the monomer PO_4^{3-} but there is only one in the chain PO_3^-. Therefore these excess Na^+ ions must interact with the Si-O-Si bond in $Si(OSi)_4$. As the metal oxide plays an important role in the sodium silicate glass structure [41], the excess Na_2O in combination with SiO_4 tetrahedra could form Q_3 $[Si(OSi)_3O^-Na^+]$ bonded to $[PO_3^-Na^+]$. The chemical reaction which might be responsible can be represented by two steps as :

$$2Na_3PO_4 + P_2O_5 + SiO_2 \longrightarrow 4NaPO_3 + Na_2O + SiO_2 \quad ... \quad (6.10)$$

$$2Na_3PO_4 + P_2O_5 + 2SiO_2 \longrightarrow 4NaPO_3.(Na_2O.2SiO_2) \quad ... \quad (6.11)$$

The possible formation of Si-O-P bonds between $NaPO_3$ and Q_3 according to (6.11) can be shown as :

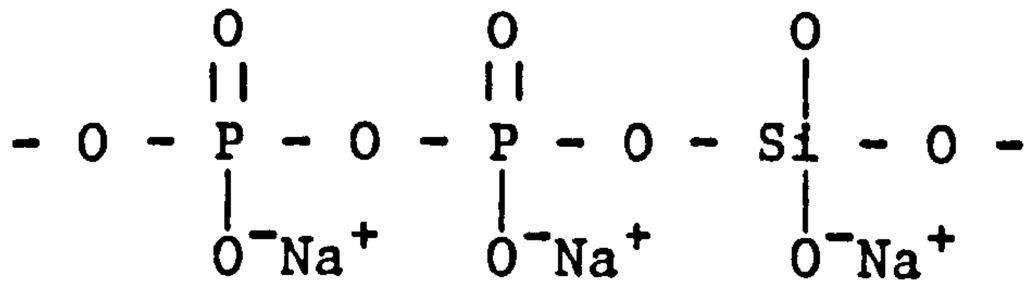

The ^{31}P chemical shift mainly depends upon the value of n [49,50] and on the next nearest neighbour. If the reaction (6.11) occurs then the value of n is less than for 16 mol% P_2O_5 containing sample and the association of the phosphorus with the silicon via oxygen could result in low shielding at the site of ^{31}P nucleus. Thus the ^{31}P resonance (-12.0 PPM) in NSP6 is lower than the reported chemical shifts (-15 to -27 PPM) for metaphosphate. This also explains the cause of higher ^{29}Si chemical shift (-99 PPM) in NSP6 sample, i.e.

higher shielding due to phosphorus as the next nearest neighbour of silicon shifts the peak position to a more negative value.

The increase of P_2O_5 polymerises the metaphosphate unit PO_3^- in the glass structure [49]. This leads to extraction of O^-Na^+ from the Q_3 portion of the glass and thus some Q_4 may appear. The resultant glass structure is therefore a combination of $PO_3^-Na^+$, $Si(OSi)_3O^-Na^+$ and $Si(OSi)_4$ units. The chain P-O-P affects both the ^{31}P and ^{29}Si resonances, i.e. the peak positions for them would be more negative. This is a possibility for NSP7 and NSP8 because ^{31}P resonates at -12.4 and -13.8 PPM and ^{29}Si resonates at -102.7 and -106.8 PPM respectively. The ^{29}Si chemical shift in NSP8 is very close to the $Si(OSi)_4$ unit and is indicative of the presence of more Q_4 species than in NSP7. Both the ^{29}Si and ^{31}P chemical shifts are also an indicative of the polymerisation of $[NaPO_3]_n$ and $Si(OSi)_4$ species which increase with the increase of P_2O_5. The chemical shifts -102.7 and -106.8 PPM do not suggest the formation of $Na^+PO_3^-$-$Si(OSi)_4$ bond at these concentrations (11-20 mol%) of P_2O_5 because that would give a chemical shift of at least <-112.0 PPM. Thus a possible model for the glass structure at this range of P_2O_5 can be shown as :

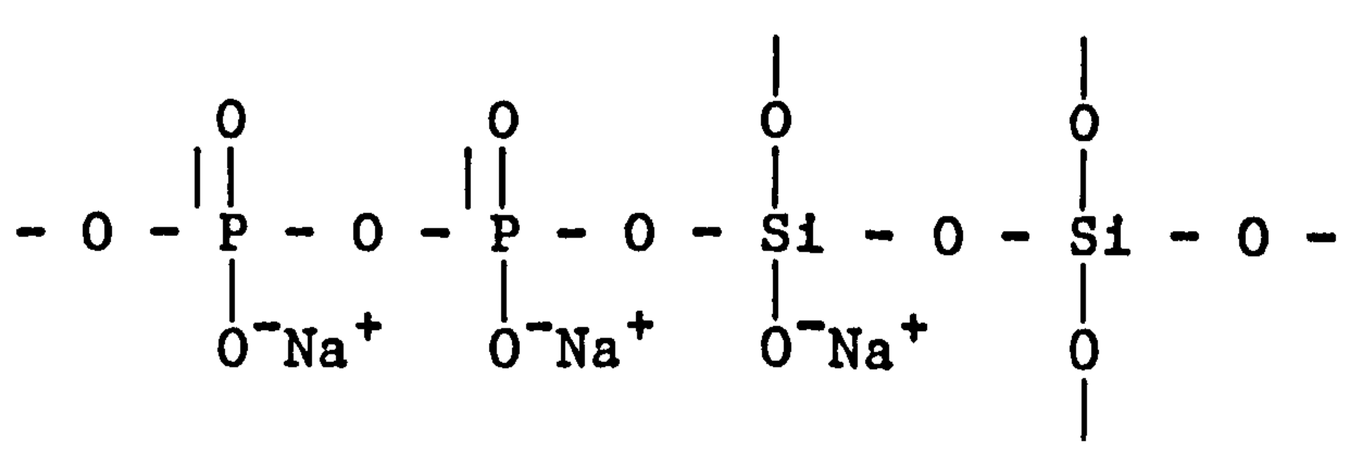

In the ^{29}Si spectra for NSP7 and NSP8 no separate peaks corresponding to $Si(OSi)_3O^-Na^+$ and $Si(OSi)_4$ are observed. The

$Na^+PO_3^-$-$Si(OSi)_3O^-Na^+$ bond shifts the ^{29}Si resonance towards the more negative value and $Na^+O(OSi)_3Si$ - $Si(OSi)_4$ provides a less negative shift for the ^{29}Si in $Si(OSi)_4$ environment. Therefore the shifts become very close to each other and hence only one peak corresponding to two different local orders of the ^{29}Si is observed. The amounts or the peak position for them can only be obtained by fitting uncertain number of gaussians to the spectra. However interesting information about the formation of Q_3 bonded to phosphorus can be obtained from the linewidth (FWHM) of the spectra (Table 6.5). The FWHM for the ^{29}Si in NSP6 and NSP7 is 18 PPM but that in NSP8 is 21 PPM which are greater than the normal linewidths for Q_3 and Q_4 (~ 11 PPM for Q_3 and 12-14 PPM for Q_4) [41,45]. Formation of the Si-O-P bond increases the ^{29}Si linewidth [15] and this is the cause of wider linewidths in NSP6 and NSP7, i.e. 18 PPM instead of 11 PPM. The increased linewidth (21 PPM) in NSP8 must reflect the fact that there is another species present. In other words Q_3 and Q_4 tend to resonate according to their own local environment and hence yield a wider lineshape. The same linewidth but a more negative shift, i.e. more shield ^{29}Si environment, in NSP7 in comparison to NSP6 indicates that there may be little Q_4 present in the former material. But in NSP8 there is a lot more Q_4 resonance. Further evidence can be put forward for the diminishing of Q_3 and the increasing of Q_4 by the Na:P ratio. The analysed compositional ratios (Na/P) in NSP6 - NSP8 are 2.45, 1.60 and 1.24 ($\pm$0.04) respectively but that in metaphosphate is 1.0. This indicates that a lot more Na^+ metal ion in the relatively low phosphate containing samples than the high phosphate containing ones is available to form

Q_3 species which decreases with increasing P_2O_5 content, i.e. more and more Q_4 units form at the expense of Q_3-P as the amounts of P_2O_5 are increased in the system.

The chemical shift anisotropy, $|\Delta\sigma|$, associated with the phosphorus in $(NaPO_3)_n$ is about 220 PPM [50,51] but the observed $|\Delta\sigma|$ for phosphorus in NSP6-NSP8 is 168 PPM. The formation of Si-O-P could change the average shielding around the phosphorus in $(NaPO_3)_n$ and this may be the cause of the lower $|\Delta\sigma|$ value. The absence of spinning sidebands in the ^{29}Si spectra represent the small anisotropy around the ^{29}Si nucleus in Q_3 $[Si(OSi)_3O^-Na^+]$ bonded to $(NaPO_3)_n$. This situation is rather complicated because the powder pattern for pure Q_3 is near axially symmetric with $\sigma_{xx} = -48\pm5$, $\sigma_{yy} = -55\pm3$, $\sigma_{zz} = -162\pm5$ PPM [80] and the spinning spectrum for rotational frequency 3 kHz (< static linewidth) provides spinning sidebands.

Addition of more P_2O_5 to the system continues the scavenging of Na^+ ions from the $-\overset{|}{\underset{|}{Si}}-O^-Na^+$ matrix and grows more SiO_4 tetrahedra in the system. Ultimately all the phosphorus and silicons become characteristic of metaphosphate and Q_4 species respectively. This is a possibility for NSP9 (~25 mol% P_2O_5) where the ^{29}Si resonates at -109 PPM, characteristic of pure Q_4 species, and the ^{31}P resonates at -16.0 PPM which is characteristic of metaphosphate $(NaPO_3)_n$. Thus the chemical reaction which appears to be taking place within the NSP9 glass structure can be written as

$$NaPO_3 + Na_2O.2SiO_2 + P_2O_5 + 3SiO_2 \rightarrow 3NaPO_3 + SiO_2 \quad \ldots \quad (6.12)$$

The metaphosphate species may appear either as a ring or a chain but definite prediction is not possible at this stage. However chemical shifts of the two species suggest that there is no Si-O-P bond at this level of P_2O_5 (- 25 mol%). Thus isolated arrangements of the phosphate group and SiO_4 tetrahedra suggest the enhancement of phase separation and indeed sporadic nucleation, observable to the naked eye, was observed during quenching from the melt. The FWHM for the ^{29}Si is in this case reduced from 21 PPM (for 19.7 mol% P_2O5) to 14 PPM which is also a characteristic of a pure Q_4 resonance. The compositional ratio Na/P in NSP9 is 0.91 $\pm$ 0.03 and is very close to metaphosphates (Na/P) = 1.0. This ensures the scavenging of all the sodium in NSP9 from the silicate matrix of the glass and hence the ^{29}Si isotropic line shape is found corresponding to $Si(OSi)_4$ environment without being accompanied by spinning sidebands.

The Na : Si ratio is constant throughout the compositional range but their ratio to phosphorus decreases with increasing P_2O_5 content. Therefore the number of metaphosphate units decreases with the increase of P_2O_5, i.e. excess P^{5+} becomes available (for > 25 mol% P_2O_5) to share its additional charge. In order to balance this charge the PO_4 tetrahedra have to extract non-bridging oxygens(nbo) from somewhere in the system. There may not be any nbo left in the silicate portion and those can only be found at the phosphorus site. The mean <P-O> distance in metaphosphate is 1.53 Å [81] but that for <Si-O> in SiO_4 tetrahedra is 1.62 Å [64]. The Pauling bond strength [82] for a P-O bond is 1.25 and that for Si-O in tetrahedral arrangement is 1.0. The difference in ionic radius between P and Si (0.02 Å) is less than the [<Si-

O> - <P-O>] distance. This evidence make the P-O bond much stronger than the Si-O bond. Therefore excess P^{5+} could dissociate Si-O-Si bonds to neutralize the extra positive charge. If this is the case then P^{5+} could occupy the silicons position and once again form Si-O-P bonds between SiO_4 and PO_4 tetrahedra, that is the ^{29}Si chemical shift must be <-112 PPM due to increased shielding created by phosphorus at the site of Si in $Si(OSi)_4$. The dramatic change of chemical shift from -109 (NSP9) to -116.6 PPM (NSP10) therefore infers the formation of this new $(OSi)_4SiPO_4$ bond. However the unusual peak at -212.6 PPM along with -116.6 PPM (Figure 6.12.b) suggests further modification within the structure.

The tetrahedron PO_4 is more close packed than SiO_4. Therefore the degree of condensation of the SiO_4 network decreases due to incorporation of P^{5+} into the SiO_4 matrix. In other words the freedom of a tetrahedron increases relative to its neighbours. This freedom to expand the Si-O bond length in addition to the extra positive charge of P^{5+} introduces some instability which helps to form $[SiO_6]$ octahedra where the <Si-O> distance is 1.72 A [64]. Thus the resonance at -212.6 PPM characteristic of the Si-O-P bond in "SiP_2O_7" occurs. The metaphosphate environment remains intact at this level of P_2O_5 (38 mol%).

Further addition of P_2O_5 polymerises the $(OSi)_4Si-PO_4$ environment and also increases the number of SiP_2O_7 species. As the polymerisation increases the shielding, the ^{29}Si chemical shifts corresponding to the former environment are -118.4, -119.9 PPM in NSP11 and NSP12 respectively. The shifts for SiP_2O_7 like environment are -213.1, -212.8

PPM respectively, i.e. the same within the experimental error.

The <P-O> bond distance in PO_4 tetrahedra is 1.60 Å [35,36] but that in SiP_2O_7 is 1.52 Å [61]. Therefore the phosphorus in the SiP_2O_7 like environment has greater ability to attract oxygen than the other phosphorus environments. Thus the unit like SiP_2O_7 grows at a faster rate with the increase of P_2O_5 content and forms at the expense of the $(OSi)_4Si-PO_4$ environment.

The diminishing tendency of the metaphosphate resonance is evident from the ^{31}P resonance (Figure 6.13.b). In the ^{31}P spectrum for NSP10, the peak at -22.9 PPM corresponding to metaphosphate is clear but that in NSP11 is faint. Identification of metaphosphate in NSP12 and NSP13 is not possible from the peak position unless a gaussian is fitted to the spectra. The amounts of $NaPO_3$ are so low in these two materials that the respective peak is possibly merged within the broad peak at -40 PPM.

There can be six crystallographically distinct sites of silicon in SiP_2O_7 [61]. If these glasses (NSP10-NSP12) contain structural units similar to those in SiP_2O_7, thus the ^{29}Si resonance of $[SiO_6]$ might be expected to be multiple or broadened. This is not so - the resonance in fact being relatively narrow (9 PPM) compared with vitreous silica (12-14 PPM) or the Q_4 units in these glasses (16 PPM). This indicates that the range of distribution of $[SiO_6]$ octahedra in these glasses is smaller than in the crystalline material (linewidth is 12.4 PPM).

The anisotropy associated with phosphorus in SiP_2O_7 is 80 PPM but that in $NaPO_3$ is 220 PPM [50,63]. The calculation

of anisotropy from the spectra (Figure 6.13) for the individual species is complicated because of poorly resolved peaks. Despite this complication an estimate of 215 $\pm$ 10 PPM can be made either by using the method of Herzfeld and Berger [48] or from the static spectra. This also indicates the presence of the ^{31}P local order like $NaPO_3$ in the glasses NSP11-NSP13. The reported chemical shift range for ^{31}P in SiP_2O_7 in -46 to -54 PPM [63]. However, the maximum ^{31}P shift observed in these materials is -40 PPM. This suggests that the resonance due to relatively low $NaPO_3$ environment is merged within the SiP_2O_7 peak and the resultant effect is the shifting of peak position towards low field as the relative amount of $NaPO_3$ increases.

The change of environment with phosphorus content in most of the steps for all the nuclei is evident from the Figure (6.21). The chemical shift as well as the line width changes with the P_2O_5 concentration due to formation of different species. The most alteration of environments occurs when Si^{4+} switches to Si^{6+}. The discontinuity between 25 and 38 mol% P_2O_5 reflects that the shielding around Na^+ changes following the change of P^{5+} environment. The wide ^{23}Na linewidth (26-31 PPM) is mainly caused by chemical shift dispersion.

The change of environment of the Al^{3+} impurity ion is evident from the Figure (6.19) with increasing P_2O_5 content. In NSP6 glass (11 mol% P_2O_5) only one peak at +49 PPM is found. The position of this peak moves towards high field with the successive addition of P_2O_5, e.g. +45 PPM in NSP7 (16 mol% P_2O_5), +44 PPM in NSP8 (19.7 mol% P_2O_5) and +42 PPM in NSP9 (25 mol% P_2O_5). These peaks correspond to Al^{3+}

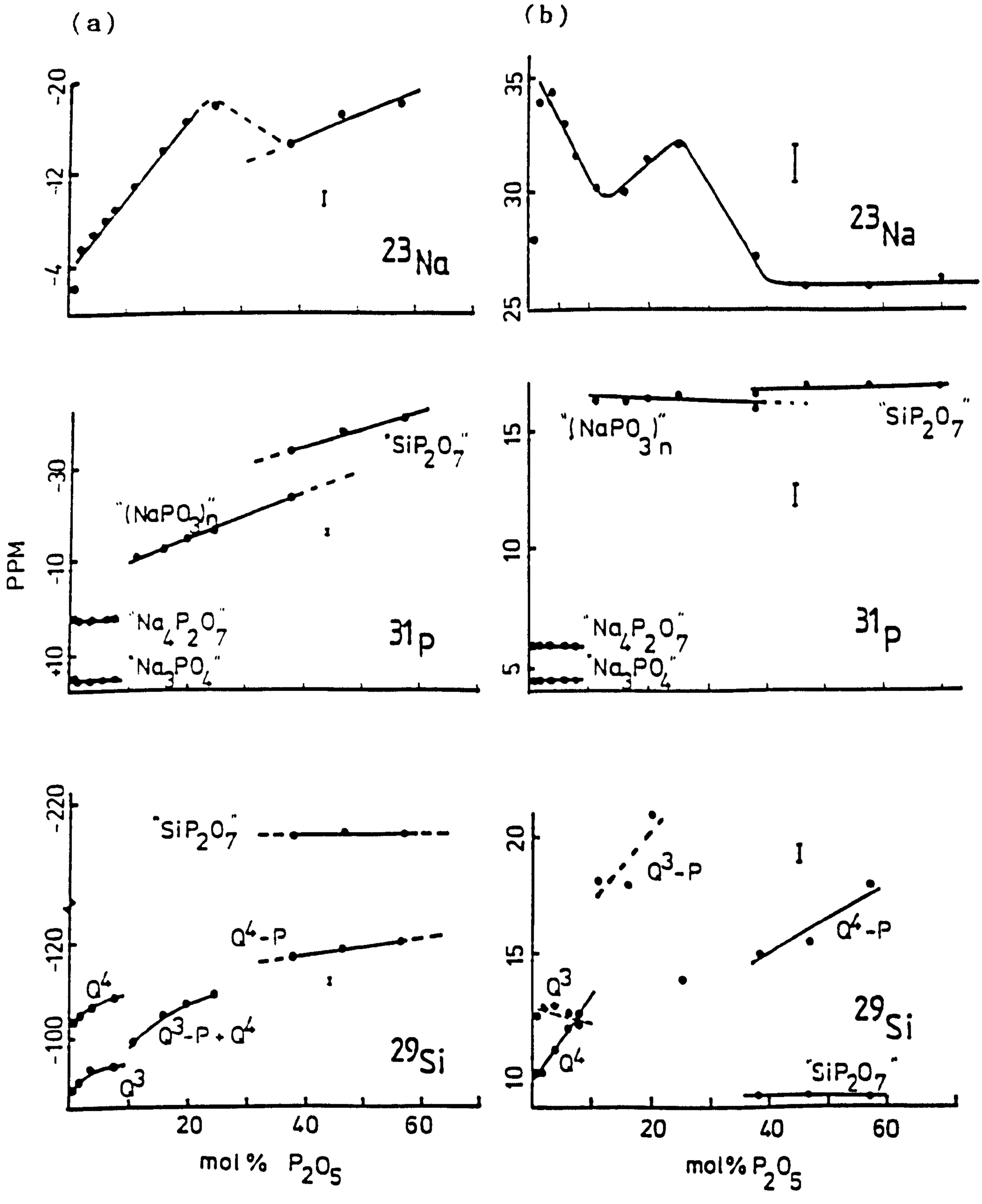

Figure 6.21 Variation of (a) chemical shift and (b) FWHM with P_2O_5 content for Na, P and Si resonances in $Na_2O.\ 2SiO_2\ .ZP_2O_5$ (Z= 1 to 57) glasses.

tetrahedrally coordinated to phosphorus in $AlPO_4$ [77]. These peak positions also correspond to Al^{3+} tetrahedrally coordinated to silicon [83]. Addition of P_2O_5 increases the shielding around the ^{27}Al nucleus and shifts the peak position towards the more negative side of the PPM scale [79]. In NSP8 and NSP9 another peak at -14 PPM is a characteristic of Al^{3+} octahedrally coordinated via oxygen to phosphorus [46]. Further addition of phosphorus shifts the position of the peak more negative. This latter peak is the only one observed in NSP10,11,12 and 13. This implies that Al^{3+} is substituting for Si^{4+} and shows a similar change from 4- to 6- coordination with increasing phosphorus content.

The ^{29}Si and ^{31}P spectra of partially devitrified NSP9 (Figure 6.16 and 6.17.a) show a major structural change. It appears that Na^+ somehow forms Q_3 species and phosphorus enters into the Si^{4+} network resulting in the broad resonance -92 to -104 PPM. The change of phosphorus environment from $NaPO_3$ to $Na_5P_3O_{10}$ indicates the creation of excess phosphorus per sodium which might be responsible for the Si-O-P bond in the devitrified state. This may also depolymerise the $NaPO_3$ chain which could give a lower ^{31}P chemical shift value (-12.6 PPM) as observed in the case of low P_2O_5 (11-20 mol%) containing glasses.

The effect of heat treatment in $[SiO_6]$ unit containing glasses are completely different. As it has already been mentioned that phosphorus in SiP_2O_7 has greater affinity to attract oxygen, all the $[SiO_4]$ tetrahedra show a tendency to become $[SiO_6]$ units and eventually all the Si^{4+} become Si^{6+}. This has been confirmed by a single ^{29}Si resonance at -213 PPM (Figure 6.16. 3). The SiO_6 unit is more ordered than the SiO_4

unit and the glasses containing higher amounts of SiO_6 units show a greater tendency to be crystallised. The sample NSP10 contains only about 13% SiO_6 units and the rate of crystallisation is very low. For the heat treatment at 775°C for 720 hours, the SiO_6 : SiO_4 ratio changes to 0.20 $\pm$ 0.05 from 0.15 $\pm$ 0.05 (for base glass). This indicates that the sample NSP10 might crystallise for a long heat treatment (more than a month) at an appropriate temperature. Alternatively this ratio for NSP12 is infinity for the heat treatment 825°C/48 hours. Comparison of the glass and crystalline FWHM (9.0 and 12.4 PPM respectively) clearly reveal the ordered state of SiP_2O_7 in glass. Although the metaphosphate peak is not clear in the glass spectra for NSP11 and NSP12, the peak is evident in the spectra for crystalline materials (Figure 6.17.c and .d).

Except in NSP9 where a major change is observed via ^{29}Si and ^{31}P NMR, the ^{23}Na environment does not change abruptly with heat treatment. The ^{23}Na NMR reflects a small change of peak position and a slight deviation of the line shape from its base glass.

The small change (0 - 4 PPM) of peak position for the ^{27}Al due to heat treatment indicates the change of bond angle and bond length for the Al^{3+} coordination. In NSP9 (725°C/12h) the peak at -21 PPM may be due to substitution of Al^{3+} in place of Si^{4+} as has already been explained for glass. The assignment of the peak at +38.7 PPM (Figure 6.19.a) to $AlPO_4$ is reasonable because ^{31}P also resonates corresponding to $AlPO_4$ environment (Figure 6.17.a). The area of the peak is also consistent with the concentration of Al^{3+} (3 mol%) in the material. Thus multinuclear NMR is essential to study

such a system.

The line width of the tetrahedral Al^{3+} site becomes narrower than the octahedral site reflecting a relatively more ordered state due to the same heat treatment in NSP9 (Figure 6.19.a). The two octahedral Al^{3+} sites in the heat treated NSP11 (Figure 6.19.c) may arise from the Si-O-Al (-9.4 PPM) and P-O-Al (-16.0 PPM) bonds. Only the change of bond angle and bond length is observed in other glasses (NSP12,13).

Formation of different phases (Figure 6.20) in different amounts of P_2O_5 containing samples indicate the different reaction mechanism during heat treatment. The minor crystalline phases, e.g. $Na_5P_3O_{10}$ and $AlPO_4$ in devitrified NSP9 are not observed by XRD. Formation of cubic SiP_2O_7 in NSP12 due to heat treatment is consistent with Chakraborty et al. [19] but the other phase $3SiO_2.2P_2O_5$ along with SiP_2O_7 in NSP11 clearly indicate that the heat of reaction depends upon the concentration of P_2O_5.

6.4 ANALYSIS OF STRUCTURAL PROPERTIES

6.4.1 DIFFERENTIAL THERMAL ANALYSIS

The glass transition temperature, T_g, crystallisation temperature, T_x, and the liquidus temperature, T_{ls}, (or the softening points where T_{ls} is not obtained), for the sodium phosphosilicate glasses are recorded in Table (6.8). The T_g and T_x appear to increase for the 8 to 25 mol% P_2O_5 containing glasses. The sharp fall in T_g for high P_2O_5 containing glasses indicates a major change of glass structure. No crystallisation temperature is observed for NSP10, i.e. the rate of crystallisation is very low at this level of P_2O_5 (38

mol%) in the sodium disilicate system. However for the other samples (NSP11,12) the relative area under the exothermic peak increases with the increase of P_2O_5 (diagram is not shown) which is an indication that the rate of crystallisation increases with P_2O_5 content.

TABLE NO. 6.8 THE GLASS TRANSITION, CRYSTALLISATION AND LIQUIDUS TEMPERATURE OF SODIUM PHOSPHOSILICATE GLASSES.

Sample	Amounts of P_2O_5 mol% ±2%	T_g (°C) ±3	T_x (°C) ±2	T_{ls} (°C) ±2
NSP1	0.91	454	683	867
NSP2	1.85	454	721±5	842±5
NSP3	3.98	444	718±9	925±9*
NSP4	6.12	-	-	905±20*
NSP5	7.92	-	765	938
NSP6	11.04	654±6	887±62	1420±7
NSP7	16.07	661±7	978±32	1420±11
NSP8	19.69	450±11	839±15	1041±9*
NSP9	25.02	456	519,810	1411±10
NSP10	38.12	373	-	958*
NSP11	46.79	445±7	753±18	854-1014±5
NSP12	57.26	248±6	815,953	915-1021±5

* softening point

6.4.2 INFRARED SPECTROPHOTOMETRY

Although the infrared spectroscopic study of the sodium phosphosilicate glasses has already been done with limited success [19], a careful observation in combination with nuclear magnetic resonance can reveal some information about Si-O-P, P=O, Si-O-Si bonds etc. However the presence of absorption bands at the same place or in the neighbourhood of each other often creates a problem. In this section the infrared absorption bands obtained from the sodium phosphosilicate system are assigned to different stretching vibrations on the basis of previous workers [19,84-85].

The infrared spectra of $Na_2O.2SiO_2.ZP_2O_5$ (Z=0-57) are shown in Figure (6.22). The infrared bands for the SiP_2O_7 glass have been found at 1331, 1100, 1040, 794, 487 and 453 cm^{-1} and those for vitreous SiO_2 are 1180, 1060, 810 and 440 cm^{-1} [19]. In SiO_2 the first two bands (1180, 1060 cm^{-1}) have been assigned to Si-O stretching vibrations of which 1060 cm^{-1} is relatively strong and the last two (810, 440 cm^{-1}) have been attributed to O-Si-O and Si-O-Si bending motions respectively [84]. The infrared bands for vitreous P_2O_5 have been found at 1285, 1150, 950, 780, 650 and 475 cm^{-1} [85]. Using these wave numbers the bands in SiP_2O_7 glass have been assigned as follows [19] :

(i) 1331 cm^{-1} to P=O bond,

(ii) 1100 cm^{-1} to P-O of P-O-P and Si-O-P bonds,

(iii) 1040 cm^{-1} to Si-O of Si-O-P and Si-O-Si bonds,

(iv) 487 cm^{-1} to O-P-O bending vibration and

(v) 453 cm^{-1} to Si-O-P and Si-O-Si bending vibration.

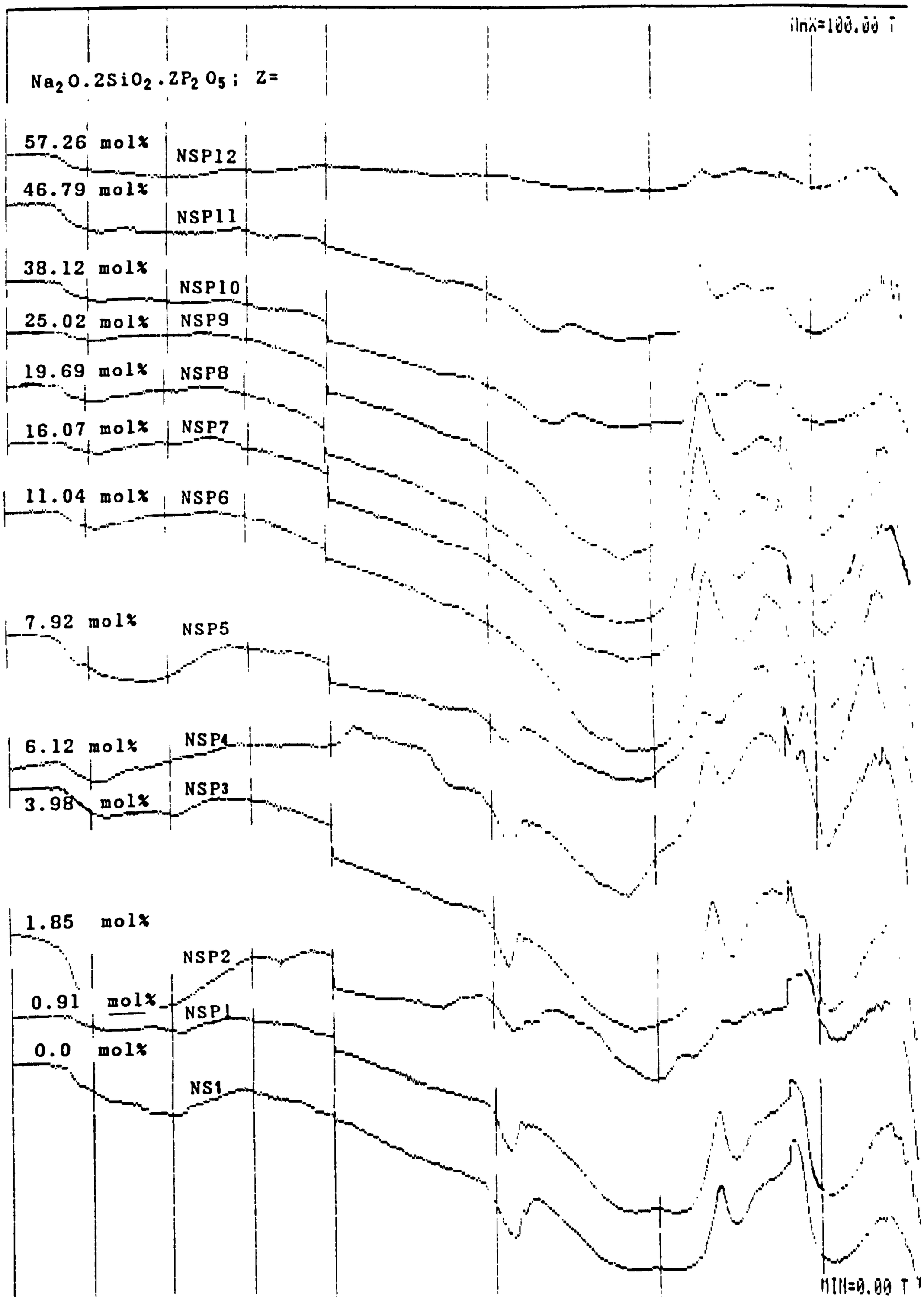

Figure 6.22 Infrared spectra of $Na_2O.2SiO_2.ZP_2O_5$ (Z= 0 to 57) glasses.

The principal regions of absorption for orthophosphate and pyrophosphate are almost the same [86]. The bands generally appear within the region 1400-850 cm^{-1} for orthophosphate and 1350-690 cm^{-1} for pyrophosphate. The strong bands for orthophosphate occur between 1060-1000 cm^{-1}. The metaphosphate bands occur in the 1315-1205 cm^{-1}, 870-850 cm^{-1} and 770 cm^{-1} regions [86]. Therefore in a glass containing multiphosphate groups overlapped, unresolved and broad bands may often occur.

In NSP1-NSP5 a strong band is observed around 1446 cm^{-1} which may be assigned to non-bridging oxygen in the system. This band is not observed in the high phosphate containing glasses (NSP6-NSP12). In the spectra (Figure 6.22) of NSP1-NSP12, there is a broad absorption region in the vicinity of 1350 cm^{-1} which could be due to a P=O stretching vibration of the phosphate group. However a strong absorption band around 1075 cm^{-1} may be due to Si-O stretching vibration in SiO_4 tetrahedral environment. This band disappears in the high P_2O_5 containing glasses (NSP10-NSP12). The plateau like absorption in NSP10-NSP12 around 900 cm^{-1} is due to O-Si-O bending vibrations of SiO_6 octahedra [87]. The other absorption bands between 650 and 900 cm^{-1} can also arise from $[SiO_6]$ units O-Si-O and Si-O-Si bending vibrations. The weak absorption in the region 900-950 in the glasses represents p-O-P link.

6.4.3 STRUCTURAL RELAXATION AND FICTIVE TEMPERATURE

It has already been explained that cooling through the transition region of a glass at a different rate changes the fictive temperature (T_f). Several kinetic parameters to

explain the glass properties have been measured using the correlation between the cooling rate and the fictive temperature [32,33]. However the structural relaxation caused by the cooling rate and hence the correlation with T_f has not yet been presented. In this section the sample NSP12 is chosen to show the relationship between T_f and the change of species.

The ^{29}Si spectra for NSP12 showing the change of area, which is a measure of the amounts of the species due to different cooling rates are shown in Figure (6.23). The different techniques of cooling, resulting fictive temperatures and the relative amounts of six- and four-coordinated silicons are recorded in Table (6.9). A plot of $\ln([SiO_4]/[SiO_6])$ versus $10^3/T_f$ show a linear relationship (Figure 6.24).

6.4.4 DISCUSSION

The T_g and T_{1s} for the samples containing 11-18 mol% P_2O_5 are fairly high. As has been explained from the NMR data that at these levels of P_2O_5 $Na_+PO_3^-$ - $Si(OSi)_3O^-Na^+$ forms, and this may be the reason of high T_g and T_{1s}. The samples NSP6-NSP9 crystallise more rapidly than the high P_2O_5 containing samples (NSP10-NSP12). For all the samples $(T_g/T_{1s}) < 0.55$, which indicates that volume nucleation may occur during heat treatment [56]. However this assumption is not well recognised and a rough estimate can only be made [56].

Assignment of the infrared spectroscopic bands is consistent with NMR data. The presence of Si-O-P bond and the absorption in the region 900 cm^{-1} in the NSP10-NSP12 indicate

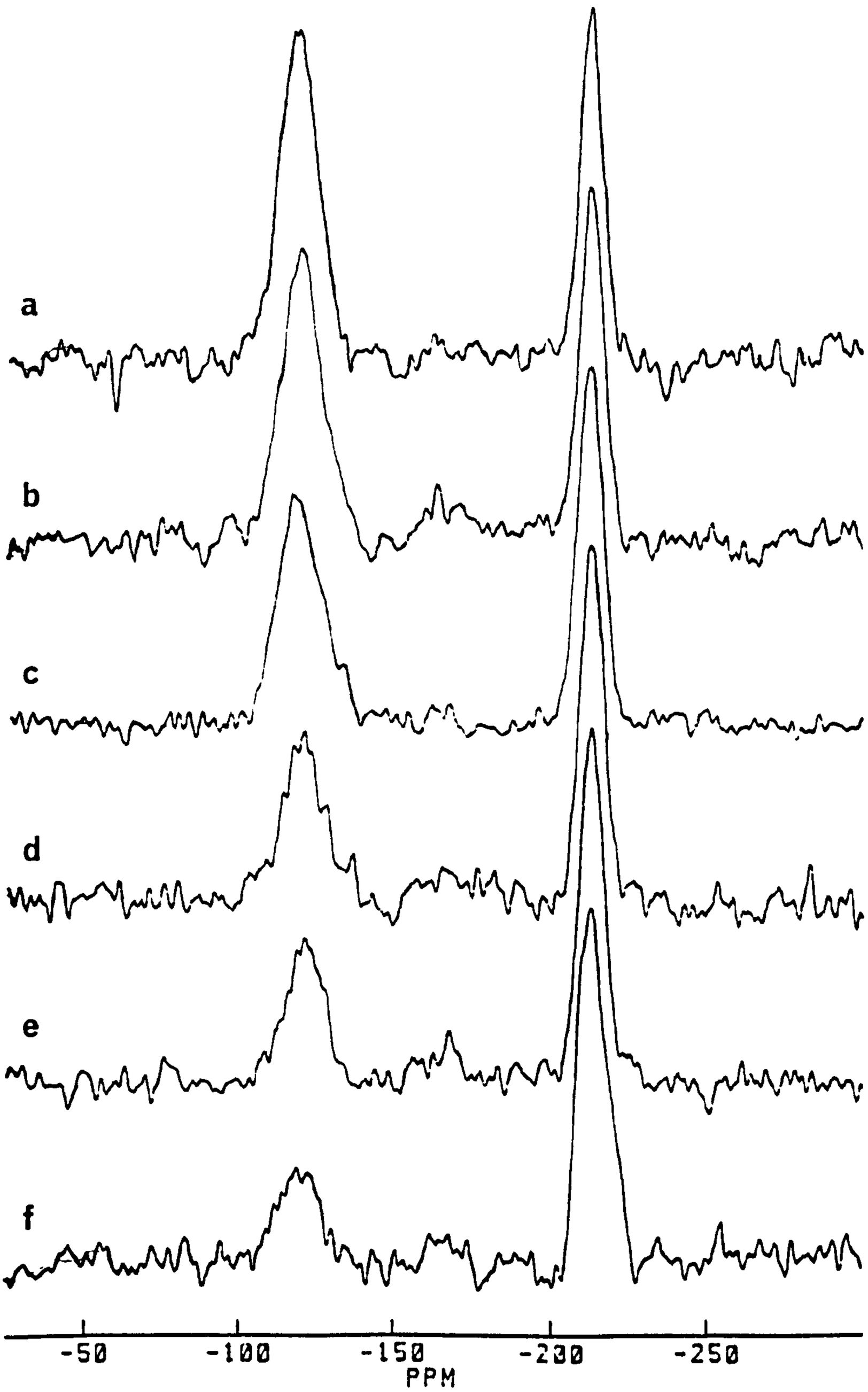

Figure 6.23 MAS NMR spectra of Si in $Na_2O.2SiO_2.60P_2O_5$ prepared with different fictive temperatures (a) poured into liquid N_2, other samples splat cooled at (b) -10 °C, (c) +30 °C, (d) +100 °C, (e) +200 °C, (f) +400 °C.

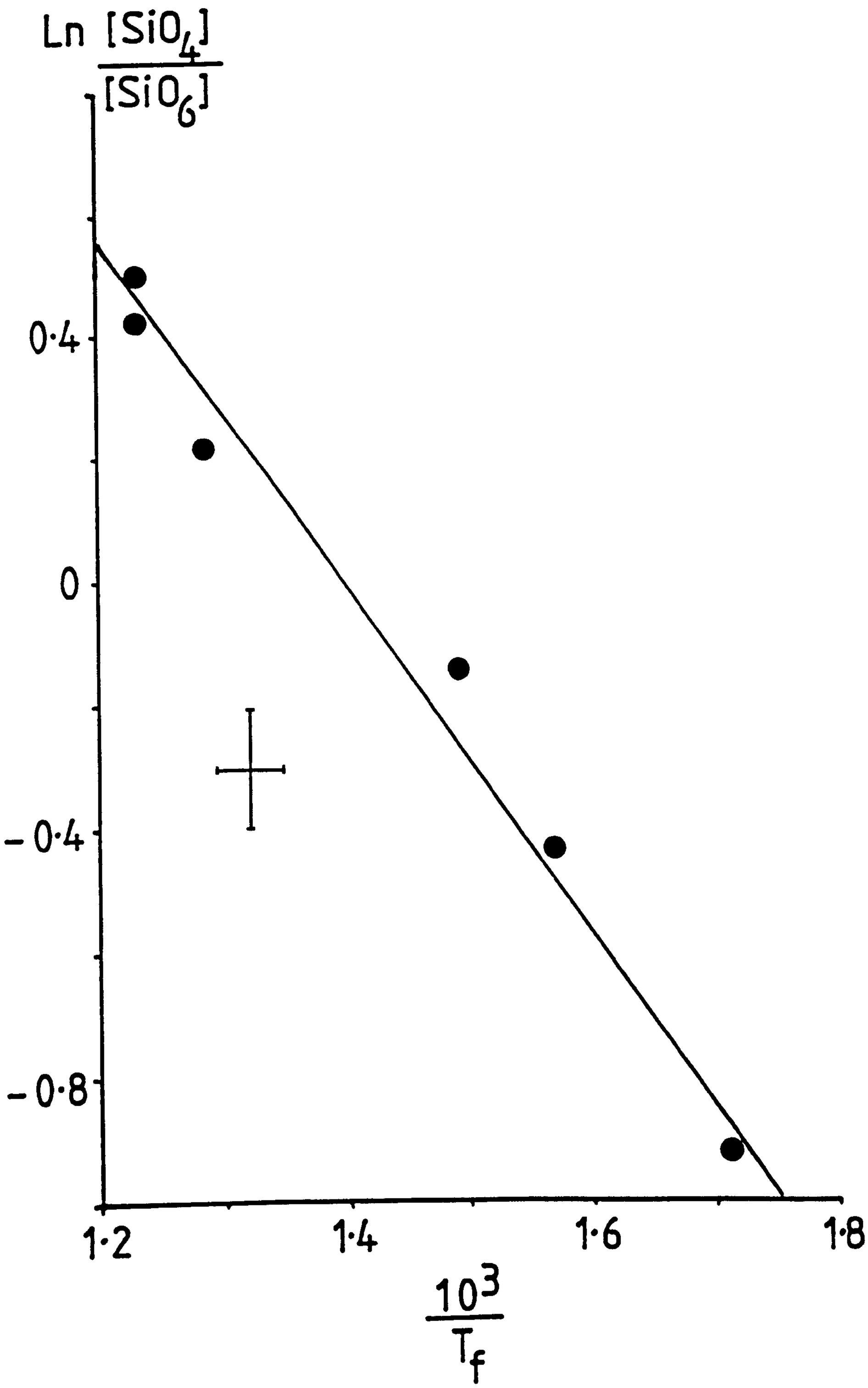

Figure 6.24 Variation of six and four coordination of silicon in $Na_2O.2SiO_2.60P_2O_5$ with fictive temperature.

TABLE NO. 6.9 DATA FOR FICTIVE TEMPERATURE AND STRUCTURAL RELAXATION DUE TO VARIOUS COOLING RATES IN SODIUM PHOSPHOSILICATES

Sample	$Na_2O.2SiO_2.60P_2O_5$		
State of the sample/ cooling procedure $^oC/h$ $\pm5^oC$	Fictive temp. T_f ^oK ±10	$\frac{SiO_4}{SiO_6}$	$\ln\frac{SiO_4}{SiO_6}$ ±0.09
splat cooled at 400^oC	585	0.397 ± 0.045	-0.93
splat cooled at 200^oC	638	0.645 ± 0.059	-0.44
splat cooled at 100^oC	670	0.87 ± 0.07	-0.14
splat cooled at room temperature	778	1.25 ± 0.11	0.22
splat cooled at -10^oC	813	1.54 ± 0.14	0.43
poured into liquid N_2	812	1.67 ± 0.16	0.51

the presence of [SiO_6]. However other phosphate groups also show absorption in this region and definite prediction from the infrared spectra is problematic. A sharp band at 650 cm^{-1} has been shown in the heat treated SiP_2O_7 glass in comparison to its base glass [19]. A band around 654 cm^{-1} is observed in all the high phosphate containing glasses (NSP10-NSP12) which has not been observed in the other glasses. This band may therefore correspond to [SiO_6] octahedra.

Structural relaxation in glasses is a complex phenomenon. However Ritland [30] derived an equation relating to fictive temperature and the cooling rate as

$$\frac{d\ln|q|}{d\,(1/T_f)} = -\Delta h/R \quad \ldots \quad \ldots \quad (6.12)$$

where q = cooling rate through the transition region,
Δh = activation enthalpy and
R = gas constant.

In the sodium phosphosilicate system the ratio (SiO_4/SiO_6) is proportional to the cooling rate, i.e.

$$q = k\,\frac{SiO_4}{SiO_6}$$

Therefore equation (6.12) can be written as :

$$\frac{d\ \ln\ [SiO_4/SiO_6]}{d\ (1/T_f)} = -\ \Delta h/R \quad \ldots \quad (6.13)$$

Thus the slope of the plot $\ln(SiO_4/SiO_6)$ versus $10^3/T_f$ (Figure 6.24) gives Δh/mole = -0.23 ± 0.03 ev. Therefore the energy required to form one mole of [SiO_6] unit from the parent [SiO_4] unit is 0.25 ev. The -ve sign indicates that the heat is absorbed during the process.

6.5 GENERAL DISCUSSION

In the lithium phosphosilicate system only PO_4^{3-} group forms but in sodium and potassium system both PO_4^{3-} and $P_2O_7^{4-}$ form. The rate of dimerisation appears to become negative in the neighbourhood of a 4 mol% P_2O_5. The mean <P-O> distance in $Na_4P_2O_7$ is 1.544 Å [88] but that in Na_3PO_4 is 1.560 Å [89]. Energetically dimerisation is more favourable than the formation of monomers and thus dimer form at a faster rate for low P_2O_5 concentrations. However the excess addition of P_2O_5 ($\geqslant$5 mol%) accelerates monomerisation at the expense of dimerisation. Both the orthophosphate and pyrophosphate occupy the holes in the glass structure. In order to accommodate these phosphate species the hole dimension must be comparable to the size of the phosphate groups. The pyrophosphate is almost twice as big as the orthophosphate. Therefore the creation of pyrophosphate may not be continued and this may accelerate the orthophosphate formation. The dimerisation is even more important in $K_2O.2SiO_2$-P_2O_5 with low (0-4 mol%) amounts of P_2O_5. This means that monomer starts to grow at the expense of dimer before the critical concentration of P_2O_5 in the sodium system. This fact can be explained by the large radius of the K^+ ion in comparison to the Na^+, i.e. $K_4P_2O_7$ is larger in volume than $Na_4P_2O_7$.

The models (equs. 6.5 - 6.7) predicted to describe the structure of low phosphate containing samples diverge for high P_2O_5 content. For Z=(1/3)X the ratio (Q_4/Q_3) in equ. 6.5 becomes infinity, i.e. all the species may become Q_4 with this amount of P_2O_5 when all the phosphorus appear as PO_4^{3-}. Similarly when only pyrophosphate forms, Z=½X may give the

silicate portion of the glass as Q_4. The situation in model (b-iii) (equ.6.7) is rather complex when both PO_4^{3-} and $P_2O_7^{4-}$ form. In this case $2 \leqslant (3m + 2n) \leqslant 3$, i.e. all the silicons may appear as $Si(OSi)_4$ for $\frac{1}{2}X \leqslant Z \leqslant (1/3)X$. Therefore the value of Z depends on the values of m and n. In a sodium silicate composition if X=0.3 and n=0, then a 10 mol% P_2O_5 containing sample should give all the silicons as Q_4 units. This is indeed consistent with, within the experimental error, the experimentally obtained Q_4/Q_3 ratios. Thus the models are only valid to explain the glass structure for $\leqslant$10 mol% P_2O_5 alkali phosphosilicate glasses provided that further nucleation of Q_2 species does not occur.

Formation of SiP_2O_7 is energetically less favourable in comparison to SiO_4 tetrahedra because of the large <Si-O> bond distance and lower bond strength in $[SiO_6]$ octahedra [64]. Therefore additional voids created by the comparatively compact PO_4^{3-} tetrahedra in Na_3PO_4, which allow the Si-O bond in SiO_4 to expand, may be responsible for the formation of $[SiO_6]$ octahedra. The similar trend in the potassium system suggests that $[SiO_6]$ octahedra may also form in the K_2O-SiO_2-P_2O_5 system when proper amount of P_2O_5 is added. Although in the $Li_2O.2SiO_2$-P_2O_5 system the trend is dissimilar, one sample with 50 mol% P_2O_5 was made and $[SiO_6]$ octahedra were also obtained with a ratio $[SiO_4]/[SiO_6]$ similar to that in the sodium system. However in SiP_2O_7 glass such octahedral coordination of Si has not been observed [24] which indicates that the alkali metal ion plays an important role to form the $[SiO_6]$ units in the glasses. The ratio (SiO_2/P_2O_5) in SiP_2O_7 glass is 1 but that in SiO_6 units containing alkali phosphosilicate glasses is $\leqslant$1. Some of the phosphorus form

metaphosphate, some form bonds with [SiO_4] tetrahedra and the rest form SiP_2O_7 like environments in alkali phosphosilicate glasses. Thus it can be concluded that the alkali metal ion plays an important role to maintain the charge neutrality by sharing its charge with phosphorus via oxygen. There may be a critical value of the alkali-metal ion : silicon : phosphorus proportion for which six- coordinated silicon can form in the glass but this is yet to be determined.

Raman study [90] of Na_2O-SiO_2-P_2O_5-Al_2O_3 system has been shown to change Al^{3+} coordination from 4 to 6 at higher Al_2O_3 concentration (~13 mol%) and P^{5+}, Al^{3+} do not incorporate into the silicate network. Whereas this study shows that the coordination may change at the low level even for ~3 mol% Al_2O_3 and also incorporates into the network if the concentration of P_2O_5 is high enough.

All the chain, dimer and monomer observed by Raman study [20] in the sodium phosphosilicate system for high P_2O_5 concentration have not been found in this study. Monomer and dimer form up to 10 mol% P_2O_5 and then only metaphosphate forms for higher concentrations of P_2O_5 (> 10 mol%). The metaphosphate is the most stable form of the phosphate groups under normal conditions because of its short <P-O> distance (1.53 Å) [81]. This may be the reason why the glasses retain the structure of metaphosphate throughout the configuration once it has formed.

REFERENCES

1. P.W. McMillan, Glass Ceramics, Academic Press, London, 1964.

2. P.W. McMillan and G. Patridge, Proc. Brit. Ceram. Soc., No.3, 241 (1965).

3. P.F. James and P.W. McMillan, Phil. Mag., 18, 863 (1968).

4. H. Harper, P.F. James and P.W. McMillan, Discuss Faraday Soc., 50, 206 (1970).

5. H. Harper and P.W. McMillan, Phys. Chem. Glasses, 13, 97 (1972).

6. P. Hing and P.W. McMillan, J. Mater. Sci., 8, 340 (1973).

7. P. Hing and P.W. McMillan, J. Mater. Sci., 8, 1041 (1973).

8. P.W. McMillan, in Advances in Nucleation and Crystallisation in glasses, A. Ceram. Soc., P.224 (1971).

9. P.W. McMillan, Proc. xth Int. Cong. on glass, 14, 1 (1974).

10. K. Matusita, S. Sakka, T. Muki and M. Tashiro, J. Mater. Sci., 10, 94 (1975).

11. H. Tomoza, in Advances in Nucleation and crystallisation in glasses, Am. Ceram. Soc., P.41 (1971).

12. P.F. James and P.W. McMillan, Phys. Chem. Glasses, 11 (3), 59 (1970).

13. P.F. James and P.W. McMillan, Phys. Chem. Glasses, 11 (3), 64 (1970).

14. P.F. James and P.W. McMillan, J. Mater. Sci., 6, 1345 (1971).

15. R. Dupree, D. Holland and M.G. Mortuza, Nature, 328, 416 (1987).

16. R. Dupree, D. Holland and M.G. Mortuza, Phys. Chem. Glasses, 29(1), 18 (1988).

17. R. Dupree, D. Holland, M.G. Mortuza, J.A. Collins and M.W.G. Lockyer, J. Non-Cryst. Solids., 106, 403 (1988).

18. News, Ceramic Bulletin, 65 (8), 114 (1986).

19. I.N. Chakraborty and R.A. Condrate, Snr., Phys. Chem. Glasses, 26 (3), 68 (1985).

20. C. Nelson and D.R. Tallant, Phys. Chem. Glasses, 25 (2), 31 (1983).

21. C. Nelson and D.R. Tallant, Phys. Chem. Glasses, 26 (4), 119 (1985).

22. F. Liebau, Structural Chemistry of silicates, Springer Verlag, 1987, P.39.

23. E. Tillmanns, W. Gebert and W.H. Baur, J. Solid State Chemistry, 7, 69 (1973).

24. T.L. Weeding, B.H.W.S. de Jong, W.S. Veeman and B.G. Aitken, Nautre, 318, 353 (1985).

25. D.A. McKeown, F.L. Galeener and G.E. Brown, Jr., J. Non-Cryst. Solids, 68, 361 (1984).

26. M. Taylor and G.E. Brown, Geochim. Cosmochim Acta., 43, 1467 (1979).

27. G.E. Brown, Jr., F.D. Dikmen and G.A. Waychumas, SSRL Rept. No. 1983/01, proposal No. 741.

28. D.R. Tallant and C. Nelson, Phys. Chem. Glasses, 27 (2), 75 (1986).

29. A.Q. Tool, J. Am. Ceram. Soc., 29 (9), 240 (1946).

30. H.N. Ritland, J. Am. Ceram. Soc., 39 (12), 403 (1956).

31. O.S. Narayanaswamy, J. Am. Ceramic Soc., 54 (10), 491 (1971).

32. C.T. Moynihan, A.J. Easteal, M.A. DeBolt and J. Tuckner, J. Am. Ceram. Soc., 59 (1-2), 12 (1976).

33. M.A. DeBolt, A.J. Easteal, P.B. Macedeo and C.T. Moyniham, J. Am. Ceram. Soc., 59 (1-2), 16 (1976).

34. I.B. Johns, H.E. Ulmer and J.W. Edwards, J. Chem. Phys., 35 (4), 1271 (1961).

35. D.W.J. Cruickshank, Acta. Cryst., 17, 677 (1964).

36. D.W.J. Cruickshank, Acta. Cryst., 17, 679 (1964).

37. C.H. Macgillavry, C.H.J. De Decker and L.M. Nizland, Nature, Lond., 164, 448 (1949).

38. G.C. Hampson and A.J. Stosick, J. Am. Chem. Soc., 60, 1814 (1938).

39. A.-R. Grimmer, Private Communication.

40. R. Dupree, D. Holland and D.S. Williams, J. Non-Cryst. Solids, 81, 185 (1986).

41. R. Dupree, D. Holland, P.W. McMillan and R.F. Pettifer, J. Non-Cryst. solids, 68, 399 (1984).

42. R. Dupree, D. Holland and D.S. Williams, J. de-Physique, Colloque C8, supplement Au No.12, Tome 46, C8-119 (1985)

43. A.-R. Grimmer, M. Magi, M. Hehnert, H. Stade, A. Samoson, W. Wicker and E. Lippmaa, Phys. Chem. Glasses, 25 (4), 105 (1984).

44. J.B. Murdoch, J.F. Stebbins and I.S.E. Carmichael, Am. Miner., 70, 332 (1985).

45. R. Dupree and D. Holland, in New horizons in glass and glass ceramics, Ed. M.H. Lewis, Chapman and Hall (1988).

46. I.L. Mudrakovskii, V.P. Shmachkova, N.S. Kotsarenko and V.M. Mastikhin, J. Phys. Chem. Solids, 47 (4), 335 (1986)

47. G.L. Turner, K.A. Smith, R.J. Kirkpatrick and E. Oldfield J. Mag. Reson., 70, 408 (1986).

48. J. Herzfeld and A.E. Berger, J. Chem. Phys., 73, 6021 (1980).

49. S. Prabhakar, K.J. Rao and C.N.R. Rao, Chem. Phys. Lett., 139 (1), 96 (1987).

50. L. Griffiths, A. Root, R.K. Harris, K.J. Paker, A.M. Chippendale and F.R. Tromans, J. Chem. Soc. Dalton Trans., 2247 (1986).

51. T. M. Duncan and D.C. Douglass, Chem. Phys., 87, 339 (1984).

52. J. Boehm, D. Fenzke, H. Pfeifer, J. Magn. Reson., 55 (2), 197 (1983).

53. A.-R. Grimmer and U. Haubenreisser, Chem. Phys. Lett., 99 (5,6), 487 (1983).

54. Wang-Hong Yang, R.J. Kirkpatrick and G. Turner, J. Am. Ceram. Soc., 69 (10), C222 (1986).

55. B.O. Mysen, F.J. Ryerson and D. Virgo, Am. Mineral, 66, 106 (1981).

56. P.F. James, J. Non-cryst. solids, 73, 517 (1985).

57. B.C. Bunker, D.R. Tallant, C.A. Balfe, R.J. Kirkpatrick, G.L. Turner and M.R. Reidmeyer, J. Am. Ceram. Soc. 70 (9), 675 (1987).

58. J.A. Wilder, J. Non-cryst. Solids, 38 and 39, 879 (1980).

59. W.H. Zachariasen, J. Am. Chem. Soc., 54, 384 (1932).

60. V.H. Mayer, Montash Fur. Chemie, 105, 46 (1974).

61. E. Tilmans, W. Gebert and W.H. Baur, J. Solid State Chemistry, 7, 69 (1973).

62. A.-R. Grimmer, F.V. Lampe and M. Magi, Chem. Phys. Lett., 132 (6), 549 (1986).

63. I.L. Mudrakovskii, V.M. Mastikhin, V.P. Shmachkova, and N.S. Kotsarenko, Chem. Phys. Lett., 120 (4,5), 425 (1985)

64. F. Liebau, structural chemistry of silicates, Springer Verlag, 1987.

65. W. Sinclair and A.E. Ringwood, Nature, 272, 714 (1978).

66. G. Bissert and F. Liebau, Acta. Crystallogr., B26, 233 (1970).

67. K.-F. Hesse, Acta. Crystallogr., B35, 724 (1979).

68. T.-Y. Tien and F.A. Hummel, J.Am. Ceram. Soc., 45 (9), 423 (1962).

69. E.T. Turkdogan and W.R. Maddocks, J. Iron and Steel Inst., 172, 1 (1952).

70. R. Dupree, M.H. Lewis and M.E. Smith, J. Appl. Cryst., 21, 109 (1988).

71. N.D. Butler, R. Dupree and M.H. Lewis, J. Mater. Sci., 3, 469 (1984).

72. R. Dupree, I. Farnan, A.J. Forty, S. El-Mashri and L. Bottyan, J. Phys (Paris), 46, C8-113 (1985).

73. R.J. Kirkpatrick, R. Oestrike, C.A. Weiss, Jr., K.A. Smith and E. Oldfield, Am. Miner., 71, 705 (1986).

74. R.A. Kinsey, R.J. Kirkpatrick, J. Hower, K.A. Smith and E. Oldfield, Am. Mineral, 70, 537 (1985).

75. B.L. Phillips, F.M. Allen, R.J. Kirkpatrick, Am. Mineral., 72, 1190 (1987).

76. U. Haubenreisser, G. Scheler and A.-R. Grimmer, Z. Anorg. Allg. Chem., 532, 157 (1986).

77. D. Muller, E. Jahn, G. Ladwig and U. Haubenreisser, Chem. Phys. Lett., 109 (4), 332 (1984).

78. JCPDS powder diffraction files.

79. D. Muller, G. Berger, I. Grunze and H. Ladwig, Phys. Chem. Glasses, 24 (2), 37 (1983).

80. J.F. Stebbins, Nature, 330, 465 (1987).

81. B.K.H. Jost, Acta. Cryst., 16, 640 (1963).

82. L. Pauling, The Nature of Chemical Bond, Cornell University Press, 1960.

83. D. Muller, W. Gessner, A. Samoson, E. Lippmaa and G. Scheler, J. Chem. Soc., Dalton Trans., 1277 (1986).

84. R.J. Bell, N.F. Bird and P. Dean, J. Phys. C., 1, 299 (1968).

85. J. Wong, J. Non-Cryst. Solids, 20, 83 (1976).

86. D.E.C. Corbridge and E.J. Lowe, 493 (1954).

87. Q. Williams and R. Jeanloz, Science, 239, 902 (1988).

88. K.Y. Leung and C. Calvo, Canad. J. Chem., 50 (16), 2519 (1972).

89. D.M. Wiench and M. Jancen, Z. anorg. Chem., 461, 101 (1980).

90. D.R. Tallant and C. Nelson, Phys. Chem. Glasses, 27 (2), 75 (1986).

CHAPTER 7

^{29}Si RELAXATION IN ALKALI SILICATE AND ALKALI PHOSPHOSILICATE GLASS AND GLASS CERAMICS

7.1 INTRODUCTION

Even using high resolution NMR techniques, nuclei with only subtle environmental differences may not be distinguishable [1-18]. Measurement of spin-lattice relaxation time (T_1) of fast relaxing nuclei, e.g. ^{7}Li, ^{23}Na, ^{1}H etc. as a function of temperature in broad line NMR has been used to reveal structural detail of polymers and glasses [19-23]. Recently Liu et al. [24,25] have presented the variation of ^{29}Si T_1 relaxation time with temperature (T) for $650 < T < 1450^{o}K$ and that of ^{23}Na for $25 < T < 1450\ ^{o}K$ in albite and alkali silicate glasses. However normally the glass transition temperature (T_g) and the liquidus temperature (T_{ls}) of oxide glasses are within 250-1600°C and the measurement of relaxation time under the conditions of high resolution at such a high temperature is not feasible.

The ^{29}Si in any material should provide a single resonance for crystallographically equivalent sites and double, triple, etc. for non equivalent sites depending upon their number. But the degree of non-equivalency, wide range of FWHM etc. often creates problems [13,14] in resolving details within a lineshape. It is well known that in silicates the Q_m connected to Q_{m-1} ($0 \leqslant m \leqslant 4$) or vice versa give different chemical shifts which depend upon the amounts of Q_m or Q_{m-1}, e.g. Q_3 in $25Li_2O.75SiO_2$ has a chemical shift of -92.7 PPM but that in $40Li_2O.60SiO_2$ is -87.0 PPM (see section 4.2.1). Unfortunately in glasses MAS NMR cannot resolve Q_m connected to different numbers of Q_{m-1}.

In silicates the network former 'silicon' has a long relaxation time at room temperature, typically 10-60 minutes,

which discourages T_1 measurements. However ^{29}Si T_1 in liquids is comparatively short and has been measured for a number of systems [26-28]. Attention has been given recently to the solid state and a few studies have been performed for silicates and aluminosilicates [29-33] at room temperature. However the results are controversial to some extent [34].

Although some data on the ^{29}Si spin-lattice relaxation in glass and crystalline alkali silicates has been given by Selvaray et al. [8], Schneider et al. [12] and Liu et al. [25], no systematic studies have been reported to date on these systems at room temperature. A better understanding of the ^{29}Si T_1 relaxation time in silicates might provide unknown structural detail [13,14,34], particularly in glasses. The results of the ^{29}Si relaxation measurements presented in this section are shown to be sensitive to the site asymmetry and provide sometimes a single and sometimes a two component relaxation time for Q_m species. An attempt is made here to use ^{29}Si T_1 measurements in alkali silicates and alkali phosphosilicates to obtain information about the silicate network.

7.2 RELAXATION OF ^{29}Si IN SODIUM SILICATE GLASS AND GLASS CERAMICS

7.2.1 ^{29}Si RELAXATION AS A FUNCTION OF ALKALI CONTENT

In order to observe the effect of modifier content on the ^{29}Si relaxation the samples NS7-NS9 (28.6 - 20.0 mol%) were made with varying concentration of Na_2O. Semilogarithmic plots of intensity (recovered magnetisation) versus relaxation delay for the samples (NS7 - NS9) are shown in Figure 7.1 together with NS3 (32.6 mol% Na_2O; ^{29}Si relaxation data of NS3

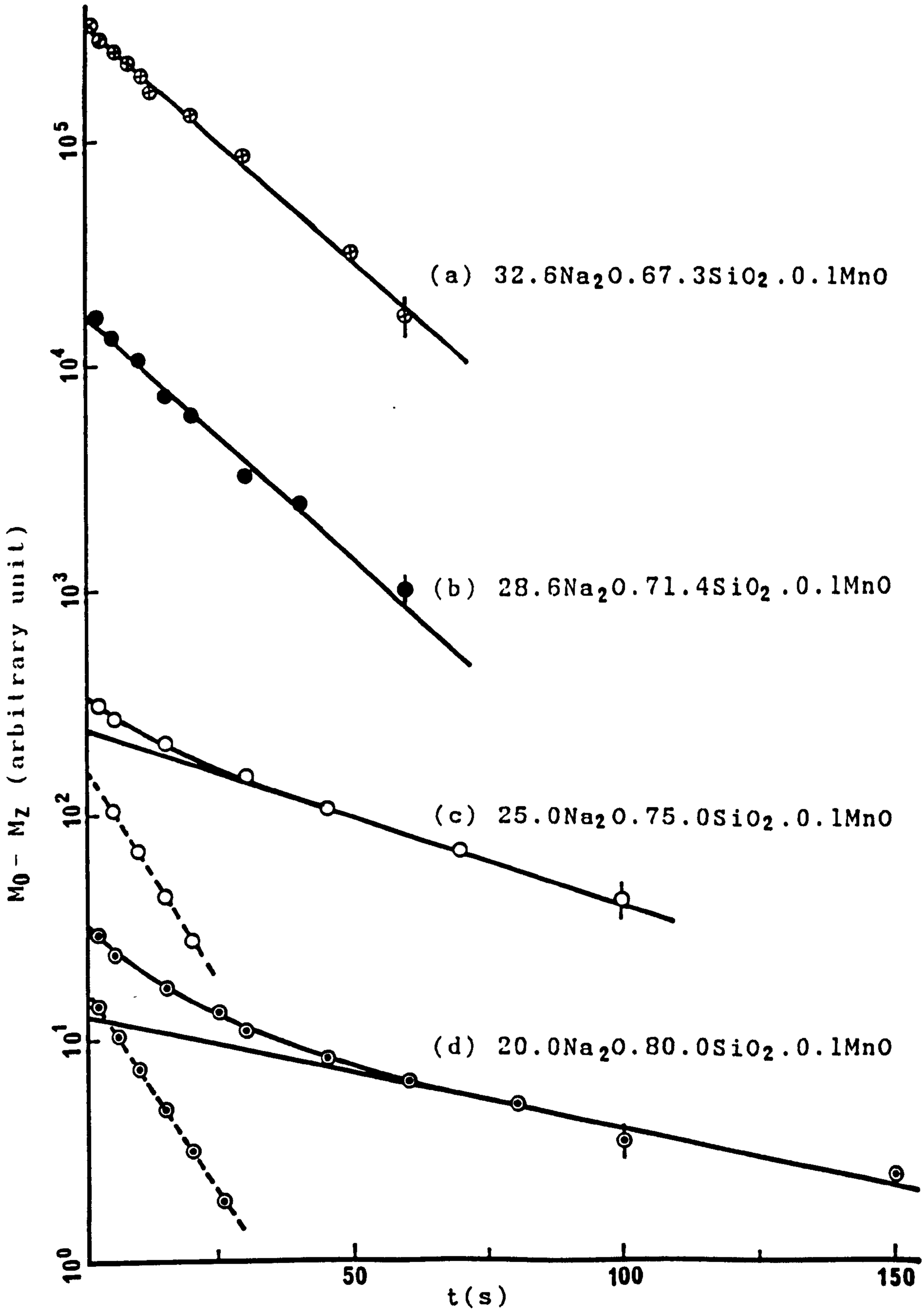

Figure 7.1 ^{29}Si relaxation in Q_3 of varying modifier content sodium silicate base glasses. The plots have been shifted arbitrarily to prevent overlapping. The differences between curved and straight portion of the plots are presented by the broken lines. (b) to (d) are nominal compositions.

TABLE NO. 7.1 ^{29}Si RELAXATION TIMES AND COMPOSITIONS OF Q_m SPECIES IN SODIUM SILICATES

Sample	Nominal composition (mol%)			T_1 relaxation times (s)				Composition (%) of ± 4%				$\frac{Q_4}{Q_3}$
				Q_3		Q_4		Q_3 corresponding to		Q_4 corresponding to		
	Na_2O	SiO_2	Mno	Long	Short	Long	Short	Long T_1	Short T_1	Long T_1	Short T_1	
NS3*	32.7 (33.3)	67.3 (66.7)	0.1	20.0±2.0	-	-	-	-	-	-	-	-
NS7	28.6	71.4	0.1	19.5±2.1	-	-	-	-	-	-	-	-
NS8	25.0	75.0	0.1	52.5±4.3	10.0±1.2	-	-	78.9	21.1	-	-	0.53 ±0.05
NS9	20.0	80.0	0.1	80.0±7.0	12.0±1.7	100.0±9.0	14.0±1.8	44.9	55.1	40.7	59.3	1.17 ±0.12

* Analysed compositions are given. The numbers in the brackets are nominal compositions.

TABLE NO. 7.1 ^{29}Si RELAXATION TIMES AND COMPOSITIONS OF Q_m SPECIES IN SODIUM SILICATES

Sample	Nominal composition (mol%)			T_1 relaxation times (s)				Composition (%) of ± 4%				$\frac{Q_4}{Q_3}$
				Q_3		Q_4		Q_3 corresponding to		Q_4 corresponding to		
	Na_2O	SiO_2	MnO	Long	Short	Long	Short	Long T_1	Short T_1	Long T_1	Short T_1	
NS3*	32.7 (33.3)	67.3 (66.7)	0.1	20.0±2.0	-	-	-	-	-	-	-	-
NS7	28.6	71.4	0.1	19.5±2.1	-	-	-	-	-	-	-	-
NS8	25.0	75.0	0.1	52.5±4.3	10.0±1.2	-	-	78.9	21.1	-	-	0.53 ±0.05
NS9	20.0	80.0	0.1	80.0±7.0	12.0±1.7	100.0±9.0	14.0±1.8	44.9	55.1	40.7	59.3	1.17 ±0.12

* Analysed compositions are given. The numbers in the brackets are nominal compositions.

has already been presented in Chapter 5). From the figure it is clear that two exponentials grow from the single exponential with the decrease of Na_2O content. The rate of growth seems to be continuous rather than discrete with the change of alkali metal ion concentration.

The T_1 relaxation time of each component for the two exponentials is determined from the slope of the extrapolated straight line and from the differences between the curved portion and the straight line. As the signal intensity is proportional to the number of nuclei observed, the amounts of different sites can be obtained from the intersection of the straight lines with the Y (intensity) axis at t=0. The T_1 relaxation times and the compositions obtained from the relaxation data of the base glasses (NS7 - NS9) are given in Table (7.1). The variation of relaxation time as a function of Na_2O content is shown in Figure (7.2).

In any of the Q_m species in glasses, spins may exist in a variety of different environments and the measured relaxation decay is a sum of contributions from all the spins. Therefore one might expect single relaxation behaviour if the spins of the nuclei remain in a single environment. According to Equ. (3.8) the T_1 relaxation plot should be a straight line with slope $(-1/T_1)$ on a log scale; but the curvatures of Figures (7.1.c and .d) clearly show at least two relaxation times.

7.2.2 ^{29}Si RELAXATION AS A FUNCTION OF HEAT TREATMENT

The effect of paramagnetic impurities in the ^{29}Si relaxation rate in sodium disilicate composition has already been discussed in Chapter 5. However, samples NS1, NS3 and

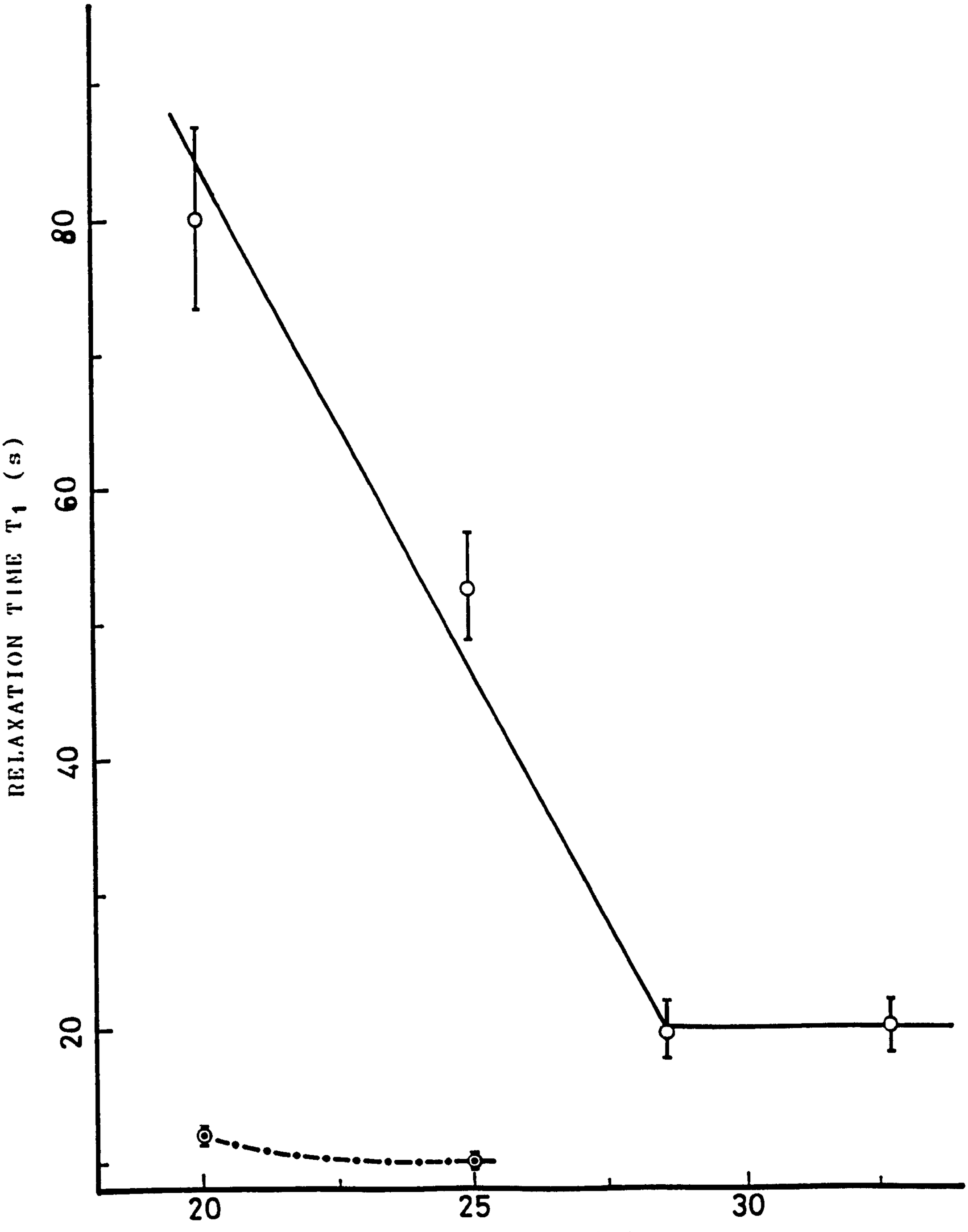

Figure 7.2 ^{29}Si relaxation time in Q_3 as a function of Na_2O content in sodium silicate base glasses. Solid line is for long component and broken line is for short component.

TABLE NO. 7.2 ^{29}Si RELAXATION TIMES AND COMPOSITIONS IN SODIUM DISILICATE BASE AND HEAT TREATED GLASSES

Sample	Heat treatment	Level of MnO	Q_3			
			Long Component		Short Component	
	T^oc/th	mol%	Relax. time (s)	Composition (%) ± 6.4%	Relax. time (s)	Composition (%) ± 6.4%
NS1	NHT*	0.0	112.0± 10.0	-	-	-
	425/3		1027.0±126.0	-	-	-
	425/6		1235.0±163.0	-	-	-
	475/6		1828.0±159.0	85.5	126.3±13.5	14.5
	525/6		2113.0±250.0	75.6	161.0±15.0	24.4
NS3	NHT	0.1	20.0± 2.0	-	-	-
	425/3		102.0± 5.7	-	-	-
	425/6		114.2± 8.4	58.2	13.6± 1.5	41.8
	425/9		1014.3± 93.5	48.8	28.3± 2.2	51.2
	425/12		1097.0±145.0	29.2	78.1±10.8	70.8
	475/6		135.6± 11.5	50.5	14.4± 2.0	49.5
	525/6		169.0± 12.0	13.5	19.0± 2.5	86.5
NS4	NHT	0.2	8.1± 0.7	-	-	-
	425/6		13.3± 1.1	56.7	2.3± 0.3	43.4
	425/9		20.0± 3.2	58.0	3.0± 0.3	42.0
	475/6		13.0± 1.0	64.1	3.1± 0.3	35.9
	525/6		22.6± 2.0	68.2	4.2± 0.4	31.8

* NHT = no heat treatment (base glass)

NS4 used in that study were further chosen to study the structural change due to heat treatment.

The semilogarithmic plots of relaxation decay for $Na_2O.2SiO_2.0.0MnO$ (NS1) as a function of heat treatment are shown in Figure (7.3) and those for NS3 (0.1 mol% MnO) and NS4 (0.2 mol% MnO) are shown in Figures (7.4 and 7.5) respectively. In all the samples two exponentials appear to grow from the single exponential following the sudden rise of relaxation times compared to un-heat treated glass. The variation of relaxation time as a function of heat treatment for a fixed period and that as a function of time for a fixed temperature is shown in Figure 7.6. For undoped material this tendency is less marked than for the doped materials. The relaxation times and the compositions obtained as a function of heat treatment are recorded in Table (7.2). Both the long and short T_1 relaxation times are found to be increased with the increase of either heat treatment temperature or heat treatment time. The concentration of the short component increases and that of long component decreases in NS1 and NS3 but that in NS4 is reversed.

There may be more than two T_1 times but data manipulating problems restrict the assignment of more than two values of T_1. The relaxation decay is not always single exponential in amorphous and polycrystalline materials [19,20] and this also creates a problem of interpretation of T_1 in glasses.

Non-homogeneous distribution of paramagnetic centres may influence the relaxation rate in a different way. Heat treatment may also cause one region to become Mn^{2+} rich at the expense of the other regions but the similarity of the results

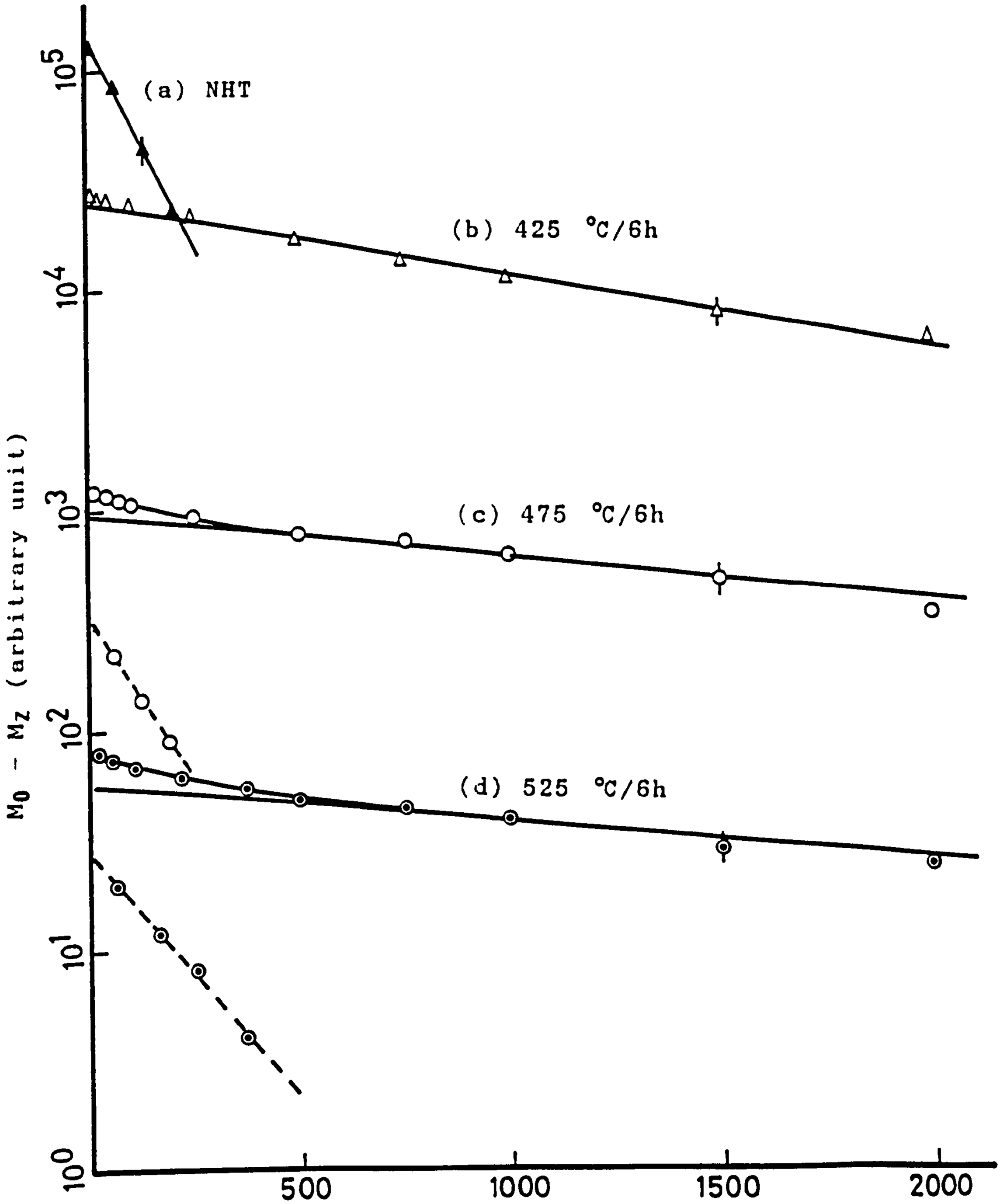

Figure 7.3 ^{29}Si relaxation decay of $32.7Na_2O.67.3SiO_2$ (NS1) for various heat treatments. Successive curves have been displaced vertically one cycle to prevent overlapping. Broken lines are obtained as Figure 7.1.

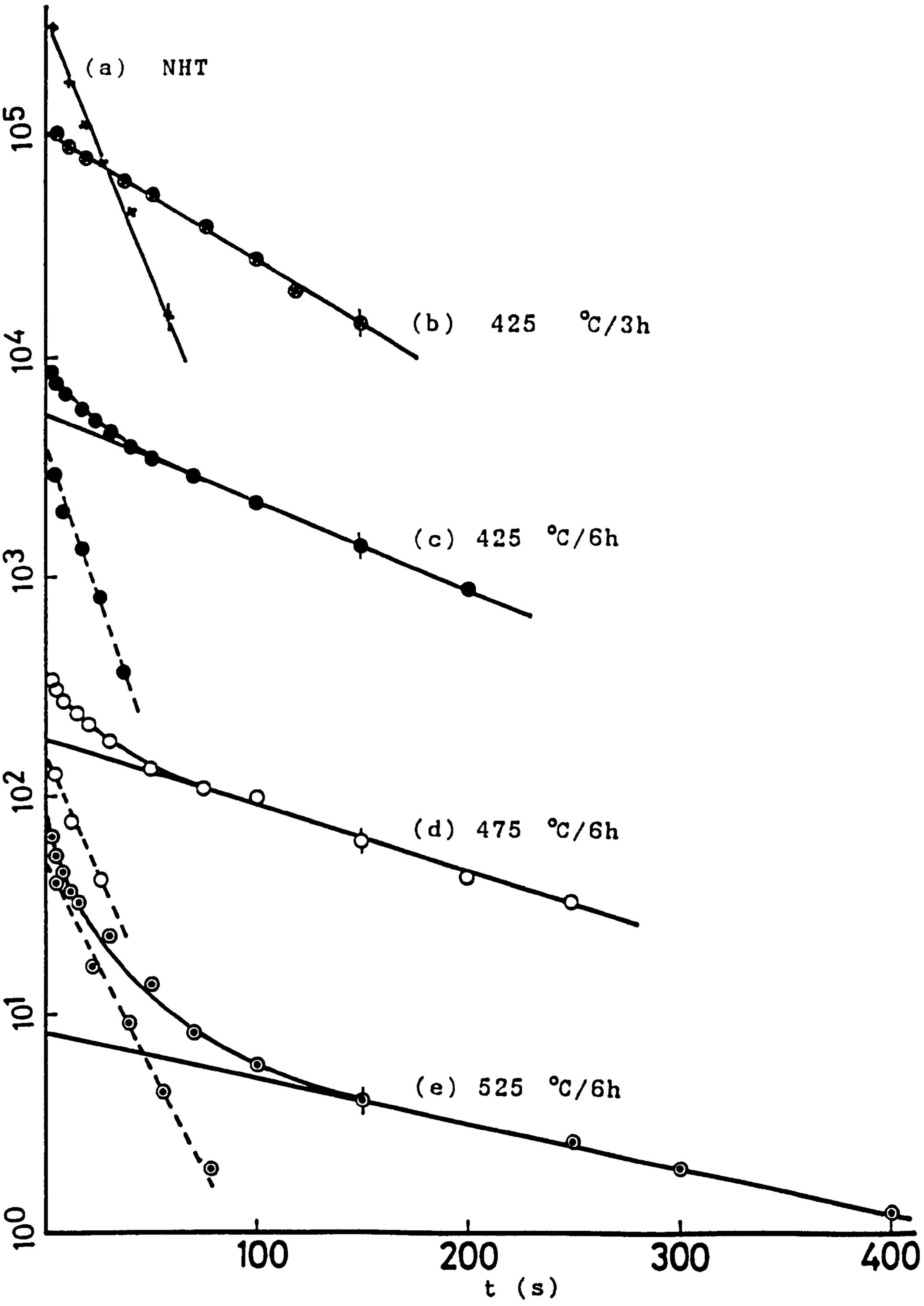

Figure 7.4 ^{29}Si relaxation decay of $32.6Na_2O.67.3SiO_2$ 0.1MnO (NS3) for various heat treatments. Each of the plots has been shifted by two cycles.

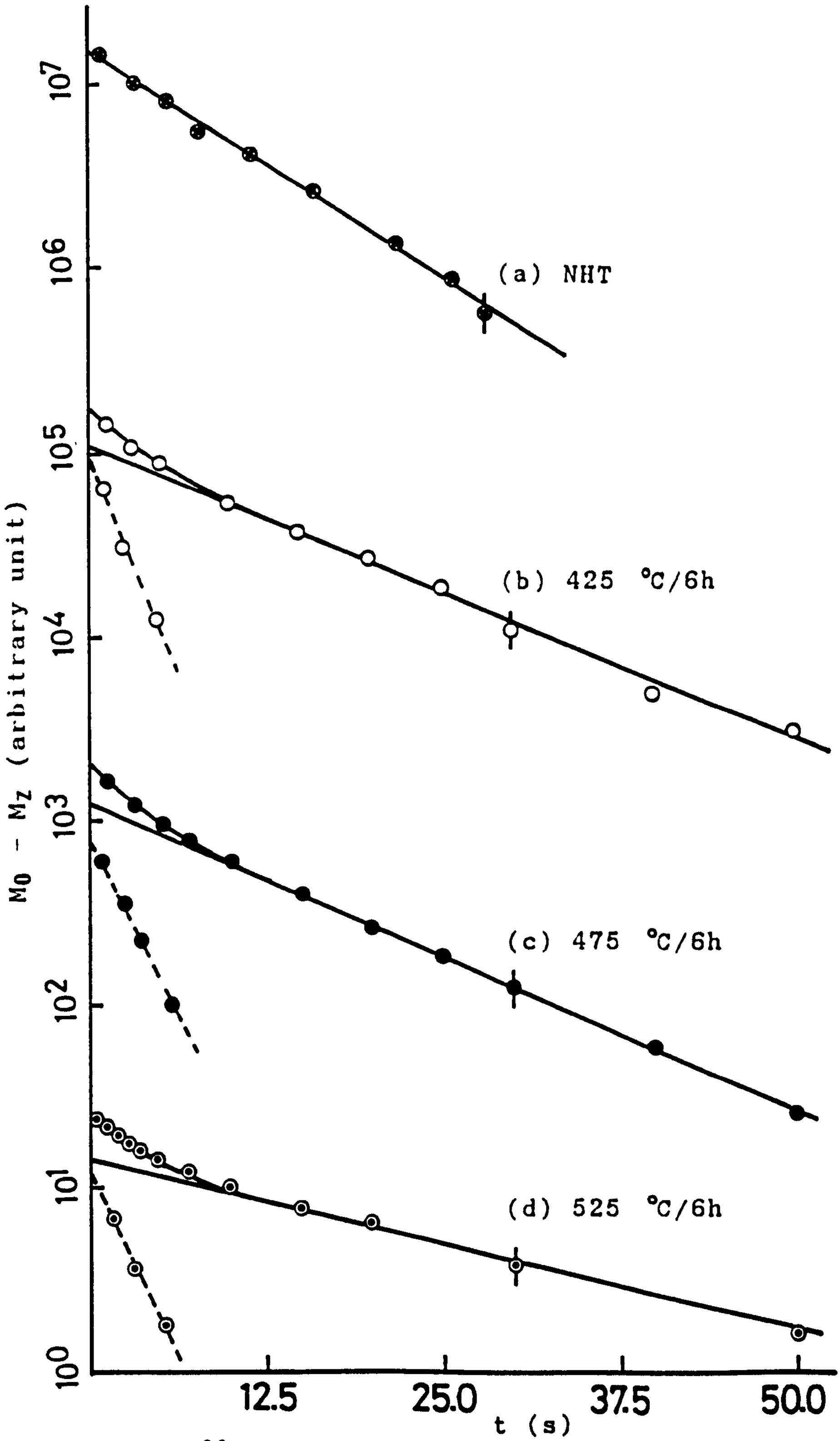

Figure 7.5 ^{29}Si relaxation decay of $32.1Na_2O.67.7SiO_2$ 0.2MnO (NS4) for various heat treatments. Each of the plots has been shifted by two cycles.

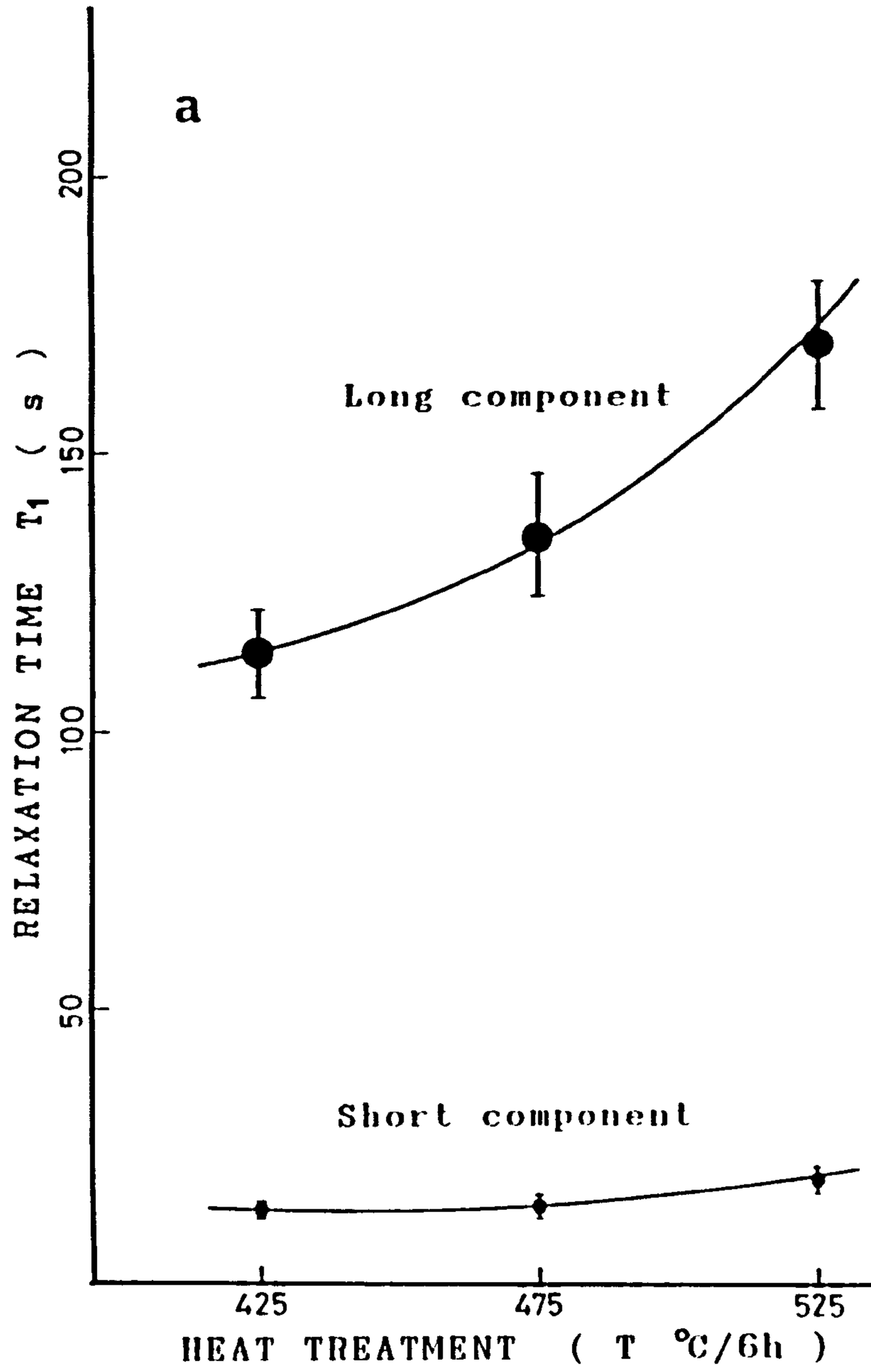

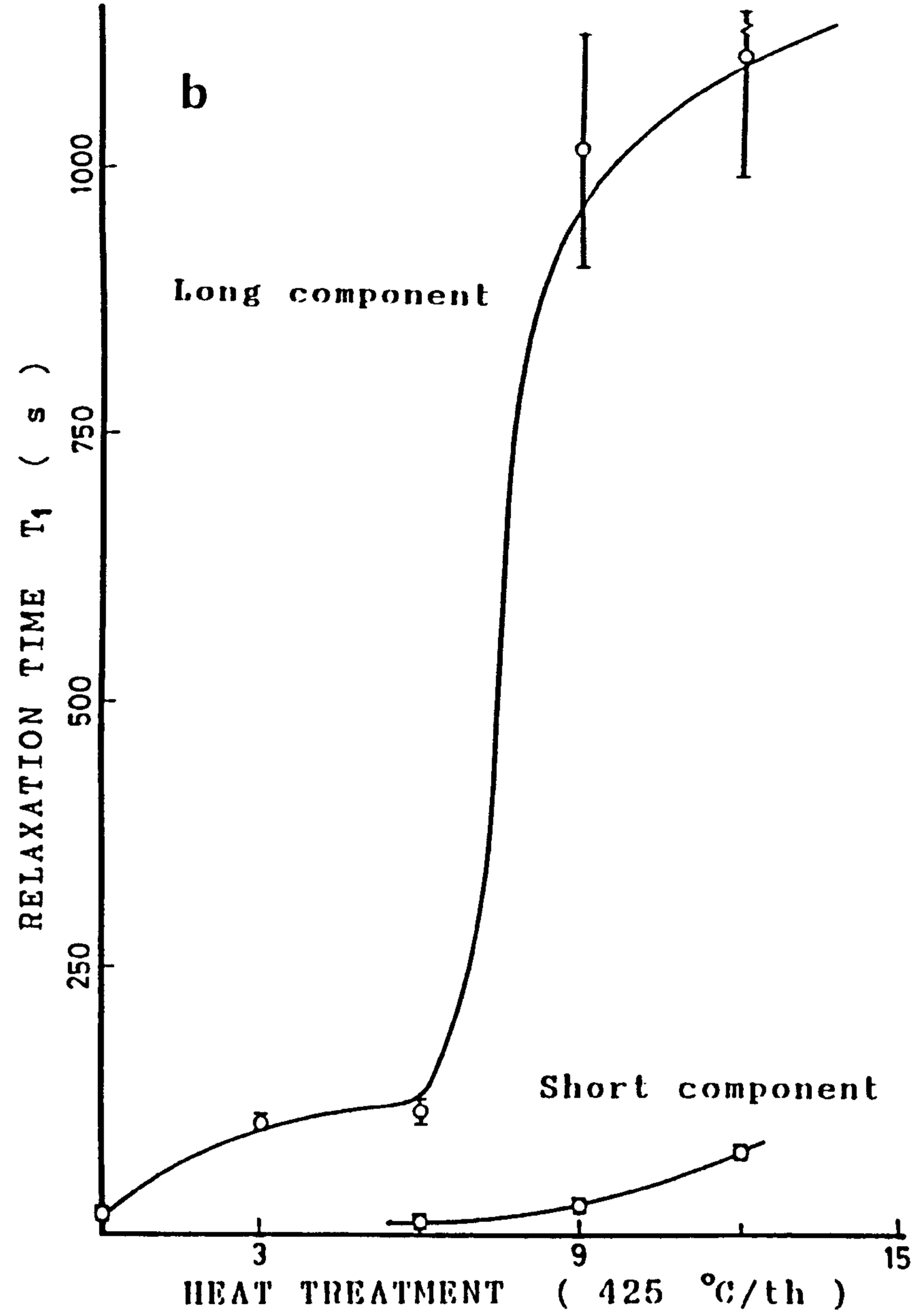

Figure 7.6 Variation of long and short component relaxation times with heat treatment (a) temperature and (b) time in $Na_2O.2SiO_2.0.1MnO$ (NS3) base glass.

obtained from undoped sample encourages confidence in the results. The results presented here would provide a way of quantifying the various species and may also give a method for detecting phase separation in glasses.

7.3 RELAXATION OF ^{29}Si IN LITHIUM SILICATE SYSTEM

Figure (7.7) shows the plots of intensity versus relaxation delay for LS1, LS1 heat treated at 475^{o}C for 6 hours, henceforth referred to as LS1H, and LS3 samples. In the lithium silicate system all the base and heat treated glasses show two component relaxation times. The T_1 relaxation times and the concentrations corresponding to each component are determined exactly the same way as before (See 7.2) and are presented in Table (7.3).

Although the experimental conditions for the samples LS1 and LS1H were the same the intensity distributions of the Q_m species are not the same. Figure (7.8) shows the ^{29}Si spectra of the samples for various delays. The differences in intensity between Q_3 and Q_4 may provide some information about the effect of heat treatment.

7.4 DISCUSSION OF SODIUM AND LITHIUM SILICATES ^{29}Si T_1 RELAXATION TIMES

7.4.1 ^{29}Si RELAXATION IN $xNa_2O.(1-x)SiO_2$ (x=28.6,25.0,20.0)

Although relaxation in glasses is complicated, the appearance of a two component relaxation time in the low Na_2O ($\lesssim$ 25 mol%) containing samples compared to high Na_2O($\gtrsim$ 28.0 mol%), where only single exponential is observed (Figure 7.1), provides some information about the system. The samples contain a paramagnetic impurity which is assumed to be

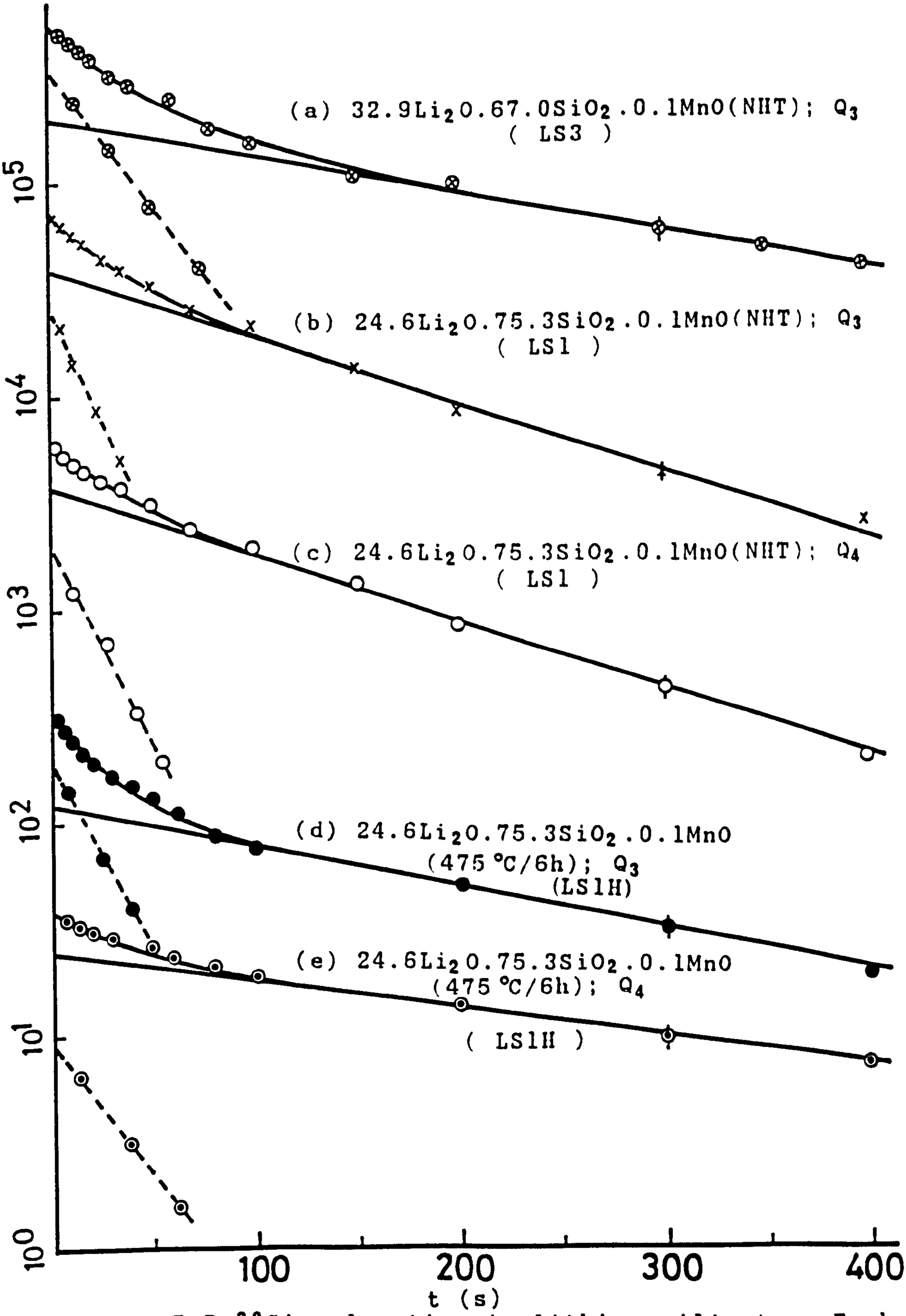

Figure 7.7 ^{29}Si relaxation in lithium silicates. Each plot is shifted by one cycle. The broken lines are obtained as before(Fig. 7.1).

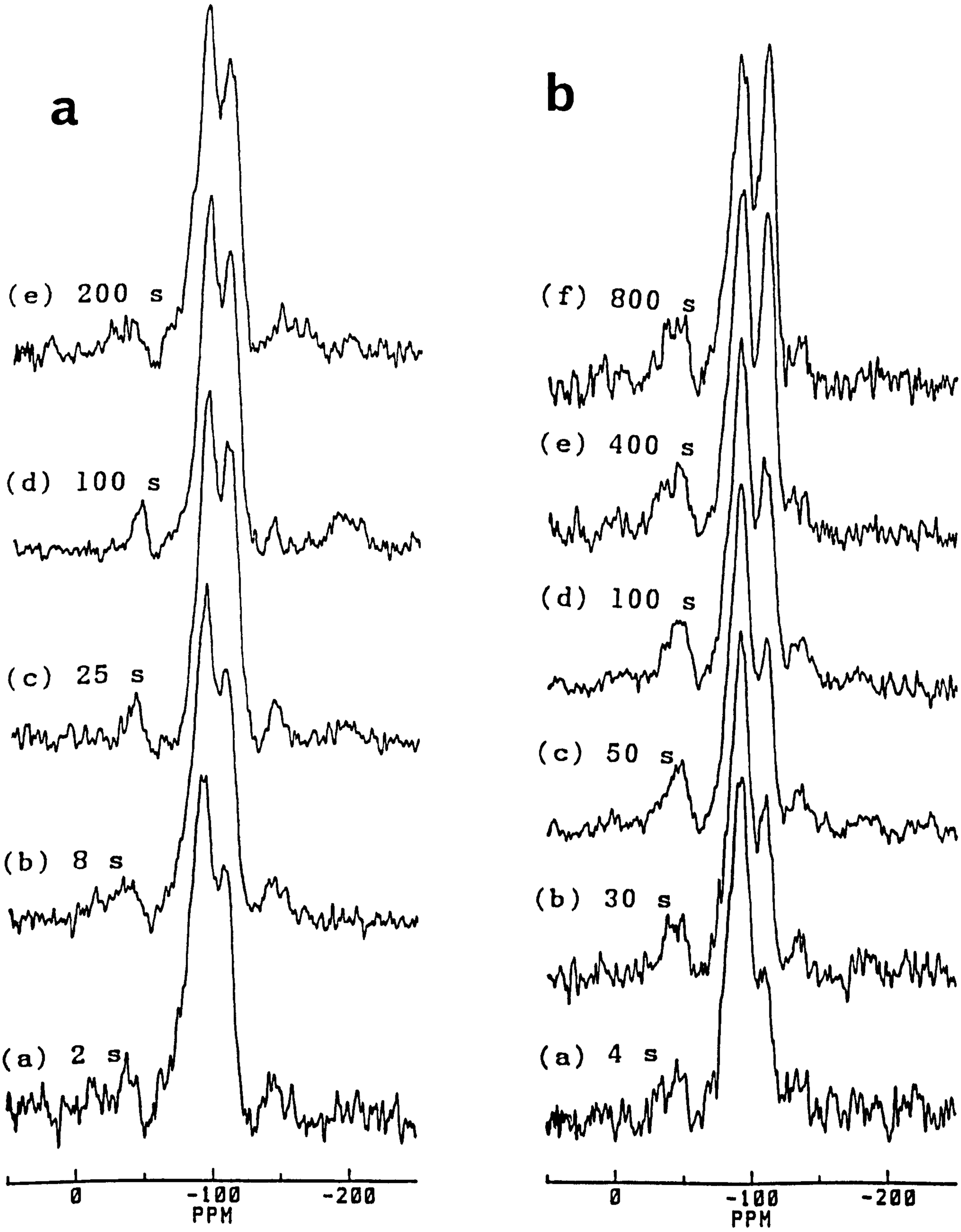

Figure 7.8 ^{29}Si spectra of $24.6Li_2O$. $75.3SiO_2$0.1MnO (LS1) (a) base glass and (b) heat treated at 475 °C/6h(LS1H) for various delays.

TABLE NO. 7.3 DATA FOR THE ^{29}Si RELAXATION TIMES AND COMPOSITIONS OF Q_m SPECIES IN LITHIUM SILICATES

Sample	T_1 relaxation times (s)				Compositions (%) of ± 6.0(%)			
	Q_3		Q_4		Q_3 corresponding to		Q_4 corresponding to	
	Short	Long	Short	Long	Short T_1	Long T_1	Short T_1	Long T_1
LS1	18.9±2.2	130.0±15.0	23.9±2.7	143.0±16.0	38.4	61.6	33.9	66.1
LS1H	26.5±3.0	232.0±20.0	35.5±3.5	302.0±25.0	60.2	39.8	25.8	74.2
LS3	32.0±4.2	250.0±22.0	-	-	66.1	33.9	-	-

TABLE NO. 7.3 DATA FOR THE ^{29}Si RELAXATION TIMES AND COMPOSITIONS OF Q_m SPECIES IN LITHIUM SILICATES

Sample	T_1 relaxation times (s)				Compositions (%) of ± 6.0(%)			
	Q_3		Q_4		Q_3 corresponding to		Q_4 corresponding to	
	Short	Long	Short	Long	Short T_1	Long T_1	Short T_1	Long T_1
LS1	18.9±2.2	130.0±15.0	23.9±2.7	143.0±16.0	38.4	61.6	33.9	66.1
LS1H	26.5±3.0	232.0±20.0	35.5±3.5	302.0±25.0	60.2	39.8	25.8	74.2
LS3	32.0±4.2	250.0±22.0	-	-	66.1	33.9	-	-

randomly distributed throughout the volume and provides centres for nuclear relaxation via spin diffusion.

The transition probability for dipolar interaction of the ^{29}Si is $W \sim 10^{-1}$ s^{-1} and the diffusion coefficient is $D \sim 10^{-19}$ m^2 s^{-1}. Thus the time taken by the nuclear spins to diffuse energy [37.a] over the distance of $10^{-9}m$ is ~ 20 s. Therefore the diffusion process is very slow and for a time <20 s spin diffusion does not allow to develop a common spin temperature amongst the ^{29}Si atoms, and so the magnetisation recovery curves will not necessarily be single exponentials for the first 20s approximately. This is what is observed in Figure 7.1 for NHT glasses. But increase of ^{23}Na content will reduce the spin duffusion by unlike-spin dipolar interaction and hence increase the time to attain a spin temperature. This is not what is observed. Also there is no reason why heat treatment should lengthen the time to establish a spin temperature if the glass remains homogeneous, whereas this time appears to increase in some cases by a factor of 10 (e.g. Figure 7.3). Figure 7.3 suggests that a spin temperature is only achieved after $\sim 500s$, which may possibly indicate phase separation on heat treatment in this glass on a scale $d \sim (Dt)^{\frac{1}{2}}$, i.e. 70 Å .

Now if spin diffusion occurs throughout the bulk of the material the rate of relaxation of all the nuclei of the

same kind are expected to be the same. If this is the case then it may be said that the sodium silicate glasses with $\geq$28 mol% Na_2O form single phase glass and as a result the single exponential decays of the ^{29}Si in NS3 and NS7 are found (Figure 7.1.a,.b). Alternatively sodium silicate glasses with $\leq$ 25 mol% Na_2O might not form homogeneous glass which may result in the two exponential decays of the ^{29}Si in NS8 and NS9 glasses (Figure 7.1.c,.d). The relaxation decay of Q_4 in NS9 shows similar trend (Table 7.1). Thus, if we assume that the two component T_1 is a measure of non-homogeneity, i.e. phase separation then it may be said that the sodium silicate glasses containing $\leq$ 25 mol% Na_2O separate into two phases. The increasing difference between the extrapolated straight line and the experimental curvature due to decreasing Na_2O content (Figure 7.1) may represent the degree of phase separation.

Further evidence can be put forward in support of phase separation in low Na_2O (< 25 mol%) containing samples using the values of the ^{29}Si relaxation times (Figure 7.2). The T_1 values for Q_3 in NS3 (32.7 mol% Na_2O) and NS7 (28.6 mol% Na_2O) are almost the same ($\sim$ 20 s) and that in NS8 (25 mol% Na_2O) and NS9 (20 mol% Na_2O) are significantly different (Table 7.1) and increase with the decrease of Na_2O concentration. Thus the longer relaxation time of Q_3 in NS8 and NS9 may be due to the effect of phase separation.

The ratio of the compositions (Q_4/Q_3) of NS9 (1.17 $\pm$ 0.12) and that of NS8 (0.53 $\pm$ 0.05) is consistent with the constrained model [1] (Table 7.1). This consistency reassures the absence of more than two species in this compositional range. The single component T_1 in NS3 and NS7 suggests that spin diffusion occurs throughout the sample.

7.4.2 ^{29}Si RELAXATION IN HEAT TREATED SODIUM DISILICATES

It has been discussed in Chapter 5 that all the sodium disilicate base glasses, irrespective of MnO concentration, show single exponential T_1 (Figure 5.2). So that there appears to be a spin temperarture. Heat treatment for a short time and at a low temperature retains the single exponential behaviour but increases the relaxation time abruptly in the glasses NS1 and NS3 (Figures 7.3.b, 7.4.b, 7.6). The sudden rise of T_1 may be due to nucleation at those heat treatments. The ^{29}Si relaxation in this case may also be considered as showing a spin temperature because a two component relaxation time is not observed. However for further heat treatment two component relaxation times grow as have already been observed in sodium silicate glasses with 25.0 and 20.0 mol% Na_2O (Figure 7.1). It is well known that heat treatment just above T_g can cause glass-in-glass phase separation for less than $\sim$ 20% Na_2O, i.e. phase separation without being crystallised [38]. The T_g for sodium disilicate is 455^oC and therefore the heat treatment at 475^oC for 6 hours may cause phase separation. Thus the two component T_1 in the heat treated glasses are possibly due to phase separation. The sharp rise of relaxation time for

the heat treatment 425°C/9 h (Figure 7.6) may also be due to nucleation but the number of nuclei is more than in the heat treatment for short time (425°C/6h). Unfortunately high resolution NMR is unable to detect such a change.

Comparison of the relaxation times (Table 7.2) in undoped and doped materials shows a similar trend of increase of T_1 with heat treatment time and temperature. But the compositional data (Table 7.2) for NS4 (0.2 mol% MnO) show anomalous behaviour in respect of NS1 and NS3. The concentration in NS1 and NS3 of the long component T_1 decreases with heat treatment but that for the short component increases. The anomalous compositional data for NS4 is not easily explained but that may be due to relatively high concentration of impurity. The sluggish formation of two component from single component T_1 in the undoped material (NS1) may be due to a low rate of spin flip-flop because of a low level of impurity caused by the impurities in the starting materials.

7.4.3 ^{29}Si RELAXATION IN LITHIUM SILICATES

The trend of the increase or decrease of relaxation times and the composition of the LS1 and LS1H are the same as NS1 and NS3 (Table 7.2). Thus similar interpretations as NS1 and NS3 may be applicable to lithium silicate glasses. Therefore the two component relaxation times (Table 7.3; Figure 7.7) in all the base and heat treated lithium silicates indicate that the glasses (LS1, LS1H, LS3) could be phase separated. Relatively longer relaxation times in LS1H (Table 7.3) indicate that the sample might be more phase separated than LS1.

7.5 EFFECT OF P_2O_5 ADDITIONS ON THE ^{29}Si RELAXATION IN ALKALI DISILICATES

It has been shown in Chapter 6 that addition of P_2O_5 has a profound effect on the glass structure. Silicon-29 relaxation measurements were carried out on alkali disilicates containing varying amounts of P_2O_5. In this section the effect of low amounts of P_2O_5 in $R_2O.2SiO_2$ (R = Li, Na, K) and high amounts of P_2O_5 in only $Na_2O.2SiO_2$ system are presented.

7.5.1 LITHIUM PHOSPHOSILICATES

The ^{29}Si relaxation decays for LSP1 and LSP3 on semilogarithmic plot are shown in Figures (7.9). In both the samples the decays represent two exponentials for all the species. The T_1 in LSP1 is measured only for Q_3 species because Q_4 is not well resolved.

7.5.2 SODIUM PHOSPHOSILICATES

The semilogarithmic plots of ^{29}Si relaxation in sodium disilicates with 0.9, 1.9 and 4.0 mol% P_2O_5 (NSP1-NSP3) are shown in Figure (7.10) and those with 50.0 and 60.0 mol% P_2O_5 (NSP11c and NSP12b) are shown in Figure (7.11). The relaxation decay in the pure sodium disilicate composition is single exponential (Figure 7.4.a) but on addition of low amounts (1-4 mol%) of P_2O_5 the decays become a combination of more than one exponential. However in the case of 50 mol% P_2O_5 the decay is single exponential whereas for 60 mol% it is at least two exponential.

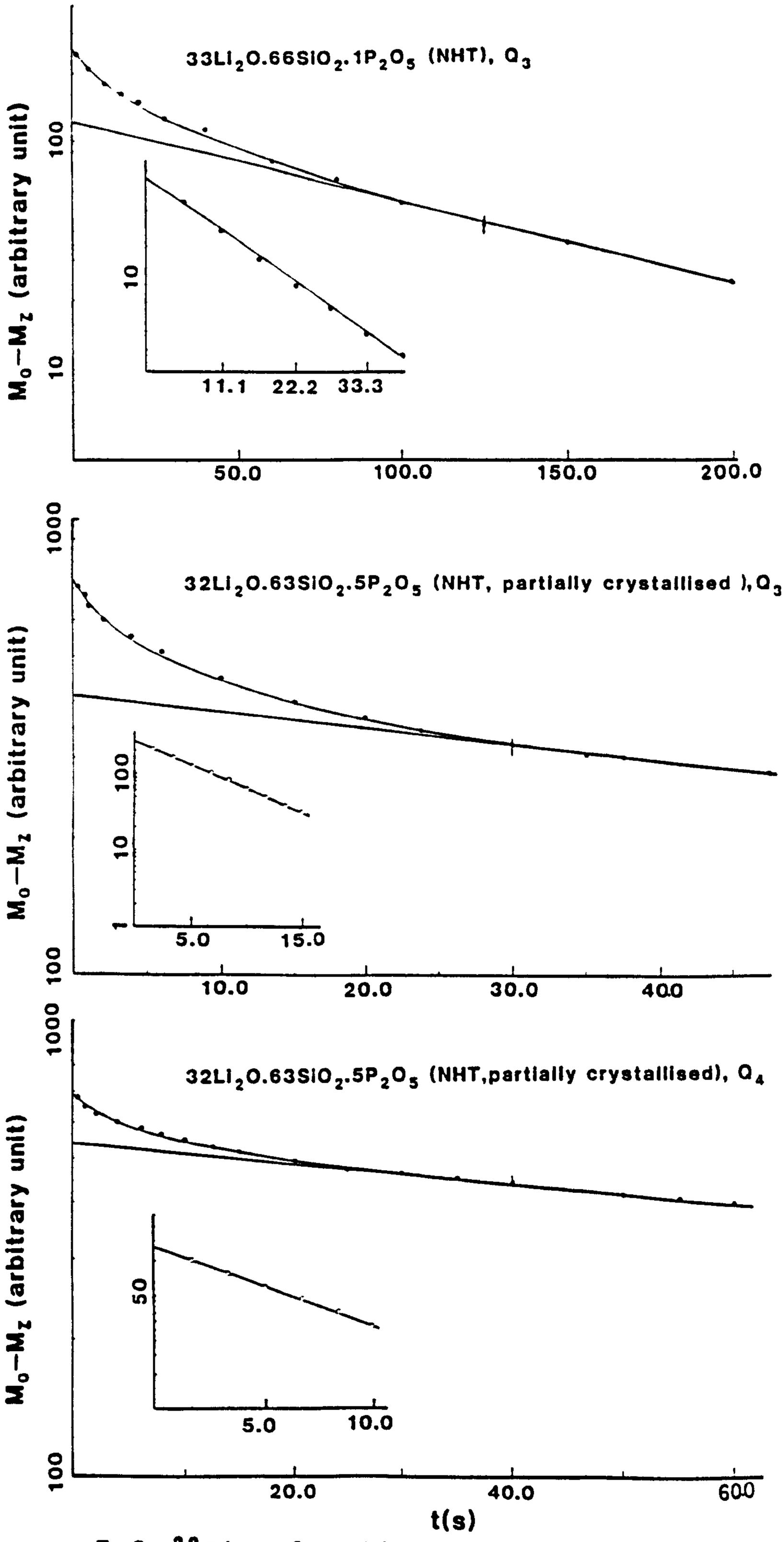

Figure 7.9 ^{29}Si relaxation decay in lithium phosphosilicates. The difference between curved and straight portion is shown by inset.

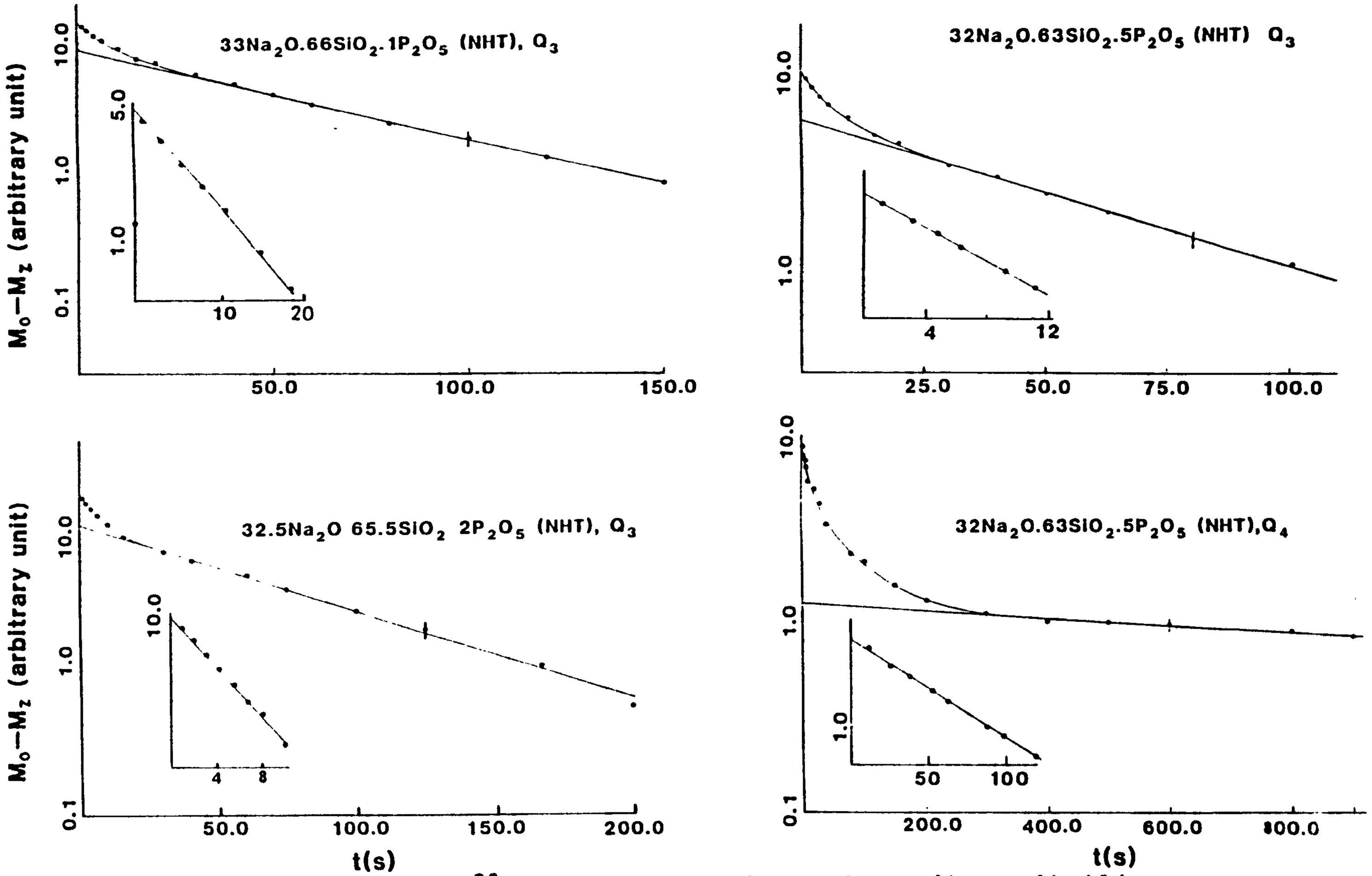

Figure 7.10 ^{29}Si relaxation decay in sodium disilicate with low amounts of P_2O_5. The difference between curved and straight line is shown by inset.

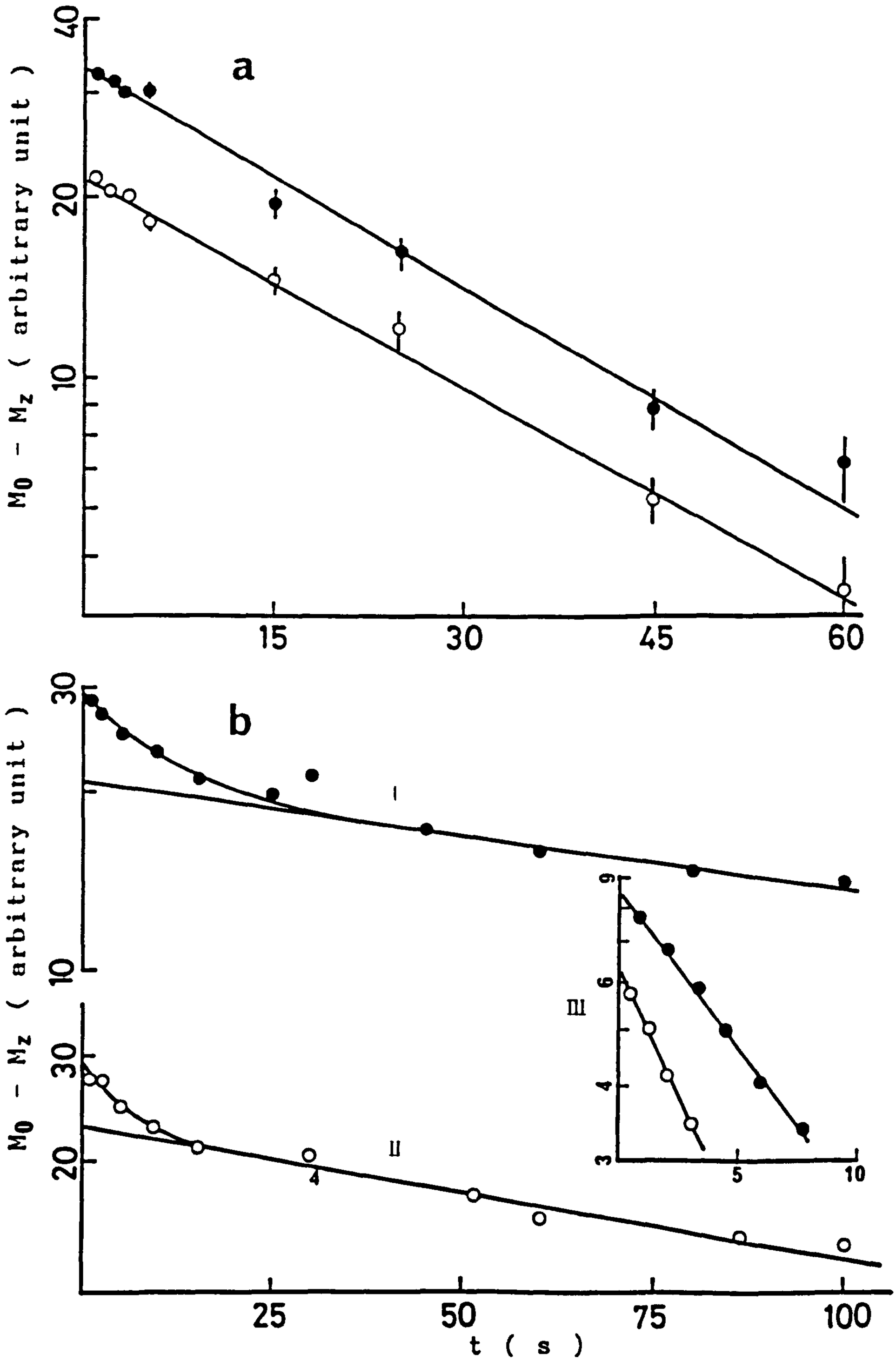

Figure 7.11 ^{29}Si relaxation decay in (a) $16.67Na_2O.33.33SiO_2.50.0F_2O_5$ and (b) $13.33Na_2O.26.67SiO_2.60.0P_2O_5$. (●) Q_4 - P and (○) SiO_6 - P. b.III is the difference between the curved and straight portion of the lines. Error bars for (b) are the same as (a).

7.5.3 POTASSIUM PHOSPHOSILICATES

The results for the potassium disilicates with low amounts (0.9 and 4.0 mol%) of P_2O_5 are similar to those of lithium and sodium phosphosilicates and are not shown.

The relaxation times and the compositional data of all the alkali phosphosilicates are presented in Table (7.4).

7.6 DISCUSSION OF THE ALKALI PHOSPHOSILICATES ^{29}Si RELAXATION

7.6.1 LOW (1-4 mol%) P_2O_5 CONTENT

The phosphate group (orthophosphate and pyrophosphate) in alkali disilicates with low amounts of P_2O_5 are known to occupy the holes in the glass structure [39; see 6.2]. Both the Q_3 and Q_4 are three dimensional chain-like structures [40-42]. The boundary of the phosphate species may be distinct from the Q_3 and Q_4 network. This makes the interpretation of ^{29}Si relaxation in these materials more difficult. Moreover the phase separation and the interfacial effect between the continuous network of the silicate matrix and the phosphate species may affect the relaxation rate.

The ratio for the compositions of long to short T_1 (Table 7.4) in Q_3, within the experimental error, is almost the same in all alkali phosphosilicates with low (1-4 mol%) amounts of P_2O_5. The Q_3 relaxation times for the short and long component T_1 in the NSP1 - NSP3 are 7 and 60 s respectively. Alkali to silicon ratio in all the samples is 0.5. Thus the same relaxation time and compositions are expected for the same extent of phase separation. However, the long component T_1 relaxation time for Q_4 in NSP3 is extremely long (2342 s). This may happen due to either

TABLE NO. 7.4 RELAXATION TIMES AND COMPOSITIONS OF ALKALI PHOSPHOSILICATES

Sample	T_1 Relaxation times (s)								Compositions (%) of ± 6%							
	Q_3		Q_4		Q_4-P		SiO_6-P		Q_3 corresponding to		Q_4 corresponding to		Q_4-P corresponding to		SiO_6-P corresponding to	
	short	long	short	long	short	long	short	long	short T_1	long T_1	short T_1	long T_1	short T_1	long T_1	short T_1	long T_1
LSP1	21.0±2.6	118.0± 8.0	-	-	-	-	-	-	47.5	52.5	-	-	-	-	-	-
LSP3	8.3±1.2	114.-±10.0	6.0±2.0	19.0±11.0	-	-	-	-	37.6	62.4	22.0	78.0	-	-	-	-
NSP1	7.5±1.5	53.0±7.0	-	-	-	-	-	-	37.1	63.9	-	-	-	-	-	-
NSP2	6.6±1.7	63.0±9.0	-	-	-	-	-	-	46.5	53.5	-	-	-	-	-	-
NSP3	6.7±2.0	57.5±6.5	57.0±6.0	2342.0± 185.0	-	-	-	-	43.1	56.9	79.0	21.0	-	-	-	-
KSP1	84.±1.0	50.0±7.3	-	-	-	-	-	-	38.0	62.0	-	-	-	-	-	-
KSP3	8.0±1.1	56.0±6.8	-	-	-	-	-	-	31.5	68.5	-	-	-	-	-	-
NSP11d	-	-	-	-	35.6±3.8	-	37.5±3.2	-	-	-	-	-	60.8	-	39.2	-
NSP12b	-	-	-	-	8.4±1.2	242±26.0	5.0±0.8	191.0±21.0	-	-	-	-	28.8	71.2	22.2	77.8

distribution of MnO or phase separation. Relaxation caused by interfacial effects may be ignored because the number of phosphate species varies with P_2O_5 content (see 6.2) which would change the relaxation rate.

The same argument may be applicable to the potassium phosphosilicate system but the results for the lithium phosphosilicates show some differences (Table 7.4). This could be due to the presence of $Li_2O.SiO_2$ nuclei because of early phase separation in LSP3 glass (see 6.2).

7.6.2 HIGH (50, 60 mol%) P_2O_5 CONTENT

For the high concentrations of P_2O_5 ($\gtrsim$ 38 mol%) phosphorus forms Si-O-P bonds in both Q_4-P and $[SiO_6]$-P and thus octahedral silicon like - SiP_2O_7 occurs in the base glasses (see 6.3). The sample with 50 mol% P_2O_5 (NSP11C) contains less SiP_2O_7 than NSP12b (60 mol% P_2O_5). The rate of crystallisation in SiO_6 octahetra is higher than that in SiO_4 tetrahedra because the Gibbs free energy for the former is less than that of the latter [43]. The larger amounts of SiP_2O_7 like environment in NSP12b would enhance the rate of nucleation and glass-in-glass phase separation. Alternatively in NSP11c phase separation might not occur due to the smaller amount of SiO_6 octahedra. This suggests that all similar species in NSP11c could be randomly oriented and spin diffusion might occur among them. If we think that this is the case then the single component ^{29}Si T_1 relaxation in NSP11c as shown in Figure (7.11.a) is expected for both the Q_4-P and $[SiO_6]$-P units. But possible phase separation in NSP12b may not allow spin diffusion and two components relaxation times are obtained (Figure 7.11.b).

7.7 GENERAL DISCUSSION

Identifications of phase separation of the sample of composition similar to NS9 (20 mol% Na_2O) have been carried out by several authors [44,45] using water durability experiments. According to their investigations the samples with $\lesssim$20 mol% Na_2O phase separate although they appear transparent. The reason of this transparency was explained by the fact that concentration of the phase separated droplets was very low and the size of the droplets was very small. Fictive temperature measurement of Na_2O-SiO_2 system with 1-20 mol% Na_2O showed that these glasses phase separate by spinodal decomposition (Figure 7.12) [46]. If the assumption - two component relaxation time is an indication of phase separation then this work has shown that the sample with $\lesssim$25 mol% Na_2O may phase separate. Although data for the water durability experiment and fictive temperature up to 25 mol% are not available, the occurence of phase separation in $\lesssim$25 mol% Na_2O is in substantial agreement with Jen et al. [45] and Mazurin et al. [46]. For higher concentration of Na_2O (> 25 mol%) the coulombic repulsion between the Na^+ ion will be much stronger than with lower concentrations. This force might help to scatter the species randomly throughout the volume of the glass melt and hence may produce a homogeneous glass for >25 mol% Na_2O in sodium silicates.

The creation of two component relaxation times from single component due to heat treatment was first observed by Nishi et al. [47] in polymer mixtures. They predicted that the effect is due to phase separation in mixtures. In their case the long component T_1 became longer and the short

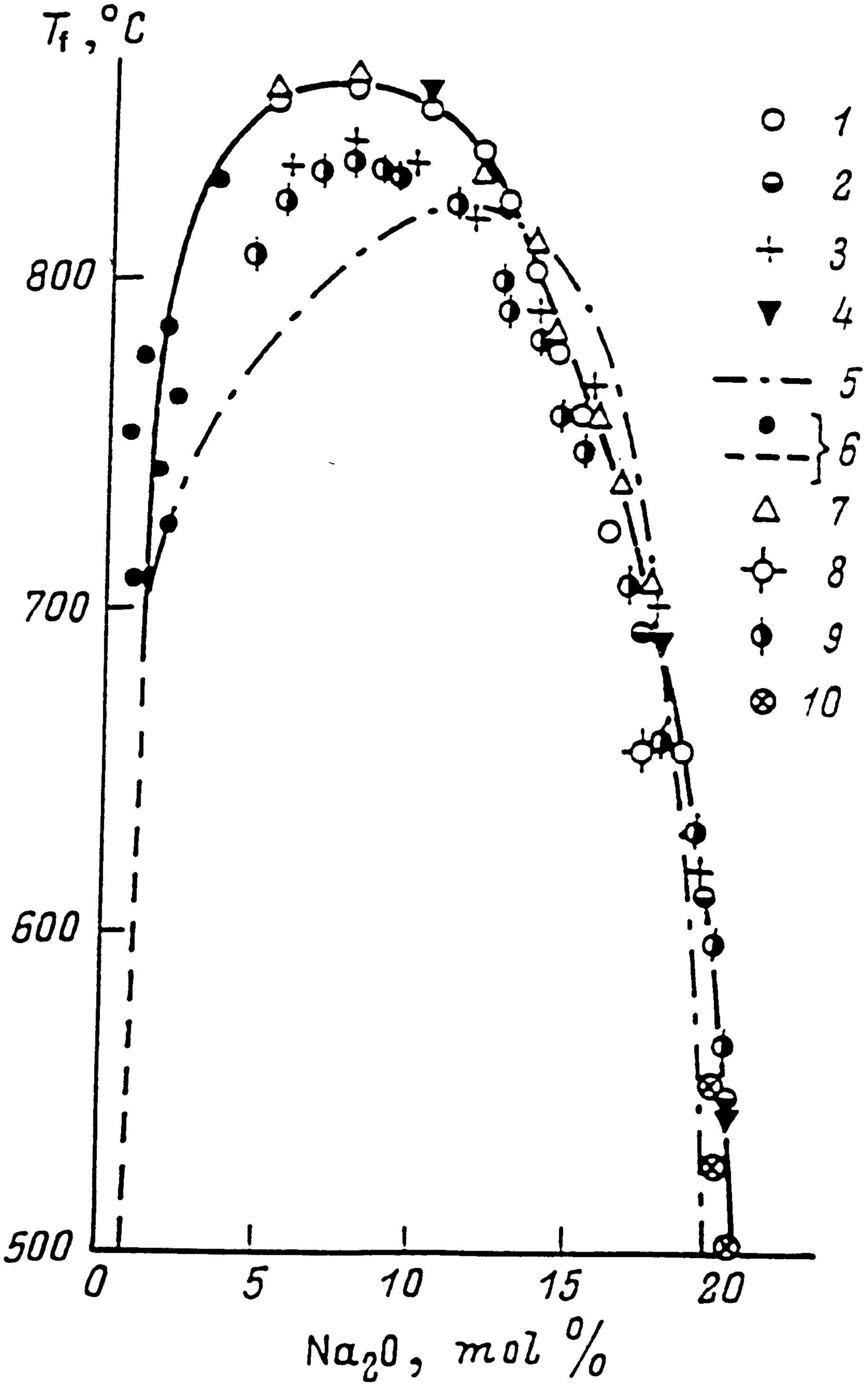

Figure 7.12 Variation of miscibility temperature, T_f with Na_2O in sodium silicate system (ref. 46).

component T_1 became shorter due to heat treatment. The ^{29}Si relaxation in sodium disilicates clearly shows the growth of two T_1 components from single T_1 due to heat treatment of the base glass. The only difference in this case is that both the short and long component T_1 became longer with heat treatment. This dissimilarity may be due to different type of material. Thus the formation of two T_1 components from single T_1 may possibly be considered as a measure of phase separation in alkali silicate glass.

The different relaxation times (Table 7.3) in LS1 and LS1H suggest to do further investigation of the system. The TEM micrographs of LS1, LS1H and LS1H's electron diffraction pattern are shown in Figure (7.13). In LS1 there is no indication of globular structure but that in LS1H may be due to phase separation. The diffuse rings in the diffraction pattern (Figure 7.13.c) are due to glass in which there is no sign of crystal formation. It may be said that the sample LS1H has phase separated into two liquids prior to its crystallisation [48]. The relaxation decay in LS1 is similar to that in LS1H but the decays in both the samples are different from NS1, NS3 and NS4 (Figures 7.3.a-.5.a). Therefore it may be said that microphase separation has occured in LS1 which is beyond the detection limit of TEM.

Not only the NMR results, nucleation and crystallisation kinetics of $Li_2O.2SiO_2$ has been shown to be different from other alkali silicates [49]. The magnitude of the rate of nucleation in $Li_2O.2SiO_2$ does not follow the classical nucleation theory whereas in other systems it does [49]. This perverse nature of $Li_2Si_2O_5$ may be due to some nucleation kinetics which might have occured during quenching from the

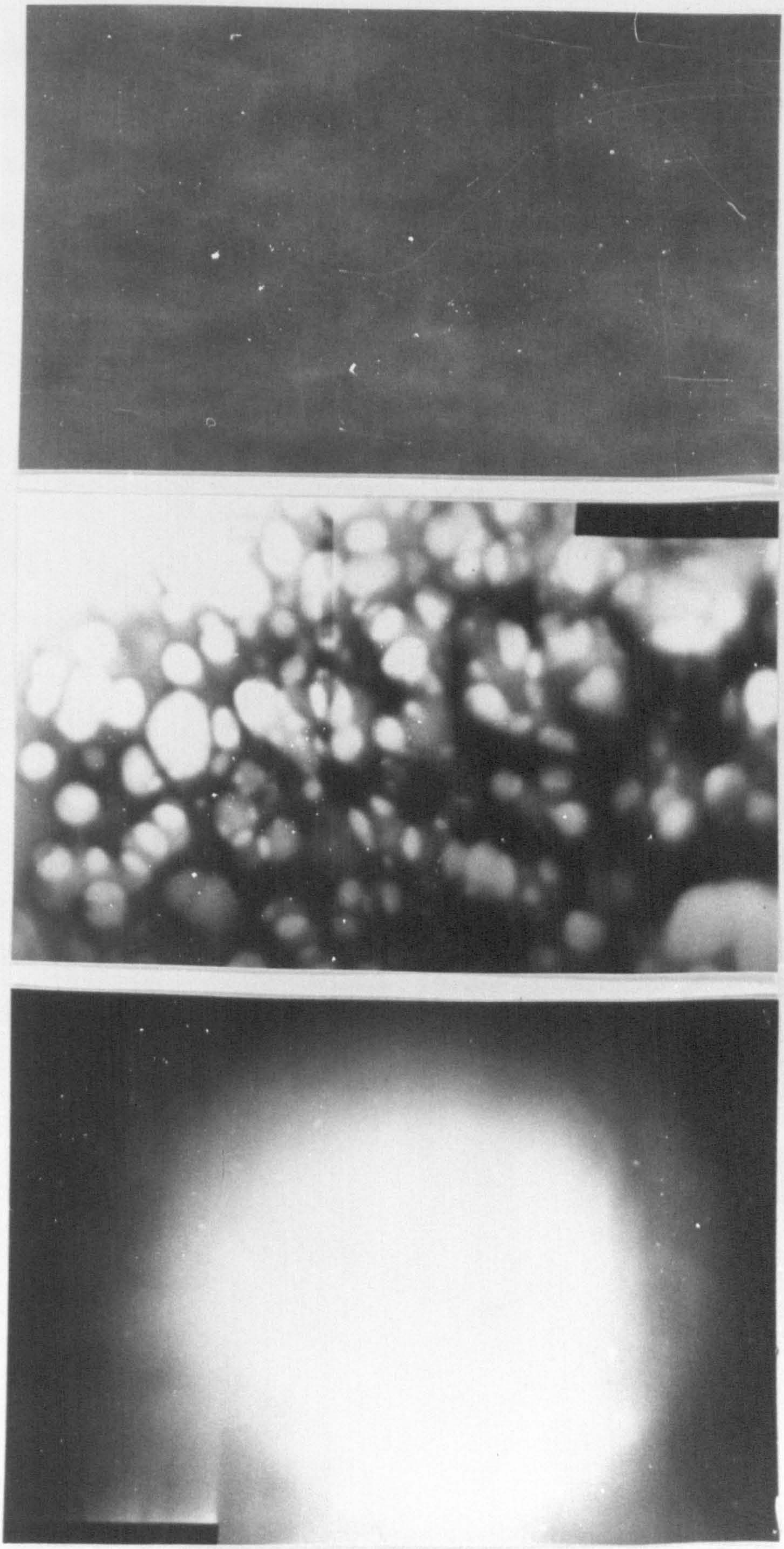

Figure 7.13 Transmission electron micrographs of 24.6 $Li_2O.75.3SiO_2$ sample. (a) Base glass; original mag.* 66000. (b) Heat treated at 475 °C/6h; original mag.* 50000. (c) Selected area diffraction pattern of (b) showing broad intensity maximum.

melt. Experimental nucleation rate is many times greater than the theoretically predicted value. This suggests that pre-nucleation in the system could accelerate the nucleation rate. Thus the outcome of MAS NMR experimentations as two component relaxation times in approximately lithium disilicate composition might be due to either nucleation or amorphous phase separation.

T_1 measurements of proton with structural heterogeneity in polymers [19,20,50] showed single component relaxation time. In heterogeneous material different regions should have different relaxation times. But the fact was explained by the small separation between two regions which can allow spin diffusion to cancel out the difference in relaxation times. For the heat treated polymers, as observed by Nishi et al. [47], the distinct boundary between two regions separated by certain distance might not allow spin diffusion and hence a two component relaxation time might occur. Thus in the case of alkali silicate glasses two component relaxation times may grow from a single T_1 as a result of phase separation caused by either heat treatment or during quenching from the melt.

REFERENCES

1. R. Dupree, D. Holland, P.W. McMillan and R.F. Pettifer, J. Non-Cryst. Solids, 68, 399 (1984).

2. R. Dupree, D. Holland and D.S. Williams, J. Non-Cryst. Solids, 81, 185 (1986).

3. R. Dupree, R.F. Pettifer, Nature, 308, 525 (1984).

4. I. Farnan, S.C. Kohn and R. Dupree, Geochim. Cosmochim. Acta, 51, 2869 (1987).

5. R. Aujla, R. Dupree, I Farnan and D. Holland, 2nd International Conference on the Affects of Models of Formation of the Structure of Glass, Nashville, U.S.A., Vol.2, June 8-12, 1987.

6. R. Aujla, R. Dupree, I. Farnan and D. Holland, The Physics and Technology of Amorphous Silica, France, June 20 - July 3, Plenum press (1987).

7. C.M. Schramm, B.W.H.S. de Jong and V.E. Parziale, J. Am. Chem. Soc., 106, 4396 (1984).

8. U. Selvaray, K.J. Rao, C.N.R. Rao, J. Klinowski and J.M. Thomas, Chem. Phys. lett., 114 (1), 24 (1985).

9. A.-R. Grimmer, M. Magi, M. Hahnert, H. Stade, A. Samoson, W. Wicker and E. Lippmaa, Phys. Chem. Glasses, 25 (4),105 (1984).

10. C.N.R. Rao, J.M. Thomas, J. Klinowski, U. Selvaraj, K.J. Rao, G.R. Milward and S. Ramdas,Phys.Chem.,24 (1) 61 (1985).

11. J.B. Murdoch, J.F. Stebbins and I.S.E. Carmichael, Am. Miner., 70, 332 (1985).

12. E. Schneider, J.F. Stebbins and A. Pines, J. Non-Cryst. Solids, 89, 371 (1987).

13. R. Dupree, D. Holland, in New Horizon in glass and glass-ceramics, Ed. M.H. Lewis, Chapman and Hall (1988).

14. R. Dupree, M.E. Smith, Rept. Prog. Phys. (1989) (to be published).

15. R. Dupree, D. Holland and D.S. Williams, J. de Phys. colloque C8, supplement au no.12, Tome 46, December 1985.

16. R. Dupree, D. Holland and M.G.Mortuza, Phys. Chem. Glasses, 29 (1), 18 (1988).

17. R. Dupree, D. Holland and M.G. Mortuza, Nature, 328, 4176 (1987).

18. R. Dupree, N. Ford and D. Holland, Phys. Chem. Glasses 28 (2), 78 (1987).

19. V.J. Mcbrierty and D.C. Douglass, J. Polymer Science : Macromolecular Reviews, Vol. 16, 295 (1981).

20. K.J. Packer, J.M. Pope and R.R. Yeung, M.E.A. Cudby, J. Polymer Science, Symposium, 22, 589 (1984).

21. E. Gobel, W. Warmuth and H. Olyschglager and H. Dutz, J. Magn. Reson., 36, 371 (1979).

22. W. Muller-Warmuth and E. Schick, J. Non-Cryst. Solids, 453 (1977).

23. E.R. Andrew, W.S. Hinshaw, M.G. Hutchins and A. Jasinski, Chemical Phys. Lett., 27 (1), 96 (1974).

24. S.B. Liu, A. Pines, M. Brandriss and J.F. Stebbins, Phys. Chem. Minerals, 15, 155 (1987).

25. S.B. Liu, J.F. Stebbins, E. Schneider and A. Pines, Geochim Cosmochim. Acta., 52, 527 (1988).

26. G.C. Levy, J.D. Cargiole, P.C. Juliano and T.D. Mitchell, J. Magn. Reson., 8, 399 (1972).

27. G.C. Levy, J. Am. Chem. Soc., 94, 4793 (1972).

28. G. Engelhardt, Z. Chem. 15, 495 (1975).

29. T. Watanabe, H. Shimizu, A. Masada and H. Saito, Chem. Lett., 1293 (1983).

30. P.F. Barron, R.L. Frost and J.P. Skjemstad, J. Chem. Soc., Chem. Commun., 581 (1983).

31. P.F. Barron, P. Slade and R.L. Frost, J. Phys. Chem., 89, 3305.

32. D.J. Cookson and B.E. Smith, J. Magn. Reson., 63, 217 (1985).

33. J. Klinowski, T.A. Carpenter and J.M. Thomas, J. Chem. Soc., Chem. Commun., 956 (1986).

34. G. Engelhardt and D. Michel, High Resolution Solid State NMR of Silicates and Zeolites, John Wiley and Sons, 1987.

35. W.E. Blumberg, Phys. Rev., 119 (1), 79 (1960).

36. H.E. Rorschach Jr., Physica, 30, 38 (1964).

37. A. Abragam, Principles of Nuclear Magnetic Resonance, Oxford, (a) p.139, (b) p.385, 1985.

38. M. Tomozawa, Phys. Chem. Glasses, 13 (6), 161 (1972).

39. Wang-Hong Yang, R.J. Kirkpatrick and G.L. Turner, J. Am. Ceram. Soc., 69 (10), C-222 (1986).

40. A.K. Pant and D.W.J. Cruckshank, Acta. Cryst., B 34 13 (1968).

41. R.N.G. Wyckoff, Crystal structures, Wiley, New York, 1964.

42. A.K. Pant, acta Cryst., B 24, 1077 (1968).

43. F. Liebau, Structural Chemistry of Silicates, Springer Verlag, 1985, P.15.

44. J.H. Simmons, S.A. Mills and B.F. Howell, Effect of Phase separation on the Physical and Chemical Properties of Glasses-Density and Chemical Durability, NMSIR 74-510 (National Bureau of Standards, Washington, D.C., 1974).

45. J.S. Jen and M.R. Kalinowski, J. Non-Cryst. Solids, 38 and 39, 21 (1980).

46. O.V. Mazurin, G.P. Roskova and E.A. Porai-Koshits in 'Phase Separation in Glass', Eds. O.V. Mazurin and E.A. Porai-Koshits, North Holland, 1984, p.109.

47. T. Nishi, T.T. Wang and T.K. Kwei, Macromolecules,8 (2), 227 (1975).

48. P.F. James and P.W. McMillan, Phys. Chem. Glasses, 11 (3) 59 (1970).

49. D.R. Uhlmann and H. Yinnon, The Formation of Glasses, in Glass : Science and Technology, Ed. D.R. Uhlmann and N.J. Kreidl, Vol.1, Glass Forming Systems, Academic Press, P.1, 1983.

50. V.J. McBrierty and D.C. Douglass, Physics Reports, 63, (1980).

CHAPTER 8

CONCLUSION

8.1 COMPARISON OF GLASS SYSTEMS

The concentration of Q_m species in alkali silicates varies with alkali content. Figure 8.1 compares the amounts of Q_m in the Li_2O-SiO_2 system obtained in this study with the constrained random [1] and unconstrained random [2] models. For lower concentrations of Li_2O (< 30 mol%) the result of this study is similar to constrained random model, i.e. not more than two species appear to be present. For higher concentrations of Li_2O (> 30 mol%) there is deviation but this study is closer to the constrained random than that of unconstrained random, i.e. the major species will be Q_m and Q_{m-1} with small amounts of Q_4. Similar results are obtained for Na_2O-SiO_2 glasses. Thus for higher concentrations of alkali, an intermediate situation exists between the two models.

The ^{29}Si chemical shift for the Q_m ($0 \leqslant m \leqslant 4$) species in different binary alkali silicates differ slightly. The variations of the Q_3 and Q_4 shift with alkali content are the most significant. This indicates that the Q_3 and Q_4 environments in vitreous state are different from their crystalline form. The relatively small difference of Q_2 chemical shift between glass and crystal suggests that the ^{29}Si local order in glass and crystalline Q_2 are not very different from each other. Devitrification of R_2O-SiO_2 (R=Li,Na) systems results in different polymorphs of $R_2Si_2O_5$ and the observed NMR spectra are consistent with XRD results.

Addition of P_2O_5 to the $R_2O.2SiO_2$ (R=Li,Na,K) gives the most interesting results. It appears that, in alkali disilicate glasses with 0-10 mol% P_2O_5, phosphorus itself does

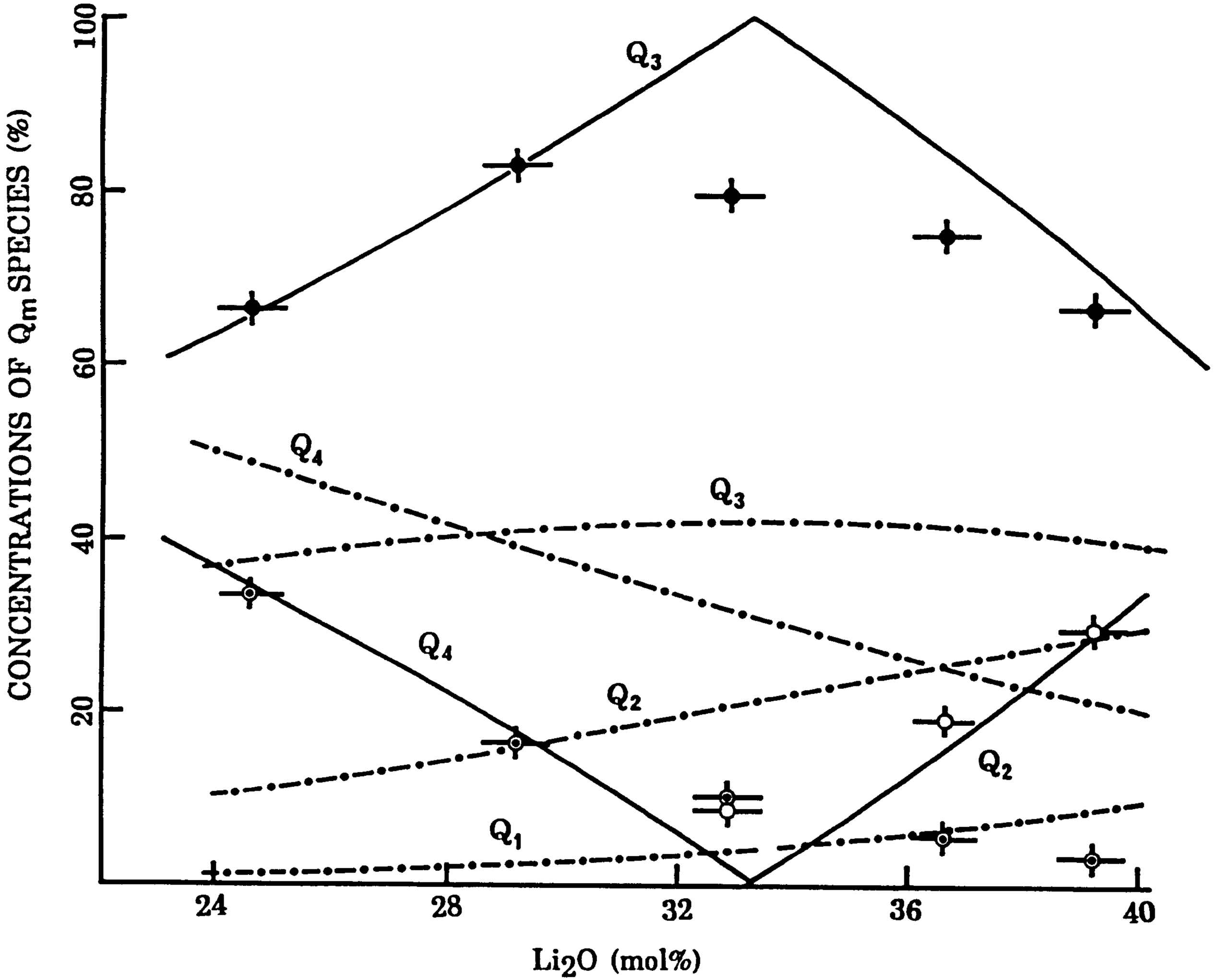

Figure 8.1 A comparison of the amounts of observed Q_m species with the constrained random(———) and unconstrained random(—•—•—) models. Experimental data are indicated as ⊙ (Q_4), ● (Q_3) and O (Q_2).

not participate in the network but increases the polymerisation of the silicate network by the effective removal of modifier cations. Thus amounts of Q_3 decrease and those of Q_4 increase with the increase of P_2O_5. The phosphorus environment resembles "Li_3PO_4" in the $Li_2O.2SiO_2$ system but in $R_2O.2SiO_2$ (R=Na,K) glasses it is present as "R_3PO_4" and "$R_4P_2O_7$". More than 10 mol% P_2O_5 changes the silicon environment to Q_3 with some phosphorus next nearest neighbour, i.e. Q_3-P. The Q_4 - like environment again appears to form at the expense of Q_3-P as P_2O_5 content increases and finally for 25 mol% P_2O_5 only Q_4 is present. Further addition of P_2O_5 (> 38 mol%) produces Q_4-P and an SiP_2O_7 like environment. The phosphorus environment is metaphosphate - like "$NaPO_3$" at these (≳ 11 mol%) concentrations of P_2O_5. The metaphosphate units remain unchanged with P_2O_5 content. Formation of SiP_2O_7 species is the first evidence of 6- fold coordination of silicon in the vitreous state.

The ^{29}Si relaxation times in the vicinity of the sodium disilicate composition range seem to be single exponential whereas those in lithium silicates are not. The ^{29}Si relaxation in all the alkali phosphosilicates except those with 50 mol% P_2O_5 show similar effects to the lithium silicate system. Both heat treatment and addition of low amounts of Na_2O (≲ 25 mol%) gives a two component ^{29}Si relaxation time. These two component relaxation times may be explained by the effect of nucleation or glass-in-glass phase separation.

8.2 NMR AS A TOOL FOR GLASS CERAMIST

The sensitivity of NMR to the local order of nuclei rather than long range order gives additional information to the glass ceramists. This study has clearly showed that NMR can be used to quantify species, even to 1%, in silicate glasses. MAS NMR has provided valuable information on the interaction of P_2O_5 with alkali disilicate glasses and on the environments of ^{29}Si, ^{31}P, ^{27}Al, ^{7}Li and ^{23}Na in these systems. The technique has also given confirmation that the precursors of crystalline Li_3PO_4 are present in lithium disilicate glasses containing P_2O_5 as a nucleating agent. This clearly confirms the proposed mechanism behind the dramatic increase of nucleation rate in Li_2O-SiO_2 system with small amounts of P_2O_5 [3]. Although the lack of long range order in glasses broadens the lineshape with respect to its crystalline environment, the MAS NMR lineshape obtained from the vitreous state can be used to provide structural information. Thus NMR can be considered as a potential tool for present and future glass ceramists.

8.3 PROPOSAL FOR FUTURE WORK

The discovery of six coordinated silicon in glasses provides a new area in the field of glass research. The increase of "SiP_2O_7" with increasing P_2O_5 suggests that a glass, within the detection limit of x-ray, can be made entirely of SiO_6 units. However this task is yet to be completed. XRD results of heat treated high phosphate ($\geqslant$ 25 mol%) containing glasses show different type of nucleation and hence crystallisation properties, which are solely dependent upon P_2O_5 concentration. Therefore a thorough microscopic

study is essential to understand the nucleation and crystallisation of such glasses. The formation of [SiO_6] units from SiO_4 units as a function of heat treatment allows one to determine the equilibrium constant for the reaction. Therefore an estimate of configurational entropy as a function of heat treatment would be possible. Measurement of fictive temperature for various cooling rates as a function of P_2O_5 concentration would provide a value for the enthalpy of the system from which useful information can also be obtained.

The formation of doublets in ^7Li spectra suggests that the lithium atoms occur in pairs. However application of the theoretical equation for an $I=\frac{1}{2}$ system (equ. 2.40) to calculate the distance between two lithium atoms ($I = 3/2$) in Li_2O-SiO_2 (see Chapter 4) may not be appropriate. Thus a theoretical development for strong dipolar interaction in an $I = 3/2$ system is of future interest.

CaO-Na_2O-SiO_2 with small amounts of P_2O_5 form bioactive glasses which can be used for medical applications. The structure of this glass system is yet to be established and the ^{29}Si, ^{31}P NMR would provide useful information. The effect of phosphorus in R_2O (R = Li, Na, K) meta and tetrasilicates or as a function of alkali content would also be of interest. This would provide information on the mechanism for formation of SiO_6 unit in glasses in presence of alkali metal ions. Most of the rock forming silicate melts, e.g. CaO-Al_2O_3-SiO_2, CaO-MgO-SiO_2, contain small amounts of P_2O_5 [4] and the structural analysis of these glasses will be of both scientific and technological interest. Measurement of the relaxation times of the network formers in the glasses may provide additional information about the subtle environmental differences.

Most of the nuclei in the periodic table are now accessible to NMR investigation. Therefore in addition to the ^{29}Si, ^{31}P, ^{27}Al, ^{23}Na, ^{7}Li, ^{1}H other nuclei, for example ^{17}O, ^{51}V, ^{135}Ba, ^{25}Mg, ^{87}Sr, ^{89}Y, ^{6}Li, ^{19}F may also be probed in glasses.

Although ^{17}O is a quadrupolar nucleus with low natural abundance (0.037%) and moderate gyromagnetic ratio, it has a wide chemical shift range (~900 PPM) [5]. Thus ^{17}O NMR has sometimes been successful in investigating structure and ionic nature determinations [6-8]. The ^{17}O NMR results obtained from the recently developed "double angle spinning" technique [9,10] supersedes previous results and can be used to identify oxygen local order in glasses. ^{17}O is readily available in the form of isotopically enriched water and the glasses can be made with such water. As the oxygen is the nearest neighbour of silicon in silicate glasses some information about nucleation kinetics, glass-in-glass phase separation and equilibrium concerned with oxygen exchange because of bond angle, bond length variation due to heat treatment can be obtained.

^{51}V may be a good NMR nucleus and it can be incorporated in some of the alkali silicate glasses in small amounts. However the effect of large amounts of vanadium in glasses may be difficult to observe because of possible unpaired d-electron. Ba, Mg and Sr are constituent elements of rock-forming glasses and their investigation can help in understanding various properties of magmas. However, they are quadrupolar (I = 3/2, 5/2 and 9/2 respectively) nuclei and large electric field gradients and low natural abundance may hinder such an investigation to some extent. ^{89}Y is a $I=\frac{1}{2}$ nucleus and information can readily be obtained from NMR

signal. However, the sensitivity of ^{89}Y NMR relative to protons is very low (1.2×10^{-4}) and this creates a problem in investigations of the local order of the yttrium ions.

In Li_2O-SiO_2 glass ^{7}Li - ^{7}Li couplings form homogeneous interaction which is difficult to narrow. Therefore ^{6}Li NMR can provide information about non-homogeneous dipolar interaction between ^{6}Li and ^{7}Li. ^{19}F is a 100% abundant nucleus with $I=\frac{1}{2}$ and dissolves in mineral glasses. The local order of fluorine in this system is not clearly understood and creates a need for future study. Thus with the introduction of new nuclei in NMR research, this broadens the area of investigation for a wide range of glasses, glass ceramics and other materials.

THE END

REFERENCES

1. R. Dupree, D. Holland, P.W. McMillan and R.F. Pettifer, J. Non-cryst. Solids, 68, 399 (1984).

2. C.M. Schramm, B.W.H.S. de Jong and V.E. Parzialy, J. Am. Chem. Soc., 106, 4396 (1984).

3. P.F. James and P.W. McMillan, J. Mater. Sci., 6, 1345 (1971).

4. B.O. Mysen, F.J. Ryerson and D. Virgo, Am. Miner, 66, 106 (1981).

5. C. Rodger, N. Sheppard, C. McFarlane and W. McFarlane in NMR and The Periodic Table. Edited by R.K. Harris and B.E. Mann, Academic Press, 1978, London.

6. H.A. Christ, P. Diehl, H.R. Schneider and H. Hahn, Helv. Chim. Acta., 44, 866 (1961).

7. B.N. Figgis, R.G. Kidd and R.S. Nyholm, Proc. Roy. Soc. A269, 469 (1962).

8. G.L. Turner, S.E. Chung and E. Oldfield, J. Magn. Reson., 64, 316 (1985).

9. A. Samoson, E. Lippmaa and A. Pines, Mol. Phys., 65, 1013 (1988).

10. B.F. Chmelka, K.T. Muller, A. Pines, J. Stebbins, Y. Wu and J.W. Zwanziger, Nature, 339, 42 (1989).

Appendix A

Nuclear properties of some nuclei

Nucleus	Nuclear Spin	Operating frequency at B_0 = 8.45 T (MHZ)	Sensitivity at natural abundance relative to ^1H	line width* factor, L $x10^{54}$
^1H	1/2	360.13	1.0	-
^7Li	3/2	139.908	0.27	0.05
^{23}Na	3/2	95.3	0.09	0.33
^{27}Al	5/2	93.848	0.21	1.0
^{29}Si	1/2	71.535	3.70×10^{-4}	-
^{31}P	1/2	145.78	0.07	-

* From equ. (2.34) one can have

$$\nu_{\frac{1}{2}}^{(2)} = \frac{-9\,(e^2q)^2}{64\,\nu_L\,h^2}\,\frac{Q^2}{I^2\,(2I-1)^2}\,(a-3/4)\,(1-\mu^2)\,(9\mu^2-1)$$

The term $\dfrac{Q^2}{I^2\,(2I-1)^2}\,(a-3/4) = L$

is generally called the linewidth factor.